

Institut für Experimentelle Genetik
GSF-Forschungszentrum für Umwelt und Gesundheit,
Neuherberg



Search for New Steroid Hormone Metabolizing Enzymes: Functional Genomics of the Short-Chain Dehydrogenase/Reductase Superfamily

Brigitte D. Keller

Vollständiger Abdruck der von der Fakultät Wissenschaftszentrum Weihenstephan für
Ernährung, Landnutzung und Umwelt der Technischen Universität München
zur Erlangung des akademischen Grades eines

Doktors der Naturwissenschaften

genehmigten Dissertation.

Vorsitzender: Univ.-Prof. Dr. Martin Hrabé de Angelis

Prüfer der Dissertation: 1. Univ.-Prof. Dr. Johannes Buchner
2. Univ.-Prof. Dr. Dr. Adelbert Bacher
3. apl. Prof. Dr. Jerzy Adamski

Die Dissertation wurde am 02.06.2006 bei der Technischen Universität München eingereicht und durch die Fakultät Wissenschaftszentrum Weihenstephan für Ernährung, Landnutzung und Umwelt am 18.10.2006 angenommen.

Meinen Eltern

Contents

Abbreviations	xi
Zusammenfassung	1
Abstract	3
1. Introduction	5
1.1. The Short-Chain Dehydrogenase/Reductase superfamily	5
1.1.1. Structural characteristics of SDRs	6
1.1.2. Enzymatic characteristics and substrates of SDRs	7
1.1.3. Medical impact of SDR superfamily	8
1.2. Hormones	8
1.2.1. Steroid hormones	10
1.2.2. Distribution and action of steroid hormones	10
1.2.3. Classes of steroid hormones	11
1.2.4. Biosynthesis of steroid hormones	12
1.3. Steroid metabolizing enzymes: Biosynthesis and pre-receptor control of steroid action	15
1.3.1. 20 α -Hydroxysteroid dehydrogenases	15
1.3.2. 3 α -Hydroxysteroid dehydrogenases	15
1.3.3. 3 β -Hydroxysteroid dehydrogenases/isomerases	15
1.3.4. 11 β -Hydroxysteroid dehydrogenases 1 and 2	16
1.3.5. 17 β -Hydroxysteroid dehydrogenases	16
1.4. The aim of the study	17
2. Results	19
2.1. Introducing remarks	19
2.2. Identification of SDR candidate enzymes and classification as SDRs	19
2.2.1. Identification of putative SDRs using SDR Finder	19
2.2.2. Verification of the SDR Finder identified enzymes and classification as SDR enzymes	23
2.2.3. Identification and verification of MGC4172 and MGC18716	24
2.2.4. Annotation of the identified SDR type enzymes to the genome	24
2.3. Selection of identified SDRs for in-depth characterization	28

Contents

2.4.	Expression patterns of candidate enzymes	33
2.4.1.	Development of an automated <i>In Silico</i> Northern Blot (ISNB)	33
2.4.2.	Expression analysis of the candidate genes in silico and wet lab	35
2.4.3.	Expression pattern of murine orphan Sdr (mSdr-o)	37
2.4.4.	Expression pattern of human retSDR3	38
2.4.5.	Expression pattern of rat dhrs7b	38
2.4.6.	Expression pattern of rat dhrs8	39
2.4.7.	Expression pattern of murine Rdh12	40
2.4.8.	Expression pattern of human RDH12	41
2.4.9.	Expression pattern of human RDH13	42
2.4.10.	Expression pattern of murine Dhrs4	43
2.4.11.	Expression pattern of human DHRSX	43
2.4.12.	Expression pattern of human WWOX	44
2.4.13.	Expression pattern of murine Wwox	45
2.4.14.	Expression pattern of human MGC4172	46
2.4.15.	Expression pattern of murine MGC18716	47
2.5.	First hints to substrate specificity: phylogenetic analyses	48
2.6.	Investigation of substrate specificity: test of steroidogenic substrates	51
2.6.1.	Selection of substrates and establishment of measurement	51
2.6.2.	Establishment of substrate conversion assays	52
2.6.3.	Conduction of conversion assays for enzymes under investigation	58
2.6.4.	Expression plasmids	60
2.6.5.	Test of overexpression	60
2.6.6.	Enzymes not converting the tested substrates	61
2.6.7.	Human retSDR3 oxidizes 17 β -estradiol to estrone	62
2.6.8.	Human RDH12, human DHRSX, and murine Dhrs4 reduce dihydrotestosterone to androstanediol	63
2.6.9.	Murine Dhrs4 has reductive enzymatic activity not only versus dihydrotestosterone but also towards androstenedione and estrone	65
2.6.10.	Murine Wwox reduces androstenedione to testosterone and androsterone to androstanediol	68
2.7.	Investigation of subcellular localization	71
2.7.1.	Bioinformatic means to predict subcellular localization	72
2.7.2.	Vectors and system of analysis	72
2.7.3.	Murine Sdr-o is a mitochondrial protein	75
2.7.4.	Human retSDR3 localizes to the cytoplasm	76
2.7.5.	dhrs7b from rat is localized in the endoplasmic reticulum	77
2.7.6.	Rat dhrs8 is an ER-localized SDR enzyme	78

2.7.7. Murine Rdh12 is endoplasmic reticulum-localized	79
2.7.8. Human RDH12 localizes to the ER	80
2.7.9. Human type 13 retinol dehydrogenase localizes to the mitochondria	81
2.7.10. Murine Dhrs4 is neither a peroxisomal SDR nor mitochondrial but cytoplasmically distributed	82
2.7.11. Human DHRSX co-localizes with ER-staining	83
2.7.12. MGC4172 and MGC18716 may both be ER-localized	84
3. Discussion	87
3.1. General remarks	87
3.2. The set-up - is it functional genomics?	87
3.3. Identification of candidate proteins and classification as SDRs	88
3.3.1. The SDR Finder - friend or foe?	88
3.3.2. On NCBI NonRedundant Database	89
3.3.3. Annotation of identified SDRs to chromosomal location	90
3.4. Analysis of the expression patterns	92
3.4.1. Need of expression analysis	92
3.4.2. Experimental expression analysis by Northern Blot	93
3.4.3. In silico expression analysis	93
3.5. Use of phylogenetics in predicting substrate specificities	96
3.6. The substrate conversion assay	98
3.6.1. Prokaryotic or eukaryotic overexpression?	98
3.6.2. A steroid hormone conversion assay in living cells - what are the advantages?	100
3.6.3. Considerations on the cell line used	100
3.6.4. The conversion assay in living cells - is it <i>in vivo</i> ?	103
3.6.5. Michaelis-Menten kinetics in living cells	103
3.6.6. Measurement of progestin conversion	105
3.7. Studies on subcellular localization	105
3.7.1. Prediction of subcellular localization	105
3.7.2. Considerations on the experimental design	106
3.8. Conclusions about the enzymes under investigation	111
3.8.1. Murine orphan Sdr (Sdr-o)	111
3.8.2. Human retSDR3	113
3.8.3. Rat SDRs under investigation: dhrs7b and dhrs8	115
3.8.4. Retinol dehydrogenases under investigation: murine type 12, human types 12 and 13	116
3.8.5. Murine Dhrs4	118
3.8.6. Human DHRSX	119

Contents

3.8.7. Human and murine WW-box containing oxidoreductases	120
3.8.8. MGC4172 and MGC18716	122
3.9. What else could be done?	124
3.10. Outlook	125
4. Methods	127
4.1. Work with <i>E. coli</i>	127
4.1.1. Culture media	127
4.1.2. Inhibitory and selective media supplements	127
4.1.3. Growing of bacteria	127
4.1.4. Short- and long-term-storage of bacterial culture	128
4.1.5. Production of competent <i>E. coli</i> and transformation of plasmid DNA	128
4.2. Methods with eukaryotic cell lines	129
4.2.1. Cultivation of cells	129
4.2.2. Maintenance of cell culture: Splitting, thawing, freezing, and long-term storage of eukaryotic cells	130
4.2.3. Transfection of eukaryotic cells	131
4.2.4. Seeding of cells and transfection in different formats	131
4.2.5. Immunocytochemical methods for subcellular localization studies .	132
4.3. DNA-based molecular biological methods	134
4.3.1. Isolation and purification procedures	134
4.3.2. Measurement and quality assessment of DNA solutions	135
4.3.3. Cloning strategies	137
4.3.4. PCR-based methods	138
4.4. RNA-based methods	139
4.4.1. Synthesis of RNA by in vitro transcription and digoxigenin labelling	139
4.4.2. Isolation and purification methods	139
4.4.3. Handling and measurement	140
4.5. Analysis of Gene Expression	141
4.5.1. Reverse transcription of mRNA into cDNA	141
4.5.2. Hybridization of cDNA probes to membrane bound RNA: Northern Blot	141
4.5.3. Analysis of gene expression in mouse embryos	142
4.6. Measurement of substrate specificity	144
4.6.1. Measurement of substrate conversion in living cells	144
4.6.2. Determination of Michaelis-Menten kinetics	144
4.6.3. Purification of HPLC samples by solid phase extraction	146
4.6.4. HPLC measurement	147
4.7. Bioinformatic methods	148

4.7.1. Identification of SDR candidate genes	148
4.7.2. In silico Northern Blot	148
4.7.3. Alignments and phylogeny	149
4.7.4. Bioinformatic assessment of subcellular localization	149
5. Programs, organisms, material	151
5.1. Programs	151
5.2. Organisms	152
5.2.1. E. coli strains used	152
5.2.2. Cell lines used	153
5.3. Material	153
Bibliography	153
A. Appendix	171
A.1. Accession numbers of the dataset for the phylogenetic trees	171
A.2. Primers used	172
A.2.1. Primers used for test of overexpression of the constructs and generation of northern blot probes	172
A.2.2. Primers and restriction sites used for cloning	173
A.3. IMAGE clones ordered (RZPD)	174
A.4. List of publications	175
Danksagung	177

Contents

Abbreviations

A	androstenedione
A-diol	androstanediol
A-on	androsterone
aa	amino acid
AKR	aldo-keto reductase
APS	ammoniumperoxodisulphate
BLAST	basic linear alignment search tool
b(p), kb(p)	base (pair), kilo base (pair)
BSA	bovine serum albumin
C-ol	cortisol
C-on	corticosterone
cDNA	complementary DNA
CDS	coding sequence
CNS	central nervous system
CYP	cytochrome P450
DAB	diaminobenzidine
DHEA	dihydroxyepiandrosterone
DHT	dihydrotestosterone
DNA	deoxyribonucleic acid
dpc	days post coitum
NTP	nucleotide triphosphate
ds	double-stranded
E1	estrone
E2	estradiol
E. coli	Escherichia coli
EDTA	ethylenediaminetetraacetic acid
ER	endoplasmic reticulum
EST	expressed sequence tag
FBS	fetal bovine serum
fig	figure
GAPDH	glyceraldehyd-3-phosphate dehydrogenase

GR	glucocorticoid receptor
GST	glutathione S-transferase
HPLC	high performance liquid chromatography
HSD	hydroxysteroid dehydrogenase
IPTG	isopropyl-beta-D-thiogalactopyranoside
ISNB	in silico northern blot script
kDa	kilo Dalton
K _m	Michaelis-Menten constant
LB	Luria-Bertani
LCFA	long chain fatty acid
MR	mineralocorticoid receptor
mRNA	messenger RNA
NAD	β -nicotinamide adenosine dinucleotide
NADP	β -nicotinamide adenosine dinucleotide 3'phosphate
NADPH	β -nicotinamide adenosine dinucleotide 3'phosphate, reduced form
OHP	20 α -hydroxy progesterone
P, P4	progesterone
nt	nucleotide
PAGE	polyacrylamid gel electrophoresis
PBS	phosphate buffered saline
PCR	polymerase chain reaction
qRT-PCR	quantitative reverse-transcriptase PCR
RDH	retinol dehydrogenase
RNA	ribonucleic acid
rpm	rotations per minute
RT-PCR	reverse transcriptase PCR
SDS	sodium dodecylsulfate
SDR	short-chain dehydrogenase/reductase
SHGB	sex hormone binding globulin
ss	single-stranded
T	testosterone
TEMED	tetramethylethylenediamine
VLCFA	very long chain fatty acid
V _{max}	maximal velocity
w/v, w/w	weight/volume, weight/weight
X-Gal	5-bromo-4-chloro-3-indolyl-beta-D-galactopyranoside

Zusammenfassung

Die Enzym-Superfamilie der Short-Chain Dehydrogenasen/Reduktasen (SDRs) zeichnet sich durch gemeinsame strukturelle Elemente aber einen geringen Grad an Konservierung auf Aminoäure-Ebene (15-30%) aus. Zum größten Teil besteht die Familie aus Oxidoreduktasen, die eine Vielzahl von Substraten umsetzen, darunter Retinole, Steroidhormone, Zucker, Aminosäuren und Xenobiotika. Ziel der vorliegenden Arbeit war ein funktionell genomicscher Ansatz zur Identifizierung und Charakterisierung neuer SDRs. Für die enzymatische Charakterisierung lag der Fokus auf Steroidhormon-Umsetzung.

Mit Hilfe des “SDR Finders” wurden mehrere hundert Kandidaten aus den Genomen von Mensch, Maus und Ratte identifiziert. Nach mehreren Verifizierungsschritten verblieben 38 SDRs als mögliche Ziele der Doktorarbeit; 13 wurden in Hinblick auf Expressionsmuster, enzymatische Aktivität gegenüber Steroidhormonen und subzelluläre Lokalisation charakterisiert.

Zur Expressionsanalyse wurde ISNB, ein automatisiertes System zur Evaluierung von EST-Häufigkeiten in Datenbanken, etabliert und getestet. Experimentell wurden diese Ergebnisse mit Northern Blots und PCR bestätigt und komplementiert. Alle 13 Enzyme weisen unterschiedliche Expressionsmuster auf. Während die Expression einiger gewebe-spezifisch ist, sind andere in einer größeren Anzahl von Geweben oder ubiquitär exprimiert.

Phylogenetische Untersuchungen ergaben erste Hinweise auf die Substratspezifität der neuen SDRs. Alle sind mit bereits charakterisierten Steroid- und Retinoldehydrogenasen verwandt. Die Untersuchung der Substratspezifität wurde in lebender Zellkultur durchgeführt. Nach transienter Transfektion wurde die Interkonversion von Steroidhormonen unter Bedingungen gemessen, die physiologischen Umständen sehr ähnlich sind. Hierdurch konnte erstmalig der Steroidumsatz von fünf der gewählten Enzyme gezeigt werden. Die humane retSDR3 oxidiert Estradiol zu Estron. Die anderen vier aktiven Enzyme wirken als Reduktasen. Die murine Dhrs4 zeigte mit drei umgesetzten Steroidhormonen (Androstendione, Dihydrotestosterone, Estron) das breiteste Substratspektrum. Die humanen Enzyme RDH12 und DHRSX setzen ebenfalls Dihydrotestosteron zu Androstandiol um. Murine Wwox kann die Reduktion von Androstendion und Androsteron katalysieren. Dieses Ergebnis zeigt zum ersten Mal die enzymatische Aktivität von Wwox gegenüber Steroidhormonen, die bereits in mehreren Publikationen postuliert aber nicht gezeigt wurde. Es ist damit wahrscheinlich, dass auch das humane Homolog Steroide umsetzen kann, die in der vorliegenden Arbeit nicht getestet wurden. Für alle gezeigten Umsetzungen wurde im Anschluss Michaelis-Menten-Kinetik durchgeführt. Die Ergebnisse hieraus zeigen K_m -Werte bei physiologischen Konzentrationen der jeweiligen Steroidhormone.

Die subzelluläre Lokalisation von zehn SDRs wurde im Endoplasmatischen Retikulum,

in den Mitochondrien oder im Cytosol gezeigt.

Diese Arbeit zeigt nicht nur, dass über SDRs im Steroidmetabolismus noch vieles entdeckt werden kann. Sie vermittelt zudem neue Erkenntnisse über die Expression, Aktivität, und Lokalisation einiger Enzyme dieser Familie.

Abstract

Short-chain dehydrogenases/reductases (SDRs) form an enzyme superfamily with common structural elements but a quite low overall amino acid identity of only 15-30%. As oxidoreductases, SDRs can convert a variety of substrates including retinoids, steroid hormones, sugars, amino acids, and xenobiotics. Aim of the work at hand was a functional genomics approach towards identification and characterization of new SDRs with focus on steroid hormone conversion abilities.

By use of ‘SDR Finder’ I could identify several hundred putative SDRs from the genomes of human, mouse, and rat. After several steps of verification, 38 enzymes remained as possible targets of this thesis. 13 enzymes were selected to be characterized with regard to expression pattern, steroid conversion, and subcellular localization.

For expression analysis, an automated system for evaluation of EST frequencies in databases was established and tested (ISNB). Experimentally, these results were underlined and complemented by northern blot and PCR. I could show that all enzymes have distinct expression patterns, some being exclusively expressed only in few tissues while others showed a broader or ubiquitous expression.

Using phylogenetic analyses evolutionary relationship of these SDRs to characterized retinoid and steroid dehydrogenases of the SDR family was shown and first hints to substrate specificity gained. Substrate conversion was analyzed by a conversion assay in intact cells. After transient transfection, I was thereby able to test for interconversion of steroid hormones under close-to-physiological conditions. Five of the selected enzymes were active towards the steroid hormones tested. This is a novel observation. Human retSDR3 oxidizes estradiol to estrone while the other four enzymes display reductive activity. Murine Dhrs4 shows the broadest substrate spectrum with conversion of estrone, androstenedione and dihydrotestosterone. Human RDH12 and human DHRSX also have activity towards dihydrotestosterone, reducing it to androstanediol. Also for the first time, I was able to show enzymatic activity of murine Wwox: the catalysis of the reduction of androstenedione and androsterone. This finding underlines that its human homologue also could have activity towards steroidogenic substances - a fact that has been proposed several times but up to now could not be shown. All conversion measurements were followed by Michaelis-Menten kinetics. These results indicate values for K_m at physiological concentrations of the respective steroid hormones.

I could determine the subcellular localization of ten enzymes, finding them in endoplasmic reticulum, mitochondria or cytoplasm.

The work at hand shows that there is still much to be discovered about SDR type enzymes and steroid metabolism but also delivers new insights into several enzymes of this family.

1. Introduction

Over the last century, biological sciences have changed from a merely descriptive level to the analysis of the molecular basis of metabolic functions. By these in-depth analyses, many hypotheses about life could be acknowledged or declined. This way knowledge has been gained on the four classes of macromolecules which life depends on: polysaccharides, lipids, nucleic acids, and proteins. Two out of these four macromolecule classes depict the focus of two fields of modern biology, and also the focus of many studies on inborn errors of metabolism: genetics, the science of inheritance and its regulation, and biochemistry which comprises the action of catalytically active proteins, the enzymes. The focus of this thesis lies on one family of enzymes with large implication on inborn errors of metabolism, the Short-Chain Dehydrogenase/Reductase (SDR) family. Among many substrates SDR type enzymes can convert steroid hormones. These hormones play a crucial role in many metabolic pathways as the sexual reproduction of mammals.

By sexual reproduction, the genetic material is not only passed to the next generation for maintenance of a species but also comprises mechanisms for adaptation to changes in environmental conditions. This process of adaptation is rather slowly gaining importance during evolution. Steroid hormones have been shown to be key regulators of fertility and thus of the ability of sexual reproduction. All living processes are tightly regulated within the organism, and so is the endocrine system. Dysfunction and imbalance lead to severe diseases - not only infertility but also cancer, malformation syndromes, osteoporosis, obesity, and, last but not least, Alzheimer's disease. Research on steroid hormones and the enzymes that regulate their anabolism, activity, and catabolism can help to understand the mechanisms by which these diseases develop and therefore lead the way to curing or bypassing their development.

1.1. The Short-Chain Dehydrogenase/Reductase superfamily

The first SDR type enzymes were described in the 1970's with the primary structure of prokaryotic ribitol dehydrogenase [25, 79] and alcohol dehydrogenase from *D. melanogaster* [106, 113]. Few more enzymes were added and the family was considered to consist of prokaryotic dehydrogenases and insect alcohol dehydrogenase. When the mammalian NAD⁺-dependent 15-hydroxyprostaglandin dehydrogenase [55] and the first 17 β -hydroxy-steroid dehydrogenase (17 β -HSD) [88] were added to this family [55] the interest on SDRs

1. Introduction

(then called Short-Chain Alcohol Dehydrogenases, SCAD) began to rise. In 1994, over 60 enzymes had been subordinated to this family [48]; in 2003, the family already consisted of about 3000 members in all taxa [86]. SDRs span several EC classes. The majority of SDRs belongs to the oxidoreductases (EC 1.x.x.x) but also lyases (EC 4.x.x.x) and isomerases (EC 5.x.x.x) have been described [48].

There have been attempts to find an understandable and reliable system for the subordination of the SDR superfamily. Five families have been described to belong to SDRs, namely divergent, classical, intermediate, extended, and complex SDRs. Classical SDRs have been further subdivided into eight subfamilies, extended SDRs comprise three subfamilies [50]. However, this system has not been accepted by the research community so far. For the aldo-keto-reductase family, a system has been established for the subordination according to structural features. Alike attempts for a general and expandable nomenclature are on-going also for the SDR superfamily (personal communication, Prof. J. Adamski).

1.1.1. Structural characteristics of SDRs

Most SDRs described so far have an amino acid (aa) chain of 250 to 400 residues in length but share quite low sequence identity of 15 to 30%. Due to this rather low conservation, SDRs are subordinated to this family according to the existence of certain motifs which are usually well conserved. These motifs are shown in table 1.1.

Table 1.1: Typical SDR motifs [86] in order of appearance in the primary structure.

Motif	Function
TGxxxGxG	Coenzyme binding region, maintenance of the central β -sheet
D	Stabilization of adenine ring pocket, weak binding to coenzyme
NNAG	Stabilization of the central β -sheet
N	Active site
S-Y-K	Active site
N	Connection of the substrate binding loop and the active site
PG	Reaction direction
T	H-bonding to carboxamide of nicotinamid ring

Despite the low sequence identity shared by these enzymes, SDRs have been shown to fold into a typical one-domain structure with a highly similar α/β folding pattern including a Rossmann fold. The Rossmann fold [101] is a typical cofactor binding structure of enzymes using NAD^+ or NADPH/H^+ . Interestingly, the Rossmann fold is one of the most often found protein motifs in PDB [54]. It consists of a central β -sheet flanked by

1.1. The Short-Chain Dehydrogenase/Reductase superfamily

α -helices. This coenzyme-binding region typically forms the N-terminal part of the SDR protein while the C-terminus is responsible for substrate binding.

The one-domain-folded SDR-monomers (average molecular weight: 27 kDa [91]) are usually inactive and have to form dimers or tetramers for activity. The quaternary structure is also highly similar. To this rule, few exceptions have been described among them the porcine carbonyl reductase which is active as a monomer [35].

1.1.2. Enzymatic characteristics and substrates of SDRs

SDR-type oxidoreductases interconvert hydroxy- and keto-groups on many substrates. The reaction performed is pictured at position 17 of a standardized steroid backbone in fig. 1.1.

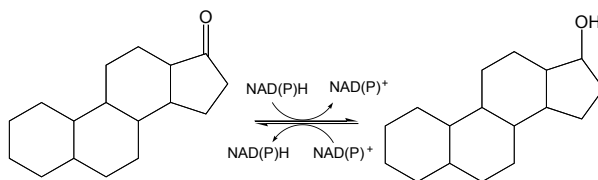


Figure 1.1: Oxidoreductase activity at sterane position 17. In most SDRs, NADPH/H⁺ is preferred as a cofactor for reduction, for oxidation, NAD⁺ [93].

In the course of characterization especially of human SDR-type enzymes, the variety of substrates they are able to convert became apparent. They play a central role in many intermediary metabolic pathways. Some SDRs have been described to fulfill house-keeping activities as GAPDH. Besides sugars (prokaryotic glucose dehydratase, human UDP-galactose epimerase), naphtalenes (*M. crisea* 1,3,8-trihydroxynaphthalene reductase), amino acids, and retinoids (retinol dehydrogenases), steroids are substrate to SDR conversion (examples are depicted in fig. 1.2). Examples for pathways involving SDRs are the bile acid, steroid hormone, fatty acid, retinol and neurotransmitter metabolism.

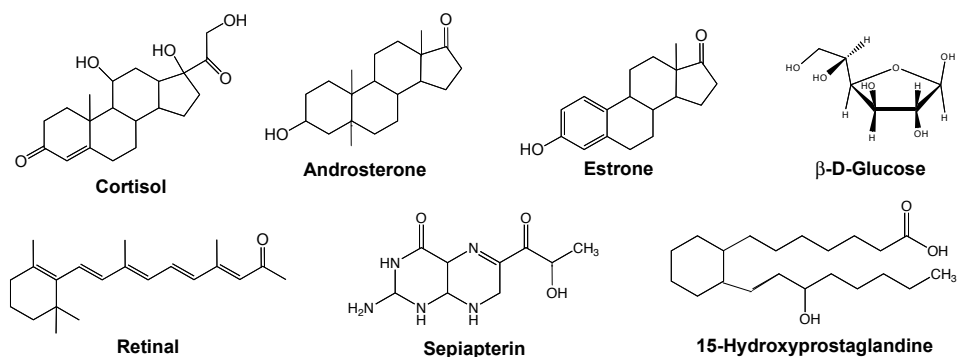


Figure 1.2: SDRs can act on a variety of substrates.

1. Introduction

1.1.3. Medical impact of SDR superfamily

It is not surprising from the wide variety of functions that SDRs have been shown to be involved in many wide-spread diseases. Some SDR enzymes are important in the development of steroid-dependent cancers [120]. Other SDRs have been associated with inflammation and degenerative defects [77,117,121]. Table 1.2 depicts examples of disease-causing dysfunctional SDRs. The fact that SDRs are involved in several serious diseases makes them a popular target for medically relevant studies. Many of these concern inhibitor screens (e.g. [22,23,28,62,94,112,119]). Broadening knowledge about this enzyme family could therefore not only lead to more detailed understanding of the metabolism but also bring up new targets for drug development.

Table 1.2: Examples for inborn errors of metabolism and cancers caused by dysfunctional SDRs

SDR	Inborn error of metabolism caused
UDP-galactose 4'epimerase	Galactosemia type III
Sepiapterin reductase, Dihydropterine reductase	Tetrahydrobiopterin deficiency
NAD(P)H-steroid dehydrogenase like	Congenital hemidysplasia with ichyoform erythroderma and limb defects (CHILD)
3 β -HSD 2	Congenital adrenal hyperplasia (CAH)
11 β -HSD 2	Apparent mineralocorticoid excess syndrome
17 β -HSD 3	Male pseudohermaphroditism
17 β -HSD 4	D-specific bifunctional protein deficiency syndrome
Type of cancer caused	
17 β -HSD 1	Breast cancer
17 β -HSD 2	Epithelial cancers, e.g. intestinal cancer
17 β -HSD 3	Prostate cancer

1.2. Hormones

For regulation of cell proliferation and differentiation, development of the organs and interaction of different tissues, multicellular organisms need complex mechanisms of control and communication. This is achieved by use of hormones as chemical signaling molecules. Depending on their chemical nature, hormones are subdivided into several classes as peptide and protein hormones (e.g. insulin), amino acid-related hormones (e.g. adrenaline),

fatty acid-derived hormones (e.g. prostaglandins), small inorganic molecules (e.g. NO), and steroid hormones (see below), the latter being derived from cholesterol as common precursor.

Hormones execute their function by binding to specific receptors that may be an integral membrane protein such as the insulin receptor or intracellular proteins as is the case for the nuclear steroid hormone receptors. Biosynthesis of hormones or their precursors mainly takes place in specialized endocrine glands. Several mechanisms of action have been described according to the distance of hormone action. They are named systemic (endocrine), paracrine, autocrine, and intracrine (for hormone action, see [2] , for introcrinology, see [57]).

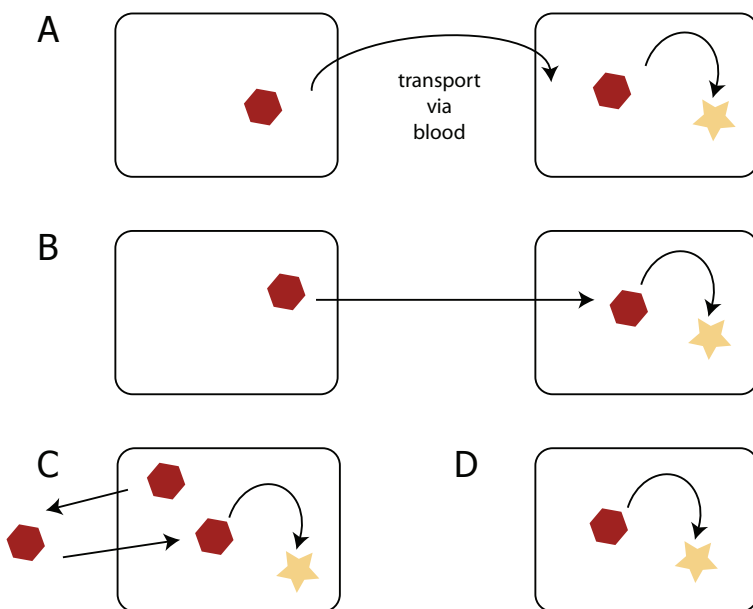


Figure 1.3: Modes of hormone action (inactive hormones are depicted by hexagon, active ones by a star). A: endocrine action on distant cells after transport via the blood, B: paracrine action on neighbored cells, C: autocrine action after secretion on the synthesizing cell or on cells of the same type, D: intracrine action within one cell.

Ways of hormone action are depicted in fig. 1.3. For endocrine action, hormones secreted to the blood are transported bound to proteins. In the human blood these can be for example albumin (nonspecific carrier) or specific carrier proteins as the sex hormone binding globulin (SHGB). Only about 3% of the hormones in the blood are transported unbound. In contrast, paracrine mode of hormone action is on neighbored cells. The secreting cell type differs from the target cell type. Autocrine action can take place on the same cell or one the same cell type in the immediate surroundings as has been described for neurotransmitters. Intracrine action has been described for androgens [57]. In summary,

1. Introduction

hormones can be synthesized as inactive precursors and activated by special enzymes at their point of action. Alternatively, the active hormone are synthesized locally.

1.2.1. Steroid hormones

Steroid hormones are derivates of cholesterol and exhibit the same backbone. The parent ring structure of steroids, sterane, and its numbering are shown in fig. 1.4.

According to structural features and the number of carbon atoms (C), steroid hormones are divided into six groups (see fig. 1.7): the sex hormones (estrogens: 18 C, androgens: 19 C, gestagens: 21 C), mineral- and glucocorticoids consist of 21 C each and vitamin D and its daughter metabolites of 27 C.

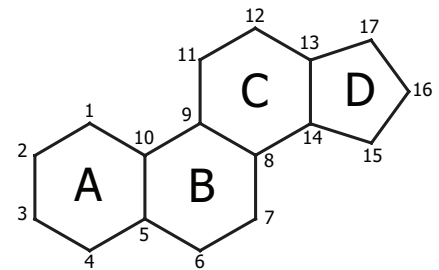


Figure 1.4: Sterane, the backbone of steroid hormones and its numbering.

1.2.2. Distribution and action of steroid hormones

Distribution and action of steroid hormones is delivered by the four ways described in fig. 1.3. The classical genomic way of endocrine steroid hormone action is outlined in fig. 1.5.

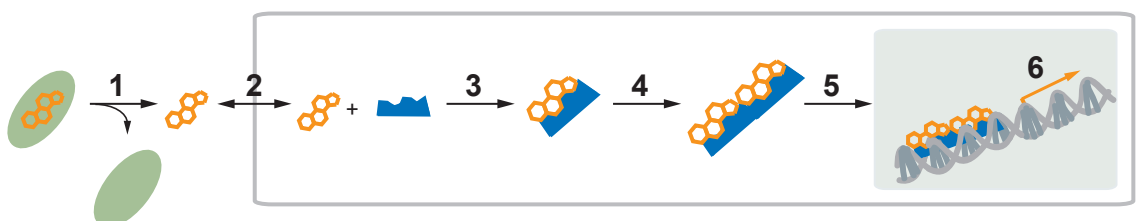


Figure 1.5: Classical mechanism of steroid hormone action. Numbers reflect pathway progression.

For systemic distribution, steroid hormones are bound to transport proteins. These transport proteins release the hormones at the cellular surface (1). Two ways have been described for steroids entering the cell (2): by passive diffusion (free hormone hypothesis) or assisted by transporter proteins [65]. Megalin was described to mediate endocytosis of the SHGB-hormone complex thus being crucial for optimal internalization [1]. It is yet unclear whether the free hormone hypothesis will persist or whether receptor-mediated uptake is the predominating mechanism for steroid hormone entry to the target cells.

There, steroid hormones bind to their specific receptors (3). Before receptor-binding occurs, steroid hormones usually have to be activated by intracellular enzymes. Further modifying enzymes can inactivate excess hormone. Upon receptor-binding of the activated hormone, the hormone-receptor complex dimerizes (4) and is translocated to the nucleus (5). Steroid hormone-receptor dimers then bind to specific binding sites on the DNA and act as transcriptional regulators influencing target-gene expression (6) and the protein content of the affected cell.

Beside these effects on transcriptional activity steroid hormones have been described to perform non-genomic effects which occur in the range of seconds after confrontation with the hormone. This very rapid way of action was shown to be mediated via activation of kinases and membrane receptors. This has been shown for progestins [58]. Even for the non-genomic effects receptor-binding is a prerequisite. At present, many respects of the non-genomic way of steroid hormone action remain puzzling (for a review on non-genomic steroid actions, see [66]). Recent findings indicate that the non-genomic effects caused by estradiol are early steps of a newly discovered estradiol-mediated signaling pathways [122]. This could also be true for the non-genomic effects of other steroid hormones.

1.2.3. Classes of steroid hormones

Physiologically important steroids are divided into seven groups, six of which act as hormones. Hormonally active are the classes androgens, estrogens, progestins, mineralocorticoids, glucocorticoids, and the hormones of vitamin D group. The seventh class of steroids, bile acids, are hormonally inactive and synthesized in the liver emulgating dietary lipids in the intestine. Hormonally active steroids are depicted in fig. 1.7. Tissues relevant for the steroid hormone biosynthesis are shown in fig. 1.6). Many of the steroid hormones classically considered as sex steroids (progestins, androgens, estrogens) exert neurosteroidogenic [99, 128] in addition to their classical functions.

Progestins. Progesterone is the only biologically active progestin. It plays a major role in preparing and maintaining pregnancy. Anti-progestins are used as contraceptives. In addition, progestins are of major importance as intermediate products in the biosynthesis of the other steroid hormones except for those of the vitamin D group. Progesterone has also been shown to operate neurosteroidogenically in rat glial cells [49].

Androgens. Androgens are the main determinants for male sexuality and behavior. The active androgens are testosterone and 5α -dihydrotestosterone. Androgen analogues are ingested to increase muscle anabolism; anti-androgens are used in the treatment of some cancers (e.g. prostate cancer). Androgens display inhibitory effects on apoptosis in prostate

1. Introduction

cancer [53] and last but not least exert neurosteroidogenic actions: they display a central negative feedback on the hypothalamic-pituitary-gonadal axis [95].

Estrogens. Estrogens drive the development of the reproductive system and functions in female vertebrates. Medically important are estrogens as substitution therapy after the menopause and as anti-estrogens in the therapy of certain cancers, e.g. estradiol-dependent breast-cancer. Estradiol, the biologically active estrogen, has been proposed to enhance apoptosis needed for the regression of the corpus luteum [118] though usually, estrogens are described to rather increase proliferation.

Corticoids. **Glucocorticoids** (in human cortisol and cortisone, in rodents deoxycorticosterone and corticosterone) regulate the glucose metabolism [117]. Dysregulation of the biosynthesis of glucocorticoids can cause diseases like adrenal hyperplasia or Cushing's syndrome with unregulated secretion of cortisone. Glucocorticoids are pharmaceutically important in the treatment of adrenal insufficiency. As glucocorticoids in high doses also show immunosuppressive and antiinflammatory effects, synthetic analogues are used in the treatment of autoimmune and rheumatic diseases but also given after transplantation to suppress the rejection of the graft.

Mineralocorticoids, especially aldosterone, are essential regulators of mineral metabolism and blood pressure. High levels of aldosterone lead to aldosteronism with low potassium in plasma and high blood pressure. Glucocorticoids have, though to a much lesser extent, mineralocorticoid effects. Also progesterone can bind to the mineralocorticoid receptor (MR).

Vitamin D group. Vitamin D and its metabolites are synthesized from cholesterol by UV-induced cleavage of the B ring which takes place in the skin. In mammals, vitamin D is a key regulator of calcium and phosphate metabolism and therefore indispensable for anabolism and maintenance of the bones. Abnormal vitamin D levels cause rickets, osteomalacia, and osteoporosis (for a review on vitamin D, see [29]).

1.2.4. Biosynthesis of steroid hormones

Biosynthesis of endocrine active steroid hormones is not ubiquitous but takes place in specialized endocrine glands (cf. to fig. 1.6). However, also local biosynthesis and activation of steroid hormones are indispensable for correct function of the endocrine system.

The common precursor of all steroid hormones is cholesterol. Though cholesterol is ubiquitously spread over the organism (it is an essential part of the plasma and mitochondrial membranes), its biosynthesis in the adult organism is mainly restricted to the liver, while it displays a distinct and spatial pattern throughout embryogenesis [59, 60]. Rather

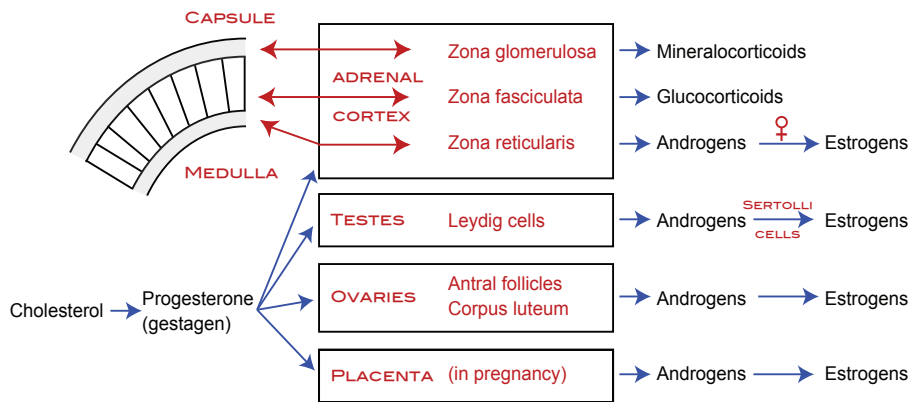


Figure 1.6: Steroid biosynthesis relevant tissues. Modified after [74].

than dietary uptake of cholesterol, *de novo* biosynthesis secures the supply of the organism with this molecule.

Rate-limiting step of the steroid-hormone biosynthesis is the trifunctional cholesterol monooxygenase complex at the inner mitochondrial membrane. The monooxygenase complex is expressed in steroidogenic tissues (adrenal, placenta, gonads, brain) predominantly but not exclusively: lower levels are also found in liver and intestine. This enzyme-complex forms pregnenolone. The bifunctional steroid- Δ -isomerase and 3β -hydroxy- Δ^5 -steroid dehydrogenase in the smooth endoplasmatic reticulum then form progesterone. Both classes of corticoids are synthesized in the adrenal cortex but in different areas: glucocorticoids in the zona fasciculata and mineralocorticoids in the zona glomerulosa.

Two groups of enzymes play an important role in the biosynthesis of steroid hormones from cholesterol: Cytochrome P450 enzymes and hydroxysteroid dehydrogenases (HSDs).

Progesterone is the precursor also of androgens and estrogens. The enzymes involved are members of the Cytochrome P450 family: 17α -hydroxylase/ $17,20$ -lyase (Cyp17A1) is responsible for formation of androgens. P450-aromatase (Cyp19A1) aromatizes the A ring of the steroid backbone and thus forms estrogens of androgens. The enzyme is predominantly found in female specific tissues but is also present in the adrenal (formation of DHEA and DHEA-S takes place in the zona reticularis), the testis and other tissues.

Hydroxysteroid dehydrogenases (HSDs), the other group of enzymes metabolizing steroids belong to two families, aldo-keto-reductases (AKR) and SDRs. These enzymes exert their functions (activation and inactivation of the hormones) at the specific site of steroid hormone action in pre-receptor control of activity. Some of them are also responsible for inactivation of active steroids delivered to non-target tissues.

1. Introduction

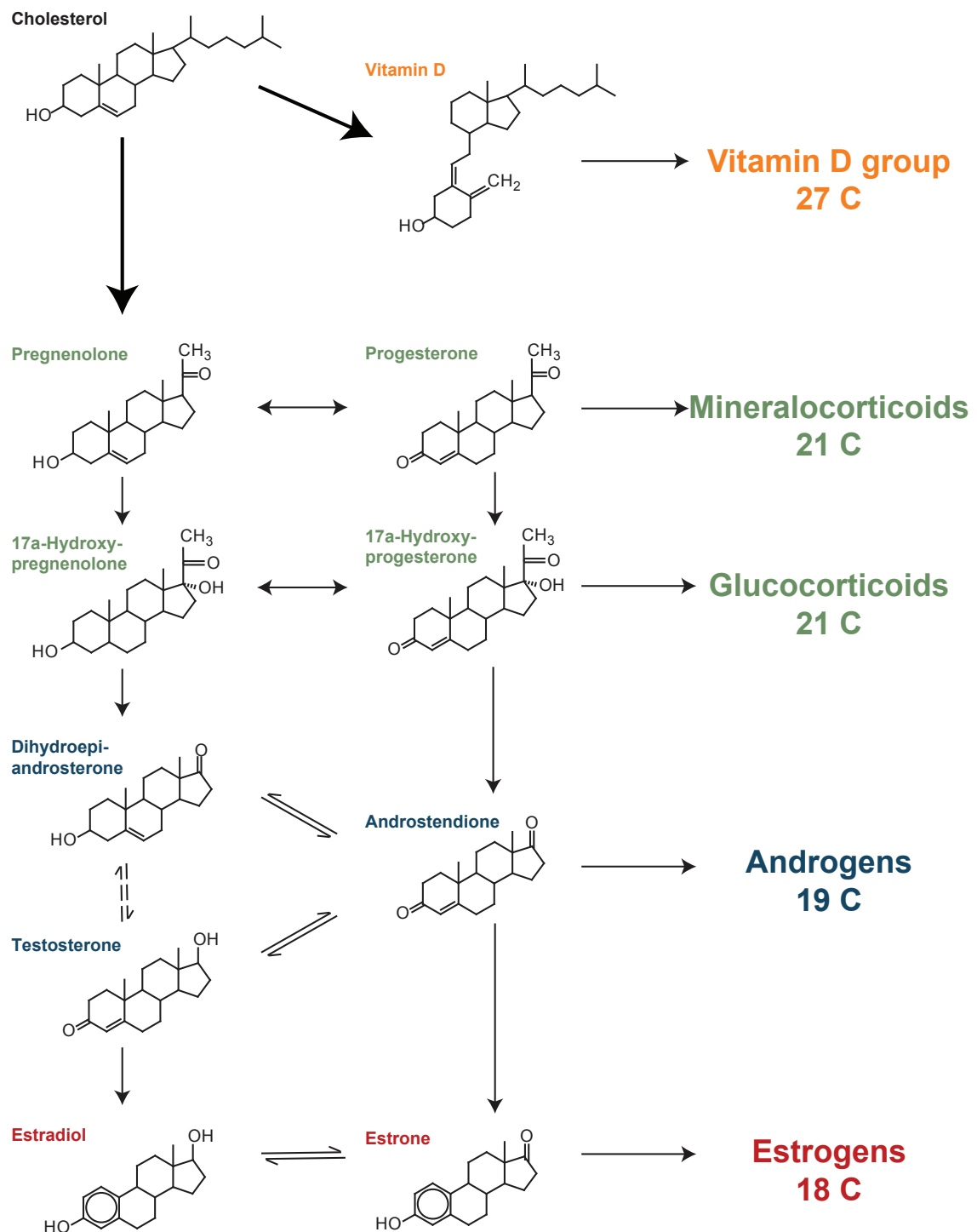


Figure 1.7: Steroid hormone biosynthesis. Cholesterol is the common precursor of all steroid hormones.

1.3. Steroid metabolizing enzymes: Biosynthesis and pre-receptor control of steroid action

Hydroxysteroid dehydrogenases (HSDs) can act on several positions of the steroid backbone, namely 3 (α and β), 11 β , 17 β , and 20 α . Accordingly, they are called 3 α -, 3 β -, 11 β -, 17 β -, and 20 α -HSDs. 3 α - and 20 α -HSDs, as well as type 5 17 β -HSD are mainly not SDR but aldo-keto-reductase (AKR)-type enzymes though also SDRs have been shown capable of these reactions. These enzymes are important switches of pre-receptor control by activating and inactivating the respective hormones according to the need of the organism. Most HSDs have been shown to be multifunctional enzymes acting on several substrates [78].

1.3.1. 20 α -Hydroxysteroid dehydrogenases

The AKR family members with 20 α -HSD activity (AKR1C1, AKR1C3) are responsible for the interconversion of progesterone and its biologically weaker counterpart, 20 α -progesterone [126]. 20 α -HSD may furthermore have a protective role against high levels of this steroid [127]. 17 β -HSDs type 1 and 2, two SDR-type enzymes, have been described to have 20 α -HSD activity. Type 2 17 β -HSD catalyzes the activation of 20 α -progesterone.

1.3.2. 3 α -Hydroxysteroid dehydrogenases

Several 3 α -HSDs seem to regulate the access of androgens to the androgen receptor (AR) [10]. While 3 α -HSD types 2 and 3 (AKR1C3, AKR1C2) catalyze the inactivation of 5 α -dihydrotestosterone to 3 α -androstaneadiol, the latter is also able to perform the reverse reaction [91]. SDRs with 3 α -HSD activity are for instance 11-cis-retinol dehydrogenase and RoDH-like enzyme.

1.3.3. 3 β -Hydroxysteroid dehydrogenases/isomerases

3 β -HSDs/isomerases are a group of membrane-bound, microsomal or mitochondrial SDRs [87, 108]. They are bifunctional enzymes with hydroxysteroid dehydrogenase and isomerase function. The interconversions that have been described for human type 1 3 β -HSD/isomerase are: pregnenolone to progesterone (via pregn-5-ene-3,20-dione) and dehydroepiandrosterone to androstenedione (via 5-androstene-3,17-dione) [114]. The enzymes perform a two-step reaction. First, the 3 β -hydroxyl group is dehydrogenated, yielding a Δ^5 -3-keto-intermediate and NADH. The latter then activates isomerization resulting in a Δ^4 -3-keto-intermediate. In total, 2 human and 6 murine isoforms have been described with tissue-specific expression patterns matching the needs in steroid biosynthesis. In the rat, 4 types of 3 β -HSD/isomerase are found.

1. Introduction

1.3.4. 11β -Hydroxysteroid dehydrogenases 1 and 2

11β -HSDs catalyze the final steps in the biogenesis of glucocorticoids. Both characterized 11β -HSDs are SDR-type enzymes regulating the activity of glucocorticoids by interconversion of hormonally active cortisol and inactive cortisone [26]. In rodents, corticosterone and dehydrocorticosterone are interconverted. Type 1 11β -HSD is a bidirectional enzyme but *in vivo* mainly acts as reductase supplying cortisol to the glucocorticoid receptor (GR). Type 2 11β -HSD on the other hand shows only dehydrogenase activity. Similar to 20α -HSD, 11β -HSD type 2 displays protective function towards the occupation of the MR by cortisol.

1.3.5. 17β -Hydroxysteroid dehydrogenases

Table 1.3: Known 17β -HSDs, substrates and enzymatic direction.

17β -HSD	mainly active on	other activities known	in vivo enzymatic direction
1	E1	20α -HSD	Red
2	DHEA, E2, T	20α -HSD, 3β -HSD	DH
3	A		Red
4	E2	β -oxidation	DH
5	DHEA, A	3α -HSD	Red
6	DHT, E2	3α -HSD	DH
7	E1, zymosterone	3β -HSD, 3α -HSD	Red
8	E2		DH
9	A-diol	3α -HSD, RDH	DH
10	DHT	3α -HSD, β -oxidation	DH
11	A-diol		DH
12	E1, A	(V)LCFA-synthesis	Red

Type 5 17β -HSD does not belong to SDR but to AKR family. Type 6 and type 9 17β -HSD exert this function only in rodents. A - androstenedione, A-diol - $3\alpha,17\beta$ -androstadienol, DH - dehydrogenase, DHEA - dehydroepiandrosterone, DHT - dihydrotestosterone, E1 - estrone, E2 - 17β -estradiol, RDH - retinol dehydrogenase, Red - reductase, T - testosterone, (V)LCFA - (very) long chain fatty acid. See [77] for references. For type 12 17β HSD, cf. to [68].

17β -HSDs conduct oxidation and reduction reactions at position 17 of the steroid backbone by interconversion of keto- and hydroxy groups. A standardized reaction is shown in fig. 1.1 (p. 7). These reactions are of utter importance for the activation and inactivation of androgens and estrogens as they regulate the biological potency of the

respective hormones. Like 11β -HSDs catalyzing the final steps in glucocorticoid formation, 17β -HSDs catalyze the final steps in the biogenesis of sex steroid hormones.

Until 2004, it was thought that under physiological conditions, 17β -HSDs exert either the oxidative (dehydrogenase) or the reductase function [5]. More recent findings show however that some enzymes act bidirectionally also under physiological conditions [52]. As outlined in table 1.3, 12 enzymes of this group have been described up to now. Type 13 17β -HSD seems to be on the way of characterization - the name has already been reserved. Human type 6 and 9 17β -HSDs are not active in steroid but in retinol metabolism; murine enzymes conduct the reaction described in this table. Like for other steroid metabolizing enzymes, 17β -HSDs vary with regard to tissue- and substrate specificity, to enzyme kinetics as well as to the reaction direction.

1.4. The aim of the study

Steroid hormone metabolizing enzymes are members of three protein families: the cytochrome P450s, aldo-keto-reductases, and short-chain dehydrogenases/reductases (SDRs). Many SDRs have been identified over the last years. Nevertheless, their respective functions in metabolic context are still unknown. The aim of this thesis therefore was the identification and characterization of new steroid hormone-metabolizing SDRs using a functional genomics approach towards this protein family.

The identification should be conducted as a genome-wide process, leading to a large number of putative characterization targets. Due to the low conservation within SDR family, their identification is technologically challenging as is the selection of putatively steroid-metabolizing candidates. Their characterization should be done at a medium-throughput-scale. Therefore, several aspects were anticipated: (1) the expression pattern, (2) the substrate specificity towards steroid hormones, and (3) the localization of these enzymes in the cell. These three aspects were thought to reveal insights to the metabolic role of the selected enzymes.

Bioinformatic methods become increasingly important and allow processing of many ‘samples’ at the same time. The analysis of tissue specificity and subcellular localization should thus be conducted both by *in silico* and wet lab experiments. For expression analysis *in silico*, there was no fast and reliable tool to screen the EST data available. Therefore, (4) an adequate tool had to be developed.

For the analysis of substrate specificity, an applicable assay for measurement had to be established. In order to better address physiologically relevant conversions, (5) an assay in living cells should be set up. (6) The determination of subcellular localization required the set-up of reasonable assay design as well.

1. Introduction

2. Results

2.1. Introducing remarks

The challenge of this thesis was a functional genomics approach towards SDR family members, focussing on so-far uncharacterized proteins with putative steroid-metabolizing properties. Characterization of selected enzymes was done at a medium-throughput scale. Functional genomics imply that all genes under investigation are - as far as possible - analyzed under the same aspects. Minor deviations from this way will be outlined. To facilitate comprehension of this approach the results will be shown sorted methodologically. Therefore, identification, bioinformatic analyses, expression analyses, substrate conversion assays and studies on subcellular localization of the respective enzymes will not be sorted by candidate genes but by analytical approach. To facilitate the overview, results will additionally be summarized in tables at the end of each section.

2.2. Identification of SDR candidate enzymes and classification as SDRs

2.2.1. Identification of putative SDRs using SDR Finder

Short-Chain Dehydrogenases/Reductases (SDRs) are a large family of enzymes sharing common structural features highlighted in conserved amino acid motifs. SDRs share rather low overall sequence identity of as little as 15-20%. Therefore, the identification of not yet annotated SDRs becomes a tedious task as conserved patterns within these motifs are too short to be subjected to blastp or other similarity search algorithms. In this work, the program SDR Finder was used for the identification of protein sequences belonging to SDR family. This program is a proprietary software owned by BioNetWorks GmbH but was available for this work within a cooperation. SDR Finder is an implementation of the BioNetWorks patent filing for an algorithm to find SDR proteins among sets of proteins of known sequence but unknown or incompletely assigned function.

Algorithm properties of SDR Finder. The SDR Finder algorithm is based on the five known SDR characterizing amino acid motifs TG***G*G (MT1), NNAG (MT2), N (MT3), S and Y*ASK (MT4) and PG(MT5) which have to appear in this order within a defined

2. Results

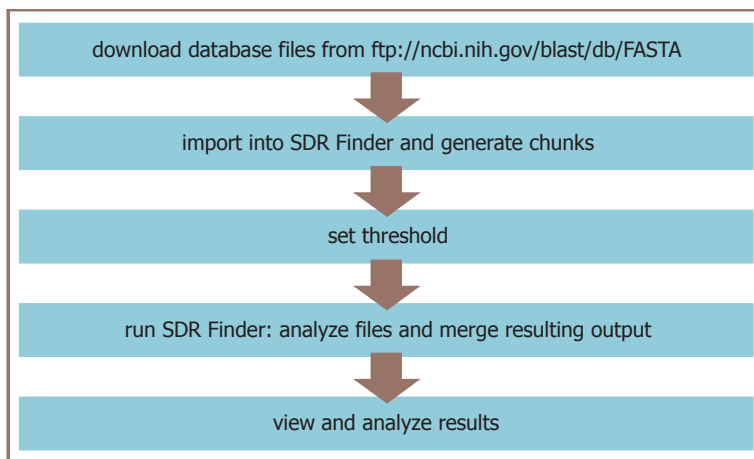


Figure 2.1: Workflow for using the SDR Finder. Search criteria are refineable at several stages of analysis, e.g. by increasing the threshold when analyzing the data or by including other database files.

amino acid window sizes (refer to table 2.1). MT1 comprises the cofactor binding region, MT4 the active center of SDR type enzymes. The other motifs have catalysis and structure supporting function.

Table 2.1: Amino acid motifs of SDRs as used by SDR Finder.

	amino acids
MT1	TG***G*G
MT2	NNAG
MT3	N
MT4	S ... Y*ASK
MT5	PG

Protein sequences are scored on the number of exact matches in the five motifs, resulting in the highest score of 16 (1 per exact match) [51]. Though SDR motif definition has meanwhile expanded [86] the definition given here will be used in description of the SDR Finder if not stated otherwise. The asterisks within the motifs are given following the description of the SDR Finder.

Identification of putative SDRs - database analysis and SDR Finder usage.

An outline of this procedure is given in fig. 2.1. As indicated in the legend, changes to the initial set-up can be applied at several stages. To begin,

protein database files in FASTA format were downloaded from the NCBI ftp-Server. I was reaching for a nearly complete search and thus downloaded not only the Monthly Updates of several months (january 2003 - march 2003) but the complete non redundant (NR) protein database from NCBI as well. The respective files were then loaded into SDR Finder for conversion to the proper file type (.sfd). Though database files can be kept *in toto* and converted to '.sfd' files, search for SDRs is facilitated by splitting the output file into smaller data-sets, 'chunks'. These files contain a previously defined number of sequences. Due to computer performance 10000 sequences per chunk were chosen.

2.2. Identification of SDR candidate enzymes and classification as SDRs

For running SDR Finder after the generation of the input files, a minimum number of conserved amino acids within the motifs MT1-MT5 is set as threshold. Though some SDRs have been reported with only 9 amino acids conserved out of the total of 16 (personal communication Dr. Ariane Volkmann, BioNetWorks GmbH) I chose 11 as a threshold to reduce the number of false positives. After running the program through all chunks, results were merged into one SDR Finder Output file (.sfo) and viewed as a results table. A slightly adapted example is given in table 2.2 - the original table contains, in addition, the GenBank ID and species information. Both were excluded here: GenBank ID is in most cases depicted as unspecified. Species information was expelled because only proteins from rat are shown. The example patterns are included only after export to excel format.

Table 2.2: Example for a results table.

Alt. Id	Score	TYR?	Example pattern
NP_037308.1	11	false	[*G*****G][NNA*][N][S][**AS*][PG]
NP_077334.1	11	false	[TG***G**][*N*G][N][S][***SK][PG]
A55148	11	false	[T****G**][**AG][N][S][**ASK][PG]
NP_112308.1	11	false	[TG*****G][NNA*][N][S][**A**][PG]
AAF14190.1	11	false	[*G***G*G][*N*G][N][S][**AS*][PG]
NP_077056.1	11	false	[*****G*G][**AG][N][S][**ASK][PG]
NP_114452.1	11	false	[T****G*G][N**G][N][S][**AS*][PG]
NP_446339.1	11	false	[*G***G*G][**AG][N][S][**ASK][P*]
AAF87312.1	11	true	[TG***G**][**AG][N][S][Y*A*K][P*]
AL RTP	11	true	[*****G*G][N*AG][N][S][Y***K][PG]
NP_059028.1	11	true	[TG***G*G][N*A*][N][S][Y****][PG]
NP_113870.1	13	true	[TG***G*G][N*AG][N][Y*ASK][P*]
NP_599214.1	12	true	[TG***G*G][NNA*][N][S][Y***K][P*]
NP_058931.1	11	true	[TG***G*G][*NAG][N][Y**SK]
AAF21040.1	11	true	[TG***G**][**AG][N][S][Y*A*K][P*]
S11021	12	true	[TG***G*G][NNA*][N][S][Y****][PG]
NP_620253.1	11	true	[TG***G*G][*NA*][N][S][Y**S*][P*]
NP_446459.1	14	true	[TG***G*G][NN*G][N][S][Y*ASK][P*]
AAD25486.1	11	true	[TG***G**][*NA*][N][S][Y***K][PG]
NP_058877.1	11	true	[*G***G**][**A*][N][S][Y*ASK][PG]

Depicted are the rat proteins found by SDR Finder with a threshold of 11 from NCBI NR database.

(Alt. - Alternate)

From the results table, several informations can be gained. The first column gives the accession of the sequence in the originating database (Alt. ID - contrasting the GenBank

2. Results

ID). Second, ‘score’ depicts the number of conserved amino acids within the five motifs MT1 - MT5. The next column, ‘TYR?’ indicates whether motif MT4 contains the tyrosine (tyr in three letter code; depicted by ‘false’ or ‘true’). In the ‘example pattern’, every searched motif is included in square brackets. Conserved amino acids are depicted by their abbreviation in one-letter code, not-conserved ones by an asterisk. Also amino acids within motifs but usually not conserved (as the *** in the first motif) are depicted by asterisk. These, however do not lead to a decrease of the score.

From this result table, a first overview of the results can be gained. It is possible to sort the sequences according to ‘score’, ‘species’, or ‘TYR?’. Additionally, parts of the results (for example, bacterial sequences or sequences with or without the described tyrosine) were either discarded or regained.

Table 2.3: Numbers of human, murine and rat proteins found in NR database by SDR Finder.

	true	false	Σ
Mouse	35	30	65
Rat	12	8	20
Human	33	17	50

For verification, the results retained from the SDR Finder output were first sorted according to the originating species. Parts of the result table entries contained no species information. These were looked up in the database but turned out to be of prokaryotic origin altogether. Table 2.3 shows the number of database entries for human, mouse and rat proteins. All other species were not considered for further analyses. Reason for the restriction to these three species is the fact, that the characterization of steroid metabolizing enzymes from SDR family should also lead to the identification of putative new drug targets for human steroid caused diseases. Many metabolic conditions are studied in mouse models as these models mimic the human disease. On the other hand, from a steroid researcher’s point of view, the rat is closer to humans in way of this metabolic pathway [97] [12]. Furthermore, many rat proteins are only annotated to the genome but not characterized and therefore urged to gain new insights.

The rest of the sequences was then sorted by the tyrosine content of motif MT4. This information is very useful in the analysis of the results as the tyrosine of MT4 is an essential amino acid in the active center and conserved in all SDRs described so far. In order to secure the right recognition of the active center, ‘false’ were overviewed and discarded if MT4 was really not conserved. Based on this overview over motif conservation, the next steps of verification could be performed.

2.2. Identification of SDR candidate enzymes and classification as SDRs

2.2.2. Verification of the SDR Finder identified enzymes and classification as SDR enzymes

In order to control the performance of SDR Finder and in order to get an overview over the found proteins, all genes were subjected to manual supervision. First, the sequences of all identified proteins were downloaded from NCBI protein database. As no SDRs have been described with more than 450 amino acids [86], all enzymes with more than 500 amino acids were excluded from further analysis. Within the remaining sequences, the typical SDR motifs [86] were searched manually and the conservation monitored. Additionally, the sequences were aligned with previously described and characterized SDRs in multiple alignments using clustalW. Multiple alignments were not only helpful for the identification of the conserved motifs but also helpful for excluding double hits. Fig. 2.2 exemplarily shows one alignment of some of the proteins chosen later on for more in-depth characterization.

Rdh12_mm	-----MLFILVLLTSFLSILYL TAPSIRKFFAGGVCTTNVQIPGKVVVI	TGANTGI GKETAR	57
DHRSX_hs	-----MSPLSAARAALRVYAVGA A VILAQLLRRCRGGFLEPVFP P RDRVAIV	TGGTDGI GYSTAK	61
retSDR3_hs	-----	MATGTRYAGKV VVVT GGGRGI GAGIVR	27
Dhrs4_mm	-----MQKAGRLLGGWTQAWMSVRMASSG--I	LTRRNPLSNKVALV TASTDGI FAIAR	51
LOC287380_rn	MISPSSRKGM LKERAMDLVTQTTIPLLFGCLGIFSLFRLLQRTRSKAYLRNAV VV TGATSGL GKECAR	70	
dhrs8_rn	-----MKYLLD LLLLPLLIVFCIESFIKRLIPKKKSVAGEIVLIT TGAGHGI GRLTAY	54	
Rdh12_mm	ELARRGARV YIACRDVLKGEASA EIRADTKNS---QVLVRKLDLS DTKSIRAF AERFLAEKKLHILI		123
DHRSX_hs	HLARLGMHVIIAGNNDSKAKQVVS KIKEETLND---KVEFLYCDLASMTSIRQFVQKF MKKIP LHVL		127
retSDR3_hs	AFVNNSGARVVICDKDESGGRALEQELPG-----AVFILCDVTQEDDV KTLVSETI RRFGRLDCVV		107
Dhrs4_mm	R LAEDGAHVVVSSRKQQNVDRAVATLQGEGLS-----VTGIVCHVGKAEDREKLT TALKRHRGIDILV		115
LOC287380_rn	V F H AAGAKV VLGRNVKA LEFTRELADSSSQG QTHQPCVVTFDLADPGAIAPAAE I LQCFGYV DILI		140
dhrs8_rn	EFAKLNTKLV LWDINKNGIEETA AKCRKLGAQ-----VHFVVD C SQREIY SAVRKVKEEVGDV S ILV		118
Rdh12_mm	NNAG VMCPYS---KTDGFETHFGV N H LGHFL LTYLLLERLKESAP---ARVVNLSSIAH LIGKIRFH		190
DHRSX_hs	NNAG VMMPQR---KTRDGFEHFGL NY LGHFL LTN LLLDTL KESGSPGH SARV VTSSA THYVAELNMD		194
retSDR3_hs	NNAG HHP PPPRPEETSQ GFRQ LLEENL LGT YLT KLA LPY LRKS QG----N VNISS S LVGAIGQA---		157
Dhrs4_mm	S NAVNPF PGNIMD VTEEVWDKVL S IN V TATA MMKAVVPEM KRGG---GSV VIVG SVAG FTRFP--		185
LOC287380_rn	NNAG IS-YRGAISDTIVD VRKMEIN YFGPVALT KALLPSMVERKR---GHIVAISS I QGKISIP--		209
dhrs8_rn	NNAG VVY TADLFATQDPQ-I EKT FEV N VLAHF WTTKAFLPAMMKNH---GHVVTVAS A AGHTVV P---		187
Rdh12_mm	DLQGQKRYCSAFA Y GHHS K LAN LLFT RELAKR LQGTG---V TAYA VH P GV VLSI E TRNSY LLCLLWR-LFS		256
DHRSX_hs	D LQSSAC YSPHA Y AQS K L ALV LFTY H LQRLAEGSH-VTA N VVD P GV VN T DLYKHVFWATR LAK-KLL		264
retSDR3_hs	-----QAVPYVATK GAVT AMT KAL DES PYG---V RVNC IS P GNI WT PLWEELA ALMPDPR-ATI		210
Dhrs4_mm	-----SLGP YNVS K T ALL GLTKN FAELA PKN---IRV N CLAP G L IKT R FSSV L-WEEKARE-DFI		239
LOC287380_rn	-----FRSA Y AASK HAT QAFF D C LRA EMKD SD---IE TV V IS P GYIH T NLS VNA V TAD GS RY GALD		263
dhrs8_rn	-----FLLAYC SSSKFA AVFG H RALT D E A LGCT G VR ST CLCPNF INTG FIKNP ST NLGPT LEE PEE		241
Rdh12_mm	--PFFKSTS QGA QTSLHC ALA EDLEPLSGKYFSDCKRMW VSS RARNK KTAERLWNVSC ELLGI QWE--		316
DHRSX_hs	GWLLFKTPD EGA WT SI A V TPELEG V GGR YLYNE KETKS LHV TYNQKLQ QOLW SKS CEMT G VLD VT		330
retSDR3_hs	REGMLAQPLGR MGQ PAEV GAA VFLASEAN FCTG-IE LLV TGG AEL GY GCK ASR ST PVD AP DIPS--		270
Dhrs4_mm	KEAM QIR---RLG K PEDC AGI VS FLC SED ASY INGET VV VGGG TPS RL-----		279
LOC287380_rn	KNTA QGR S AVE V A QD IF D A V G K K K D V L L TDF LPT M A V I R T L A P R L F F R I M A S R K E R K S K NS--		325
dhrs8_rn	V VE HLMHG I L TNQKM IF V PGS I ALL T V LER V P FER FL DV L K R R IN V K F D A V V G Y K D K-----		298

Figure 2.2: Alignment of several SDRs identified by SDR Finder. Marked in red are the conserved motifs as described in table 1.1 (see p. 6). It is interesting to note the high level of conservation within those regions in comparison to the extremely low degree of conserved amino acids in other regions of the proteins. Rat dhrs7b is depicted under the name LOC287380.

2. Results

Taking a closer look on the alignment, some issues are notably interesting:

- Especially in the middle part, murine Rdh12 (first line) and human DHRSX (second line) share considerable similarity.
- Typical motifs of murine Dhrs4 show a lower degree of conservation in comparison with the other proteins aligned.
- The PG...T motif in rat dhrs8 protein can not be undoubtedly allocated. While at the relative position of the same motif in the other proteins only P and T are conserved, there is one PG...T motif closer to the C-terminus of the protein though separated by five instead of three amino acids. To address the localization of this motif, deletion mutants could be considered but were not in the scope of experiments at this stage of the thesis.

Similar observations could be made also from other alignments. To complete the exclusion of redundant hits, all sequences were annotated to their positions in the respective genomes.

2.2.3. Identification and verification of MGC4172 and MGC18716

From Dr. Udo Oppermann (SGC, University Oxford, UK) I learned about another new human SDR-type enzyme, MGC4172. Using blastp, I could also identify the murine homologue, MGC18716. Both enzymes were not correctly annotated in the NCBI database lacking the cofactor binding region in the deduced amino acid sequence. This also accounts for the fact that SDR Finder did not identify the enzymes as SDRs. By analysis of both the human and the murine mRNA sequences from the NCBI database, I was able to identify the full-length coding sequences. Both have a total length of 780 nucleotides, resulting in proteins of 260 amino acids. On nucleotide level, CDS are 89% identical, protein comparison reveals 92% identity as shown in fig. 2.3.

As both proteins were not correctly annotated to their coding sequences, I had a closer look on the genomic organization of MGC4172 and MGC18716. Both genes are coded on the minus strand at the respective gene loci. The human MGC4172 gene is located on chromosome 17q12 (genomic sequence: NT_086873), murine MGC18716 is located on chromosome 11C (NT_096135). Both genes consist of seven exons. From the annotation results I could deduce that the exons and introns had correctly been annotated before but the protein sequence had not been correctly deduced from the resulting mRNA sequence.

2.2.4. Annotation of the identified SDR type enzymes to the genome

While verifying and evaluating the output of SDR Finder, I checked the chromosomal localization of the identified proteins. This procedure was also helpful in identifying further

2.2. Identification of SDR candidate enzymes and classification as SDRs

```

mouse: 1 MTRAGMERWRDRLALVTGASGCCAAVARALVQQGLKVVGCARTVGNIEELAAECKSAGY 60
       M R GMERWRDRLALVTGASGGCAAVARALVQQGLKVVGCARTVGNIEELAAECKSAGY
human: 1 MARPGMERWRDRLALVTGASGCCAAVARALVQQGLKVVGCARTVGNIEELAAECKSAGY 60

mouse: 61 PGTLIPYRCDSLNEEDILSMFSAVRSQHSGVDICINNAGMARPDTLLSGSTSGWKDMFNV 120
       PGTLIPYRCDSLNEEDILSMFSA+RSQHSGVDICIINNAG+ARPDTLLSGSTSGWKDMFNV
human: 61 PGTLIPYRCDSLNEEDILSMFSAIRSQHSGVDICINNAGLARPDTLLSGSTSGWKDMFNV 120

mouse: 121 NVLAISICTREAYQSMKERNIDDGHIIININSMCGRVPPQSIVHFYSATKYAVTALTEGL 180
       NVLALSICTRAYQSMKERN+DDGHIIININSM GHRV P SV HFYSATKYAVTALTEGL
human: 121 NVLAISICTREAYQSMKERNVDDGHIIININSMSGHRLVPLSVTHFYSATKYAVTALTEGL 180

mouse: 181 RQELLEAQTHIRATCISPGLVETQFAFKLHDKDPEAAATYEHIKCLRPEDVAEAVIYVL 240
       RQEL EAQTHIRATCISPG+VETQFAFKLHDKDPEAAATYEHIKCLRPEDVAEAVIYVL
human: 181 RQELREAQTHIRATCISPGVVETQFAFKLHDKDPEKAAATYEQMKCLKPEDVAEAVIYVL 240

mouse: 241 STPPHVQVQVDIQMRPTEQVT 260
       STP H+Q+GDIQMRPTEQVT
human: 241 STPAHIQIGDIQMRPTEQVT 260

```

Figure 2.3: Alignment of MGC18716 (mouse) and MGC4172 (human). SDR motifs detected by the SDR Finder are shaded in gray, SDR motifs described in [86] are depicted in red.

redundant hits. All identified proteins remaining from earlier verification steps and results from the annotation process are depicted in table 2.4. From this table, further conclusions could be drawn: immediately, it became apparent, that candidate SDRs number 1 to 3, and 5 to 7 were all clustered on rat chromosome 6q33. A similar pattern of SDRs was detected on murine chromosome 10D3, namely candidates 4, 8, 9, 10, 11, 13 and 14.

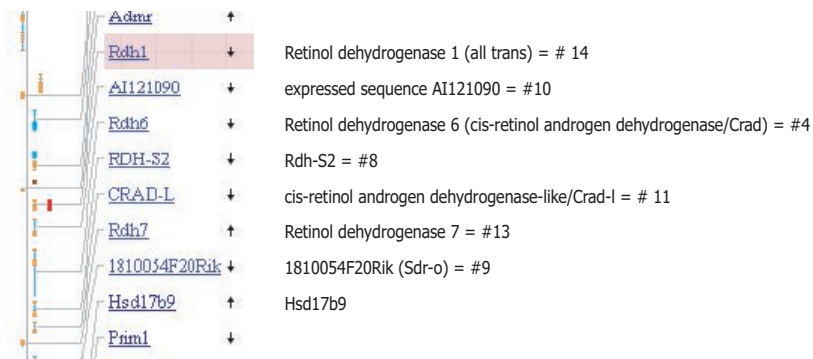


Figure 2.4: Commented detail of MapViewer (NCBI) image of murine chromosome 10D3 revealing a cluster of 8 SDRs, seven of which are included into table 2.4. The numbers next to the gene names give the candidate numbers from SDR Finder screen.

Therefore, they revealed not to be redundant hits. Instead, these SDRs are clustered at the respective genomic positions (for mouse SDRs, see fig. 2.4). The same holds true for some of the rat proteins but is not depicted. Further verification was done to exclude

2. Results

redundancy: In multiple alignments, the sequences appeared to be identical to a high percentage. *In silico* analysis revealed a similar pattern of expression (for *in silico* expression analysis, see 2.4.1), making redundant identification improbable.

To achieve easy overview of the SDR enzymes identified and encouraged by the finding of clustered SDRs, I tried a graphical annotation of the identified proteins. I took karyograms from human, mouse and rat and marked the chromosomal locations of the identified enzymes. In case of the murine genome, the denotation of the chromosomal segments as capital letters and numerals greatly facilitated this task and enabled more accurate subordination. The result for the murine genes is shown in fig. 2.5.

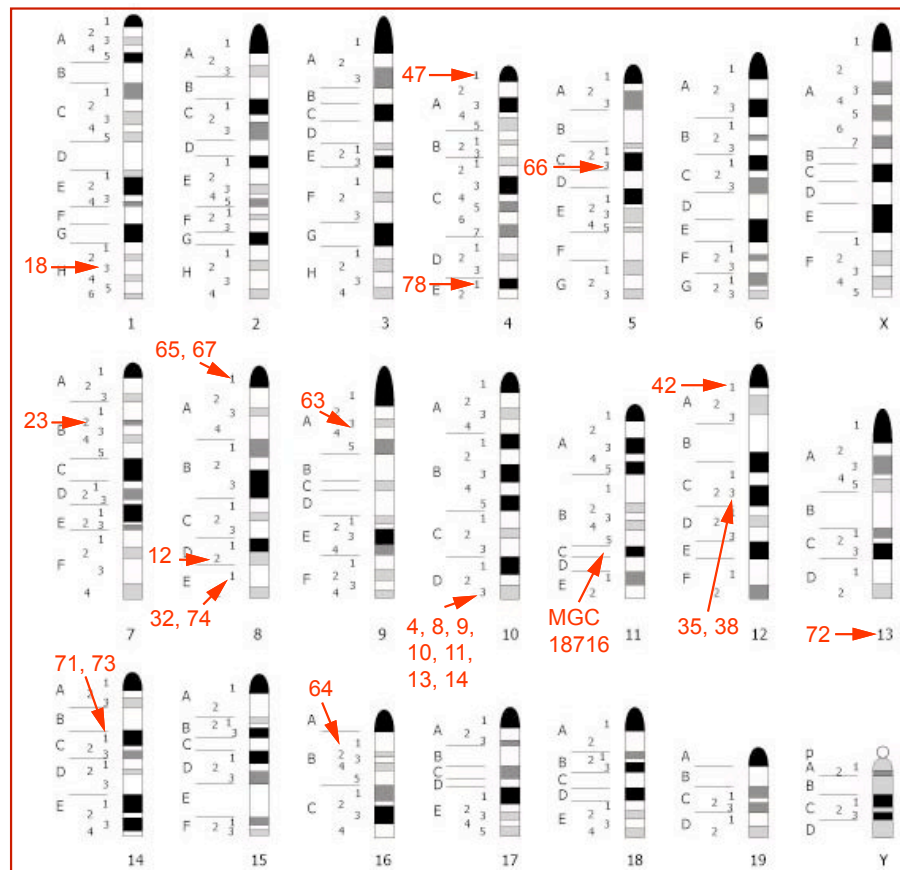


Figure 2.5: Graphical annotation of the loci coding for the identified mouse SDRs. Where arrows point to number of chromosome, no exact position was available. Numbers refer to numbering in table 2.4.

In contrast, in the rat and the human genome (see fig. 2.6), chromosomal regions are called p (for the short arm) and q (for the long arm) plus numbering. Due to the resolution of the available pictures, annotation of the respective loci was restricted to the chromosomal arms.

2.2. Identification of SDR candidate enzymes and classification as SDRs

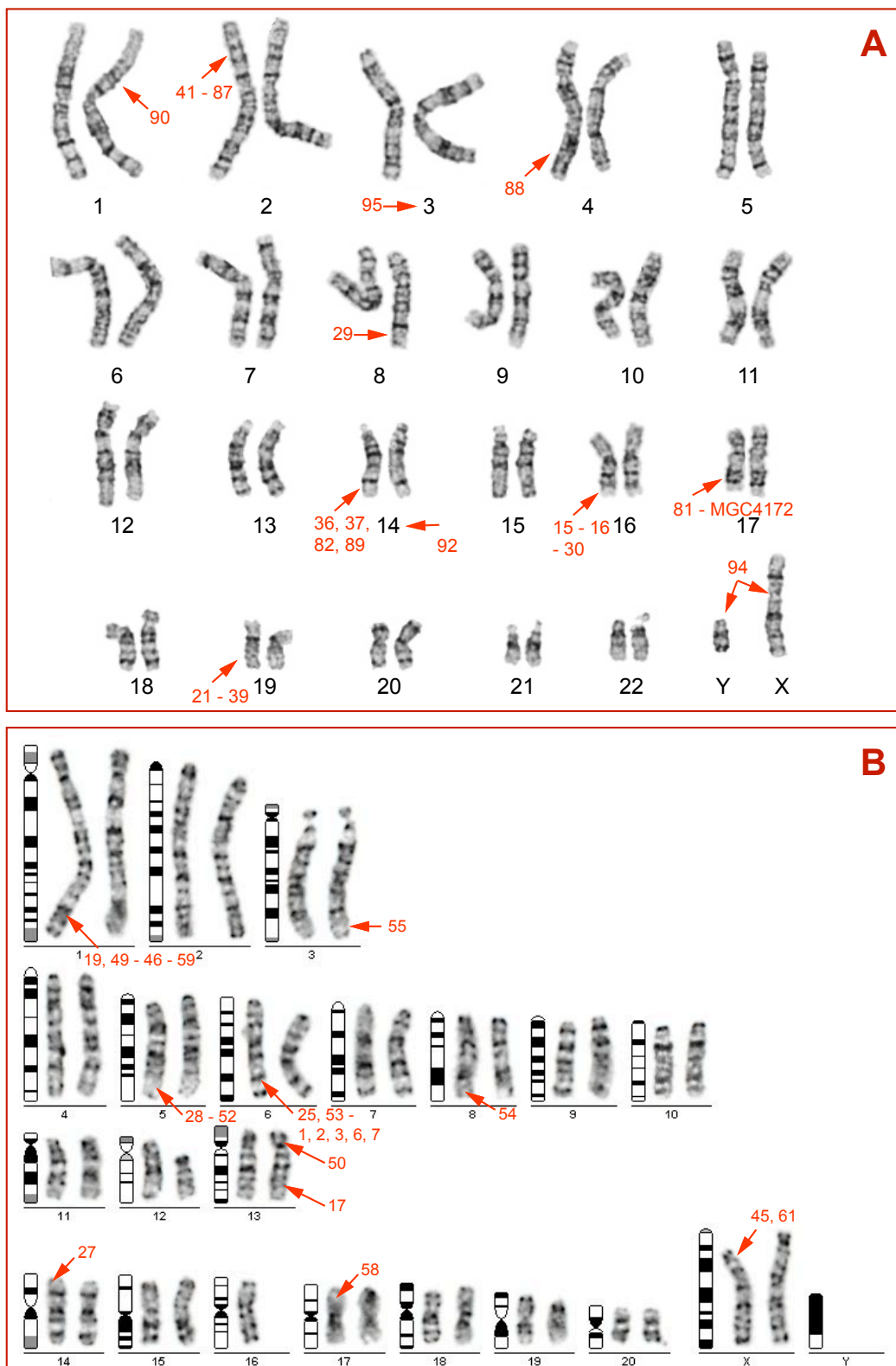


Figure 2.6: Graphical annotation of the loci coding for the identified human (A) and rat (B) SDRs. Numbers refer to numbering in table 2.4. Numerals separated by commas indicate the same loci. Genes on the same chromosomal arm but at different loci are separated by dashes. Where arrows point to number of chromosome, no exact position was available.

2. Results

2.3. Selection of identified SDRs for in-depth characterization

The results of the verification and annotation processes of the SDR Finder-identified proteins are depicted in table 2.4. The last column is used to group the candidates according to the following criteria:

The database search revealed which proteins were already characterized (indicated by 1 in the last column of table 2.4). This issue is logically not addressed by SDR Finder. Therefore, it had to be manually evaluated. At this step, proteins were seen as characterized, if after blasting the protein sequence PubMed quotations and precise description of its metabolic involvement were found or if a PubMed search with the protein's name or accession number revealed publications addressing the question of its substrate specificity.

In addition, further proteins were found to be false-positive hits (indicated by 2 in the last column of table 2.4). Obviously, very similar amino acid motifs are found not only in SDRs but also in other protein families.

During this step, several more sequences were found to be redundant. One example herefore are candidates number 26 and 27 which while annotated twice under slightly different names, turned out to be identical and homologous to human DHRS8, also referred to as 17 β -hydroxysteroid dehydrogenase type 11. Redundant proteins are indicated by 3 plus small letters in the last column of the following table. Letters identify the same enzymes.

The remaining SDRs (indicated by 4 in the last column of table 2.4) were putative targets for this thesis. Most of them were already annotated as SDRs but not further characterized.

Table 2.4: Putative SDRs identified with the SDR Finder after the first verification round.

	Name	Acc.	Organism	Gen.	Pos.	Comment
1	LOC314551	XP_234783	rat	6q33		4
2	retDH2	AAC52316	rat	6q33		1
3	retDH EC1.1.1.105	A55884	rat	6q33		3a, 4
4	Rdh6, Crad	AAB97166	mouse	10D3		2
5	retdh3	AAB07995	rat	6q33		3a
6	rdhs	XP_234786	rat	6q33		4*
7	LOC314550	XP_234782	rat	6q33		4
8	Rdh-s2	NP_671755	mouse	10D3		4
9	Sdro	XP_125913	mouse	10D3		4 [‡]
10	Rdh9, Crad-3	NP_694773	mouse	10D3		1
11	Cradl	NP_663399	mouse	10D3		4

2.3. Selection of identified SDRs for in-depth characterization

Table 2.4: (continued)

	Name	Acc.	Organism	Gen.	Pos.	Comment
12	Hsd11b2	CAA62219	mouse	8D3		1
13	Rdh7	NP_ 059501	mouse	10D3		1
14	Rdh1	AAL67915	mouse	10D3		1
15	HSD17B2	NP_ 002144	human	16q23		1
16	HSD11B2	AAH36780	human	16q22		1
17	hsd17b7	NP_ 058931	rat	13q22-23		1
18	Hsd17b7	NP_ 034606	mouse	1H3		1
19	sim. retSDR3 [bt]	XP_ 218651	rat	1q21		4*
20	retSDR3	AAF44666	human	19q13.33		3b, 4‡
21	DHRS10	AAH06283	human	19q13.33		3b
22	retSDR3	AAF06940	human	19q13.33		3b
23	Dhrs10	BAB27025	mouse	7B2		4
24	dhrs7b	XP_ 213317	rat	10q22		4‡
25	sim. CGI-86 prot. [hs]	XP_ 234304	rat	6q24		4*
26	sim. Pan1b-like [mm]	XP_ 223159	rat	14p22		3c, 4‡
27	Dhrs8	XP_ 213994	rat	14p22		3c
28	rdh10	AAO31688	rat	5q11		1
29	RDH10	NP_ 742034	human	8q21.11		1
30	WWOX	NP_ 057457	human	16q23.2		3d, 4‡
31	FORII	AAF82054	human	16q23.2		3d
32	Wwox	AAH14716	mouse	8D3-E1		3e, 4‡
33	unnamed prot.	BAB31911	mouse	8D3-E1		3e
34	Rdh12	XP_ 126957	mouse	12C3		4‡
35	RDH12	NP_ 689656	human	14q23.3		4‡
36	androgen-reg. SDR1	AAL26274	human	14q23.3		1, 3f
37	Sdr1	NP_ 067532	mouse	12C3		4*
38	unnamed prot., RDH13	BAC11591	human	19q13.4		4‡
39	Riken cDNA 8430425D21	XP_ 284259	mouse	7A1		3g, 4
40	PAN2, RDH14	NP_ 065956	human	2p24.3		1
41	Pan2	NP_ 076186	mouse	12A1		1
42	RDH11	AAH51291	human	14q23.3		3f
43	gapdh sim.	XP_ 228478	rat	Xq13		4*
44	gapdh sim.	XP_ 218807	rat	1q22		4*
45	Sdr9	XP_ 143618.1mouse		4A1		3h, 4
46	Sdr9	XP_ 143618.2mouse		4A1		3h

2. Results

Table 2.4: (continued)

	Name	Acc.	Organism	Gen.	Pos.	Comment
47	sim. bovine retSDR3	XP_218651	rat	1q21		4*
48	sim. flvt 1 [hs]	XP_222501	rat	13p13		4*
49	sim. Y-box binding prot. 1	XP_226229	rat	19p13		2
50	sim. mRiken cDNA 2610207I16	XP_232942	rat	5q22		4*
51	rdh12	XP_234334	rat	6q24		4*
52	hyp. prot.	XP_243923	rat	8q31		4*
53	hyp. prot.	XP_242022	rat	3q21		4*
54	sim. human hyp. prot. FLJ21212	XP_232988	rat	5q24		2
55	fibroblast growth factor receptor 2	XP_215092	rat	1q34		2
56	hsd17b3	NP_446459	rat	17p14		1
57	tumor associated glycoprotein E4	AAD25486	rat	1q22		2
58	fumaryl acetoacetat hydrolase	NP_058877	rat	1q31		1
59	hsd17b10	NP_113870	rat	Xq31		1
60	diacetyl-L-xylulose reductase	NP_599214	rat	not available		1
61	sim. bovine rdh8	XP_134689	mouse	9A3		4*
62	3-hydroxybutyrat dehydrogenase	NP_780386	mouse	1B11		1
63	Rdh13	XP_284259	mouse	7A1		3g
64	sim. human MARK4	XP_144372	mouse	5C3		2
65	sim. rat gapdh	XP_145308	mouse	7A1		4*
66	solute carrier family 35, member A5	NP_083032	mouse	16B4		2
67	unnamed prot.	BAC34996	mouse	5B1		2
68	unnamed prot.	BAB22553	mouse	8E1		2
69	Dhrs4	AAH03483	mouse	14C1		4‡
70	Hsd17b3	NP_032317	mouse	13		1
71	hyp. prot.	AAH03930	mouse	14C1		4
72	unnamed prot.	BAB31244	mouse	8E1		3e
73	huntingtin-ass. prot. 1 isoform A	NP_034534	mouse	11D		2
74	unnamed prot.	BAB32147	mouse	15B1		2
75	unnamed prot.	BAC26095	mouse	18E1-2		2
76	Rsdr1	NP_035433	mouse	4E1		4
77	MGC36641	NP_659171	mouse	7A3		2
78	WD repeat domain 21 isoform 1	NP_056419	human	14q24.3		2
79	dicarbonyl L-xylulose reductase	NP_057370	human	17q25.3		1
80	SDR1	NP_612461	human	14q11.2		3i, 4
81	FLJ12586	AAH47501	human	19q13.43		2

2.3. Selection of identified SDRs for in-depth characterization

Table 2.4: (continued)

	Name	Acc.	Organism	Gen. Pos.	Comment
82	Trem-like transcript 2	AAO15022	human	16p21.1	2
83	sim. lipase	XP_058404	human	10q26.12	2
84	unnamed prot.	CAD62350	human	14q11.2	2
85	sepiapterin reductase	NP_003115	human	2p14-p12	1
86	FLJ14431	AAH21973	human	4q32.3	4
87	RDH11	NP_057110	human	14q23.3	1
88	UDP-galactose-4-epimerase	NP_000394	human	1p36-p35	2
89	unknown	AAH02730	human	1p36.1	3i
90	DHRS2 isoform 2	NP_005785	human	14	1
91	IgL light chain	BAC01843	human	18 or 22	2
92	DHRSX	NP_660160	human	Xp22.33, Yp	4 [‡]
93	3-hydroxybutyrat dehydrogenase	NP_004042	human	3	1
94	smooth-muscle specific HSD	NP_114455	rat	17p14	1

Numbers in the comment column depict the following: 1 = characterized SDR, 2 = false positive, no SDR, 3 = redundant hit (letter indicates pair or group), 4 = putative target to this thesis. 4*: no IMAGE clones available. 4[‡] = selected for characterization. Abbreviations used are: Acc = Protein Accession Number in NCBI database, ass. = associated, bt = bovine, flvt = follicular lymphoma variant translocation, Gen. Pos. = Genomic Position, hs = human, hyp. = hypothetical, mm = mouse, n.a. = not available, prot. = protein or protein product, sim. = similar.

As the remaining putative targets (depicted with 4 in table 2.4) appeared too numerous for in-depth analysis of enzymatic characterization, phylogenetic and *in silico* expression analyses were conducted to narrow down the selection. As uncharacterized proteins often are closest related to other uncharacterized proteins, phylogenetic analyses were found not to elucidate this matter (for description of phylogenetic analyses, see section 2.5).

Where available, IMAGE clones containing the coding sequences were thus ordered from RZPD (Resource Center/Primary Database, Berlin) for the remaining candidate proteins (label 4 in table 2.4, asterisk: no IMAGE clones available). Their identities were confirmed by PCR and sequencing for candidates 9, 21, 24, 27, 30, 32, 34, 35, 38, 69, and 92. Human MGC4172 and its murine homologue, MGC18716 were added to this list after identification. Table 2.5 summarizes the SDR proteins chosen for further analyses.

2. Results

Table 2.5: SDRs selected for in-depth analysis.

Name annotated	Organism	Candidate number (see table 2.4)	Issues to address
Sdro	mouse	9	a, b, c
retSDR3 (DHRS10)	human	20	a, b, c
dhrs7b	rat	24	a, b, c
dhrs8	rat	27	a, b, c
RDH12, Rdh12	human, mouse	35, 34	a, b, c
RDH13	human	38	a, b, c
Dhrs4	mouse	69	a, b, c
DHRSX	human	92	a, b, c
WWOX	human, mouse	30, 32	a, b
MGC4172, MGC18716	human, mouse		a, b, c

The third column depicts the numbers given to the proteins in tab. 2.4. WWOX was previously described several times and its subcellular localization had been shown [17] but still the question of a physiological substrate remained unanswered. Where no number is depicted, the proteins were not identified by SDR Finder but were additionally included. The fourth column describes the aspects for enzymatic characterization: a = expression pattern, b = substrate specificity, c = subcellular localization

Achievements: The identification of SDR enzymes is not a trivial task, neither manually nor using SDR Finder. Within this work, 94 putatively SDR type enzymes from human, mouse and rat were identified by use of SDR Finder. After removal of 18 characterized, 17 not SDR-type, and several redundantly identified proteins, 38 SDRs remained as putative targets for in-depth characterization. For deeper characterization, 11 enzymes from this list (see table 2.5) were selected. Otherwise identified MGC4172 and MGC18716 were additionally added to this list.

2.4. Expression patterns of candidate enzymes

Regulation of expression is a major means of organisms to determine the right composition of proteins needed in a certain tissue (and its cells) at a certain time or condition. The expression pattern mirrors this need and is therefore yet another hint to an enzyme's function. The expression of estradiol biosynthesis enzyme 17β -hydroxysteroid dehydrogenase (17β -HSD) type 1 is mainly restricted to ovary and placenta in adult organisms [89, 90] while housekeeping genes as glyceraldehyde-3-phosphate dehydrogenase (GAPDH) or genes coding for cytoskeletal proteins as β -actin are ubiquitously expressed at similar levels.

2.4.1. Development of an automated In Silico Northern Blot (ISNB)

Reasons for a new automated In Silico Northern Blot (ISNB). With the ever-increasing amount of data on ESTs (expressed sequence tags) and related databases it has become possible to gain knowledge about tissue specificity prior to wet lab experiments simply by accessing EST databases. Computer-based analysis is usually referred to by the term *in silico*. As the idea of analyzing gene expression patterns with help of ESTs from databases is similar to the common wet lab method of Northern blotting, it is often called *in silico* Northern blot (ISNB). The ISNB can be manually accomplished by performing a BLAST search reflecting an EST-database of choice and subsequently counting the hits in the different libraries for the listed tissues. However, this is a rather tedious, time-consuming, and error-prone task. I therefore decided to implement an automated method. In comparison to the manual approach automation provides greater reliability, sorting by different criteria, and quick access to previous analyses. Moreover, filtering for criteria such as alignment quality or length can lead to an advanced elimination of hits of minor significance. Therefore, the ISNB does not only provide more convenient *in silico* analysis but also higher scientific output than the manual variant. However, the quality of the ISNB relies on the quality of EST databases. It is therefore important to keep in mind that EST data is always biased since some tissues are more often analyzed in cDNA databases than others.

Method and performance of ISNB. In cooperation with Korbinian Grote from the BioDV group at the Institute of Experimental Genetics, I developed a tool generating an automated output from a BLAST-search [4] of EST databases. The algorithm is outlined in the methods chapter (p. 148). In conclusion, it provides an automated version of the by-hand procedure. A given mRNA sequence is compared against the EST database of the organism of the sequence's origin at NCBI. As thresholds, minimum alignment length and quality (percentage of identical nucleotides) can be selected. Automatically, all ESTs

2. Results

meeting these thresholds are investigated for information about their origin concerning tissue and counted according to these data. The resulting profile was regarded as indicative of the general level of expression as well as of occurrence and amount of transcripts in certain tissues in relation to others.

Test of the system. Applying the automated *in silico* northern blot tool, I analyzed the expression pattern of several murine enzymes from the 17 β -HSD group (types 1, 4, and 11) for testing the system. By BLAST search, I identified 1000 ESTs for 17 β -HSD 1, 625 matching 17 β -HSD 4 and 515 for type 11 17 β -HSD. As set-up for the ISNB, I defined 85% minimal alignment similarity and 50 bp minimal EST length as analysis threshold. Out of the found ESTs, only 25 ESTs matched the conditions in case of 17 β -HSD1, 594 for type 4 and 453 for type 11. All others were accordingly excluded from the analysis (fig. 2.7, panels A to C). For experimental verification of the system, a wet-lab northern blot for the type 11 gene was included (fig. 2.7, panel D).

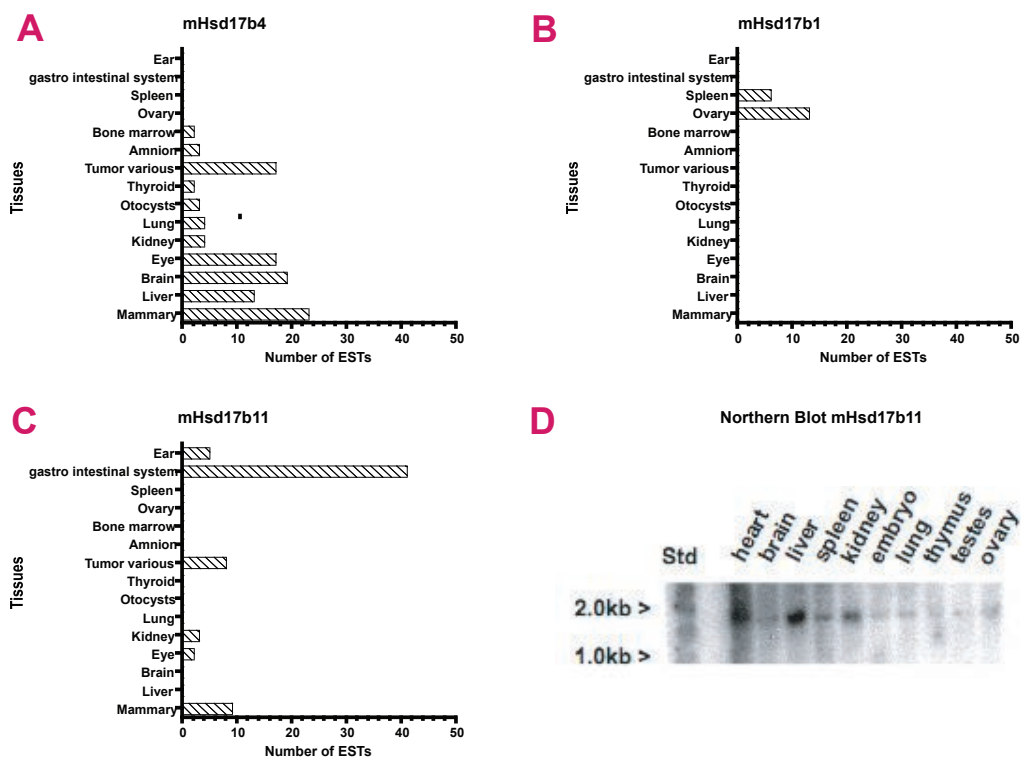


Figure 2.7: *In silico* expression patterns for murine Hsd17b4 (panel A), Hsd17b1 (panel B), and Hsd17b11 (panel C) expression. Panel D shows the experimental verification for the results in panel C, a northern blot membrane hybridized with murine Hsd17b11 cDNA.

The *in silico* results confirm the previously described ubiquitous expression pattern of

17β -HSD type 4 [83] as well as the mainly ovary-restricted one of 17β -HSD type 1 [81] (refer to panels A and B in fig. 2.7).

17β -HSD type 11 was discovered due to its homology to other 17β -HSD family members and due to its ability to convert 17β -hydroxysteroids [64]. In a more recent study, up-regulation of 17β -HSD11 by peroxisome proliferator-activated receptor alpha agonists in mouse intestine suggests involvement in lipid metabolism [80]. The *in silico* data shows broad tissue distribution of the mouse enzyme being in agreement with the hypothesis of lipid metabolism involvement. As shown in Fig. 2.7 panels C and D there is an overlap with data obtained by ISBN though not being completely congruent. This is partly due to the fact, that not all tissues are analyzed on the northern blot membrane. Furthermore, EST databases are biased due to the fact that not all tissues are analyzed at the same frequency and quality. However, for *in silico* expression analysis of many genes the new tool offers easy and versatile application.

Achievements: By developing and testing an automated system for *in silico* gene expression analysis, I could show both the advantages of automation and limitations of the *in silico* approach. The tool developed in the work at hand can help to achieve easy overview on expression patterns especially when it comes to many genes.

2.4.2. Expression analysis of the candidate genes *in silico* and wet lab

ISBN analyses for the candidate genes - set-up

In contrast to the first test of ISBN where I changed the default settings of BLAST to the output of 1000 ESTs at maximum, *in silico* analysis on the proteins under investigation in this thesis was done also with default settings of BLAST resulting in 100 ESTs maximum. The ISBN settings were the same as applied for the first test: 85% minimal alignment similarity and 50 bp minimal EST length.

Set-up and controls for wet lab expression analysis

For determination of the expression pattern of the SDRs under investigation, northern blots were as well conducted for murine and human enzymes. For the two rat enzymes characterized, RNA was isolated from a choice of tissues and RT-PCR conducted. This way, expression patterns were experimentally determined and provided further possibility to test the performance of ISBN.

Northern blots of human and murine tissues. As described in 4.5, Ambion FirstChoice Northern Blot membranes were hybridized with parts of the respective cDNAs amplified

2. Results

from overexpression plasmids. Primers and respective product lengths are depicted in the appendix. To monitor loading of the Northern Blot membranes, parts of murine β -actin CDS were hybridized. Fig. 2.8 shows quite equal amounts of RNA in each lane of the northern blots only spleen and small intestine display larger amounts of β -actin. Fig 2.9 shows the loading control for the murine northern blot. As β -actin is a highly conserved protein, murine cDNA could be used for the hybridization of both membranes. While on the membrane with human RNA, amounts of β -actin were quite similar though with higher amounts in small intestine and prostate and clearly lower amount in testis, the murine blot revealed greater differences (see fig.s 2.8 and 2.9). For easier judgement of expression levels, these figures will therefore be repeated with the each northern blot for the genes under investigation.

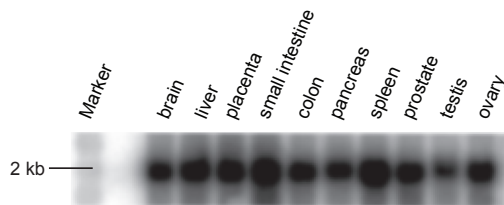


Figure 2.8: Ambion FirstChoice human blot 3 hybridized with murine β -actin cDNA as a loading control.

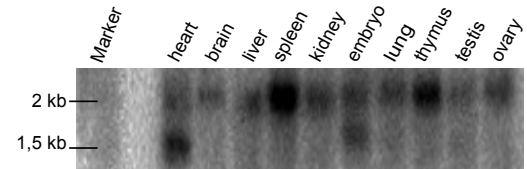


Figure 2.9: Ambion FirstChoice mouse blot 1 hybridized with murine β -actin cDNA as a loading control.

In between the experiments, the control for stripping was conducted by detection of counts with an ionization monitor. After the last experiments, the membranes were stripped from hybridization and checked for remaining signals by autoradiography. On both membranes, remaining signals from the hybridization with β -actin were detected. Signals possibly remaining from these prior hybridizations will be pointed out.

Quality control of rat cDNAs by PCR-amplification of β -actin. For expression control of the two rat enzymes included to the analysis, RNA was isolated from the following tissues of male and female rats: cerebrum, cerebellum, eye, heart, liver, kidney, spleen, lung, thymus gland, and upper thigh muscle from both genders, testis, epididymis from male and ovaries from female rat. The control-PCR (Fig. 2.10) shows approximately equal amounts of actin in all samples. Though mainly representing a qualitative control of cDNA synthesis, quantitative evaluation of the results was tried. Reasons herefore were the set-up of PCR: only the equivalent of 5 ng RNA was used and 25 cycles of amplification were conducted to avoid saturation.

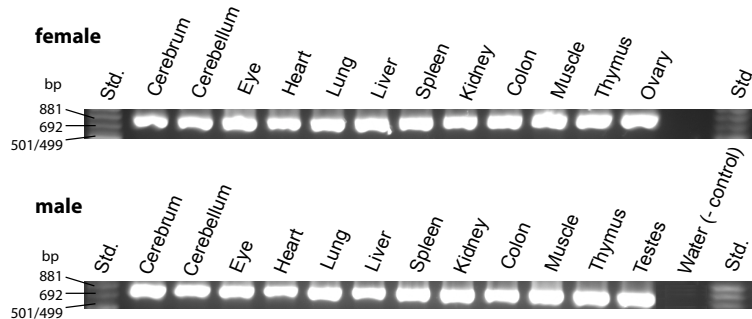


Figure 2.10: PCR with β -actin specific primers on 1:10 dilutions of cDNA of different tissues. Top panel shows female, bottom panel male tissues.

2.4.3. Expression pattern of murine orphan Sdr (mSdr-o)

Fig. 2.11 displays the expression pattern of murine Sdr-o. Even after several repetitions under slightly varying conditions (more stringent washing, lower probe amount and higher probe amount), background could not be further reduced.

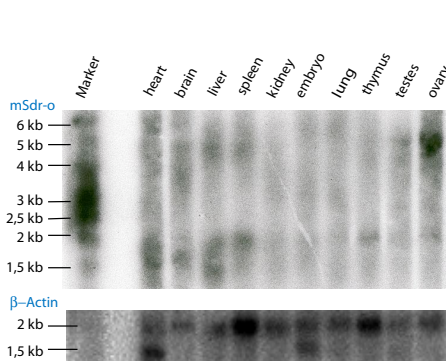


Figure 2.11: Northern Blot showing the expression pattern of murine Sdr-o.

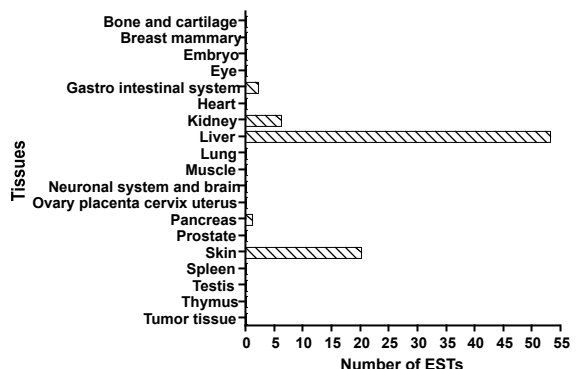


Figure 2.12: ISNB showing the expression pattern of murine Sdr-o *in silico*. Altogether, 90 out of 100 ESTs identified in databases were analyzed by ISNB.

Though with high background, a band of 5 kb is detectable showing expression in brain, liver, spleen, testis and especially in ovary. Further bands are detected at 2 and 1.5 kb. The 1.5 kb band is detectable in heart, brain, and spleen. In liver, another additional band is detected at approximately 1.3 to 1.4 kb. The 2 kb band was not described before [19] and in comparative amounts is likely to be left over from β -actin hybridization as may be the 1.5 kb band in heart - interestingly, this lower β -actin band was detected in embryo also but did not lead to a remaining signal.

In contrast to the experimental Northern Blot (see fig. 2.12) shows a very constricted expression pattern with high expression in liver and to a lesser amount in skin,

2. Results

again less in heart and in the gastrointestinal system. This is in contrast to the findings in the experimental northern blot where highest expression is observed in ovaries.

2.4.4. Expression pattern of human retSDR3

Fig. 2.13 displays the expression pattern of retSDR3 in human adult tissues, fig. 2.14 the ISNB for this gene.

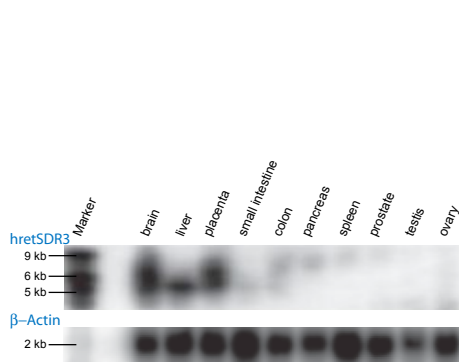


Figure 2.13: Northern blot hybridized with human retSDR3 cDNA.

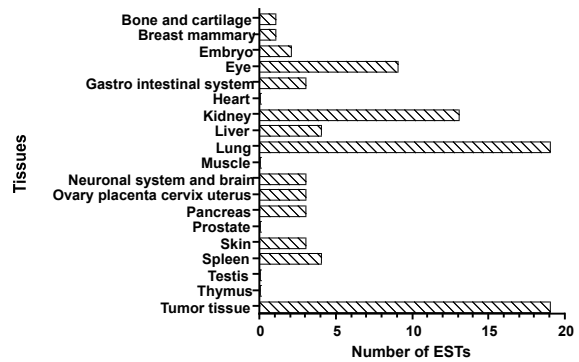


Figure 2.14: ISNB showing the expression pattern of human retSDR3 *in silico*. Altogether, 76 out of 100 ESTs identified in databases were analyzed by ISNB.

High expression is observed in brain, liver and placenta, whereas no or low signals are observed in small intestine, colon, pancreas, spleen, and gonads (testis and ovary). Two distinct sizes of specific signals are observed (approximately 5.5 and 7 kb), indicating two distinct transcription or splicing sites in brain and placenta, whereas in liver only one mRNA species is observed.

The ISNB of human retSDR3 (see fig. 2.14) shows a broad tissue distribution of expression as well. In both experimental and *in silico* northern blot, testis and prostate show no expression. The wet lab northern blot indicated expression in placenta but not in the ovaries. This is not corroborated by ISNB. Raw data displayed one EST each for cervix, ovary, and placenta. Also, the high expression in brain and liver was not detected in EST databases.

2.4.5. Expression pattern of rat dhrs7b

For rat SDRs under investigation, PCR was performed on cDNAs from several tissues both from female and male adult Sprague-Dawley rats. For control, β -actin was also investigated (refer to fig. 2.10, p. 37). Fig. 2.15 shows the expression pattern of rat dhrs7b.

2.4. Expression patterns of candidate enzymes

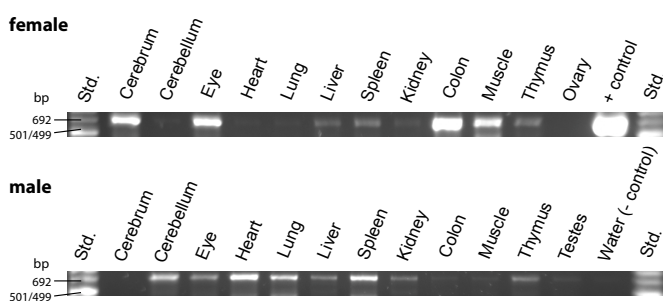


Figure 2.15: Expression pattern of rat dhrs7b in adult rat tissues. Interestingly, the pattern varies greatly between the two genders (top panel: female, bottom panel: male). Positive control: top, right – negative control: bottom, right.

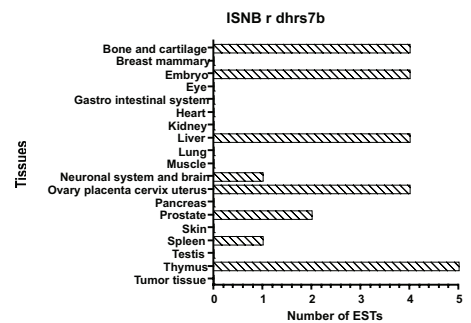


Figure 2.16: ISNB showing the expression pattern of rat dhrs7b *in silico*. Overall, only few ESTs were found from each tissue. Altogether, 36 out of 40 ESTs identified in databases were analyzed by ISNB.

Strikingly, the expression pattern of the gene is almost completely opposite between the two genders. In females, highest expression of the gene is seen in colon, where no expression in males can be seen. Medium levels of expression can be seen in female cerebrum, eye, and muscle. In male animals, dhrs7b within these three tissues is only expressed in eyes at a low level but not in cerebrum and muscle. Medium level expression can be detected in male heart, spleen, lung, and cerebellum. In females, no expression is found in these tissues except for spleen (low level). Low levels of expression can be observed in thymus and liver of both genders, female spleen, male kidney and liver.

Only little ESTs are found from each tissue in ISNB analysis. Overall, experimentally evaluated and *in silico* expression pattern do not converge well. ESTs were found from eye, heart, and kidney but expression in these tissues was not detected experimentally. The four ESTs from female reproductive tissues derive altogether from ovary, where also no expression could be seen in fig. 2.15. From tissues not tested in PCR, there is expression shown in bone and cartilage, the embryo, and prostate. No information on expression is available for breast and mammary tissue, the gastrointestinal system, pancreas, skin, and tumor tissues.

2.4.6. Expression pattern of rat dhrs8

For rat dhrs8 expression analysis, PCR was performed on cDNAs from several tissues both from female and male adult Sprague-Dawley rats (fig. 2.17).

As seen for rat dhrs7b, there are differences between the two genders: In females, dhrs8 is only in the cerebellum and not in the ovary, males express the gene only in lung, liver, kidney, and testis. No expression is seen in cerebrum, eye, heart, spleen, muscle, and thymus.

2. Results

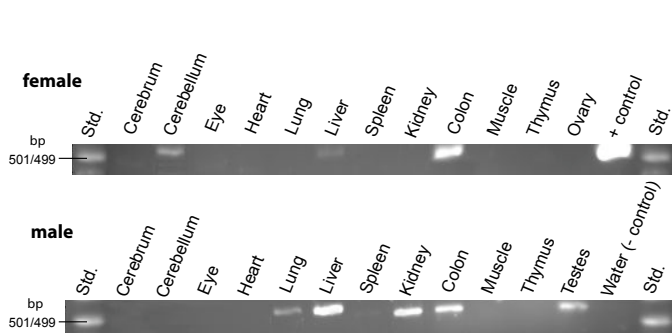


Figure 2.17: Expression pattern of rat dhrs8 in adult tissues. As for rat dhrs7b, the pattern varies between the two genders (top panel: female, bottom panel: male). Positive control: top, right - negative control: bottom, right.

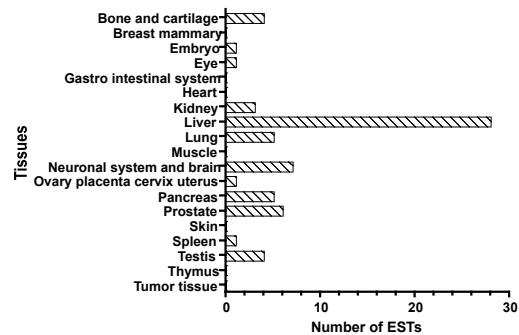


Figure 2.18: ISNB showing the expression pattern of rat dhrs8 *in silico*. All 83 ESTs identified from the databases were analyzed by ISNB.

Apart from the missing gender dissimilarity, the expression information on rat dhrs8 gained from ISNB (see fig. 2.18) fits the experimental data altogether quite well. Only minor differences are seen. Expression in the gastrointestinal system is missing, and there is 1 EST being found from spleen and eye each. Additional tissues with expression of dhrs8 are bone and cartilage, pancreas, and prostate with a rather low level of expression.

2.4.7. Expression pattern of murine Rdh12

Fig. 2.19 shows the expression pattern of murine Rdh12. It displays high background. Again, this could not be altered also by varying conditions of hybridization and washing.

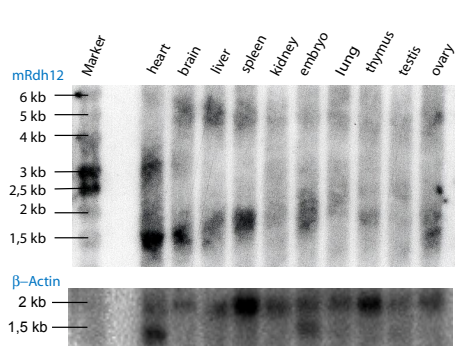


Figure 2.19: Northern blot hybridized with murine Rdh12 cDNA.

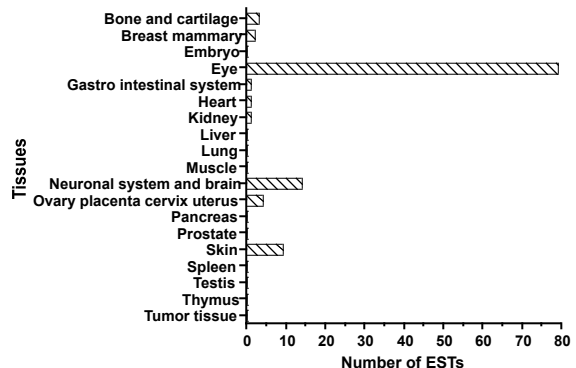


Figure 2.20: ISNB showing the expression pattern of murine Rdh12 *in silico*. All 100 ESTs identified from the databases were analyzed by ISNB.

Still, several bands can be detected: almost all tissues display a band of about 5 kb in size (brain, liver, spleen, kidney, lung, testis, ovary). Additionally, in the heart there

2.4. Expression patterns of candidate enzymes

are signals at 1.5 and 3 kb, in the brain, liver and spleen at 1.5 kb. In total, expression in kidney, liver, and the embryo is very low. Thymus and testis display two transcripts of 2 kb and 2.5 kb, respectively, the long (5 kb) transcript is almost not detectable. Ovary displays only one transcript of 1.5 kb in size. The 2 kb signal in thymus is most likely remaining from hybridization with β -actin as is the 1.5 kb signal in heart.

In contrast, the ISNB shows a expression pattern mainly restricted to the eye, being in accordance with the protein being annotated as retinol dehydrogenase. On the other hand, very low EST levels have been detected from ovaries, neuronal system and brain, heart, and kidney. Despite the rather poor quality of the northern blot due to the high background displayed, it is therefore not unlikely that Rdh12 shows a broader expression pattern as ISBN suggests. Also in earlier comparisons of ISBN and experimental northern blot results I had already observed that ISBN tends to be a qualitative rather than a quantitative method.

2.4.8. Expression pattern of human RDH12

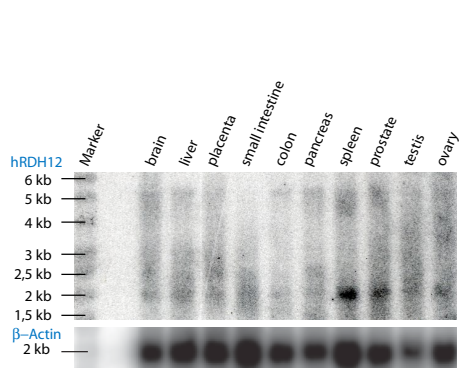


Figure 2.21: Northern blot membrane hybridized with human RDH12 cDNA.

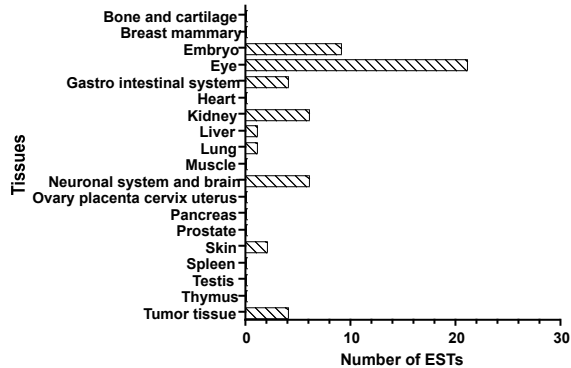


Figure 2.22: ISNB showing the expression pattern of human RDH12 *in silico*. Altogether, 42 out of 43 ESTs identified in databases were analyzed by ISNB.

Fig. 2.21 depicts the expression pattern of human RDH12. Four transcript sizes can be detected of 5.5, 3, 2.5, and 2 kb respectively. This 2 kb signal is, however, remaining from hybridization with β -actin. In the brain, low levels of the larger 5 and 3 kb sized transcript have been detected and higher amounts of the two small transcripts. This applies also to expression in the liver. In the placenta, expression seems to be restricted to the two small transcripts but uncertainty remains for the 5 kb transcript.

Interestingly, small intestine does not display the 5 kb transcript but colon does. The shorter transcripts can be detected in small intestine. Pancreas displays the 5 kb transcript as well as the 2.5 kb mRNA. Testis and ovary also display the 5 kb mRNA species but

2. Results

at medium to low amounts. Doubts about unspecific signals remain for these two tissues when comparing the result to ISNB (cf. to fig. 2.22) as for these tissues, no ESTs could be identified at all.

ISNB (see fig. 2.22) additionally shows high expression in the eye. This in accordance with the identification of human retinol dehydrogenase type 12 in the retina [37]. If not considering the 2 kb transcript human RDH12 overall expression levels are low. This is in accordance with ISNB.

2.4.9. Expression pattern of human RDH13

Human retinol dehydrogenase type 13 seems to be a gene with several mRNA species transcribed (fig. 2.23).

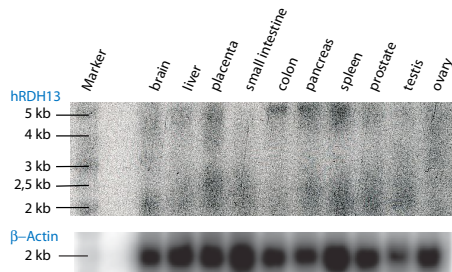


Figure 2.23: Northern blot membrane hybridized with human RDH13 cDNA.

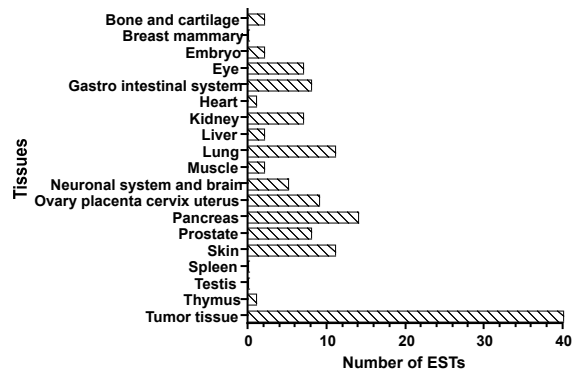


Figure 2.24: ISNB showing the expression pattern of human RDH13 *in silico*. All 100 ESTs identified from the databases were analyzed by ISNB.

In the brain, three mRNA species could be detected with lengths of 5, 3, and 2 kb respectively. Again, the 2 kb transcript is a remainder from β -actin hybridization. Liver, placenta, pancreas, spleen, and prostate show a transcript of 5 kb in size. RDH13 seems to be expressed in colon but not in small intestine. Expression in the tissues analyzed could therefore be restricted to placenta, colon, pancreas, and spleen.

The ISNB for that gene, as shown in fig 2.24, consolidates the finding of broad tissue distribution, displaying most hits in tumor tissues but similar levels in most other tissues detected. The ISNB raw data does not display a clear preference for tumors of one tissue or a certain tumor type. ESTs from ovary and placenta are evenly distributed in the raw data. This can not be seen from the wet-lab analysis in fig. 2.23.

2.4.10. Expression pattern of murine Dhrs4

Apart from the remaining β -actin levels which seem to be almost completely retained, a transcript of about 1.3 kb in size is detected in liver and kidney (see 2.25).

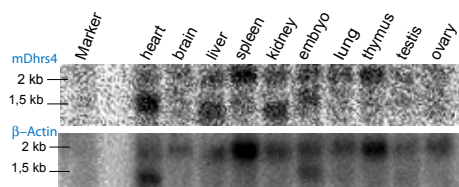


Figure 2.25: Northern blot membrane hybridized with murine Dhrs4 cDNA.

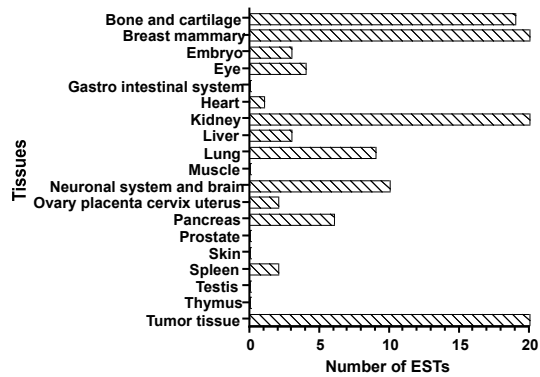


Figure 2.26: ISNB showing the expression pattern of murine Dhrs4 *in silico*. All 100 ESTs identified from the databases were analyzed by ISNB.

ISNB displays a overall high expression (fig. 2.26). Additionally to the tissues already described, it displays high expression in bone and cartilage, breast and mammary tissue, and tumor tissue. Less ESTs are found from pancreas, muscle, and spleen. Due to the broad expression pattern shown by ISNB doubts about the identity of the signals on the northern blot membrane (β -actin or mDhtrs4) are appropriate.

2.4.11. Expression pattern of human DHRSX

Human DHRSX is an ubiquitously expressed gene though with varying expression levels (see fig. 2.27). Similarly to mDhtrs4, overall expression levels are quite high. For human DHRSX, northern blot (fig. 2.27) and ISNB (see 2.28) do not converge.

Fig. 2.27 shows that the gene produces two transcripts of approximately 2.5 and 1.8 kb. While brain, placenta and colon mainly produce the longer mRNA species liver, pancreas, spleen, prostate, testis, and ovary express both transcripts to varying degrees. Strongest expression is observed in prostate, testis, and ovary.

However, when looking at the ISNB (fig. 2.28) DHRSX seems to be restricted mainly to tumor tissues and pancreas with over 50 ESTs each. Apart from lung (about 20 ESTs), 10 ESTs at maximum were identified though from a broad range of tissues. Further comparison of ISNB and its wet lab analogue is therefore obsolete.

2. Results

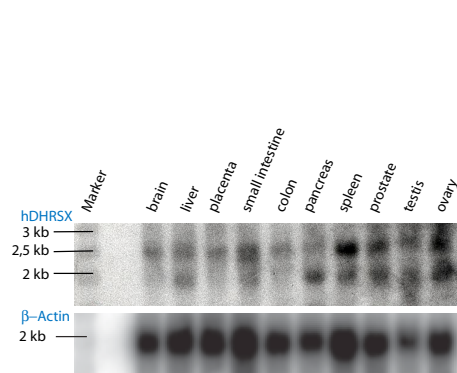


Figure 2.27: Northern blot membrane hybridized with human DHRSX cDNA.

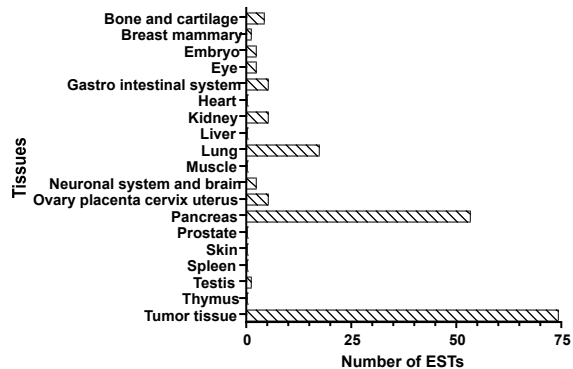


Figure 2.28: ISNB showing the expression pattern of human DHRSX *in silico*. All 100 ESTs identified from the databases were analyzed by ISNB.

2.4.12. Expression pattern of human WWOX

WWOX has been shown to be alternatively spliced with at least eight variants being described (for an overview, see Discussion, fig. 3.14, p. 121). Also from the northern blot (fig. 2.29) presented here, the existence of several mRNA species is obvious.

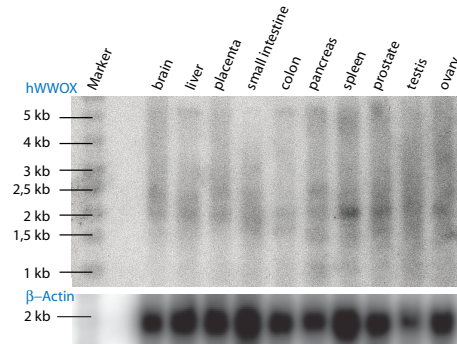


Figure 2.29: Northern blot showing the ubiquitous expression of hWWOX.

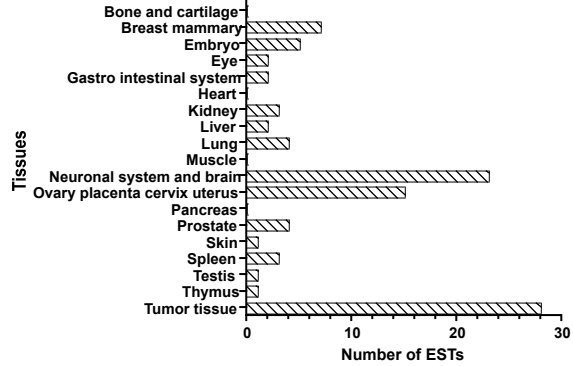


Figure 2.30: ISNB showing the expression pattern of human WWOX *in silico*. Altogether, 98 out of 100 ESTs identified in databases were analyzed by ISNB.

The first notion from fig. 2.29 is that different tissues express different variants of WWOX. The northern blot shows the largest transcripts at a size of 5 kb, the smallest with approximately 1 kb. Several transcripts have been detected with lengths between 1.5 and 3 kb. The ubiquitously detected 2 kb band is probably not a mRNA species of hWWOX but β -actin. This seems to be especially likely as the highest expression of this mRNA species is detected in spleen, where also the highest amount of β -actin was

detected. These bands will therefore not be included in the following evaluation.

Overall, WWOX seems to be ubiquitously expressed. However, alternative splicing causes distinct expression patterns for the different isoforms. In the brain, only one transcript is detected at about 2.3 kb. In addition to this, liver shows a 5 kb transcript. Placenta expresses the 2.3 kb transcript - bands could also be detected at 3 and 5 kb though not very clear. A weak signal is also detected at 1 kb. This is also true for small intestine. Colon seems to lack the 3 kb and 2.5 kb mRNA species but displays signals at 1.8 and 1 kb. Pancreas, spleen, and prostate display four signals at 5, 2.5, 1.8 and 1 kb. Especially high background hinders evaluation of expression in testis and ovary. In the latter, the 1.8 kb transcript might be expressed while the former shows the 1 kb mRNA species.

Fig. 2.30 shows the results from *in silico* expression analysis. WWOX has been described to possess pro-apoptotic effects [6, 17]. Still, many ESTs from tumor tissues were identified. Furthermore, the ubiquitous expression shown in the figure above is confirmed. Due to the applied minimal alignment length of 50 bp, all isoforms should have been identified. The ISBN can, however, not distinguish between the splice variants.

2.4.13. Expression pattern of murine Wwox

For the murine Wwox gene, expression is depicted in fig. 2.31. As for the human gene, a 5 kb transcript can be detected but is restricted to brain and liver. An approximately 2.3 kb long mRNA is ubiquitously expressed. Highest levels of this transcript are detected in ovaries, but kidney and brain also show considerable expression levels. The signals at the very bottom of mWwox-hybridized northern blot are rests of β -actin hybridization.

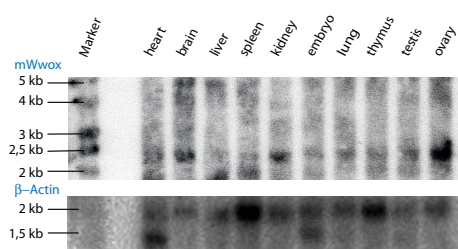


Figure 2.31: Northern Blot showing the expression of murine Wwox.

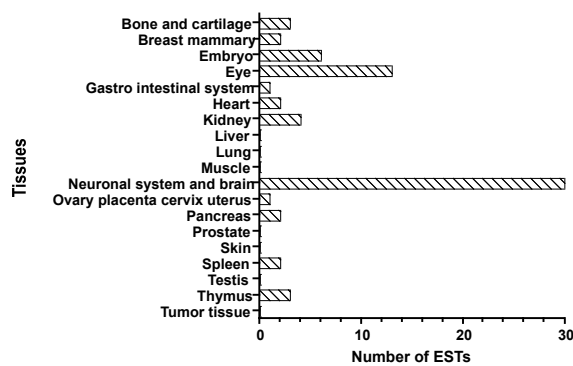


Figure 2.32: ISBN showing the expression pattern of murine Wwox *in silico*.

Human WWOX gene was shown to be ubiquitously expressed both *in silico* and by northern blot. For the murine gene, the ISBN (fig. 2.32) does not mirror the pattern

2. Results

shown experimentally.

In contrast, ISBN suggests highest expression in the brain, followed by expression in the eye and in the embryo. No ESTs were detected in the ovaries and, in contrast to the ISBN of the human gene, in tumor tissues. The fact that all 100 ESTs identified from the databases were analyzed by ISBN could provide a hint that more ESTs were available but not included by BLAST. The default value for maximal results in a BLAST search is 100 hits. Setting this value to 1000 as done in initial testing could help to improve the ISBN performance.

2.4.14. Expression pattern of human MGC4172

From the human MGC4172 gene, only one mRNA species is transcribed as shown in fig. 2.33. The transcript has a size of approximately 2 kb. Highest expression level is seen in spleen followed by prostate, ovary, and testes. At low levels, MGC4172 is expressed in all tissues analyzed. For the hybridization of this Northern Blot, the murine cDNA of MGC18716 was used. As it is 92% identical to the human cDNA, no false-positive or false-negative signals were to be expected.

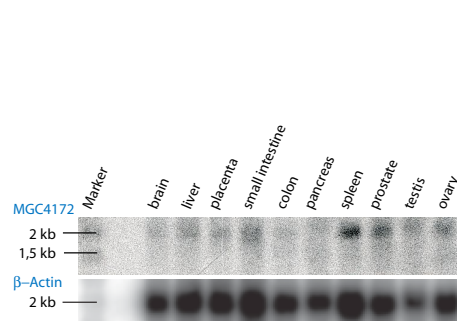


Figure 2.33: Northern blot of human tissues hybridized with murine MGC18716 cDNA.

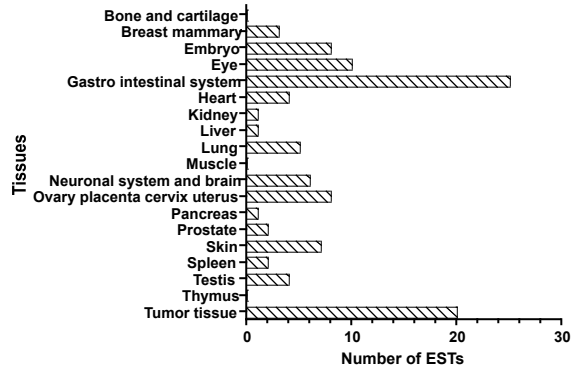


Figure 2.34: ISBN showing the expression pattern of human MGC4172 *in silico*. All 100 ESTs identified from the databases were analyzed by ISBN.

In contrast to the wet lab northern blot, most ESTs (see fig. 2.34) are found in libraries from the gastrointestinal system. Additional expression in tumor tissues is indicated. Overall, ISBN can confirm the findings from wet lab analysis. It should however be noted that the expression pattern detected here is very similar to the one displayed by β -actin. The expression level of MGC4172 is obviously extremely low. Very weak signals could be seen at a size of 1.5 to 1.7 kb in colon, pancreas, and ovary. In summary, only little conclusive results could be obtained concerning this gene.

2.4.15. Expression pattern of murine MGC18716

As for the human homologue, MGC4172, only one mRNA species could be detected for MGC18716 (cf. fig. 2.35). Again, the size of this transcript is around 2 kb. An additional signal is detected around 1.5 kb in heart, liver, and brain. Highest levels of expression are detected in spleen and thymus. While kidney and lung display low levels of expression, no discrete bands could be detected in the other tissues. Overall, MGC18716 displays very low expression levels.

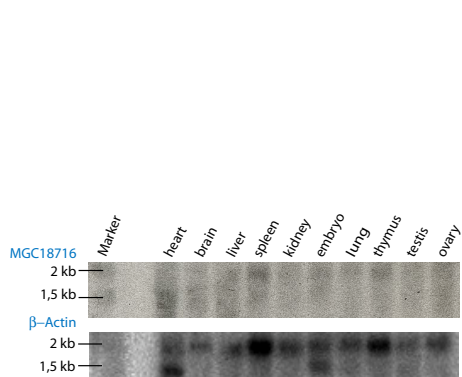


Figure 2.35: Northern blot hybridized with murine MGC18716 cDNA.

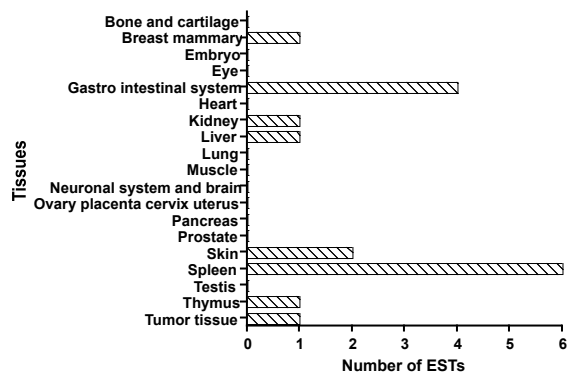


Figure 2.36: ISNB showing the expression pattern of murine MGC18716 *in silico*. Altogether, 21 out of 22 ESTs identified from the databases were analyzed by ISNB.

This might also account for the fact that only a total of 22 ESTs were identified for MGC18716 (cf. 2.36). Overall, northern blot and ISNB results match quite well, as most ESTs are detected from spleen - the tissue displaying the most prominent signal in wet lab northern blot. Furthermore, also for MGC18716 the expression pattern might be not caused by this gene but left-over from the hybridization with β -actin mRNA. However, it is then surprising that the strong signal detected at around 1.3 kb in kidney was not retained (see fig. 2.25, p. 43).

Achievements: For 13 SDR genes, expression was analyzed both *in silico* and by wet lab northern blot. All genes show unique expression patterns mostly with more than one transcript. Overall, the expression levels are rather low. The comparison of the two analysis systems for more than one gene (see chapter 2.4.1, p. 33) provides further insights into the practicability of the automated system for ISNB.

2. Results

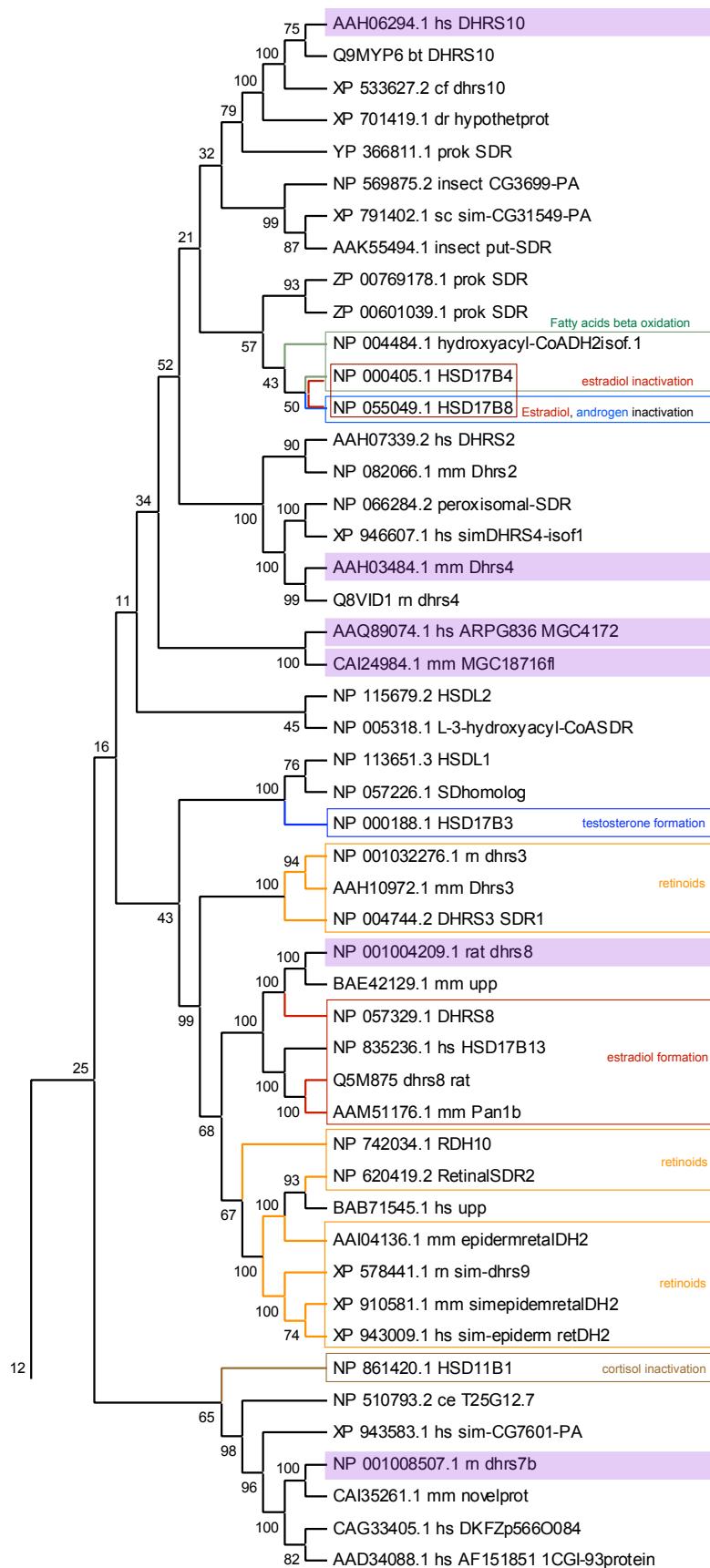
2.5. First hints to substrate specificity: phylogenetic analyses

Phylogenetic analyses have become a considerate bioinformatic means of enzyme characterization. With the growing public availability of sequences in the databases from different species it has also become possible to find evolutionary conserved and related sequences. Based on the assumption that conservation of function requires a - at least partially - conserved sequence investigators tend to compute phylogenetic trees not only for depiction of phylogenetic relationship between species but also for phylogenetic relationship concerning proteins belonging to one or several enzyme families [11]. Marijanovic *et al.* [71] and Mindnich [75] have shown that by phylogenetic analyses prediction on substrate specificities and involvement in metabolic pathways can be made. In order to get a first hint on possible substrates of the candidate enzymes, this kind of analysis has been included in this thesis. For a closer view on the evolutionary relatives of the enzymes selected for characterization I performed phylogenetic analyses using the enzymes depicted in table 2.5 and the protein sequences gained from the respective BLINK links. These analyses did not yield the expected results as most of the found relatives were not characterized. Therefore, characterized hydroxysteroid and retinoid dehydrogenases were included. Fig. 2.37 shows the relationship between the SDR genes under investigation in this study and characterized enzymes. Due to the length of the figure, it is split into half and presented on two pages.

Based on fig. 2.37, several observations could be made (from top to bottom):

1. Human DHRS10 has only few relatives in eukaryotes. The closest relationship can be seen with the 17β -hydroxysteroid dehydrogenases (17β -HSDs; depicted by HSD17Bx in the tree) type 4 and 8. While type 8 17β -HSD is restricted to inactivation of androgens and estrogens, type 4 17β -HSD in addition is part of the peroxisomal fatty acid β -oxidation. Therefore, DHRS10 could be involved in steroid and/or fatty acid metabolism.
2. Besides homologues from other species, murine Dhrs4 is closest related to Dhrs2. For both enzymes, no substrate specificity had been described. All characterized enzymes enclosed in this tree do not display very close relationship. The same observations hold true for MGC4172 and MGC18716.
3. Human and murine 17β -HSD type 11 (DHRS8) have been described to be involved in estrogen and androgen metabolism [14]. Thus, for the rat homologue, this ability seems possible.
4. Rat dhrs7b homologue, finds its place somewhere in the middle between 11β -HSDs (responsible for glucocorticoid formation and inactivation) and the closely related

2.5. First hints to substrate specificity: phylogenetic analyses



2. Results

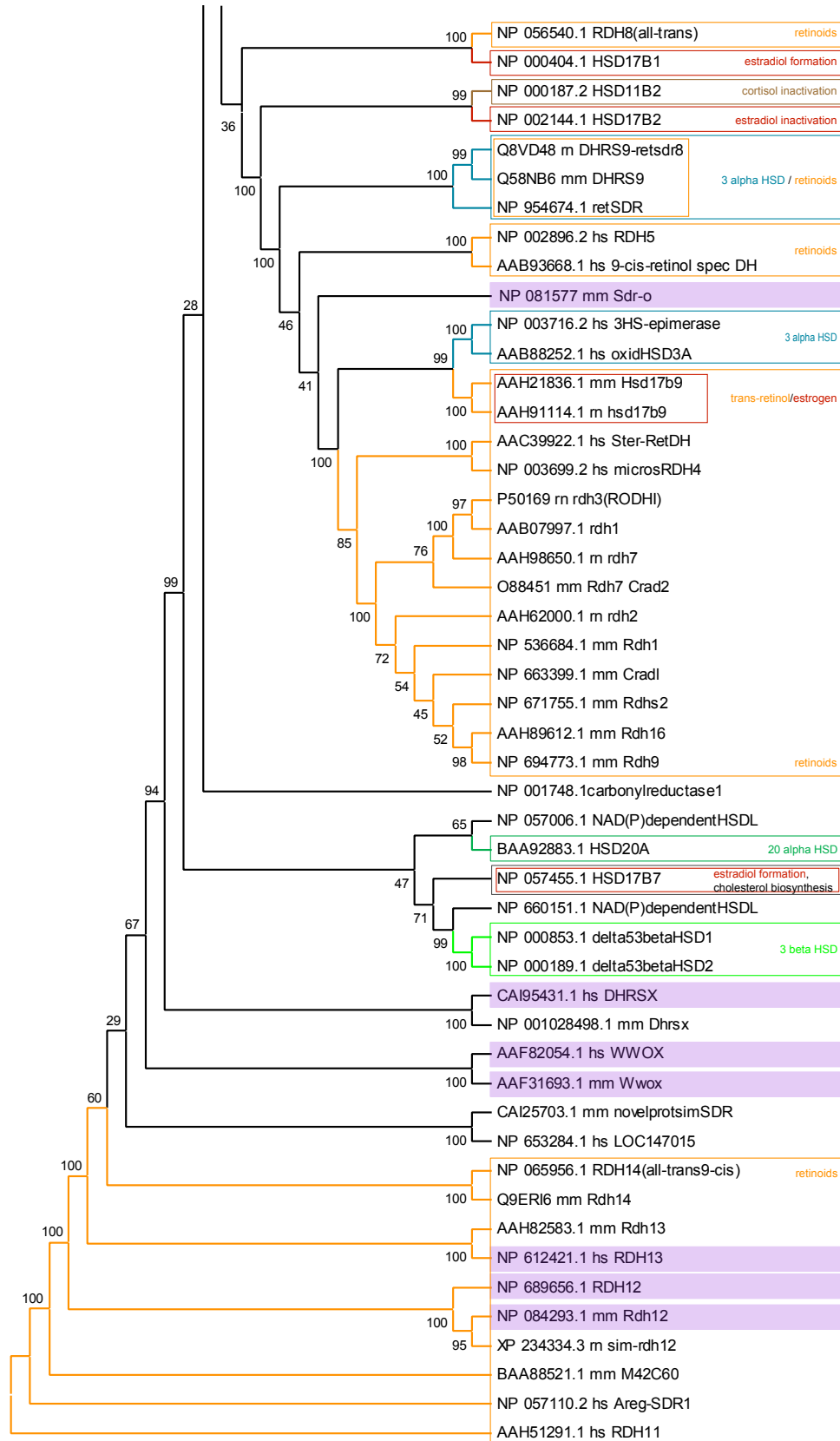


Figure 2.37: Results from phylogenetic analysis (for more details, see box on top of next page).

Figure 2.37: Tree shows SDRs selected for characterization (shaded in violet) and characterized steroid (HSDxA/By; estrogen converting enzymes in red, androgen converting enzymes in blue, other steroid dehydrogenases are marked green) and retinol dehydrogenases (RDHx, orange). Described substrate specificities are depicted in the respective boxes. Numbers on the branches indicate bootstrap values. The data-set used for this tree is presented in the appendix.

17 β -HSDs types 1 and 2 (which are balancing estradiol levels) and the photoreceptor-associated RDH8 [75].

5. Murine Sdr-o or orphan SDR was described as an SDR but with unknown substrate specificity [19]. It is located amongst retinoid and steroid (both of 3 α - and 17 β -activity) dehydrogenases.
6. DHRSX and WWOX are so far uncharacterized SDR type enzymes. Though subject to quite a high number of publications, no substrate specificity has been described for WWOX. Both WWOX and DHRSX are not very closely related to either steroid or retinoid dehydrogenases.
7. The bottom-most cluster of retinoid dehydrogenases includes the last three enzymes that are subject to investigation within this thesis: human and murine RDH12 and human RDH13. Retinoid dehydrogenases are often assigned as such according to similarities. Several RDHs were already shown to be steroid converting (e.g. 17 β -HSD9).

Achievements: Phylogenetic analyses was used to enable possible substrate specificities. This was, in large, achieved. All enzymes subject to more detailed analyses are related to characterized steroid, retinoid or fatty acid converting SDRs.

2.6. Investigation of substrate specificity: test of steroidogenic substrates

2.6.1. Selection of substrates and establishment of measurement

In this work, an assay should be established which can measure enzymatic conversion in intact cells. SDRs, due to their divergence, are involved in many intermediary metabolic pathways converting various substrates. Because not all possible substrates could be tested, due to lack of time but also, more importantly, due to lack of technical possibilities

2. Results

and established measuring methods, a screen for conversion of different steroid compounds was established. Due to the established HPLC system [3] only steroids that are available in tritiated form could be detected and be used herefore. In general, retention times were determined at concentrations used later as a tracer for enzymatic assays. This explains the noisy appearance of some chromatograms. Integration parameters are not affected hereby.

By HPLC, steroids can be separately eluted from a reverse phase C18 column in a mixture of acetonitrile and water. In all measurements, a flowrate of 1 mL/min was applied. For separation of androstenedione, testosterone, estrone and estradiol 43% of acetonitrile in water was used as previously established (personal communication, Dr. Dominga Deluca, [23]) (for chromatograms, see fig.s 2.38 and 2.39).

Fig. 2.40 shows the retention times of different androgens. Androstenedione (A, dark blue) and testosterone (T, light blue) elute from the HPLC column after 8 and 6 min, respectively. Androsterone (A-on, depicted in yellow) has the longest retention time with 14 min. Dihydrotestosterone (DHT, orange) has a retention time of 10 min. Androstanediol (A-diol, depicted in green) produces two peaks at 7 and 9 min. All androgens were separated on HPLC by application of 43% acetonitrile in water as a mobile phase.

These settings were also applied to progesterone and 20α -hydroxy progesterone. Progesterone was found to have a retention time of 18 min, while 20α -hydroxy progesterone is eluted from the HPLC column after 11.4 min (see fig. 2.41). Corticosteroids were separated with 30% acetonitrile. Cortisol eluted from the column at 5 min, corticosterone after 10 min (see fig. 2.42).

Steroids can enzymatically be modified at several positions. Due to the measuring system however, tritiated substrates were needed for use in conversion assays. The positions of modification that could be tested included 17β , 11β , 5α , and 20α . Retention times and separation conditions are summarized in table 2.6) were such chosen for test of conversion. Additionally, androstanediol had been planned for test of substrate specificity but turned out to be not available at this time.

2.6.2. Establishment of substrate conversion assays

For measurement of steroid hormone conversion, an assay in living cells was established. This approach seemed to be promising as it enables to determine whether a respective gene product under investigation can catalyze a certain reaction under physiological conditions (except for the steroid hormone concentration). Based on the assay described by Castagnetta and coworkers [15], I added the tritiated substrates directly to the living cell culture and used the cell culture supernatant after incubation for HPLC analyses. For each experiment, three independent samples were used. First, different cell lines were tested for their endogenous conversion rates of the respective steroids.

2.6. Investigation of substrate specificity: test of steroidogenic substrates

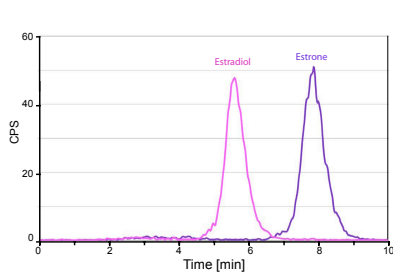


Figure 2.38: Retention times of estrone (purple, 7.5 min) and estradiol (pink, 5.5 min).

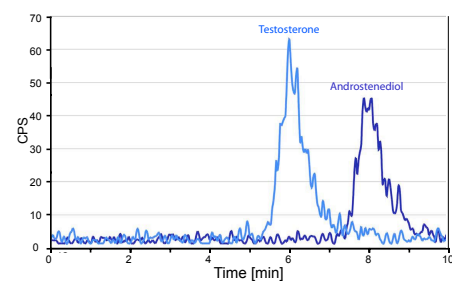


Figure 2.39: Retention times of androstenedione (dark blue, 8 min) and testosterone (light blue, 6 min).

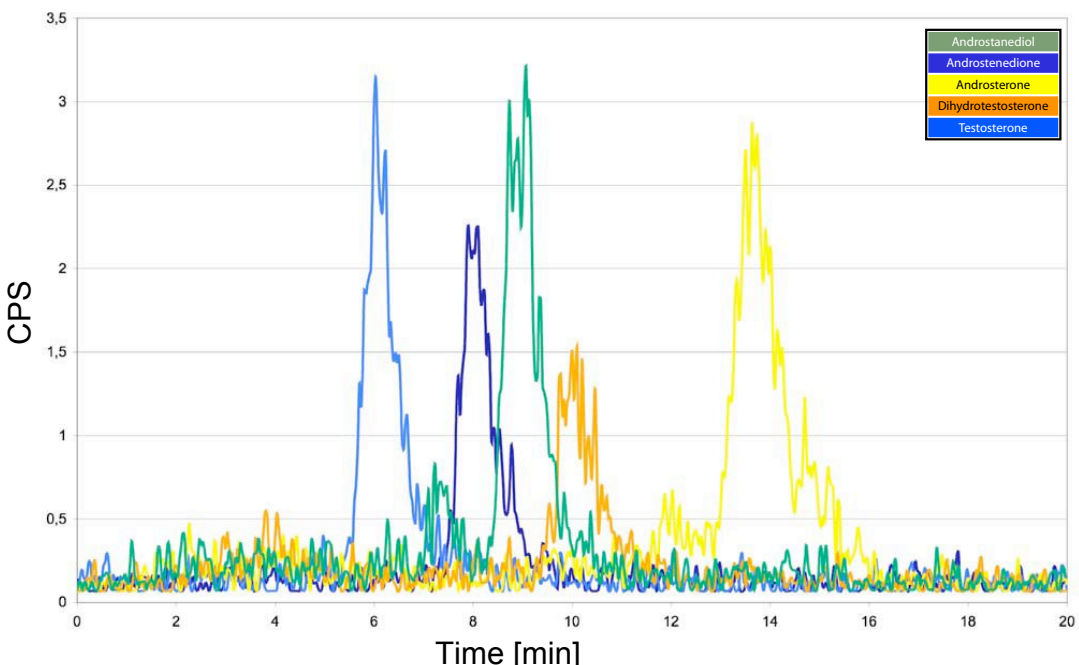


Figure 2.40: Overlay of the HPLC chromatograms of different androgens. Note that androstanediol produces 2 peaks (7 and 9 min).

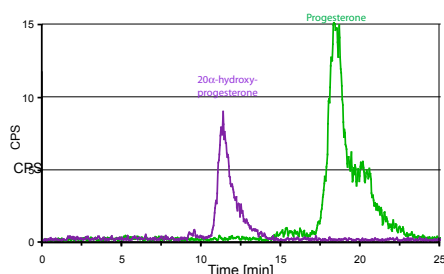


Figure 2.41: Retention times of 20 α -hydroxyprogesterone (purple, 11 min) and progesterone (green, 18 min).

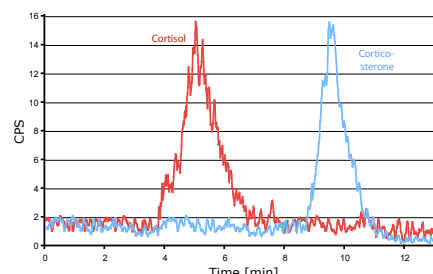


Figure 2.42: Retention times of cortisol (red, 5.5 min) and corticosterone (blue, 10 min).

2. Results

Table 2.6: Retention times and HPLC conditions for steroid separation

Steroid	Retention time [min]	% ACN
Androstanediol	7 and 9	43
Androstenedione	8	43
Androsterone	14	43
Corticosterone	9.8	30
Cortisol	5.6	30
Dihydrotestosterone	10	43
Estradiol	5.5	43
Estrone	7.5	43
20 α -Hydroxyprogesterone	11	43
Progesterone	18	43
Testosterone	6	43

% ACN = Percentage acetonitrile applied

Endogenous conversion of androstenedione, testosterone, estrone and estradiol

Supplementation of the culture medium with steroid hormones was then conducted on untransfected cells. Several cell lines were tested for endogenous conversion of the respective substrates. First, the interconversions of androstenedione (A) and testosterone (T), and of estrone (E1) and 17 β -estradiol (E2) were addressed (see fig. 2.43).

After an 8h incubation of the four substrates in HepG2, HEPA1-6, and HeLa cells, the highest endogenous conversion rates were observed in human hepatocarcinoma HepG2 cells. From all four given substrates mainly products (above 75%) were detected with retention times of around 3 minutes. Their identities have not been investigated. As they display a much lower retention time, these products possess obviously much higher polarity than the substrates applied. This points to hydroxylation reactions.

Surprisingly, murine hepatocarcinoma HEPA1-6 cells display a pattern of reactions dissimilar to human hepatocarcinoma HepG2 but rather similar to human cervix carcinoma HeLa cells. HEPA1-6 convert estrogens at rather high rates (10% of E2, 30% of E1) in comparison to androgens (both below 10%). T seems to be hydroxylated while A is interconverted into another unknown substance which elutes from the column after 11 min. The substance detected is more apolar (identity was not investigated). HeLa cells interconvert the given estrogens at low rates also by hydroxylation. They do not react on T and interconvert A into a substance of lower polarity.

For analysis of steroid conversions, 293 cells are frequently used [43]. 293T cells convert at higher rates in comparison with 293 (personal communication, F. Ströhle). 293T cells were thus selected instead of 293 cells. In tests with retSDR3 (not shown) small amounts

2.6. Investigation of substrate specificity: test of steroidogenic substrates

of endogenous conversion and highest conversion of transfected cells were seen for this cell line. Initial incubation was thus prolonged to 24 h, three times the time period as for the other cell lines. The results from these tests are also included in fig. 2.43. After 24 h they display the lowest conversion rates of E1, E2, A, and T with regard to the tested reactions and hydroxylation. Due to these tests, 293T cells were used for all conversion assays.

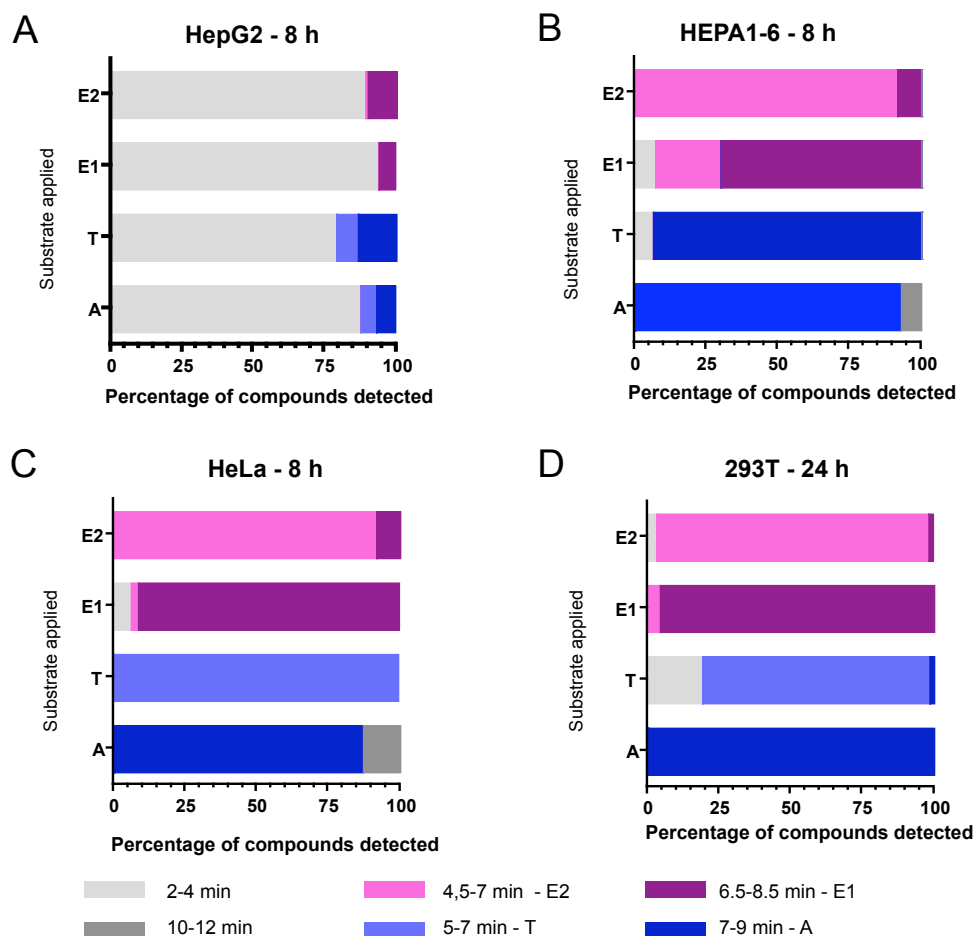


Figure 2.43: Endogenous conversion of androstenedione (A) and testosterone (T), and of estrone (E1) and 17 β -estradiol (E2) in four cell lines: HepG2 (panel A), HEPA1-6 (panel B), HeLa (panel C) and 293T (panel D). Incubation time for 293T cells was 24 h, for the other three cell lines, 8 h. For sorting by substrate, see fig. 3.8 (p. 101). Additionally to the four peaks of the substances added, peaks of unknown identity were detected at 2-4 and 10-12 min (light and dark gray).

Endogenous 20 α -conversion of progestins

The endogenous conversion was tested in HeLa, HepG2, HEPA1-6 and 293T cells. All cell lines reveal extremely high endogenous conversion rates (see fig. 2.44).

2. Results

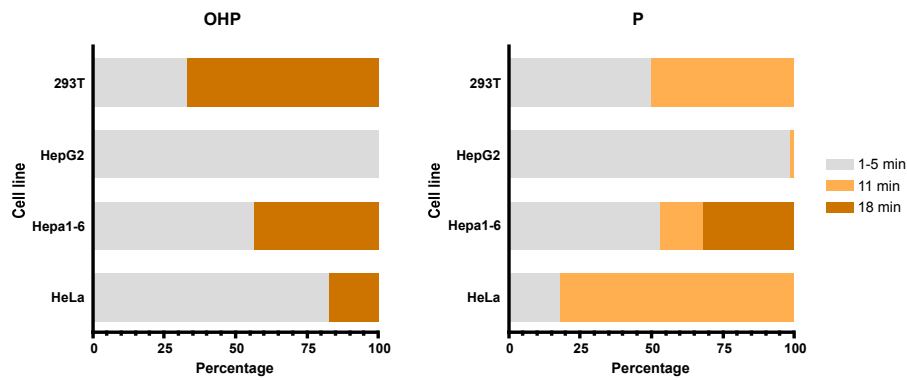


Figure 2.44: Endogenous conversion of 20α -hydroxyprogesterone (left, OHP) and progesterone (P, right) by 293T, HepG2, HEPA1-6, and HeLa cells within 24 h.

In fig. 2.45, the HPLC chromatogram is given for three samples of progesterone (P, shown in green) and 20α -hydroxyprogesterone (OHP, shown in blue). The endogenous conversion does not seem to be completely reproducible: though the same amount of substrate was applied and incubation time was identical, there is no perfect overlay between the three samples for either P or OHP. As the arrows in fig. 2.45 point out the initially applied substrates can not be detected anymore but only reaction products of the substances applied.

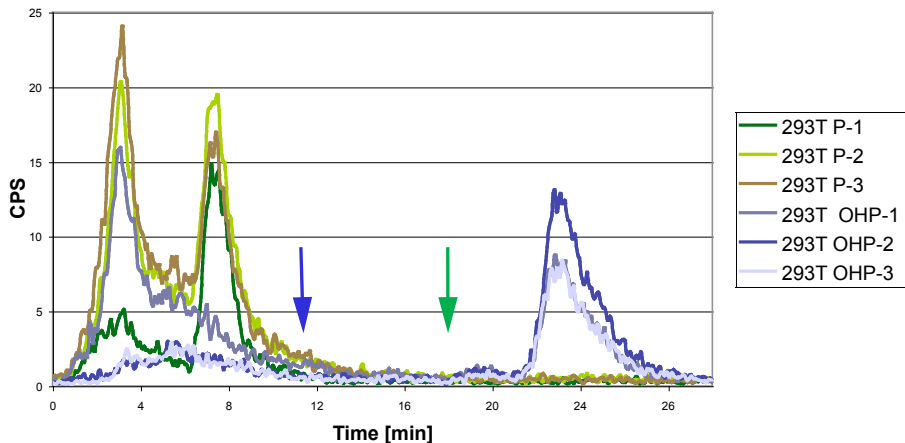


Figure 2.45: Overlay of HPLC chromatograms showing the high endogenous progestin conversion in 293T cells. Three samples of 24h incubation are shown each for 20α hydroxy progesterone (OHP, blue) and progesterone (P, green). The blue arrow points to the retention time of OHP, the green arrow to the progesterone peak. Note that the substrates applied are completely converted after 24 h.

The high conversion rates observed are little surprising, as from progestins, not only the

2.6. Investigation of substrate specificity: test of steroidogenic substrates

sex steroid biosynthesis but also the formation of mineralo- and glucocorticoids starts. In conclusion, the conversion assay presented here is not applicable for testing steroidogenic 20α -conversion.

Endogenous conversion of dihydrotestosterone

Endogenous conversion of dihydrotestosterone (DHT) was tested by 24 h incubation with the same set of cell lines as shown for the other substances, namely, 293T, HepG2, HEPA1-6, and HeLa cells. Fig. 2.46 summarizes the results displaying lowest endogenous conversion of DHT in HeLa cells. Because most suitable for conversion of A, T, E1, and E2, 293T cells were selected for conversion tests.

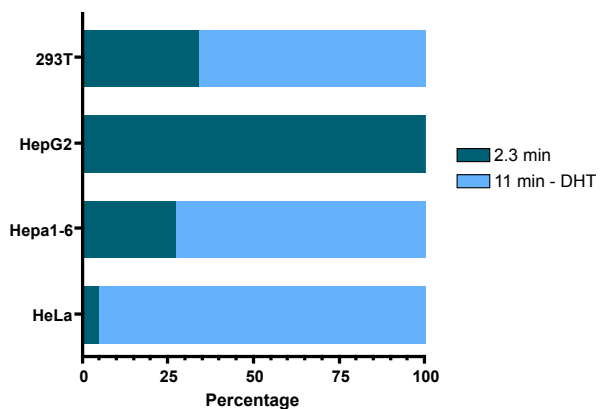


Figure 2.46: Endogenous conversion of dihydrotestosterone (DHT) by 293T, HepG2, HEPA1-6, and HeLa cells within 24 h.

Endogenous conversion of androsterone

293T cells convert approximately 20% of androsterone into androstanediol and a hydroxylated substrate. Fig. 2.47 depicts an exemplary chromatogram. For all other substances tested, 293T cells were found suitable and used for the first set of experiments with any substrate. HeLa cells show approximately the same conversion rates (data not shown). With these cells suitable also for androsterone conversion, no further tests were conducted.

Endogenous conversion of corticosteroids

Corticosteroids are found physiologically in the kidney, as they also regulate water and electrolyte balance. Little surprising, kidney-originating 293 and 293T cells are well prepared for corticosteroid conversion. They exhibited considerable conversion rates (about 10% of corticosterone, 40% of cortisol). HPLC chromatograms of this conversion are shown

2. Results

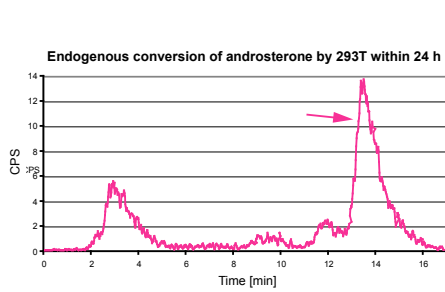


Figure 2.47: HPLC chromatogram showing the endogenous androsterone conversion rates of 293T within 24 h. Arrow points to the androsterone peak (cf. to fig. 2.40).

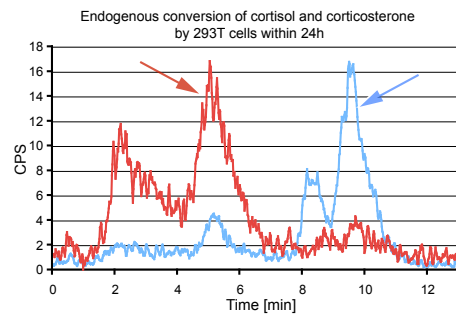


Figure 2.48: Endogenous cortisol (red) and corticosterone (blue) conversion rates of 293T within 24 h. Arrows in the respective colors point to the cortisol and corticosterone peaks (cf. to fig. 2.42).

in fig. 2.48. In order to treat all samples in the same way, corticosteroid conversion was also tested in 293T cells.

Achievements: In the work at hand, a conversion assay was established that allows the measurement of enzymatic activity towards steroid hormones in living cells, that is, under physiological conditions. The assay was shown to work for androstenediol, testosterone, estrone, estradiol, dihydrotestosterone, androsterone, and corticosteroids. Due to the fact that progestins have a key position in the biosynthesis pathway of steroids, they are converted completely within 24 h. Their conversion can thus not be measured by the assay presented.

2.6.3. Conduction of conversion assays for enzymes under investigation

After these tests of endogenous substrate conversion, I transfected pcDNA3 expressing the gene of interest, incubated the cells for 18-24 h so the protein could be built and then added steroids to the culture medium. As described earlier, I chose an incubation time of 24 h for the first tests. To proof the conversion enzymatic, time-course experiments over 84-96 h were conducted taking samples every 12 h after supplementation of substrates. During this time, the conversion curve should approach saturation even at low conversion rates. For substrates with high endogenous conversion rates, the educt decrease was considered rather than the product increase.

Next, Michaelis-Menten kinetics were performed to evaluate K_m and V_{max} . These were performed by incubation of the cells with different substrate concentrations but a constant

2.6. Investigation of substrate specificity: test of steroidogenic substrates

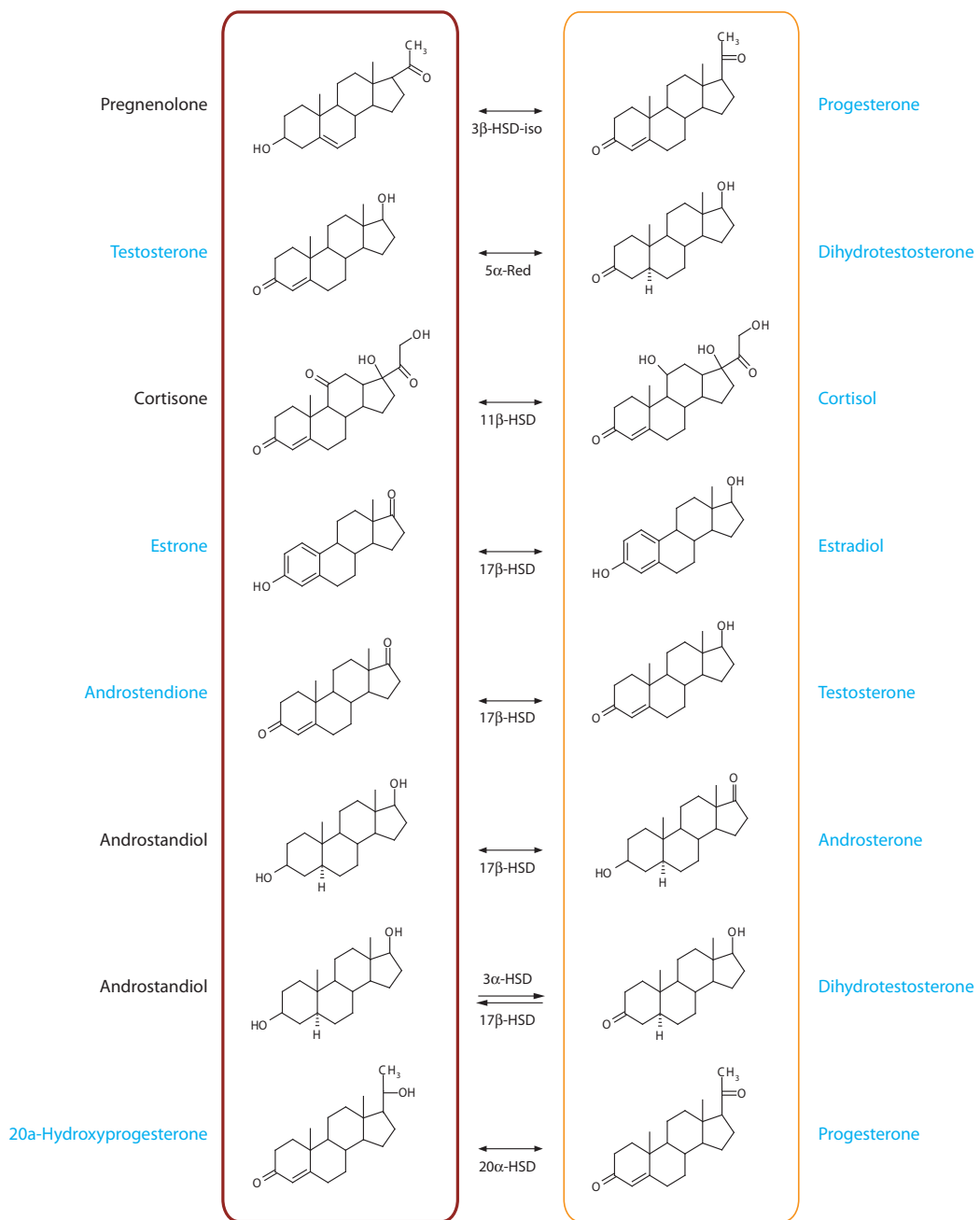


Figure 2.49: Substrates and reactions tested in the work at hand. Substrates printed in blue were available in tritiated form, substrates printed in black were not. Cortisone was not available in tritiated form and therefore was substituted with corticosterone, the rodent counterpart to cortisone. Red framed substrates have little or no biological activity, orange framed substrates depict the biologically active compounds. Interestingly, usually the active form is hydroxylated - the only biologically active ketones are progesterone and androsterone. Androsterone, however is hydroxylated at position 3 of the steroid backbone. (Modified after [2]).

2. Results

incubation time of 24 h. Michaelis-Menten kinetics were set up as shown in fig. 4.4 (p. 147). The results will be shown below. The K_m and V_{max} values presented were calculated with the Enzyme kinetics module to Sigma Plot software. The values were calculated via nonlinear regression fit to curve. All error bars shown in this section depict the standard error of the means (SEM). In order to being able to present comprehensive results, values not fitting the regular equations were forced to fit. The figures therefore represent the best fit to a given model.

On the enzymes under investigation, androgens (androstenedione, testosterone, androsterone, dihydrotestosterone), estrogens (estrone, estradiol), and glucocorticoids (corticosterone, cortisol) were tested (see also fig. 2.49).

2.6.4. Expression plasmids

For the assay in cell culture, the SDRs of interest had to be cloned in an appropriate vector (pcDNA3) and transfected for transient expression. PCR was conducted for amplification of the coding sequences of the proteins under investigation on plasmids from RZPD (cf. to appendix for names) containing a gene under investigation or on cDNA of human (293T, HeLa or HepG2) or the murine cell lines (HEPA1-6). The gained products were cloned into the pcDNA3-vector. Primers and restriction sites used for cloning are depicted in the appendix. All clones were verified by sequencing to enclose the wild-type sequence of the respective mRNAs.

2.6.5. Test of overexpression

As the proteins under investigation were previously uncharacterized, for all but WWOX an antibody does not exist. Due to the native, untagged expression from pcDNA3, RT-PCR was conducted on cDNA of transfected cells to investigate the overexpression of the transfected cDNAs at least on mRNA level. The existence of mRNA may be no proof of protein translation but at least provides a strong hint (see fig. 2.50, p. 61). Primers used as well as the expected product lengths are depicted in the appendix.

As becomes apparent from this figure, all constructs but mSdr-o and MGC4172 are overexpressed. Endogenous expression in mock-transfected cells is seen for all human genes but at much lower amounts than in transfected cells. Instead of untransfected cells, mock-transfected cells were used to exclude influence of transfection on the background level. For hWWOX, overexpression could not undoubtedly be shown. Western blot analysis for the overexpression of this protein was not established.

2.6. Investigation of substrate specificity: test of steroidogenic substrates

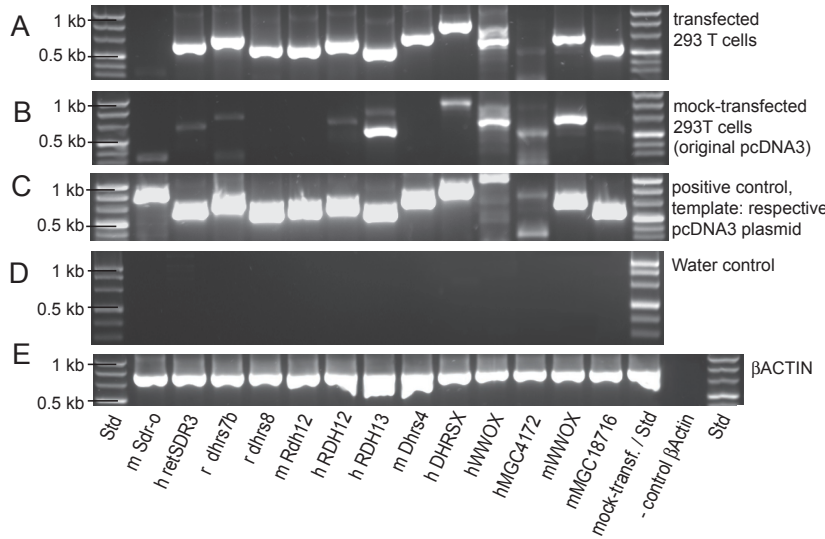


Figure 2.50: Proof of overexpression of the enzymes under investigation on mRNA level. From top to bottom, the following panels are shown: A - Test of overexpression in transfected 293T cells. B - Background level of expression in mock-transfected 293T cells. C - Positive control, performed on the respective pcDNA3 plasmids. D - Negative control, performed without template. E - Control of cDNA synthesis by amplification of human β -actin-cDNA.

2.6.6. Enzymes not converting the tested substrates

None of the enzymes investigated showed activity towards testosterone, cortisol or corticosterone.

- For murine Sdr-o, no conversion could be found. As no mRNA could be detected for that enzyme in fig. 2.50 it remains unclear whether the enzyme would be able to convert the given substrates.
- Both rat enzymes, dhrs7b and dhrs8, show a mRNA level clearly above the background signal in fig. 2.50. The weak bands in untransfected (dhrs7b) or mock-transfected cells (dhrs8) might display the cellular background of the respective homologues. The enzymes, however did not convert any of the given substrates.
- The same holds true for murine Rdh12 and human RDH13. Whether or not these enzymes are restricted to the conversion of retinoids remains unclear from this data.
- No substrate converted by human WWOX could be found. On the other hand, the overexpression of this enzyme could not undoubtedly be shown. The question whether WWOX has catalytic activity and towards which substrate could therefore not be answered in the work at hand.

2. Results

- Both MGC4172 and MGC18716 did not show activity towards any of the given substrates. The MGC4172 containing pcDNA3-plasmid does not seem to produce a mRNA. It is therefore unclear whether the enzyme does not convert the given substrates. For MGC18716, no conversion could be shown. This construct does however produce mRNA clearly above the endogenous cellular level.

In the following, the enzymes that showed activity towards one or more of the tested substrates will be described. Substrates that are not converted, will not be mentioned. All results are summarized in tables 2.11 (substrate conversion) and 2.12 (Michealis-Menten kinetics). Evaluated constants for each enzyme are shown in tables.

2.6.7. Human retSDR3 oxidizes 17β -estradiol to estrone

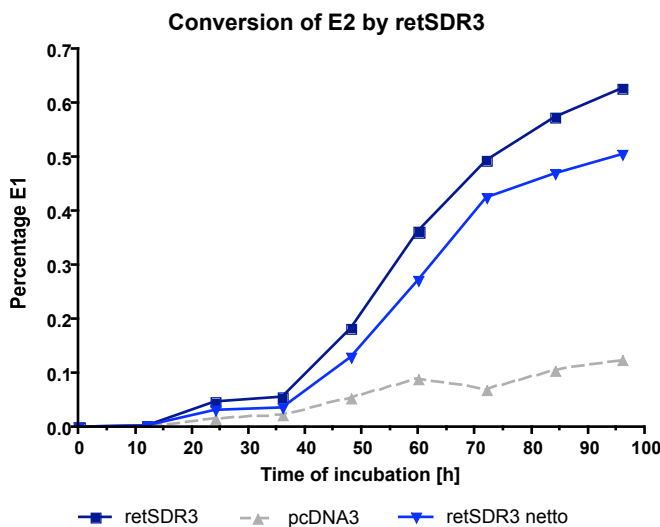


Figure 2.51: Time-course experiment showing the conversion of estradiol to estrone by retSDR3. Brutto conversion is depicted in dark blue, background (pcDNA3-transfected 293T cells) is given in gray. The retSDR3 netto conversion is depicted in light blue. Error bars show the standard deviation of the means.

I could show that under physiological conditions applied in the assay used, human retSDR3 can oxidize 17β -estradiol to estrone. In fig. 2.51, the results of the 96h-time-course experiment are given.

Though conversion takes place only at low rates, it is saturable over time. Within 96 h, retSDR3 converts about 50% of the tritiated estradiol added. Interestingly, conversion rate increases from 36 h on. This could be due to several reasons: first, expression of retSDR3 is slow in 293T cells. Second, the increase 36h after addition of the substrate is due to the fact that considerably more cells express retSDR3 as 36 h equals approximately

2.6. Investigation of substrate specificity: test of steroidogenic substrates

two doubling times of these cells. As shown in fig. 2.51, retSDR3 converts 17β -estradiol to estrone but not with a very high efficiency. The reaction appears to be quite slow and begins to saturate only after 70 h.

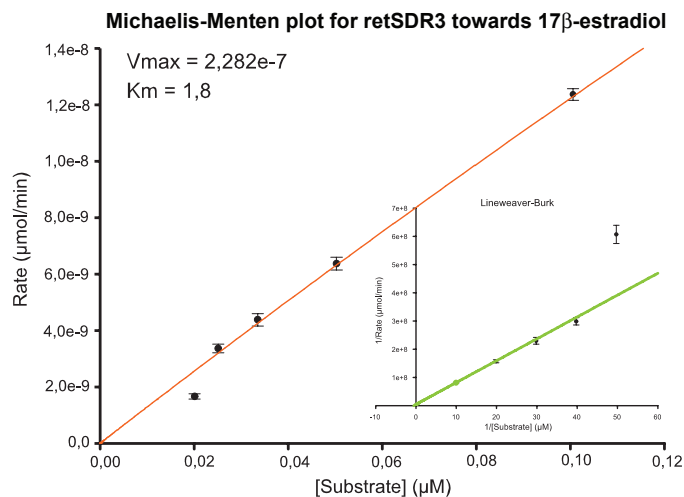


Figure 2.52: Michaelis-Menten and Lineweaver Burk plot for the conversion of estradiol by retSDR3. Error bars depict \pm SEM values.

2.6.8. Human RDH12, human DHRSX, and murine Dhrs4 reduce dihydrotestosterone to androstanediol

Table 2.7: Michaelis-Menten constant (in μM) and maximum velocity ($\mu\text{mol}/\text{min}$) for estradiol conversion by retSDR3.

	E2
K_m	1.8
V_{\max}	2.3×10^{-7}

Within the 293T cells quite high endogenous conversion of dihydrotestosterone can be observed (see fig. 2.46, p. 57). Fig. 2.53 depicts the HPLC chromatograms of a time-course experiment with human RDH12 transfected cells for dihydrotestosterone (DHT) conversion.

Fig. 2.53 depicts the different chromatograms seen on HPLC from the time-course experiment for DHT conversion by RDH12. The increase of hydroxylated substances is higher in transfected than in untransfected cells, while

the product of the conversion, androstanediol, stagnates. It thus seems that androstanediol is preferentially hydroxylated in comparison with DHT. The same holds true in case of DHRSX and murine Dhrs4 (data not shown). For these three enzymes (but not for the rest of enzymes under investigation - not shown) DHT conversion was significantly increased in comparison to mock-transfected cells (pcDNA3, see fig. 2.53). It was concluded that the measurements can distinguish this conversion from the endogenous one.

2. Results

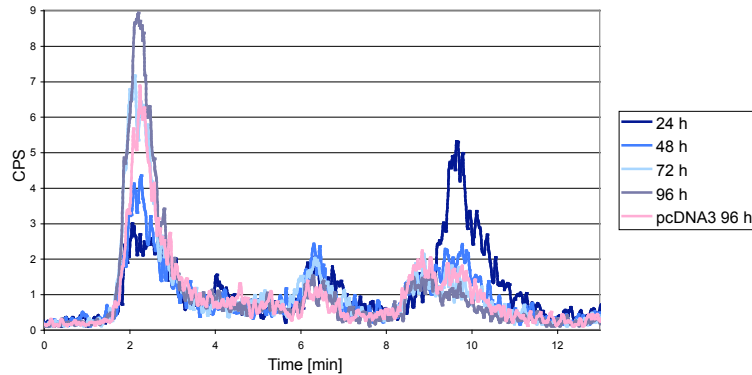


Figure 2.53: HPLC chromatograms of the time-course experiment with human RDH12-transfected 293T-cells. RDH12 samples are depicted in different shades of blue, background conversion after 96 h is given in pink. Retention time of dihydrotestosterone is 10 min, of androstanediol 7 min. The substance detected at 2 min is a product of endogenous conversion as described before.

Due to the hydroxylation of androstanediol and dihydrotestosterone, the increase of the product can not be shown in fig. 2.54. Therefore, the decrease of DHT is depicted. For easier overview, values were depicted as difference from 100% DHT applied.

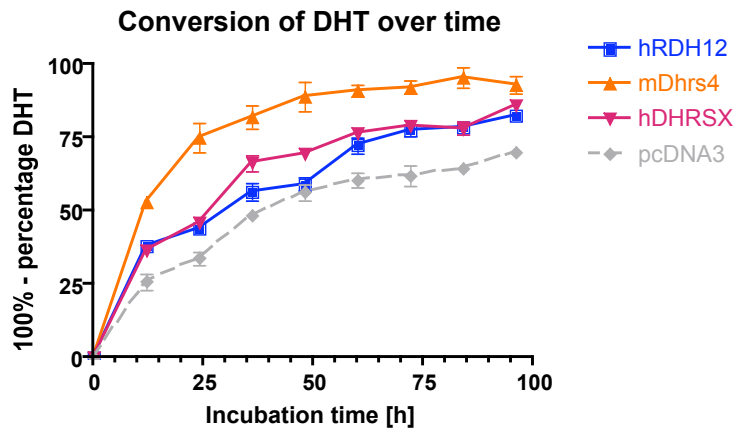


Figure 2.54: Results of the time-course experiment for dihydrotestosterone (DHT) conversion. For all three enzymes (mDhrs4 - orange, hDHRSX - red, hRDH12 - blue), there is more decrease in substrate than for mock-transfected cells (pcDNA3 - gray). Error bars show the standard deviation of the means.

Converting dihydrotestosterone (DHT) with different efficiencies: human DHRSX, human RDH12 and murine Dhrs4

For all three enzymes found to be capable of DHT conversion, the reactions were found saturable over time (cf. to fig. 2.54). Murine Dhrs4 displayed the highest rates, while hDHRSX and hRDH12 converted very similar amounts of DHT. DHRSX displayed mini-

2.6. Investigation of substrate specificity: test of steroidogenic substrates

mally higher rates. While the Michaelis-Menten constant for hDHRSX could be deduced directly from the conversion values examined, mDhrs4 and hRDH12 values had to be forced to the equations.

Table 2.8: Values of Michaelis-Menten constant (in μM) and maximum velocity for DHT conversion ($\mu\text{mol}/\text{min}$).

	mDhrs4*	hDHRSX	hRDH12*
K_m	2.7	1.8	1.6
V_{\max}	$1.2 \cdot 10^{-6}$	$3.8 \cdot 10^{-7}$	$3.7 \cdot 10^{-7}$

For enzymes depicted with *, values were forced to fit the equations.

For human RDH12, the model does not seem to fit the equation very well. This could be due to enzymatic conversion that does not follow Michaelis-Menten kinetics or to the amount of substrate given. The values calculated are depicted in table 2.8. These results reflect the findings from fig. 2.54 very well.

When comparing the V_{\max} values of the three enzymes, it becomes apparent

that the one of mDhrs4 is about 3.3 times higher than the one of hDHRSX and 3.2 times higher than of hRDH12. Obviously, of the three enzymes hRDH12 has the highest affinity towards DHT. K_m is defined as the substrate concentration, where 50% of V_{\max} is reached. It will thus reach this point at the lowest concentration (of these three enzymes). Depending on the substrate concentration present, the different enzymes have advantages: with a low concentration of DHT, human DHRSX and hRDH12 can already reach maximum velocity. For efficient conversion of high amounts of DHT however, mDhrs4 will be faster in solving the task.

2.6.9. Murine Dhrs4 has reductive enzymatic activity not only versus dihydrotestosterone but also towards androstenedione and estrone

Murine Dhrs4 was found to convert, besides dihydrotestosterone (DHT) to androstanediol, estrone (E1) to estradiol (E2) and androstenedione (A) to testosterone (T) (see fig. 2.56).

The reaction of E1 to E2 can be conducted highly efficient with a netto conversion of 50% estrone within 36 h. Testosterone formation takes longer time, with only 45% netto substrate conversion after 96 h. There are other enzymes described to possess substrate specificities towards estrone and androstenedione, for example murine 17β -HSD1. In summary, mDhrs4 is a newly identified 17β -HSD.

Michaelis-Menten kinetics for murine Dhrs4

I could show that murine Dhrs4 is able to convert estrone to 17β -estradiol and at lower rates also converts androstenedione to testosterone and dihydrotestosterone to androstanediol. Table 2.9 summarizes the values deduced.

2. Results

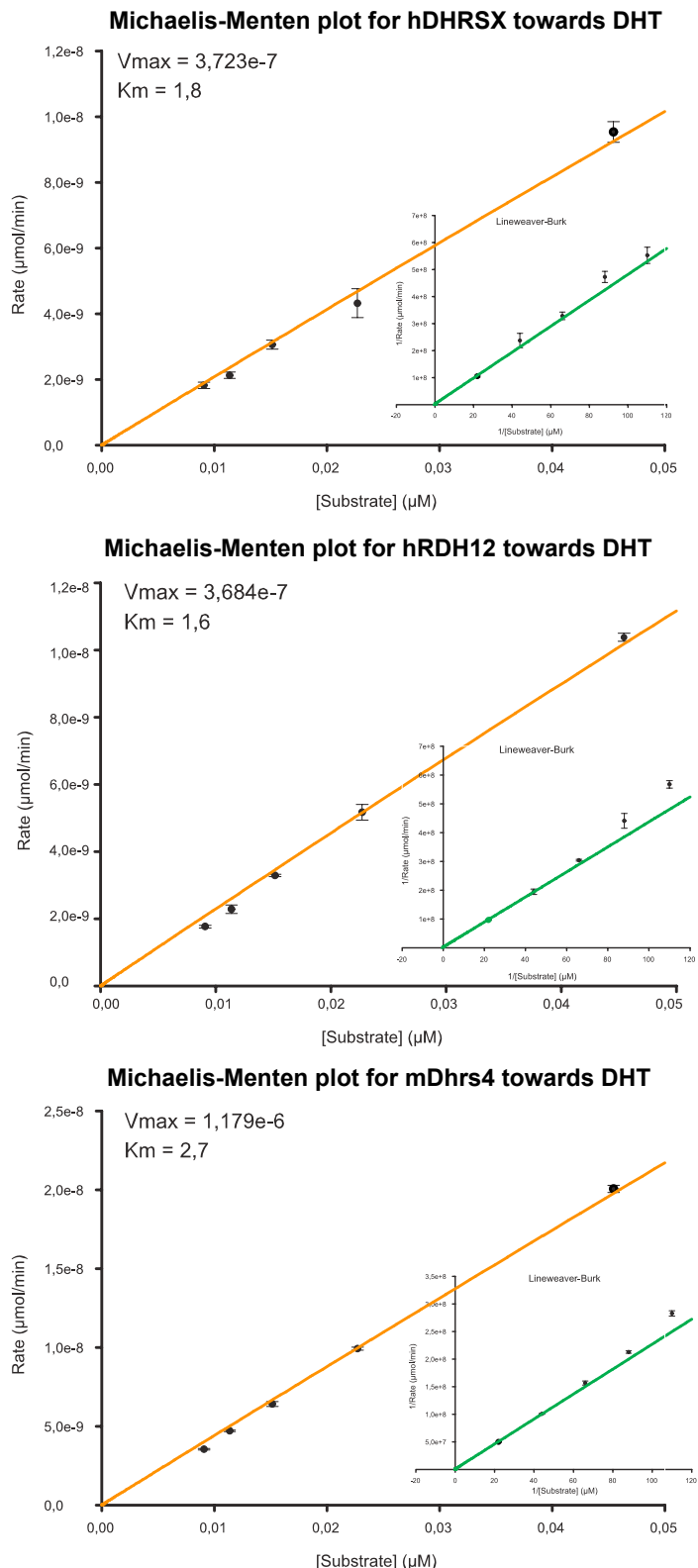


Figure 2.55: Michaelis-Menten and Lineweaver Burk plots for the conversion of dihydrotestosterone (DHT) by human DHRSX (top), human RDH12 (middle), and murine Dhrs4. Results for hRDH12 and mDhrs4 had to be forced to the curve. Error bars depict $\pm \text{SEM}$ values.

2.6. Investigation of substrate specificity: test of steroidogenic substrates

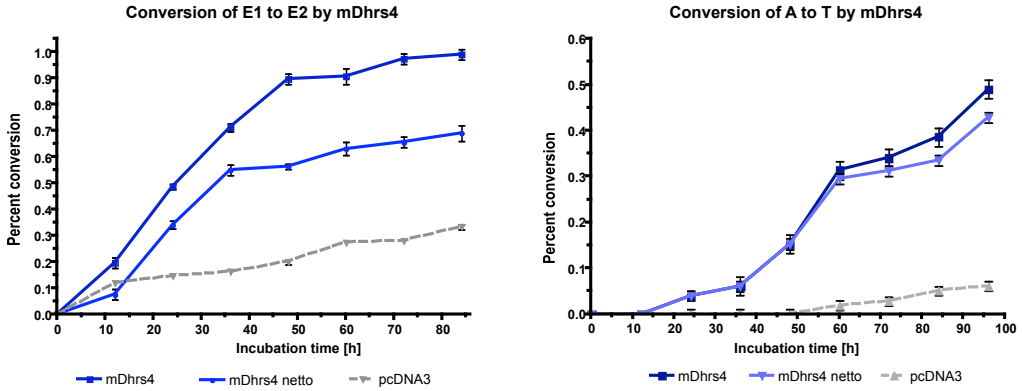


Figure 2.56: Conversions of estrone (E1) to estradiol (E2, left) and androstenedione (A) to testosterone (T, right) by mDhrs4 over time. Background activity of mock-transfected cells is depicted in gray, brutto conversion in dark blue and netto conversion in light blue. Error bars show the standard deviation of the means.

Table 2.9: Values of Michaelis-Menten constant (in μM) and maximum velocity ($\mu\text{mol}/\text{min}$) for conversions conducted by mDhrs4.

	E1	A*	DHT*
K_m	4.3	0.4	2.7
V_{max}	$1.6 \cdot 10^{-6}$	$1.9 \cdot 10^{-8}$	$1.2 \cdot 10^{-6}$

For substrates depicted with *, values were forced to fit the equations.

constant and maximum velocity for the conversion of androstenedione to testosterone. The Michaelis-Menten constant of $0.4 \mu\text{M}$ is about 10% of the one for E1 conversion. Maximum velocity of the conversion was calculated to be $1.9 \cdot 10^{-8} \mu\text{mol}/\text{min}$. This seems to reflect the findings from fig. 2.56 which shows a slower conversion of A than of E1. For the evaluation, results had to be forced to the equation. This could be due to the high deviation for the values of the lowest concentration (see Lineweaver Burk plot, highest value). If the calculations could be performed better with another fitting model should be checked in the future.

For the conversion of dihydrotestosterone (see fig. 2.55), values had to be forced to the equation as well. This seems surprising as the values depict a straight line. However, measurements should be repeated here as well with lower concentrations of substrate. Preliminary values for K_m and V_{max} are $2.7 \mu\text{M}$ and $1.2 \cdot 10^{-6} \mu\text{mol}/\text{min}$. Evaluating the Michaelis-Menten plot, it seems that the reaction velocity is already approaching

In fig. 2.57, Michaelis-Menten kinetics for formation of 17β -estradiol from estrone by mDhrs4 are shown in the upper half. K_m was found to be at a concentration of $4.3 \mu\text{M}$. V_{max} of the conversion is $1.6 \cdot 10^{-6} \mu\text{mol}/\text{min}$. This value of K_m , though preliminary, would point to a quite low affinity of murine Dhrs4 towards estrone.

The lower panel of this figure depicts the evaluation of Michaelis-Menten con-

2. Results

saturation.

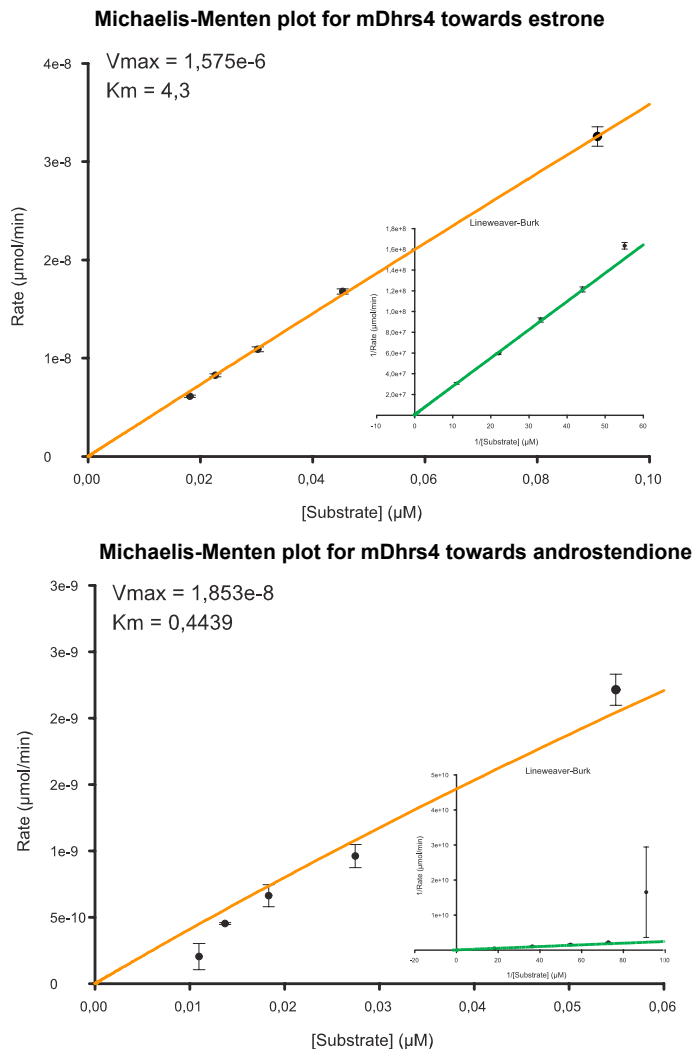


Figure 2.57: Michaelis-Menten and Lineweaver Burk plots for the conversions towards estrone (top) and androstenedione (bottom) conducted by mDhrs4. The results for the androstenedione conversion had to be forced to the curve. Error bars depict \pm SEM values.

2.6.10. Murine Wwox reduces androstenedione to testosterone and androsterone to androstanediol

In contrast to the human homologue, I could show that murine Wwox possesses reductive activity towards two 17β hydroxysteroids. It can convert androstenedione to testosterone at a very low rate and androsterone to androstanediol at higher rates (see fig. 2.58).

Similar as for retSDR3, enzymatic activity drastically increases after about 36 h of

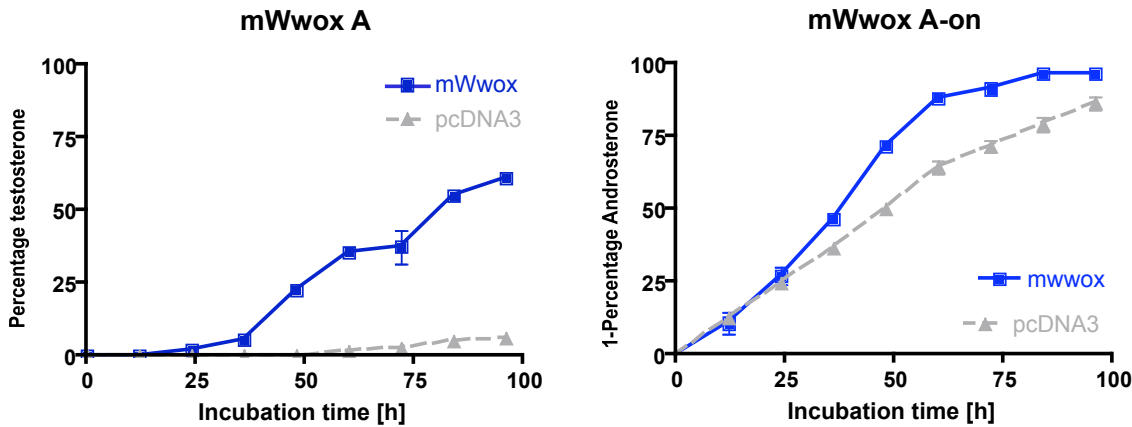


Figure 2.58: Conversions of androstenedione (A, left) and androsterone (A-on, right) by mWwox over time. Background conversion of mock-transfected cells is depicted in gray, brutto conversion in dark blue and netto conversion in light blue. Error bars depict the standard error of the means.

incubation. Between 36 and 96 h, the reaction seems to reach saturation. Also for murine Wwox, it would be wise to repeat the experiments with longer time gaps between transfection and addition of the substrate.

The conversion of androsterone to androstanediol, on the other hand seems to have an overall higher conversion rate but is, indeed lower over the time evaluated as the mock-transfected cells display much higher background. Still, the reduction of androsterone is saturable over time. For better overview, the difference between initial substrate amount (100%) and the amount of substrate measured at the given time points is depicted, resulting in an increasing curve. These data suggest that murine Wwox has a preference for androgens. Further tests on more androgenic substances should be conducted, maybe then the substrate for human WWOX could also be found.

Table 2.10: Values of Michaelis-Menten constant (in μM) and maximum velocity ($\mu\text{mol}/\text{min}$) for conversions conducted by mWwox.

	A*	A-on
K_m	0.7	2.2
V_{max}	$5.3 \cdot 10^{-8}$	$6.6 \cdot 10^{-7}$

For substrates depicted with *, values were forced to fit the equations.

Michaelis-Menten kinetics

By application of the conversion assay established in the work at hand and when overexpressing murine WW-Box containing oxidoreductase (mWwox), I found that this enzyme is capable of reducing two androgens, androstenedione to testosterone and androsterone to androstanediol. From fig. 2.58 it is difficult to deduce towards which substrate this enzyme displays higher activity due to the high background conversion of androsterone by

2. Results

293T cells. Michaelis-Menten kinetics should also address this matter.

Fig. 2.59 depicts the results of these experiments; table 2.10 summarizes the values calculated. Murine Wwox displays a higher affinity towards androstenedione than towards androsterone (K_m of 0.70 and 2.2 μM , respectively) but converts this substrate with a much lower maximum velocity: towards androstenedione it is 12 times lower than towards androsterone. This appears in line with the lower netto conversion of androsterone by mWwox in living cells (see fig. 2.58). Though complex to deduce from this figure, it seems androstenedione would be preferred to androsterone.

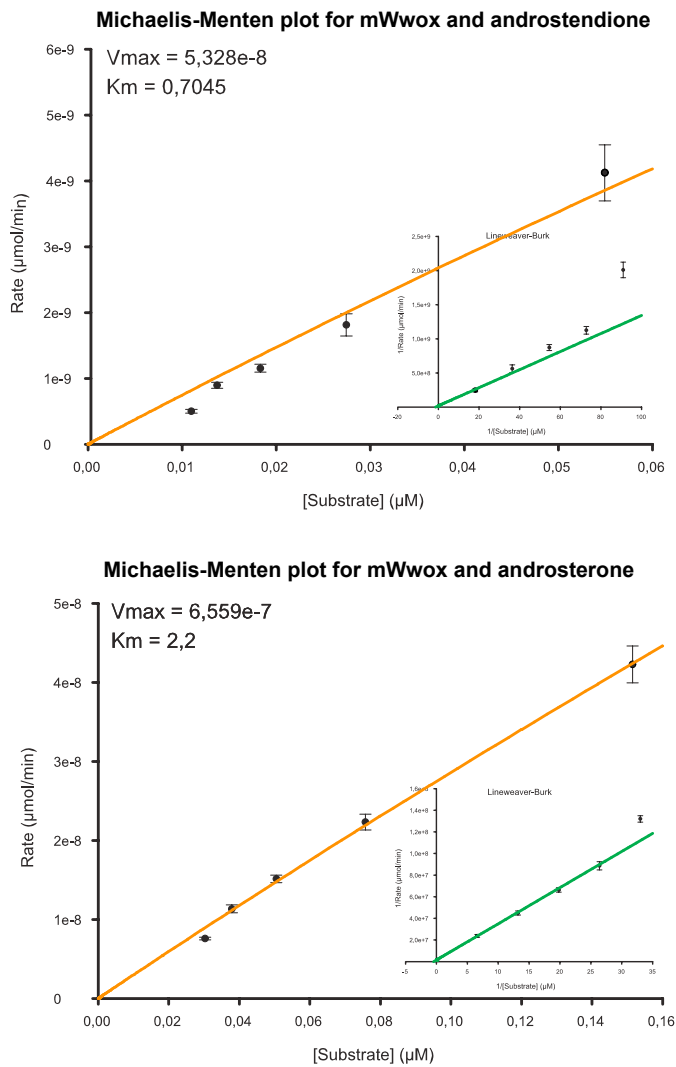


Figure 2.59: Michaelis-Menten and Lineweaver Burk plots for the conversions of androstenedione (top) and androsterone (bottom) by murine Wwox. Results for androstenedione had to be forced to the curve. Error bars depict $\pm \text{SEM}$ values.

Achievements: Five of 13 identified SDRs were shown to possess converting activities towards the steroid hormones tested. These were: human retSDR3 (E2), human RDH12 (DHT), murine Dhrs4 (A, E1, DHT), human DHRSX (DHT), and murine WWOX (A, A-on).

Table 2.11 summarizes the results of the substrate conversion assays. As the conversion assay was found to be not applicable progestins are not listed.

I was able to show that Michaelis-Menten kinetics are applicable with the conversion assay established and presented here. For the enzymes where substrate conversion was shown, the kinetics were performed. Table 2.12 summarizes the values found for Michaelis-Menten constant and maximum velocities.

Table 2.11: Summary of the results from substrate conversion assays.

	A	T	A-on	DHT	E1	E2	C-on	C-ol
mSdr-o	-	-	-	-	-	-	-	-
hretSDR3	-	-	-	-	-	+	-	-
rat dhrs7b	-	-	-	-	-	-	-	-
rat dhrs8	-	-	-	-	-	-	-	-
mRdh12	-	-	-	-	-	-	-	-
h RDH12	-	-	-	+	-	-	-	-
hRDH13	-	-	-	-	-	-	-	-
m Dhrs4	+	-	-	+	+	-	-	-
hDHRSX	-	-	-	+	-	-	-	-
MGC4172	-	-	-	-	-	-	-	-
MGC18716	-	-	-	-	-	-	-	-
hWWOX	-	-	-	-	-	-	-	-
mWwox	+	-	+	-	-	-	-	-

Abbreviations: A - androstenedione, A-on - androsterone, DHT - dihydrotestosterone, C-on - corticosterone, C-ol - cortisol, E1 - estrone, E2 - estradiol, T - testosterone.

2.7. Investigation of subcellular localization

For analysis of the subcellular localization, two methods were applied. First, subcellular localization was predicted bioinformatically by use of several servers that are publicly available through the world wide web. The CDS of the genes under investigation were then cloned into appropriate vectors (see below) and the sequence verified. Plasmids with the correct inserts were then transfected into HeLa cells, incubated and stained as described in section 4.2.5 (p. 132).

2. Results

Table 2.12: Summary of the results from Michaelis-Menten kinetics in living cells.

enzyme	substrate	K _m (μ M)	V _{max} (μ mol/min)
mDhrs4	E1	4.30 \pm 6.24*10 ⁻²	1.58*10 ⁻⁶ \pm 2.88*10 ⁻⁸
mDhrs4	A*	0.44 \pm 1.18*10 ⁻²	1.85*10 ⁻⁸ \pm 1.00*10 ⁻⁹
mDhrs4	DHT*	2.67 \pm 2.97*10 ⁻²	1.18*10 ⁻⁶ \pm 1.70*10 ⁻⁸
hDHRSX	DHT	1.78 \pm 2.74*10 ⁻²	3.72*10 ⁻⁷ \pm 1.05*10 ⁻⁸
h RDH12	DHT*	1.60 \pm 2.10*10 ⁻²	3.68*10 ⁻⁷ \pm 7.24*10 ⁻⁹
mWwox	A*	0.70 \pm 2.37*10 ⁻²	5.33*10 ⁻⁸ \pm 3.10*10 ⁻⁹
mWwox	A-on	2.19 \pm 2.55	6.56*10 ⁻⁷ \pm 7.24*10 ⁻⁷
retSDR3	E2	1.77 \pm 3.71*10 ⁻²	2.28*10 ⁻⁷ \pm 6.54*10 ⁻⁹

Values where substrates are depicted with * did not converge and were forced to fit the equations. Deviations are depicted as \pm SEM values. Abbreviations: E1 - estrone, A - androstenedione, DHT - dihydrotestosterone, A-on - androsterone, E2 - estradiol

2.7.1. Bioinformatic means to predict subcellular localization

On the world wide web, there are various public servers available which allow the prediction of subcellular localization of a given protein sequence. These tools have become a popular means to get a first hint about an enzyme's subcellular localization. Five of these servers were selected and used for the prediction of subcellular localization of the enzymes under investigation in the work at hand. The servers used are depicted in table 5.1 (p. 152). All servers used but one give the probabilities calculated according to the algorithm underlying in percent. For the LOCtree server, however, predicts the most likely result on a scale from 1 to 10 according to reliability with 10 being the maximum. In each section, I will first show the results of the different servers used and then present experimental data.

2.7.2. Vectors and system of analysis

For the investigation of subcellular localization, vectors were chosen from which the respective enzymes can be expressed as recombinant proteins in fusion with green fluorescent protein, GFP. In order to avoid masking of the terminal signal sequences, for each of the proteins two constructs, one with N- and and one with C-terminally located GFP were cloned. Alternatively, some constructs were also cloned into pcDNA4 myc-his version B, adding a C-terminal myc-his tag to the protein. Primers and restriction sites used are depicted in the appendix.

First, I transfected the original pEGFP-C2 and pAcGFP1-N1 vectors for detection of localization of the fluorescent proteins alone. pEGFP-C2 codes for protein expression with a fluorescent GFP at the N-terminus of the protein under investigation (that is, the

2.7. Investigation of subcellular localization

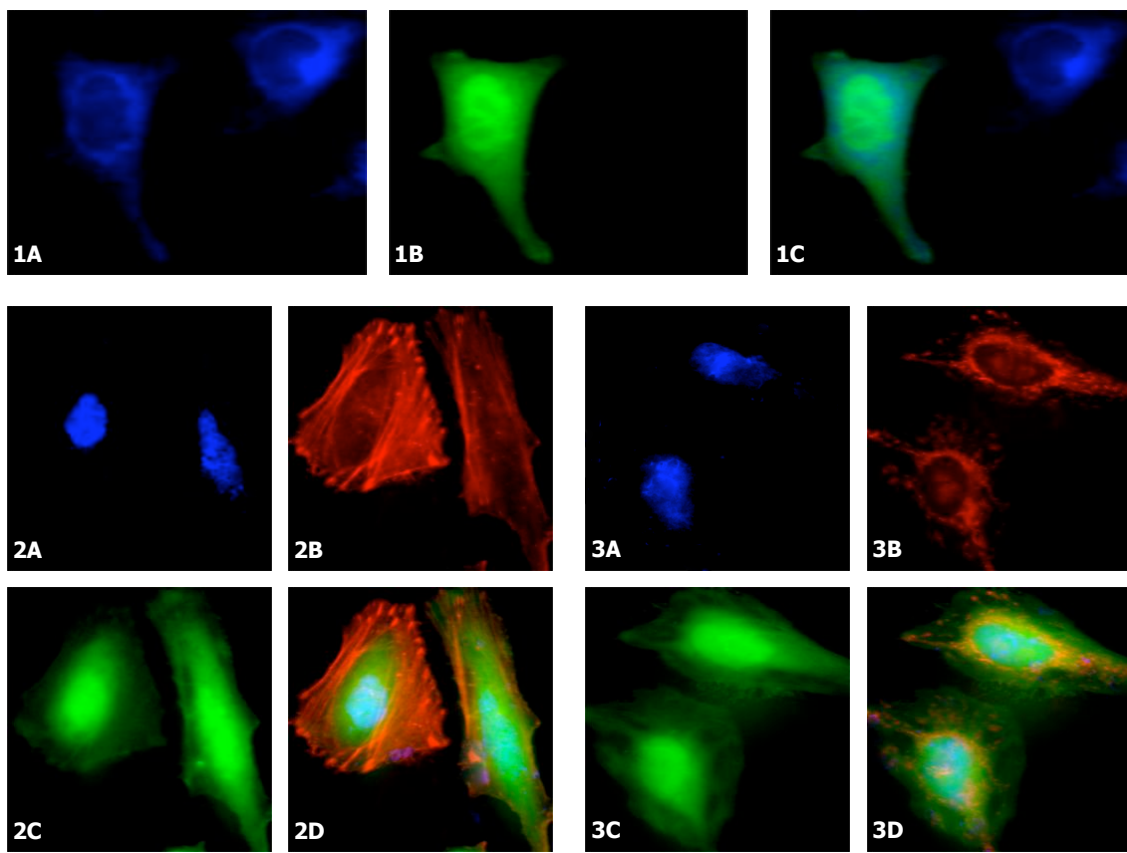


Figure 2.60: Detection of GFP expressed from pEGFP-C2 vector displaying cytosolic distribution. All images were stained as the respective images in fig. 2.61. In contrast, a nontransfected cell is seen only in panel 1 in the upper left corner.

protein under investigation is cloned to the C-terminus of GFP). In pAcGFP1-N1, the recombinant protein expressed consists of the enzyme under investigation N-terminally with GFP fused to its C-terminus (that is, the protein is cloned to the N-terminus of GFP). As proteins without a specific signal sequence are found in the cytoplasm, I also wanted to control the cytosolic distribution of GFP expressed from these vectors. Fig.s 2.60 and 2.61 show the results from these experiments. Counterstaining of endoplasmic reticulum, mitochondria, and f-actin was conducted. The phalloidin staining of f-actin is useful because cytoskeletal proteins outline the extensions of the cell.

For each of these vectors, the following panels are shown:

1. Panel 1 depicts counterstaining with ER-Tracker where 1A shows only ER-Tracker, 1B depicts the GFP detected and 1C gives an overlay of the two images shown.
2. Panel 2 depicts counterstaining with phalloidin and DAPI. Phalloidin is a fungal toxin which associates with f-actin. Image 2A depicts DAPI staining of the nucleus, 2B shows red staining of f-actin with phalloidin, 2C shows GFP distribution in the

2. Results

cell, and 2D shows an overlay of the pictures A to C. For cytosolic proteins, phalloidin staining will be shown.

3. Panel 3 depicts counterstaining with Mito-Tracker and DAPI. Image 3A depicts DAPI staining of the nucleus, 3B shows red staining of the mitochondria, 3C shows GFP distribution in the cell, and 3D shows an overlay of the pictures A to C.

The distribution of GFP expressed both from pEGFP-C2 and pAcGFP1-N1 is clearly cytoplasmic. By use of these vectors, I could also establish the staining procedures for further usage on the enzymes under investigation in this thesis. These figures are also exemplarily shown for the staining experiments conducted with the enzymes under investigation. For these enzymes, only the panels depicting co-localization will be shown.

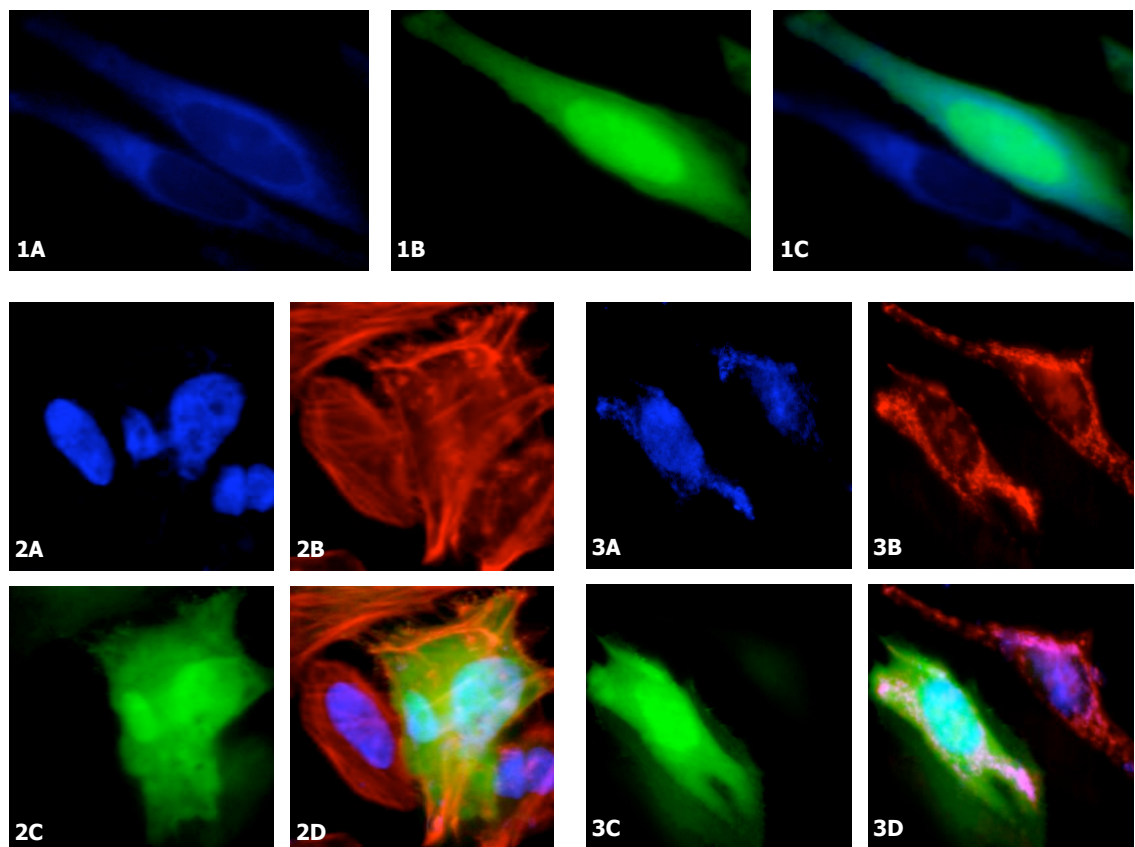


Figure 2.61: Detection of GFP expressed from pAcGFP1-N1 vector displaying cytosolic distribution. All panels show transfected and nontransfected cells in comparison. 1A-1C: ER counterstaining with A = ER, B = GFP, C = Merge; 2A-D: F-actin and nuclear counterstaining. A: DAPI - nuclear counterstaining, B: phalloidin - f-actin counterstaining, C: GFP, D: Merge. 3A-D: mitochondrial and nuclear counterstaining. A: DAPI - nuclear counterstaining, B: mitochondrial counterstaining, C: GFP, D: Merge.

2.7.3. Murine Sdr-o is a mitochondrial protein

Table 2.13: Bioinformatic predictions of the subcellular localization of mSdr-o.

Server	mSdr-o
pSORTII	73.9% cytoplasmic, 13.0% mitochondrial, 8.7 % nuclear, 4.3% vesicles of secretory system
pTarget	Mitochondria 75.1%
SubLoc 1.1	56% cytosolic
TargetP 1.1	14.7% mitochondrial, 8.5% secretory, 82.8% other
LOCtree	cytoplasmic 1

Table 2.13 depicts the results of the bioinformatic predictions on the subcellular localization of murine orphan SDR (mSdr-o). When comparing these results, it is obvious that the results between the servers differ considerably. Only pTarget correctly predicted the localization of murine orphan SDR as mitochondrial as is shown from the experimental data.

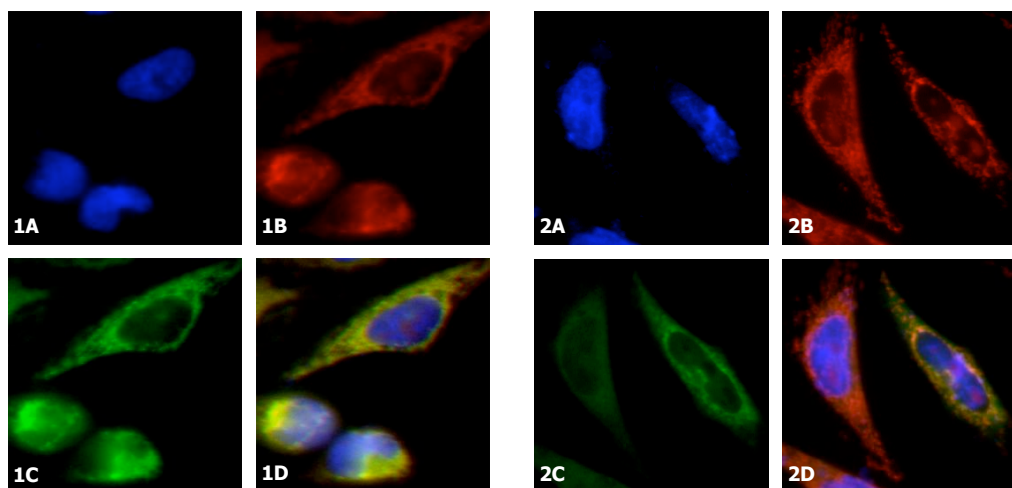


Figure 2.62: Mitochondrial localization of murine Sdr-o shown from two vectors, pAcGFP1-N1 (panel 1) and pcDNA4 myc-his Version B (panel 2). In each panel, the pictures depict: A: nuclear staining with DAPI, B: mitochondrial, 1C: GFP, 2C: detection of the myc tag, D: Overlay of the respective images A-C.

When expressed with a N-terminally fused EGFP (from pEGFP-C2), murine Sdr-o shows cytoplasmic distribution (not shown). However, with a C-terminal tag (regardless of this tag being AcGFP or myc-his), murine Sdr-o is imported to mitochondria. Fig. 2.62 shows the colocalization of murine Sdr-o with a C-terminal tag (panel 1: AcGFP,

2. Results

panel 2: myc-his). When counterstaining ER, no overlay between mSdr-o and endoplasmic reticulum could be detected (not shown). In conclusion, mSdr-o possesses a mitochondrial import signal probably N-terminally located.

2.7.4. Human retSDR3 localizes to the cytoplasm

In case of human retSDR3, again there is no clear preference for mitochondrial or cytoplasmic distribution of the protein when conducting bioinformatic predictions (cf. to table 2.14).

Table 2.14: Bioinformatic predictions of the subcellular localization of human retSDR3.

Server	hretSDR3
pSORTII	52.2% cytoplasmic, 17.4% mitochondrial, 17.4% nuclear, 4.3% vesicles of secretory system, 4.3% endoplasmic reticulum
pTarget	75.1% cytoplasmic
SubLoc 1.1	50% mitochondrial
TargetP 1.1	42.9% mitochondrial, 4.1% secretory, 45.6% other
LOCtree	cytoplasmic 3

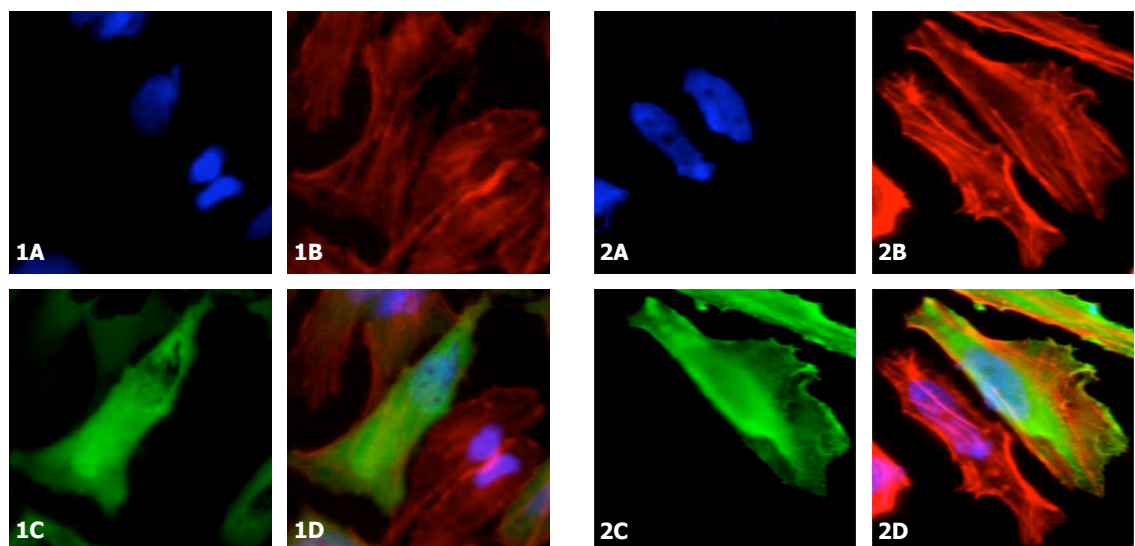


Figure 2.63: Cytosolic localization of human retSDR3 in HeLa cells. Panels 1 (expression from pEGFP-C2) and 2 (expression from pcDNA4 myc-his) show: A nuclear counterstaining using DAPI, B f-actin counterstaining with phalloidin, C localization of recombinant retSDR3, D Merge of images A-C.

Three servers were able to correctly predict the localization of retSDR3: pSORTII, pTarget and LOCtree, though the latter displayed only low reliability. Fig. 2.63 shows

the results from the staining experiments with phalloidin counterstaining. When expressing human retSDR3 in cell culture either with N-terminally fused EGFP (panel 1) or C-terminally fused myc-his tag (panel 2) both recombinant proteins show cytoplasmic distribution.

2.7.5. dhrs7b from rat is localized in the endoplasmic reticulum

Table 2.15: Bioinformatic predictions for the subcellular localization of rat dhrs7b.

Server	rat dhrs7b
pSORTII	39.1% cytoplasmic, 30.4% mitochondrial, 8.7% vacuolar, 8.7% extracellular, incl. cell wall, 8.7% endoplasmic reticulum, 4.3% nuclear
pTarget	75.1% cytoplasmic
SubLoc 1.1	50% mitochondrial
TargetP 1.1	42.9% mitochondrial, 4.1% secretory, 45.6% other
LOCtree	cytoplasmic 3

Table 2.15 depicts the results from bioinformatic predictions for the subcellular localization of rat dhrs7b. Again, most servers predict the enzyme to be cytoplasmic or mitochondrial. TargetP1.1 gives a probability of 45.6% for the enzyme to be non-mitochondria and non-secretory.

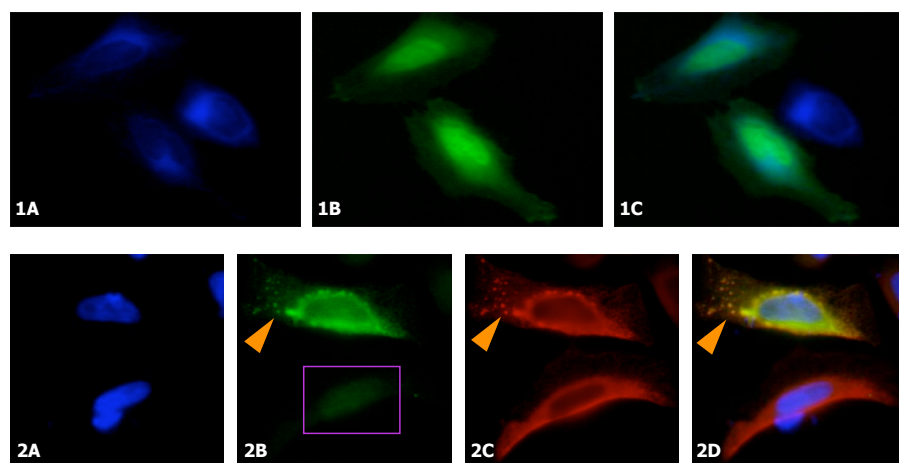


Figure 2.64: Rat dhrs7b colocalizes with ER counterstaining when expressed from pcDNA4 myc-his Version B. Panel 1: expression from pEGFP-C2 and counterstaining with ER-Tracker (A: ER-tracker, B: GFP, C: overlay). Panel 2: from pcDNA4 myc-his Version B (A: DAPI nuclear counterstaining, B: detection of myc-tagged rat dhrs7b, C: N-FLAG sarcolipin detection - ER staining, D: overlay). Arrowheads: overlap of ER and dhrs7b. Purple box: myc-background staining.

2. Results

Both in counterstaining with phalloidin and MitoTracker, no co-localization could be observed for rat dhrs7b (not shown). Further counterstaining experiments were therefore conducted. Both constructs of rat dhrs7b (in pEGFP-C2 - see fig. 2.64, top panel and in pcDNA4 myc-his - fig. 2.64, bottom) were ER-counterstained. The pEGFP-C2-expressed protein again showed cytoplasmic distribution (counterstaining by ER Tracker). In case of expression from pcDNA4 myc-his staining (detection of myc-tag, shown in red: image C) Er was counterstained by co-overexpression of N-FLAGed rabbit sarcolipin (NFSLN, FLAG-tag detection, lower panel, image B). From the colocalization of both proteins, it became apparent that the enzyme is ER localized. Especially when comparing images 2B and 2C, the same pattern of spots can be seen in the top left corner (orange arrowhead).

One more issue is interesting to note in fig. 2.64: the purple box in image 2b depicts the staining background caused the myc-epitope antibody. The lower cell shows weak nuclear staining caused by detection of the cellular c-myc-protein which is localized in the nucleus.

2.7.6. Rat dhrs8 is an ER-localized SDR enzyme

Table 2.16: Bioinformatic predictions for the subcellular localization of rat dhrs8.

Server	rat dhrs8
pSORTII	47.8% cytoplasmic, 21.7% mitochondrial, 17.4% extracellular, incl. cell wall, 4.3% vacuolar, 4.3% nuclear, 4.3% endoplasmic reticulum
pTarget	87.6% endoplasmic reticulum
SubLoc 1.1	84.0% cytoplasmic
TargetP 1.1	1.7% mitochondrial, 96.8% secretory, 6.3% other
LOCtree	mitochondrial 5

For rat dhrs8, the predictions made on its subcellular localization differ greatly between the five servers applied (cf. to table 2.16).

No co-localization with mitochondria nor cytosolic distribution was seen (not shown). The result of a counterstaining experiment is different when overexpressing rat dhrs8 from either GFP-fusion vector and counterstaining ER with the respective tracker. Fig. 2.65 shows the result of this experiment. Referring to the experimental data, it is interesting to note that neither position of GFP (N- or C terminal) fused to rat dhrs8 hinders the ER localization. In both panels of fig 2.65, a co-localization of ER and ret dhrs8 fusion protein can be observed in images C. Referring back to the bioinformatic predictions, pSORTII-server was the only one to predict the right subcellular localization.

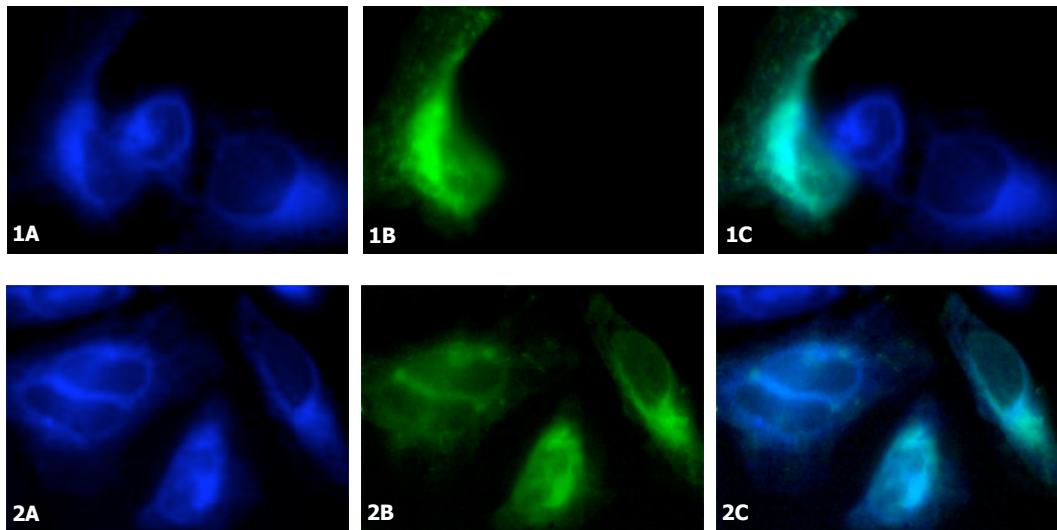


Figure 2.65: Rat dhrs8 and ER counterstaining. Expression from either vector shown leads to co-localization with ER-tracker. Panel 1: pEGFP-C2, panel 2: pAcGFP1-N1. In both panels, A depicts ER-counterstaining, B GFP, and C the overlay from pictures A and B.

2.7.7. Murine Rdh12 is endoplasmic reticulum-localized

Table 2.17: Bioinformatic predictions of the subcellular localization of murine Rdh12.

Server	mRdh12
pSORTII	55.6% endoplasmic reticulum, 11.7% cytoplasmic, 11.1% Golgi, 11.1% nuclear, 11.1% mitochondrial,
pTarget	100% mitochondrial
SubLoc 1.1	74% nuclear
TargetP 1.1	4.9% mitochondrial, 93.9% secretory, 4.2% other
LOCtree	cytoplasmic 1

Table 2.17 depicts the bioinformatic predictions on the subcellular localization of murine retinol dehydrogenase type 12 by the five servers applied in the work at hand, pSORTII, pTarget, SubLoc1.1, TargetP 1.1, and LOCtree. Again, the discrepancies of the predictions are considerable (see table 2.17). Especially for this protein, no conclusion can be drawn from these predictions. Experimental data show that pSORTII was the only server conducting the right prediction.

No obvious cytosolic distribution nor co-localization with the mitochondria could be seen (not shown). When conducting counterstaining of the endoplasmic reticulum, it became obvious that murine Rdh12 co-localized with this staining no matter from which

2. Results

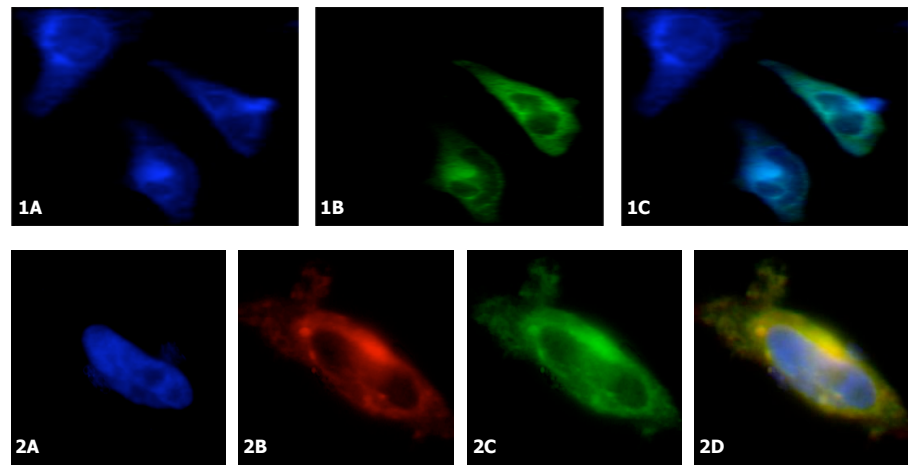


Figure 2.66: Murine Rdh12 in ER counterstained. Expression from both vectors (panel 1: pEGFPC-C2, panel 2: pcDNA4 myc-his Version B) leads to a co-localization of the enzyme with the ER staining. In panel 1, image A shows staining with ER tracker, B shows the distribution of EGFP-mRdh12 fusion protein, C shows the overlay. Panel 2 shows the distribution of mRdh12-myc-his recombinant protein. Image A: nuclear counterstaining with Hoechst, B: intracellular distribution of myc-tagged mRdh12, C: ER staining by N-FLAG sarcolipin expression (detection of FLAG-tag), D: overlay of images A-C.

of both vectors it was expressed. Obviously, murine Rdh12 is an ER-localized protein. As for rat dhhrs8, no position of the tag influences the subcellular localization of the resulting fusion protein. This may point to an internal signal.

2.7.8. Human RDH12 localizes to the ER

Table 2.18: Bioinformatic predictions of the subcellular localization of human RDH12.

Server	hRDH12
pSORTII	39.1% cytoplasmic, 17.4% nuclear, 17.4% mitochondrial, 13.0% endoplasmic reticulum, 4.3% vesicles of the secretory system, 4.3% Golgi, 4.3% peroxisomal
pTarget	62.6% endoplasmic reticulum
SubLoc 1.1	56% mitochondrial
TargetP 1.1	19.8% mitochondrial, 82.7% secretory, 2.6% other
LOCtree	organellar, secretory pathway 6

For the human homologue to the protein described in the last section, human RDH12, bioinformatic predictions do still display quite a high discrepancy but not quite as high as for murine Rdh12 (see table 2.18).

No colocalization with mitochondria or cytosolic distribution was observed for human retinol dehydrogenase type 12 (RDH12) (not shown). For the murine Rdh12 and rat dhhrs8

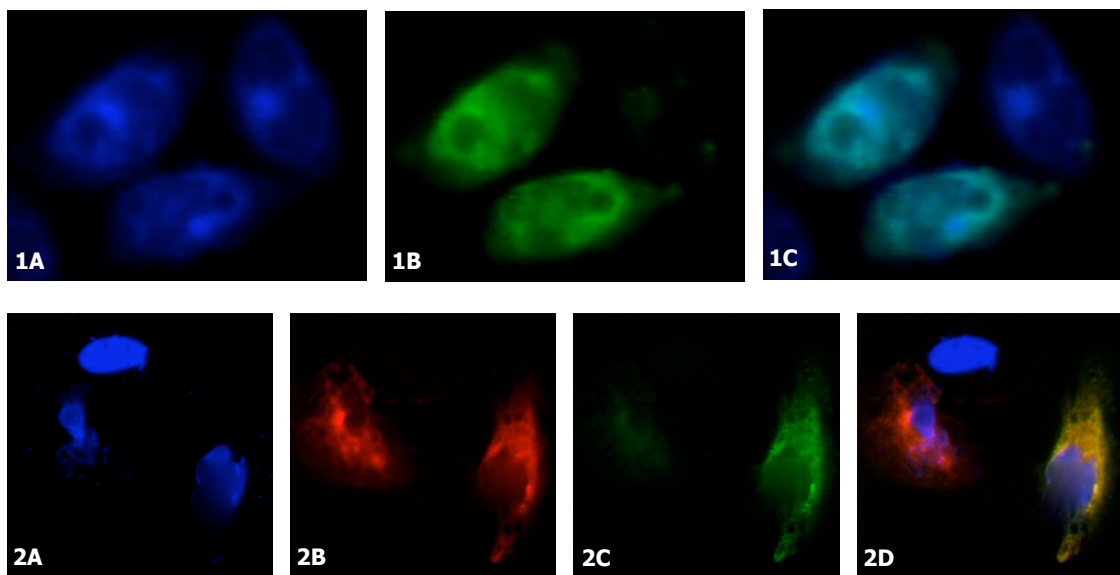


Figure 2.67: Human RDH12 and ER counterstaining. Again for both tags (N-terminal and C-terminal), colocalization with ER-staining is seen. Panel 1: expression from pEGFPC2 (A ER-staining, B GFP-fused RDH12, C overlay), panel 2: expression from pcDNA4 myc-his (A nuclear staining by Hoechst-33342, B detection of myc tagged RDH12, C ER detection by FLAG-tagged rabbit sarcolipin, D overlay of A to C)

the position of the tag did not influence the subcellular localization of the protein. Fig. 2.67 shows counterstaining of ER after transfection of hRDH12. In the top panel, human RDH12 was expressed from pEGFP-C2. For the two transfected cells included to the images, a clear overlay of ER staining and GFP-tagged hRDH12 can be observed. The two bottom panels depict expression of hRDH12 from pcDNA4 myc-his. In both cases, myc- and FLAG-detected proteins show the same distribution.

2.7.9. Human type 13 retinol dehydrogenase localizes to the mitochondria

Table 2.19: Bioinformatic predictions of the subcellular localization of human RDH13.

Server	hRDH13
pSORTII	44.4% extracell. incl. cell wall, 22.2% vacuolar, 11.1% cytoplasmic, 11.1% Golgi, 11.1% endoplasmic reticulum
pTarget	100% mitochondrial
SubLoc 1.1	74% mitochondrial
TargetP 1.1	8.3% mitochondrial, 76.9% secretory, 7.2% other
LOCtree	cytoplasmic 3

In table 2.19, the results of bioinformatic prediction for localization of human type

2. Results

13 retinol dehydrogenase are shown. Interestingly, pTarget is 100% sure of RDH13 localization to mitochondria. When comparing the results of the latter two servers to the results shown in fig. 2.68, it becomes apparent that with a C-terminally fused myc-his tag, the protein is organellarily localized (image C). Picture D shows that detection of the myc-tag co-localizes with mitochondria. Expression of RDH13 from pEGFP-C2, that is with a N-terminally fused EGFP protein, results in a cytoplasmic distribution (panels 1 and 2). Obviously, an untagged N-terminus of the protein is needed for localization to the mitochondria.

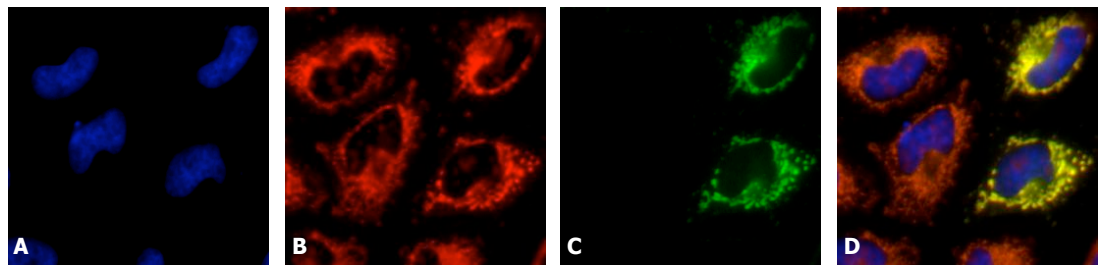


Figure 2.68: Intracellular localization of hRDH13 colocalizes with mitochondria. A shows nuclear counterstaining, B staining of mitochondria, C: localization of RDH13-GFP-fusion protein (expression from pAcGFP1-N1), D: Overlay of pictures A to C.

2.7.10. Murine Dhrs4 is neither a peroxisomal SDR nor mitochondrial but cytoplasmically distributed

mDhrs4 is the murine homologue of human DHRS4. Human DHRS4 is also called peroxisomal SDR in the database. At the C-terminus of murine Dhrs4, the last three amino acid residues comprise the weak peroxisomal retrieval signal SRL (serine, arginine, leucine, see fig. 2.2). Interestingly though, all servers predicted a mitochondrial distribution of murine Dhrs4 (see table 2.20).

Table 2.20: Bioinformatic predictions of the subcellular localization of murine Dhrs4.

Server	mDhrs4
pSORTII	52.2% mitochondrial, 26.1% cytoplasmic, 17.4% nuclear 4.3% cytoskeletal
pTarget	87.6% mitochondrial
SubLoc 1.1	74% mitochondrial
TargetP 1.1	83.8% mitochondrial, 3.2% secretory, 20.4% other
LOCtree	mitochondrial 5

Fig. 2.69 shows a from bioinformatic predictions diverging, cytosolic distribution. In other counterstaining experiments, no co-localization was observed (not shown). At this

point, it is surprising to note that all servers for bioinformatic prediction give the same but false prediction of the murine Dhrs4 enzyme.

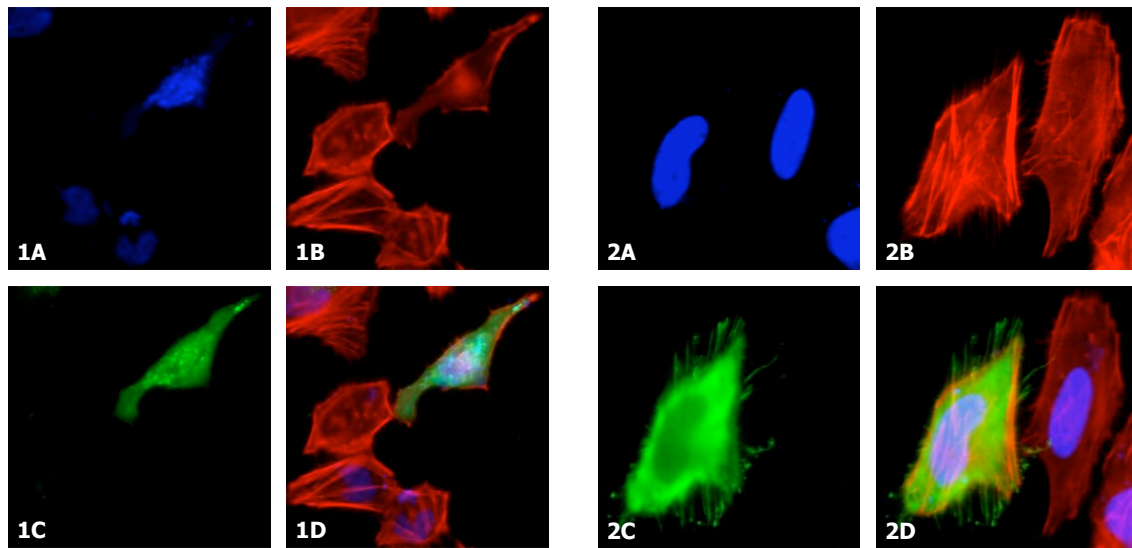


Figure 2.69: Cytosolic localization of mDhrs4. Panel 1 expressed from pEGFP-C2 (left), panel 2 expressed from pcDNA4 myc-his Version B. In both panels, the images depict: A nuclear counterstaining with DAPI, B f-actin counterstaining, C detection of recombinant mDhrs4-protein, D overlay of images A to C.

2.7.11. Human DHRSX co-localizes with ER-staining

For human DHRSX, I did not manage to clone the enzyme in pEGFP-C2. For this reason, only the results from expressing the enzyme with a C-terminal myc-his tag (pcDNA4 myc-his version B) are given. Table 2.21 shows the prediction results.

Table 2.21: Bioinformatic predictions of the subcellular localization of human DHRSX.

Server	hDHRSX
pSORTII	33.3% Golgi, 33.3% endoplasmic reticulum, 22.2% cytoplasmic, 11.1% mitochondrial
pTarget	81.4% mitochondrial
SubLoc 1.1	91% mitochondrial
TargetP 1.1	88.7% mitochondrial, 15.1% secretory, 2.8% other
LOCtree	organellar, secretory pathway 6

Fig. 2.70 describes the intracellular localization of hDHRSX as detected from C-terminal myc-tagged expression. In panel 3, ER counterstaining is shown, clearly indicating that DHRSX localizes to the endoplasmic reticulum. Only the bioinformatic prediction of the pSORTII server is therefore correct.

2. Results

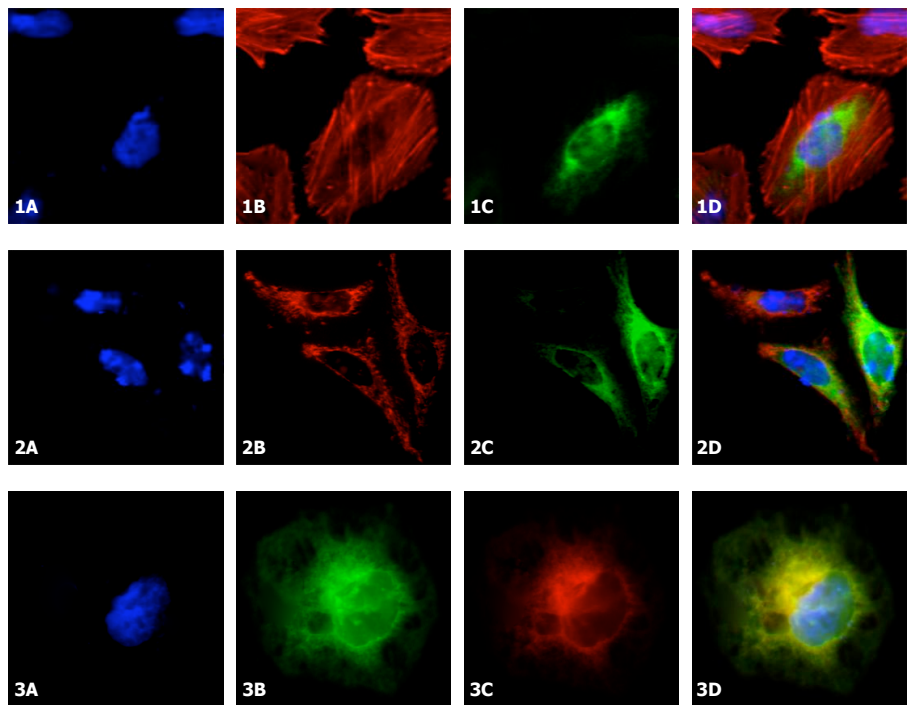


Figure 2.70: ER-localization of human DHRSX. All panels show nuclear counterstaining in picture A, counterstaining of the respective structure (1: f-actin, 2: mitochondria, 3: ER) in picture B, detection of the myc-tag in C and the overlays in D. Note that due to green staining of the FLAG tag, the myc-tag is detected red in panel 3.

2.7.12. MGC4172 and MGC18716 may both be ER-localized

All servers applied in the work at hand but pSORTII predict MGC4172 and MGC18716 to be mitochondrially localized (see table 2.22). pSORTII predicts cytoplasmic proteins in both cases. As was the case for several of the proteins described here, the bioinformatic predictions do not match the experimental data given in fig. 2.71. Red (myc-tagged MGC18716) and green staining (N-FLAG-tagged rabbit sarcolipin) show a clear overlay (picture D) indicating ER-localization of MGC18716.

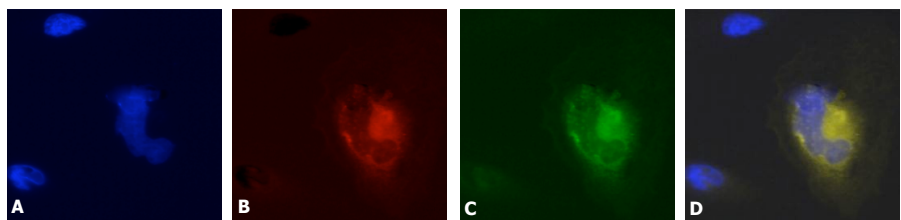


Figure 2.71: Endoplasmic reticulum-localization of murine MGC18716. A: nuclear counterstaining (Hoechst), B: MGC18716 (myc epitope detection) C: endoplasmic reticulum (sarcolipin). D: co-localization of MGC18716-myc with sarcolipin.

Experimentally, I could not determine the subcellular localization of MGC4172 due to

Table 2.22: Bioinformatic predictions of the subcellular localization of human MGC4172 and of murine MGC18716, its homologue.

Server	hMGC4172	mMGC18716
pSORTII	47.8% cytoplasmic, 21.7% mitochondrial, 13.0% nuclear, 8.7% cytoskeletal, 4.3% vacuolar, 4.3% Golgi	65.2% cytoplasmic, 17.4% mitochondrial, 8.7% nuclear, 4.3% cytoskeletal, 4.3% vacuolar
pTarget	mitochondria 62.6%	mitochondria 62.6%
SubLoc 1.1	mitochondria 84%	mitochondria 74%
TargetP 1.1	mitochondrial 66.2%, secretory 6.4%, other 19.9%	mitochondrial 68.1%, secretory 4.1%, other 26.2%
LOCtree	mitochondrial 5	mitochondrial 1

PCR problems. The gene does not seem to be strongly expressed in either cell line used in the work at hand (HeLa, SaOS-2, 293T, HepG2). In addition, it is hard to amplify its CDS also from a plasmid. This is the fact likewise for other genes, e.g. 17 β -HSD types 1 and 12. Therefore, only bioinformatic predictions on the subcellular localization have been conducted on this gene.

Achievements: For ten out of eleven enzymes under investigation in this regard, I could show their intracellular localization. Comparison of the experimental data to bioinformatic predictions revealed that the prediction servers currently available are not reliable. The experimental data of this section is summarized in table 2.23.

Table 2.23: Overview on the investigated subcellular localizations of SDRs.

subcellular localization	SDRs
cytoplasmic	hretSDR3, mDhrs4
mitochondrial	mSdro , hRDH13
endoplasmic reticulum	rdhrs7b, rdhrs8, mRdh12, hRDH12, hDHRSX, mMGC18716
not addressed	hMGC4172

Originating organisms are depicted by *h*, *m* and *r* in front of the name, meaning human, mouse, or rat, respectively.

2. Results

3. Discussion

3.1. General remarks

This thesis deals with the topic of protein identification and characterization shown for proteins belonging to SDR superfamily and putatively of steroidogenic substrate specificity. This set-up included two major focuses, the methodological approach and the protein characterization itself. Therefore, the discussion will consist of two major parts: discussion of the set-up (including what more could be done, see 3.9, p. 124) and of the results obtained with this set-up (see 3.8, p. 111ff.).

3.2. The set-up - is it functional genomics?

The work at hand was based on a functional genomics approach to the SDR superfamily. Among many terms, ‘functional genomics’ is defined here as a genome-wide attempt with regard to the function exerted by the proteins under analysis.

Is it genomics? For functional genomics approaches, usually techniques such as microarray analyses find application. These set-ups however have a different starting point as chosen in this study. For example, the initial question could be: find differences in gene expression when mutating a certain gene or: compare gene expression in different tissues. In this thesis, the question rather was vice versa: there are so many uncharacterized SDR proteins - what are they needed for? Can we identify more SDR proteins metabolizing steroid hormones?

For the identification of the putative SDR proteins, SDR Finder software was used and all protein sequences available at NCBI at this point of time were screened. Non Redundant NCBI database and Monthly Updates to it were used for this purpose. In this analysis it was important to restrict the numbers as well of false-positive hits as of false-negative hits. The threshold chosen seemed to permit a compromise between these two demands. With this threshold it was not possible to identify the complete human, rat, and mouse SDR proteins. Nevertheless the starting point of the analyses was indeed genome-wide and genomics is a term correctly used in this context.

3. Discussion

Is it functional? This thesis used several approaches to determine the functions of a set of selected SDR proteins: phylogenetics, expression analyses, studies in subcellular localization, determination of substrate specificity and their kinetics. As SDRs have multiple substrate specificities, one group of possible substrates - steroid hormones - was chosen to be tested on a set of newly identified proteins displaying SDR characteristics. As function of the genome-wide searched (and found) proteins was extensively addressed in the work at hand, the term *Functional Genomics* seems to be rightly used.

3.3. Identification of candidate proteins and classification as SDRs

SDRs form a large protein superfamily with various subfamilies described [50]. As the overall identity of these enzymes in pairwise alignment typically yields only 15 to 30% identical amino acids [86], their identification is a tedious task. The small segments within distinct motifs conserved seem to be enough to yield highly conserved proteins in structural regards [86].

3.3.1. The SDR Finder - friend or foe?

SDRs are hard-to-identify proteins in large-scale format. This was one aims of the study. Though SDR Finder considerably facilitates this task extensive verification of the results was necessary. This holds true for most if not all bioinformatic tools due to the fact that algorithms are static. From the first look on the results of SDR Finder, it became apparent that several known and characterized SDRs (as human 17 β -HSD7) were not identified by SDR Finder though containing more than the required 11 conserved amino acids. If the motifs are not found within the windows defined they can not be identified by the SDR Finder algorithm. Surprisingly though, the murine and rat homologues of HSD17B7 were identified (see table 2.4, p. 28, numbers 17 and 18).

Fig. 3.1 shows an alignment of murine, rat, and human 17 β -HSD7 (HSD17B7). In SDR Finder analysis, all three proteins should yield a score of 14. Motifs are located at the exact same positions within the three proteins. It can thus not be explained why human HSD17B7 was not identified.

SDR Finder was used for the identification process with an analysis threshold of at least 11 out of 16 amino acids conserved. If hinting at complete identification of *all* SDR enzymes contained in a genome, the threshold would have to be dramatically decreased inevitably leading to uncountable false-positive hits. This is again a logical consequence from the fact that algorithms are static while nature is not. The SDRs identified in the course of this thesis can therefore not be considered to represent a complete picture of all

3.3. Identification of candidate proteins and classification as SDRs

SDRs contained in the human, rat or mouse genome. For this task, not only SDR Finder but any bioinformatic tool will not be quite suitable. A BLAST conserved domains search could be the first step for this approach. It is however important to be aware of the fact that most functional genomics tools do not permit a global approach due to technical limitations.

Figure 3.1: Alignment of HSD17B7 from mouse, rat, and human. Sequences are named with accession numbers and MM (mouse), RN (rat), and HS (human), respectively. Motifs identified by SDR Finder are marked: in red, conserved amino acids are depicted. Shaded in gray are amino acids that are not conserved. All three proteins yield a score of 14.

When starting the identification of SDR enzymes, SDR Finder was the only available program permitting a considerably rapid and still rather reliable identification.

3.3.2. On NCBI NonRedundant Database

As indicated by its name NR database (NR = non redundant) should not contain redundancies. However, this is clearly not the case. One example is the human retSDR3. For example, the sequences of human retSDR3 (20; numbers refer to table 2.4 in the results chapter) and DHRS10 (21) differ in one amino acid. Both sequences map to the same genomic position. Under the name retSDR3 the protein was submitted to NCBI at least twice (accession numbers AAF44666 (20) and AAF06940 (22)). Further examples are depicted in table 2.4 (p. 28) and indicated by the number 3 in the last column. Sequencing mistakes or appearance of polymorphisms probably lead to these multiple entries in

3. Discussion

databases. Database management should include this annotation.

3.3.3. Annotation of identified SDRs to chromosomal location

In the process of annotation of the SDRs to their chromosomal locations, graphical outputs were drawn implementing the identified SDRs into karyograms of the three species under investigation - human, mouse, and rat.

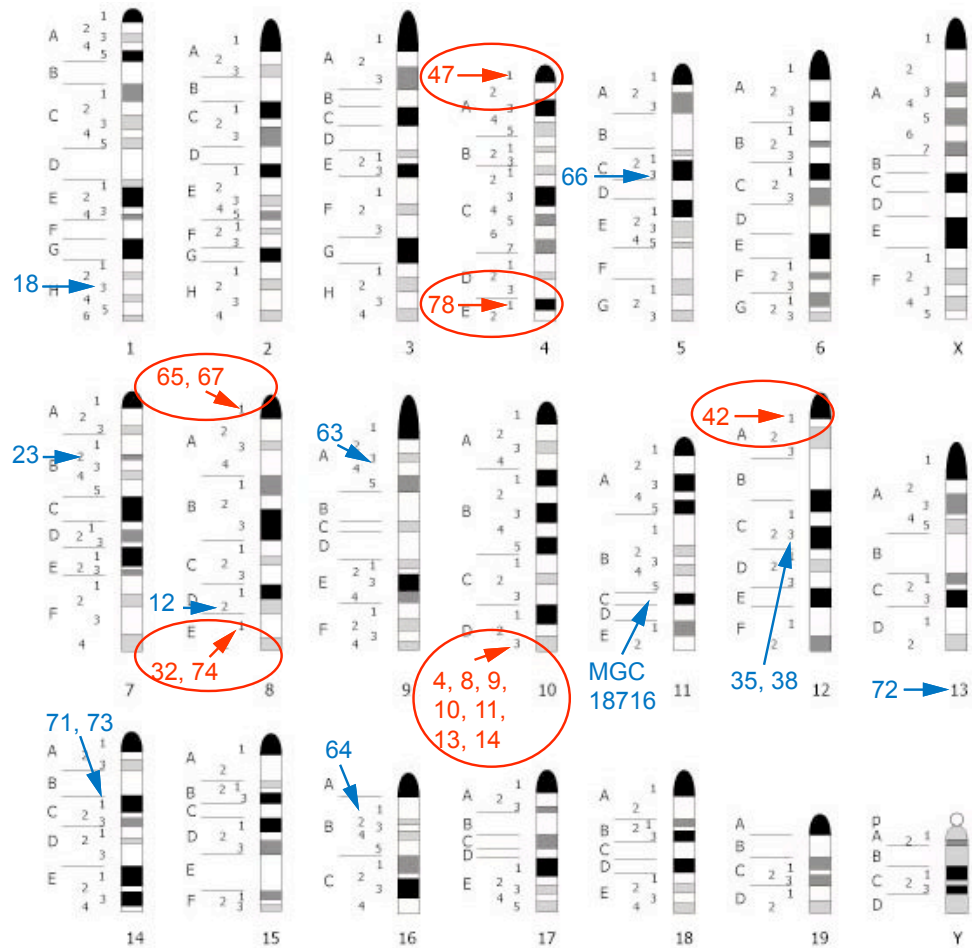


Figure 3.2: Graphical annotation of the identified mouse SDRs. 14 out of 26 genes are localized telomeric (red, framed) while the other 12 are localized at more central positions (blue).

The respective results were depicted in chapter 2 in the fig.s 2.5 and 2.6 (p. 26 f). I could thereby show that the cluster of SDRs found in the mouse genome (refer to fig. 2.4, p.25) on chromosome 10D3 can be found in the human genome on chromosome 14q and in the rat at 6q. These analyses are possible thanks to large amounts of sequence data

3.3. Identification of candidate proteins and classification as SDRs

publicly available. The comparative study of the SDRs in these species can therefore also identify synthenic regions within the genomes.

The graphical depiction of murine SDRs (see fig. 2.5, p. 26) hints at many of these genes being located at telomeric positions. This can not be deduced for the human and rat proteins: due to the resolution of the karyograms these could only be annotated to the p or q arm of the respective chromosomes. For the murine genes, this observation is shown in fig. 3.2.

While more centrally localized SDR genes are depicted in blue, telomeric ones are shown in red. In summary, out of 26 genes, 16 are located quite near to the telomers. If SDRs tend to be coded in rather telomeric areas of the chromosomes can not be deduced from this observation. It would however be interesting to follow on this and investigate all murine SDR genes. With higher resolving karyograms from human and rat, a comparative study could be performed.

Furthermore, it became apparent that there are still parts of the genomic sequences missing: two proteins, one of murine and one of human origin could only be aligned to the chromosome but not to the exact chromosomal region (murine Hsd17b3, chromosome 13, and human DHRS2 isoform 2, chromosome 14). For one rat protein, the diacetyl-L-xylulose reductase (dcxr), no chromosomal localization could be found at all. Fig. 3.3 shows the information on that gene locus taken from ENSEMBL database - it obviously maps to a chromosomal locus that is not sequenced or annotated yet. For annotated sequences, their chromosomal position would be displayed.

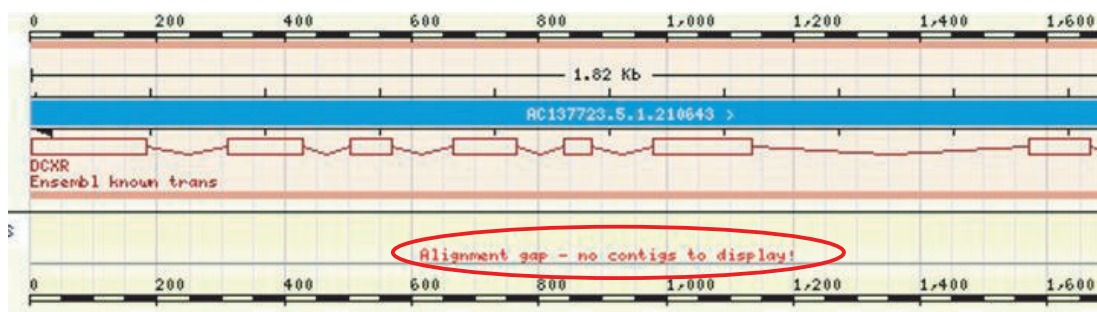


Figure 3.3: No chromosomal region could be identified for rat diacetyl-L-xylulose reductase.

Overall, the graphical depiction of the identified proteins improves the overview and therefore helps to handle the large amount of data created by the functional genomics approach.

3. Discussion

3.4. Analysis of the expression patterns

3.4.1. Need of expression analysis

Expression is tightly regulated not only in higher metazoans as vertebrates but already in bacteria. It is regulated according to the needs of the organism. That is, expression patterns mirror the need of the organism for a function to be exerted under certain conditions: for example, if there is a pregnancy to be maintained, the mammalian organism needs progesterone (among other hormones). Enzymes for the biosynthesis of this steroid hormone are then needed. Therefore, the expression pattern of a gene (and its gene product) can provide hints to the functions of this gene product.

From an ubiquitously expressed gene (such as β -actin or GAPDH) we can expect for example housekeeping functions, functions related to the structural maintenance of the cells or functions in basic metabolism. Very specialized enzymes display very distinct expression patterns: 17β -HSD1, considered to be the main enzyme of estradiol formation, is mainly expressed in the placenta [90]. Especially during embryogenesis, there are not only distinct but also spatial expression patterns - genes of cholesterol biosynthesis are expressed only in certain tissues during a defined period of time [59, 60]. Therefore, both in wet lab and *in silico* analysis it should be noted that also within the tissues the gene expression patterns are not static but adapted according to the respective circumstances.

Alternative splicing - a means of varying protein function. Most genes under investigation revealed more than one transcript in northern blot analysis. Not all genes are alternatively spliced as extensively as for example human WWOX: at least eight isoforms have been deposited to the NCBI database. In the analysis of human WWOX expression, not all of these transcripts could be detected. This could either be due to the fact, that they were not expressed in the tissues included to this northern blot membrane or to its resolution if the transcripts have very similar lengths. Assessing the size of a species' it seemed astonishing that mammals *only* should need about 35000 genes. Or, same question, differently asked: if mammals only need 30 to 35 thousand genes - why does a nematode need close to 20 thousand genes [40, 98]? The key to this riddle most likely lies in alternative splicing causing different proteins to be built from one gene. Alternative splicing probably occurs frequently in higher vertebrates but is seldomly used by nematodes as *C. elegans*. Guesses go towards 100 thousand or more proteins that can be built from a mammalian genome [40]. 60% of the mammalian genes are said to be alternatively spliced [103].

3.4.2. Experimental expression analysis by Northern Blot

All northern blot experiments were performed on one membrane each with human and murine RNA. While after the single experiments, stripping was controlled by measurement with ionization monitor, autoradiography was performed after the last experiments. It became then apparent that the β -actin mRNA hybridized had not been stripped completely from the membranes and remaining signals from this hybridizations were detected with the signals from the enzymes under investigation. Besides mostly very low expression levels of these enzymes, the degree of remaining signals can not be conclusively determined: not in all lanes, the same amounts of β -actin signals remained. If the signals remained from this control hybridization, it is unclear, why for instance the amount detected in small intestine is much lower than the level remaining in spleen in the analysis for MGC4172 (fig. 3.4, red arrows). This could also be observed for other genes.

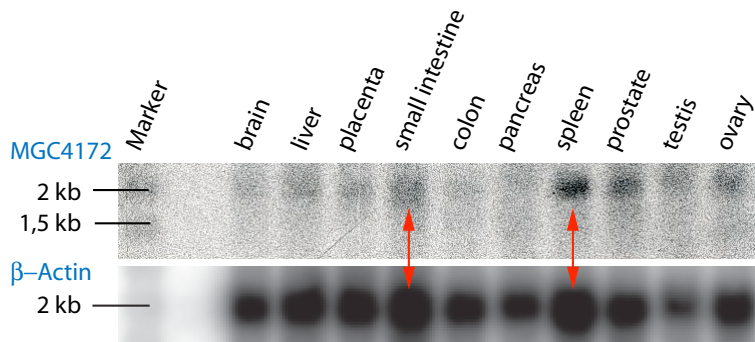


Figure 3.4: Varying amounts of remaining signals could be detected.

Two conclusions can be drawn from this observation: first, the stripping procedure should be further optimized and always be controlled by autoradiography. As labeling of the probes is done radioactively, the membrane should not be hybridized within short intervals of time but left to decline in between. Sequential hybridization of northern blot membranes should therefore only be conducted when surely no remaining signals can be detected. These problems could probably be caused by any gene with a high expression level.

3.4.3. In silico expression analysis

In many studies, *in silico* expression analysis is included to show expression patterns of enzymes. This way of analysis has become popular over the last years when EST (expressed sequence tag) amounts in databases seemed to explode. To facilitate this *in silico* northern blot and to get greater reliability out of it, this study presents an automated version of this approach, ISBN. By developing and testing this automated system I could show both

3. Discussion

the advantages of automation and limitations of the *in silico* approach. As shown in fig. 3.5, ISNB conducts the same steps as by-hand-performed *in silico* northern blot.

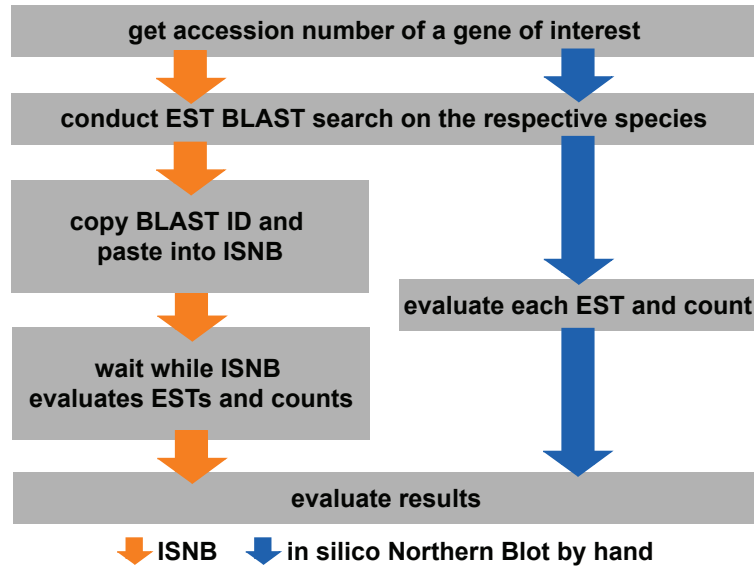


Figure 3.5: Comparison of *in silico* blot conducted automatically (orange arrows) or conducted manually (blue arrows). ISNB prevents counting errors and saves time but follows the same scheme as the manual supervision of EST data.

Pitfalls of ISNB. Generally, *in silico* expression analysis results are generally to be considered with care. Already in the first tests of ISNB, it became apparent that differences are observed between *in silico* and wet lab analysis. This observation was especially striking when concentrating on murine 17 β -Hsd11 expression in liver. Liver is regarded one of the organs often examined and should therefore be highly represented in EST collections. It is unlikely that we found only four ESTs from liver using ISNB while seeing the most prominent signal on the wet lab Northern blot (cf. Fig. 2.7, panel D). Interestingly, also in case of retSDR3 this phenomenon was observed: while the northern blot revealed high expression in liver, ISNB did not. This indicates that both for human and mouse, liver may not be as intensively studied as suggested. Otherwise, two reasons could be named for the overall differences: First, EST quality and length might not have been sufficient to be included in the ISNB analysis. This seems especially to be true for murine 17 β -Hsd1 - out of 1000 found ESTs, only 25 matched the applied conditions. Second, when analyzing EST distribution patterns with several tools available on the World Wide Web, it becomes apparent that EST relying analysis results in the same tissue distribution as ISNB does (not shown). The latter supports the reliability of ISNB output.

No question that EST database quality greatly influences the outcome influences. With

some tissues investigated more frequently than others, EST data is always biased to a certain degree. Logically there tend to be more ESTs found from tumor tissue than from liver, if there are e.g. 15 ESTs libraries from the former but only 2 libraries from the latter tissue - otherwise, the expression level in liver would have to overcome tumor expression by far. Tissues for EST databases are furthermore selected according to availability. If in this tissue a certain gene is not expressed, there will be no ESTs to detect.

During experimental expression analysis of the enzymes under investigation, further observations on the limitations of ISBN were made: ISBN cannot give information on transcript length and existence of several transcripts. As ESTs do not necessarily comprise the full coding sequences this can probably not be reliably achieved by any *in silico* analysis. However, by-hand-analysis of the found sequences could provide first hints.

The current version of ISBN does not distinguish between genders. This was achieved by RT-PCR for the two rat genes. As EST data often include gender-information, this could be included to ISBN in the future.

Furthermore, ISBN delivers rather qualitative than quantitative results. For several genes (including mWwox) all 100 ESTs identified from the databases were analyzed by ISBN. This could provide a hint that more ESTs were available but not included to the BLAST results. The default value for maximal results in a BLAST search is 100 hits. Setting this value to 1000 might help to improve the performance without having to change the underlying algorithm of ISBN.

What could be improved in ISBN? To the information of originating tissues, gender information should be included as well as the total length (and the pertinent sequences) of the identified ESTs. These additions could further improve the automated version. For the detection of splice variants, ISBN's possibilities on that part are probably limited as ESTs are not necessarily full-length verified. Gender information would enable a gender-specific analysis. The total length and sequence of the respective ESTs could help to determine alternative splice products. For even greater convenience and even easier achievable overview, a graphical output summarizing the results could be considered. This is the case for the electronic RT-PCR [105] provided by the NCBI. While the database can be directly chosen, primer sequences have to be submitted. For most genes, the results mirrored the findings from ISBN. For rat dhrs7b, no sequence tagged sites (STSs) could be found where ISBN identified 36 matching ESTs. As both methods rely on the NCBI database, this is surprising. However, if primer sequences are selected, stringency might be higher. This would then imply that reverse e-PCR results have a higher quality. At least, e-PCR results rely on the length of the virtual PCR-product produced by the primers used. In ISBN, the minimum alignment length is selected. ISBN was tested on 14 also experimentally evaluated genes and found to perform overall well. The comparison

3. Discussion

of these two systems, e-PCR and ISBN, is therefore not conclusive.

Would a new BLAST server be helpful? ISBN relies on the publicly available BLAST service at the NCBI. It is consequently depending on the integrity of this server and of its output. With a newly set-up BLAST server, an output could be generated that meets with the information needs of ISBN thereby making the tool more reliable.

The automation of the system does not only save time but also provides more reliable data because counting errors can mainly be excluded and a quality check for the identified EST sequences is implemented. Though not altogether a new approach (successful approaches have also been reported for identification of protein distribution and gene expression [34] and identification of genes involved in pathogenesis of e.g. breast cancer [107]) the tool developed in the work at hand can help to achieve easy overview on expression patterns especially when it comes to many genes.

3.5. Use of phylogenetics in predicting substrate specificities

Many studies make use of phylogenetics as the number of sequenced genomes increases. In this context, the term *phylogenomics* has been created [31]. Conserved sequence is said to code for conserved function [11]. This notion gave rise to phylogenetic shadowing - the attempt to find conserved regulatory elements within primates. Also for SDRs, several studies have used phylogenetics for the prediction of a conserved function. 17β -HSD 7 was thereby shown to be part of cholesterol biosynthesis - a finding that could be proven experimentally [71]. Identifying homologous enzymes for 17β -HSD types 1 and 3 in the zebrafish, phylogenetics have also successfully been applied [75].

The application of phylogenetics in this study had a similar but still different purpose: From relationship with substrate-characterized SDRs, first hints about the substrate specificities of enzymes under investigation should be gained. Fig. 3.6 shows the phylogenetic tree from which the conclusions were drawn. Enzymes under investigation in this thesis are shaded in violet, characterized enzymes are boxed in different colors summarizing their respective substrate specificities. Substrate specificities newly investigated in this thesis are marked by colored Xs. Even without detailed view on the tree (the original tree is depicted in the results section, see fig. 2.37, p. 49f.) it immediately becomes apparent, that minor changes in protein sequence (on which the tree is based) can lead to considerable changes in the substrate specificities of the enzymes (refer to arrows in the respective colors). Several of the depicted SDRs have multiple substrate specificities.

Homologues of the same protein from different species are not necessarily able of conducting the same reaction: rat dhrs8 did not show activity towards the tested steroids though its human homologue can convert estrogens. Human, but not murine RDH12

3.5. Use of phylogenetics in predicting substrate specificities

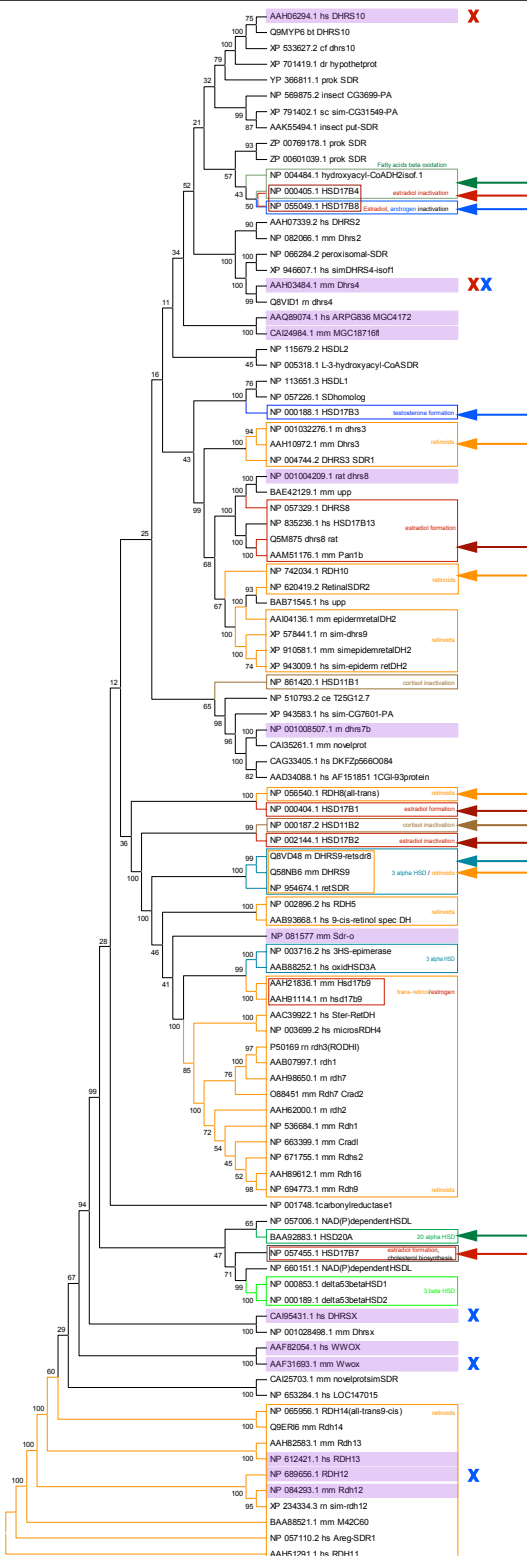


Figure 3.6: Phylogenetic tree of SDR candidate enzymes in comparison with characterized SDR type enzymes. Colors code for different substrate specificities: orange - retinoids, red - estrogens, blue - androgens, other steroid dehydrogenase functions dark green and dark blue, brown - glucocorticoids, black - cholesterol biosynthesis. Arrows also point to these substrate specificities, X in respective colors indicate substrate specificities newly investigated here. Violet box-shaded enzymes were investigated here. Numbers on the branches indicate bootstrap values. The data-set used for this tree is depicted in the appendix.

3. Discussion

can convert dihydrotestosterone to androstanediol. In case of Wwox, only the murine homologue was found to convert androgenic compounds.

The conclusions about the proteins under investigation were drawn based on these analyses. It was observed that specific functional predictions were not possible. Therefore the use of phylogenetics is limited in this regard. Phylogenetics are applicable to show relationship with enzymes previously characterized but do not tell the exact functions.

3.6. The substrate conversion assay

In the work at hand, a conversion assay was established that allows the measurement of enzymatic activity towards steroid hormones in living cells, that is, under physiological conditions. The assay was shown to work for androstanediol, testosterone, estrone, estradiol, dihydrotestosterone, androsterone, and corticosteroids. Five of 13 SDRs under investigation were shown to possess converting activities towards the substrates tested. These were: human retSDR3 (E2), human RDH12 (DHT), murine Dhrs4 (A, E1, DHT), human DHRSX (DHT), and murine WWOX showing catalytic activity towards androstanedione and androsterone. Table 2.11 summarizes the results of the substrate conversion assays. I was able to show that Michaelis-Menten kinetics are feasible with the conversion assay established and presented here. For the enzymes with substrate conversion abilities identified, these kinetics were performed. Table 2.12 summarizes the values found for Michaelis-Menten constants and maximum velocities.

3.6.1. Prokaryotic or eukaryotic overexpression?

A well-established method for steroidogenic conversions includes prokaryotic overexpression from pGEX Δ BamHI vector [61]. This method excellently works for several 17 β -HSD-type enzymes, some are, however, inactive after overexpression in bacteria. This may be due to wrong folding of the protein or to missing post-translational modifications. Prokaryotically expressed proteins may, again due to these facts, lead to artifacts. While 17 β -HSD1 and other enzymes are active after prokaryotic expression, eukaryotic expression is required for activity for instance in case of 17 β -HSD type 3 (personal communication, Dr. G. Möller). Therefore eukaryotic overexpression was chosen for characterization of the enzymes under investigation.

The adequate vector for this system also needed consideration. Tagged expression is advantageous in proving the overexpression on protein level by western blot. It may, however, also alter the subcellular localization of a protein by masking a signal sequence. As correct localization is a prerequisite of functional activity, at least in living cells, pcDNA3 (Invitrogen) appeared to be the vector of choice. From this vector, proteins are constitutively expressed via a CMV promoter. Furthermore, pcDNA3 is an easily cloned vector,

and can be amplified in bacteria in high copy number leading to plasmid isolation of high yield. However, test of overexpression proved to be challenging.

Test of overexpression by PCR. In the work at hand, transient overexpression was tested by use of PCR. This test of overexpression does, of course, only provide a first hint. Proof of mRNA existence does not necessarily mean that the protein of interest will be translated from this mRNA. Therefore, protein detection would be the experiment of choice. Another choice might be qRT-PCR. This approach would at least provide a quantification of the found mRNAs without having to ask the question whether or not the PCR reaction has reached saturation and therefore has left the linear, and thus comparable phase. In order to by-pass these limitations of PCR, the cDNA equivalent of 5 ng total RNA per reaction and 25 cycles of amplification were applied. However, intensity of the actin controls indicates that the PCR reaction was saturated (see fig. 2.50 on p. 61). Quantitative conclusion therefore have to be considered carefully.

For some of the enzymes under investigation, also mock-transfected cells showed expression of the gene. If the proteins under investigation were already expressed and active towards the substrates offered, this should result in considerable amounts of background activity. High endogenous conversion rates were seen for several substrates, most prominently the progestins but also androsterone, dihydrotestosterone and corticosteroids. Thus, overexpression could only be seen as securely proven where conversion of a given substrate was seen at least for the human enzymes. This is the case especially in case of human RDH13 and WWOX where almost no difference can be seen in mock-transfected and transfected cells from the PCR signal intensity. Also for murine Wwox, no big difference can be detected in comparison to mock-transfected cells. Due to the high degree of conservation between the human and murine homologue, primers probably bind to both species (the same, though at much lesser extent should be true for rat dhrs7b and MGC18716). For all other enzymes, signal intensities vary so greatly that overexpression on mRNA level should be acknowledged. For two enzymes, no bands were detected in either transfected nor mock-transfected cells - mSdr-o and MGC4172. In case of the former, the positive control displays a strong signal. Therefore, there does not appear to be mRNA formed. For MGC4172, also the positive control only displays a weak signal leading to an overall inconclusive result.

3. Discussion

3.6.2. A steroid hormone conversion assay in living cells - what are the advantages?

The conversion assay presented here was based on the conversion assay presented by Castagnetta and coauthors [15]. In that assay, cells were seeded on culture dishes with a diameter of 60 mm (area of approximately 28 cm²). Before addition of tritiated steroids, cells were washed twice and medium changed to FCS- and phenol red-free culture medium.

In contrast, seeding the cells on 12-well plates (area of 3.5 cm²; diameter approximately 1.2 cm) I used a considerably smaller amount of cells. Within the medium originally applied when seeding cells were transfected and substrates added. Overall, the protocol for the assay presented here was simplified (e.g. no washing steps are needed before adding the substrate). Another advantage is the fact that less cells and less culture medium require lower amounts of radioactivity. Two advantages can be named: saving costs and, more importantly, less exposure to radiation.

Luu-The and co-workers [68] have also used measurements in living cells for the characterization of 17 β -HSD12. Stable transfection seems to be a prerequisite for the assay presented in their work. The assay presented here is based on transient transfection, saving the time and work of generating these stable lines which would not be feasible for the medium-throughput scale of characterization in the work at hand. On the other hand, stable expression by-passes the problem of overexpression control. This could, however, be also avoided by tagged expression (see above). Furthermore, the assay presented by Luu-The and coworkers, uses 6-well plates, also leading necessarily to higher amounts of material and thus to higher exposure to radiation.

3.6.3. Considerations on the cell line used

For the set-up of the conversion assay, I tested several steroidogenic substances and their respective endogenous conversion within different cell lines. It was apparent that among the cell lines tested, 293T cells displayed the lowest endogenous conversion and therefore suited best the demands raised for the intracellular conversion assay. Fig. 3.8 displays the endogenous conversion rates of the four cell lines used towards androstenedione (A), testosterone (T), estrone (E1), and estradiol (E2). 293T cells have the same origin as 293

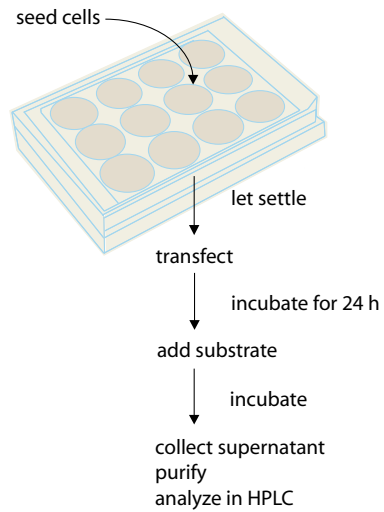


Figure 3.7: The intracellular conversion assay presented in the work at hand is easily workable due to a simplified protocol.

3.6. The substrate conversion assay

cells but are additionally transformed with SV40 T-large antigen. 293 cells are often used for steroid conversion tests (e.g. in [43]).

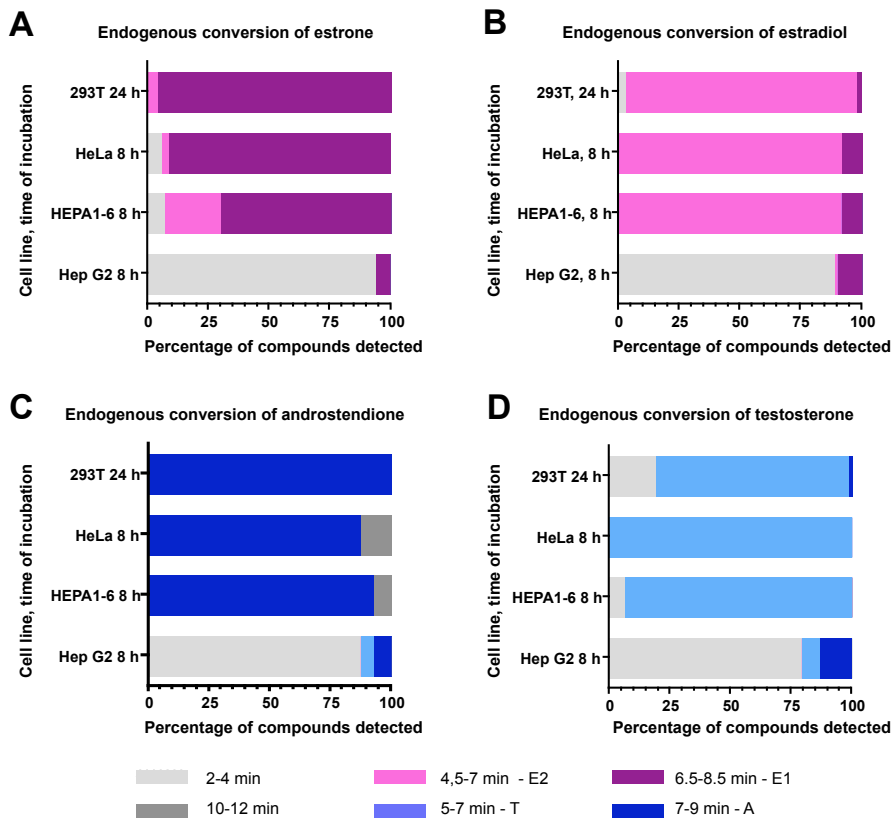


Figure 3.8: Endogenous conversion of androstenedione, testosterone, estrone and estradiol by four different cell lines, HepG2, HEPA1-6, HeLa and 293T. Please note that 293T cells were incubated with the substrates over 24 h while in case of the other three cell lines, incubation time was 8 h. Diagrams are sorted by substrate. For sorting by cell line, refer to fig. 2.43. In addition to the substrates applied, unknown substances were detected at retention times of 2-4 min and 10-12 min.

Obviously, HepG2 cells are the least suited, as within 8 h of incubation most of the substrates added was converted. This is little surprising for two reasons. First, HepG2 are liver-derived. With liver being the detoxification organ, compounds are modified for higher solubility in water. This can be achieved by hydroxylation. Second, HepG2 have been described to be steroidogenically active (e.g. [125]).

The most striking observation in context of endogenous conversion was that HEPA1-6 cells display different patterns as HepG2 cells. This was however expected as both cell lines are derived from hepatocarcinoma. Rather, they are similar to the human cervix

3. Discussion

carcinoma cell line HeLa.

When comparing the conversion of androgens, HeLa might be the cell line of choice. Fig. 3.8 shows that these cells display the lowest conversion of testosterone (for endogenous dihydrotestosterone conversion, see fig. 2.46, p. 57). With HeLa cells being of cervix origin this observation seems rational. Hela cells have also been used in context of steroidogenic research [66].

HeLa cells and 293T cells however have not the same characteristics when it comes to transfection efficiency and growth rates. From the cells tested, highest transfection efficiency could be achieved in 293T cells - a factor crucially influencing an assay with transiently transfected cells. Furthermore, in a functional genomics approach as conducted within this work, it is important to treat all samples as similar as possible in order to be able to compare the results. All substrates were thus tested in 293T cells even if for some (e.g. testosterone, androsterone) a different cell line would have shown lower endogenous conversion.

Differences in the levels of endogenous conversion of 293T cells

Background measurements were included to each experiment with either untransfected (for evaluation of endogenous conversion rates) or mock-transfected cells. Mock-transfection had no measurable influence on endogenous steroid conversion (not shown).

Endogenous conversion of steroid hormones can however change: in some time-course experiments, the cells displayed endogenous conversion of estrone over the whole time (cf. to fig. 2.56 on p. 67, conversion of estrone) at increasing rate. This increase can be explained by the fact that cells continue to divide during incubation. The linear increase of cell number is accompanied by a nearly linear increase in substrate conversion. In other time-course experiments it could be however observed (cf. to fig. fig. 2.51 on p. 62, or to 2.56 on p. 67, conversion of androstenedione), that the steroid converting ability increased significantly 36 h post steroid application in case of estradiol and 60 h in case of androstenedione. This observation could be due to changes in metabolism of the cells. However, it is unlikely be caused by genomic effects of the steroids applied. Genomic action of steroid hormones takes usually place within hours after exposure - in a whole organism it can take days, though [66]. As a cell layer is less complex than a whole organism. Genomic steroid functions should therefore be faster, not slower.

For the late onset of endogenous conversion another explanation seems more likely. With increase of cell number during time-course experiments, a higher total amount of steroids can be converted endogenously. To any detection, there is a threshold. The cells may convert the substrates at any given time without regard to the actual condition of the cells. With increasing cell number, the total amount of endogenous conversion would increase in parallel until the amount is above the detection limit and thus measurable.

In order to further determine these effects, extensive studies would be necessary but were neither within the scope nor aim of this study.

3.6.4. The conversion assay in living cells - is it *in vivo*?

Due to the lipophilic nature of steroid hormones, they are able to pass the plasma membrane as well as the intracellular membranes by passive diffusion. It was thought that likewise within the organism, steroids are released from the transporting protein at the plasma membrane and enter the target cells passively by diffusion (free hormone hypothesis) [73]. However, in contrast to this hypothesis, megalin, an endocytic receptor in reproductive tissues was shown to regulate the cellular uptake of active androgens and SHBG bound steroids [39]. In the cells cultured, this receptor is probably not expressed because neither originating tissue is reproductive.

Within the different subcellular compartments, there are different chemical situations depending on the reactions that are to be performed. There are also differences in cofactor availability and redox-potential. Due to these differences, the correct subcellular localization of the proteins is crucial. Consequently, the proteins under investigation were cloned without epitope-tagging. Though not providing 100% guarantee to correct delivery within the cell, at least no signal sequences can thus be masked.

Cell lines are of course no complete organisms but still mirror close-to-physiological conditions for the assay conducted. The conversion assay presented provides at least the possibility for substrate tests under physiological conditions.

3.6.5. Michaelis-Menten kinetics in living cells

When evaluating the results it became apparent that for half of the conversions conducted, data did not converge to Michaelis-Menten kinetics (see asterik-marked substrates in table 2.12, p. 72). Plotting the data in Excel and inserting a trend line with the accompanying formula into the diagram resulted in a line with a negative point of intersection with the y-axis. Some of the Lineweaver Burk plots (for example, retSDR3 towards E2) have a considerably steeper slope between the last two values (that is, between the two lowest concentrations). This points to the fact that despite the quite low concentrations applied, the enzymes were already approaching saturation and had left the linear region of Michaelis-Menten diagram.

For adequate evaluation of the Michaelis-Menten constant it would be necessary to repeat the experiment under application of lower substrate concentrations. For several reasons, this is however not achievable with the assay applied at this point of time:

1. The radioactively labeled substrates were typically applied at $1 \mu\text{L}$ per experiment.
Due to pipetting technology lower amounts are difficult to apply and result in larger

3. Discussion

- pipetting errors. Especially for Michaelis-Menten kinetics, a correct substrate concentration is indispensable for the outcome of correct values for Michaelis-Menten constant and maximum velocity.
2. It would of course be possible to dilute the radioactive substances prior to application to the assay. But less amount of radioactivity results, logically, in lower peaks in HPLC detection. For the evaluation with Karat-32 software, which was used in this thesis, high peaks are likewise necessary for reliable results as the evaluation of lower peaks results in relatively larger errors in the calculation of integration areas. Furthermore, for chromatograms without ideally flat baseline, the higher peaks are easier to evaluate leading to smaller overall aberrations.
 3. For Michaelis-Menten kinetics, radioactive substances were applied to the cells at $1 \mu\text{L}$ per experiment. The rest of substrate needed for higher concentrations was added from not radioactively labeled substances. Adding different concentrations of radioactively labeled substrate would at least solve the problem of peak height partially but not altogether: For low concentrations, peaks would still be at the lower evaluation limit. In addition, varying peak heights are likely to add further errors to the resulting constants due to evaluation differences.
 4. The radioactive substrates applied to the cells vary in the amount of labeled positions. If substances with a higher number of labeled positions were available, smaller concentrations might be applicable to the assay and could still be evaluated in HPLC.
 5. Theoretically, another possibility could be provided by increasing the amount of medium in the 12-well plates. If more medium was applied to the cells, the gas supply of the cells would decrease. The effect of these changes on the cells cannot be predicted. With 293T cells needing optimal circumstances for culture, this did not seem to yield the expected amelioration.
 6. Yet another possibility might be the decrease of incubation time and, of course, a completely new set-up of the assay conditions. *In vitro* measurement of Michaelis-Menten kinetics would of course also solve the problem but it was not possible to establish these measurements within the scope of this thesis.

Michaelis-Menten kinetics are performed with an excess of cofactor and often also purified proteins in most publications. In the analysis system chosen here, this was not the case. Deviations from Michaelis-Menten kinetic models could therefore be caused by the fact that the reactions observed in intact cells are more complex. Furthermore, they rely on the redox status of the cells. On the other hand, this could also be an advantage as the values determined here are evaluated within in the living system.

3.6.6. Measurement of progestin conversion

Due to the fact that progestins have a key position in the biosynthesis pathway of steroids, their conversion could not be measured under the conditions chosen. Whether or not these conversions can be tested in transfected and harvested cells, that is *in vitro* was not tested in the work at hand. Presumably, the enzymes converting progestins are still active in cell pellets especially if one assumes that the enzyme overexpressed is, too. Addition of the respective cofactor may help to force the reaction into the direction to test (but would then also increase the background activity of this direction). Probably, the safest way to test progestin conversion would be with purified proteins. This way of measurement has been described for instance recently in a publication by Steckelbroek and colleagues [111] but also in most other publications on progestin converting enzymes. Another, much older example for progestin measurement after purification is given by Edwards *et al.* [30], where solubilized preparations of the respective enzymes are incubated with progestins and cofactors for measurement.

However, an intact cell assay using 293 cells has been described by Luu-The *et al.* [69]. The main difference in comparison with the assay used here lies in the incubation time: for characterization of 20 α -conversion it was only 1 h. From experience with the assay used in the work at hand, weak activity towards progestins can probably not be measured within this time. For screening purposes, purified protein may be easier to handle - but protein purification is not easily achieved in medium throughput scale as employed here.

3.7. Studies on subcellular localization

3.7.1. Prediction of subcellular localization

Table 3.1: Wrong and false localization predictions by the servers applied

Server	Σ	correct	false
pSORTII	10	4	6
pTarget	10	4	6
SubLoc	10	1	9
TargetP	10	0	10
LocTree	10	1	9

On eleven SDRs, predictions on the subcellular localization were made by use of five different public servers: pSORTII, pTarget, SubLoc, TargetP, and LOCtree. These servers are only a small selection - over 20 servers are publicly available [104]. Table 3.1 summarizes the correct and false predictions. Predictions on MGC4172 were not included due to the fact that it was not analyzed experimentally and could therefore not be judged.

Overall, the prediction of subcellular localization is not very reliable. This was seen for more than one enzyme under investigation (for one enzyme, all predictions were different). In most cases, at least two servers agreed on

3. Discussion

one localization. In three cases, all predictions proved wrong - even where, for mDhrs4, all servers predicted the same localization. In summary, different algorithms tend to deliver different predictions. For instance, TargetP relies on the prediction of N-terminal sequences [32] while SubLoc judges the overall amino acid composition [41].

No clear preference can be deduced for certain subcellular compartments to be accurately predicted. Experimental data shows that out of ten enzymes investigated, two are localized in the mitochondria (mSdr-o and hRDH13). Both were correctly predicted by pTarget, the latter also by SubLoc1.1. From the two cytoplasmic proteins, human retSDR3 and murine Dhrs4, the latter was incorrectly predicted by all servers. The former, in contrast was precisely predicted by the pSORTII, pTarget and LOCtree servers. The same observation was made for the proteins localized in the endoplasmic reticulum.

Predictions on the subcellular localization do not provide reliability at least concerning the enzymes under investigation in this study. It is unlikely though that non-SDR type enzymes have different localization signals from the SDRs under investigation here. If conducted at all, these predictions should therefore be handled with great care. From the servers used, pSORTII and pTarget showed the best performance - with 40% correct predictions. This rather poor performance is due to several facts (for a review, see [104]): there are unconventional and, in addition, most likely many yet unknown targeting signals. Furthermore, co-translational pathways for protein import into organelles have been described [20] but can so far not be recognized by the prediction algorithms.

It should be taken into consideration however that protein localization does not have to be static but can change. For example, hWWOX has been shown to localize to mitochondria. Upon activation, it is translocated to the nucleus [17]. It is therefore not impossible that supposedly incorrect predictions are, in fact, alternative localizations under different circumstances. However, the method applied for this investigation is standardly used and should therefore provide greater reliability than bioinformatic predictions.

3.7.2. Considerations on the experimental design

For ten out of eleven enzymes under investigation in this regard, I could show their intracellular localization. The experimental data of this section is summarized in table 2.23. Subcellular localization was addressed by GFP- and by epitope-tagging of the respective proteins.

Influence of the cell type

To investigate the influence of the cell type on the investigation of subcellular localization, alternatively cervix-derived HeLa or osteosarcoma-originating SaOS-2 cells were transfected and stained. This was done exemplarily for retSDR3 as shown in fig. 3.9. Human

retSDR3 is cytoplasmically distributed in both cell types. Both cells were found suitable for this investigation as they are well transfected, possess good adhesive qualities (important as many washes are performed during the staining procedure), and have a rather large cell volume enabling good overview.

Though subcellular localization can change for certain proteins (steroid hormone receptors are localized in the cytoplasm but after ligand-binding and dimerization are translocated to the nucleus) it was observed that the localization is cell type-independent. This fact provides greater reliability to the results shown. On the other hand, in a cell type not providing the intended compartment, the protein may just localize anywhere.

Another question that might rightly be asked is whether the correct localization of a rat or murine protein can be observed in a human cell. HeLa cells are often used in studies of subcellular localization, also for non-human proteins. One example is the zebrafish 17β -HSD3: both in HeLa and zebrafish zf4 cells, is localizes to the ER [76]. The cellular system for directing proteins to the right compartments seems to be conserved at least between vertebrates: The application of HeLa cells should therefore not influence the right localization of murine or rat proteins.

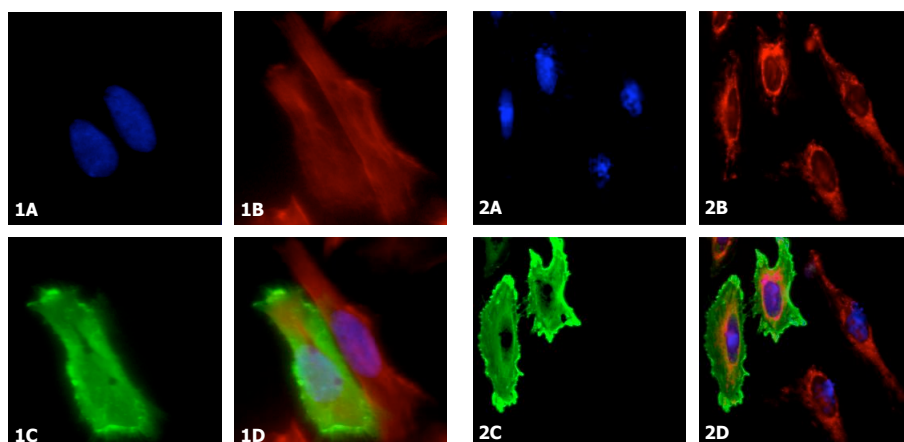


Figure 3.9: Localization of retSDR in SaOS-2 (panel1) and HeLa cells (panel2) after expression from pcDNA4 myc-his Version B. Pictures A depict nuclear staining, picture 1B f-actin counterstaining while 2B shows mitochondrial counterstaining. Pictures C show localization of the retSDR3-recombinant protein, pictures D the overlay of pictures A-C. No change in subcellular localization is observed; in both cell lines, retSDR3 is localized in the cytosol.

Both constructs show the same localization

Not only for cytosolic proteins but also for some of the ER-localized proteins it was observed that both constructs localized to the same compartment. This could hint at the

3. Discussion

presence of an internal signal. However, it should also be taken into account that both constructs might incorrectly localize. This fact can only be elucidated by identifying the signal sequence and deleting or mutating it.

The pAcGFP1-N1 vector - a problematic tool

pAcGFP1-N1 was found to be problematic for the analysis of subcellular localization. Aside from difficulties in the subcloning process the protein expressed from this vector often tends to form inclusions. This fact is illustrated in fig. 3.10 comparing the distribution of mDhrs4 with a C-terminal myc-his-tag or with C-terminally attached AcGFP. All panels in fig. 3.10 are stained in the same way. From the first glance it can be recognized that the distribution of mDhrs4 does not display identical distribution when applying different tags. However, panel B could depict cytosolic distribution when taking into account that pAcGFP1-N1-expressed proteins tend to form inclusions. Panels C and D clearly do not display a cytoplasmic distribution but only inclusions mimicking organellar distribution. However, when counterstaining different subcellular compartments, no overlay could be seen (not shown). In panel C, the inclusions colocalize with the staining of f-actin - indicated by the yellow color. However, panel A (detection of the C-terminally myc-tagged mDhrs4) undoubtedly depicts the cytoplasmic localization.

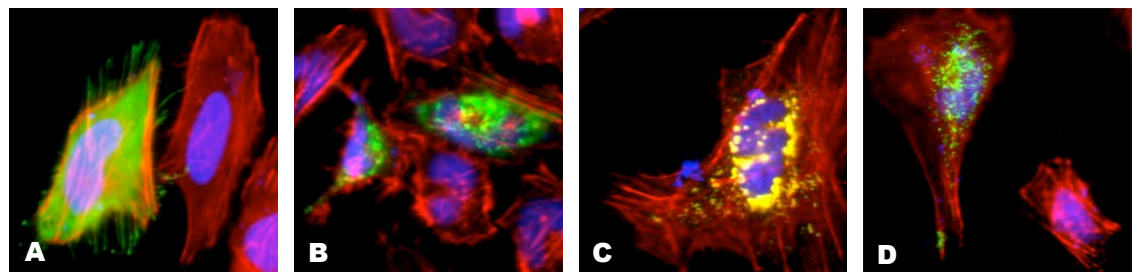


Figure 3.10: Different HeLa cells stained after transfection with C-terminally tagged mDhrs4 constructs. Blobs are inconclusive appearances due to overexpression. A: Cytosolic localization of Dhrs4-myc-his recombinant protein (expressed from pcDNA4 myc-his). B-D: Inconclusive localization of mDhrs4-AcGFP fusion protein (expressed from pAcGFP1-N1). In addition to detection of mDhrs4 recombinant proteins, cells were f-actin and nuclear counterstained.

Other constructs in pAcGFP1-N1 only showed very low or no expression. Again other enzymes, pAcGFP1-N1 delivered clear results as shown in the results chapter, also in comparison with pcDNA4 myc-his-constructs. Interestingly, the application of the original pAc-GFP1-N1 vector without fusion of another protein did not yield these results or tended to inclusions. Because of these difficulties, the system was changed and the enzymes not

yielding reliable results were cloned into pcDNA4 myc-his version B vector.

The pEGFP-C2 vector usually did not display inclusions and if so, in much lower amounts. Fig. 2.69 (see p. 83) shows inclusions by pEGFP-C2 vector in image 1C. The inclusions in this picture do not lead to the inconclusive results shown for pAcGFP1-N1-vector in fig. 3.10.

GFP- or epitope-tagging?

In the work at hand two tagging-strategies were applied for the determination of subcellular localization: addition of GFP to the protein under investigation and epitope-tagging with a myc(-his)-tag.

Two GFP vectors (pEGFP-C2 and pAcGFP1-N1) were at hand and therefore selected. The addition of GFP to a protein is rational experimental design for life-cell-imaging but not necessarily for staining of fixed cells. As shown by the example of pAcGFP1-N1, overexpression of GFP-tagged proteins can lead to intracellular inclusions and therefore hard-to-evaluate results. When expressing the fusion proteins from pEGFP-C2, this kind of artifacts could also be observed though at a much lower frequency and therefore without consequences on the results (see above).

When expressing recombinant proteins with a myc-his-tag, subcellular localization was much easier to determine. Especially small cellular structures (as the endoplasmic reticulum) could be detected more adequately. Also in the detection of the endoplasmic reticulum by overexpression of N-FLAG sarcolipin and subsequent detection of the FLAG-tag, this coincidence became clear. In the determination of subcellular localization of proteins in fixed cells epitope-tagging and subsequent detection by immunofluorescence appears to be the method of choice.

Counterstaining strategies. For counterstaining different subcellular compartments, two different methods were applied: application of an actively delivered tracker (ER, mitochondria) and counterstaining by detection of co-overexpression.

Staining of subcellular compartments using tracker. Trackers for subcellular compartments are very convenient in application: the fluorescently labeled molecule is added to culture medium, applied to the cells and incubated for 30 min. Mitochondrial tracker in general produces reliable results and is universally applicable. There were however two side-effects observed in the application of mitochondria tracker. First: it also counterstains the nucleoli (see fig. 3.11, picture 2D). This is not an artifact but characteristic of this mitochondrial tracker. Second: overexpression of a mitochondrially located fusion-protein at high level sometimes caused failure in MitoTracker staining (not shown). This was however not the fact in all cells and did therefore not influence the outcome.

3. Discussion

The mitochondrial tracker molecule is covalently bound in the mitochondria. ER tracker, in contrary is not, and thus needs to be applied as single staining method. As also indicated in the manufacturer's manual, it is washed out with subsequent permeabilization and further staining. Furthermore, ER tracker has to be freshly prepared and should not undergo various freeze and thaw cycles because otherwise the color fades considerably. For these two reasons, other methods for counterstaining the endoplasmic reticulum were applied especially in combination with antibody staining.

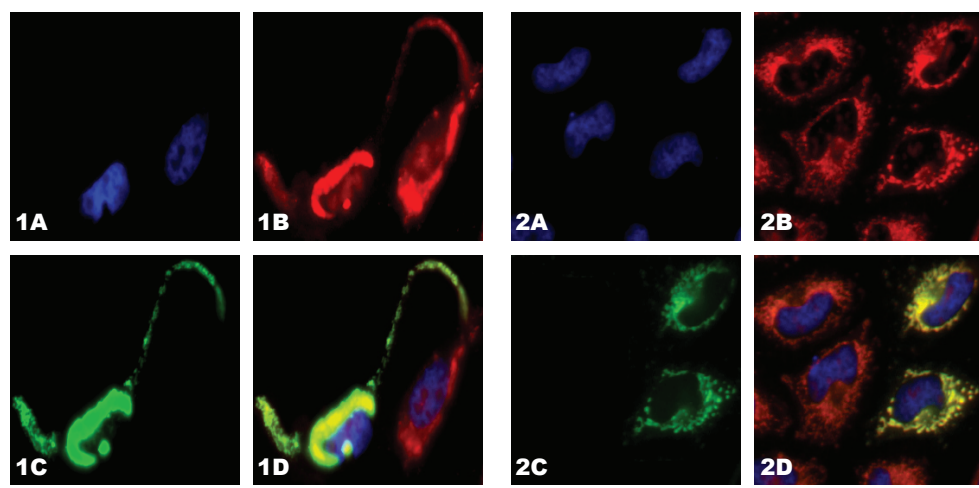


Figure 3.11: Changes in mitochondrial structure observed after the overexpression of C-terminally GFP-fused human RDH13 (expressed from pAc-GFP1-N1, both panels). Costaining of the nucleoli by mitochondria tracker is no artifact (see 2D). in both panels, the pictures depict: A - DAPI nuclear staining, B - mitochondrial staining, C - GFP distribution, D - overlays of pictures A to C.

Counterstaining by co-overexpression. Fig. 3.11 illustrates the big influence that overexpression can have on subcellular compartments even if only one protein is overexpressed. The figure depicts cell staining experiments with overexpression of human RDH13 in fusion with GFP (expressed from pAcGFP1-N1). In panel 1, the structure of mitochondria is altered in comparison with panel 2. This seems to be due to the overexpression of one recombinant protein.

The possible effect of two proteins overexpressed simultaneously can therefore be imagined. As an alternative for ER tracker in staining of the endoplasmic reticulum, N-terminally FLAG-tagged rabbit sarcolipin was co-transfected [84]. As the FLAG-tag was (like the myc-tag) detected by antibody staining, this method was reliable for the workflow applied. and not washed out. ER-staining with N-FLAG sarcolipin could be applied as the expression of this construct is rather low (personal communication, Dr. A. Oder-

matt, University of Berne, Switzerland). On the other hand, overexpression is a common practice in cell culture experiments. As it could alter the results it should be avoided if possible.

Conclusion: antibody staining. The best method of counterstaining would probably be immunofluorescent detection of an endogenously expressed protein within the given subcellular compartment. Thereby, artifacts could probably be limited to a minimum. Consequently, detection of the endogenously expressed protein by the same method would probably yield the most reliable results - but as antibodies against uncharacterized proteins are usually not available, this can not be achieved at most of the times.

3.8. Conclusions about the enzymes under investigation

After the identification of a large number of putative SDRs, thirteen enzymes were chosen for further analyses. Most of these enzymes had been annotated as SDRs in the database, but had not been further characterized at the beginning of this thesis. The results obtained from investigations on the remaining enzymes will be summarized and discussed in the following sections.

3.8.1. Murine orphan Sdr (Sdr-o)

Murine Sdr-o was described as a novel SDR by Chen and co-authors in 2002 [19], using an *in vitro* assay to address the question of substrate specificity. After transient overexpressing, no activity was found towards retinoids, 3 α -androstaneadiol, androsterone, testosterone, estradiol, and corticosterone. The authors found mSdr-o to be exclusively expressed in adult human and murine liver and additionally in the developing murine embryo (dpc 7, 11, 15, and 17). Several transcripts of 1.4, 1.5, 2.6, and 8.9 kb in size were reported.

In my experiments, the expression analysis covered several adult tissues but only one RNA sample from embryonic tissues. I detected equally high expression in murine liver, brain, spleen, testis and even higher in ovary. Furthermore, ISNB revealed expression in the skin. All transcripts but the 8.9 kb mRNA species were detected in my experiments. The lack of even distribution of mRNA species in all tissues examined might point to alternative splicing.

With the conversion assay in physiologically intact cells, I could not detect any catalytic activity towards steroids. PCR did not indicate overexpression of murine Sdr-o. However, if it was expressed (and not detected) this would be in line with the findings of Chen *et al.*. Due to lack of proven overexpression, I cannot draw further conclusions about substrate specificity of murine Sdr-o. As the myc-tagged protein was shown to be localized in

3. Discussion

mitochondria, conversion assays could be repeated with this construct, yielding further results on this topic at least in regards to determination of overexpression.

mSdr-o and vitamin D? From the high expression in ovaries, steroid metabolism involvement does not seem unlikely. High expression in liver and skin, as well as expression in the kidney (detected by ISNB), might also hint at vitamin D metabolism. These three tissues are the biological places of vitamin D biosynthesis [70]. The expression in steroidogenic tissues may not be a contradiction to this hypothesis: Hughes and coauthors have shown, that 1,25-dihydroxyvitamin D₃ can regulate the estrogen metabolism of keratinocytes at least in cell culture [44].

In determination of subcellular localization, I could show that murine Sdr-o localizes to the mitochondria. Localization of the protein was observed with a C-terminal tag. This is in line with the fact that mitochondrial import is delivered by N-terminal signal peptides. This does not fit the vitamin D-hypothesis as metabolism and biosynthesis of this steroid class are localized in the endoplasmic reticulum [70]. However, Slominski *et al.* [109] show that mitochondrially localized CYP11A1 (a member of cytochrome P450 family) can metabolize vitamin D₃. This finding opens a new alternative of vitamin D₃ metabolism. Furthermore, vitamin D₃ has been shown to induce a mitochondrial apoptosis pathway in MCF-7 breast cancer cells [123].

mSdr-o and retinoids? Regarding my own results based on phylogenetic analysis, it is surprising that Chen *et al.* [19] could not detect enzyme activity towards retinoids as I saw close vicinity of mSdr-o to retinoid dehydrogenases. Retinoid conversion thus remains a putative target of mSdr-o. Retinoid X receptor (RXR) is important in most of the fatty acids and cholesterol metabolic regulations [24]. In RXR deficiency, tissues such as eye, skin, heart, and testis are affected and the embryonic development of mice is disturbed [72, 124]. mSdr-o could therefore be an enzyme providing RXR ligands for expression regulation of target genes. As the hypothesis on vitamin D conversion, retinoid conversion by mSdr-o is supported by the expression pattern though no activity towards these substances was detected under the conditions chosen by Chen and coauthors [19].

Further studies will be necessary to determine the physiological role of mSdr-o. Another hint could be provided by promoter studies as both vitamin D and retinoids have effects on transcriptional regulation. Conversion assays with vitamin D and its metabolites should not be excluded from future studies.

3.8.2. Human retSDR3

retSDR3 was originally cloned from retinal cDNA by Haeseleer and coauthors [38]. The authors showed high (and almost exclusive) expression in the retina, but low expression amounts also in the liver. They found the enzyme to be phylogenetically related to the murine lung carbonyl reductase. In activity assays, no conversion of retinoids or steroids could be detected.

Phylogenetic analyses. In the phylogenetic analyses conducted here, murine lung carbonyl reductase was not included as it had not been detected in the BLINK search. As mentioned earlier, BLINK had not found many related SDRs except from prokaryotes and the respective homologues. The closest relatives of retSDR3 are depicted in fig. 3.12, a detail from the phylogenetic tree used for the rest of analyses. retSDR3 alias DHRS10 and its bovine, canine, and zebrafish homologues are boxed in purple, with the human enzyme (under investigation in the work at hand) shaded in violet. Exemplarily, one prokaryotic SDR of the group of related SDRs is shown and boxed in blue. Additionally, the closest characterized SDRs are boxed in green.

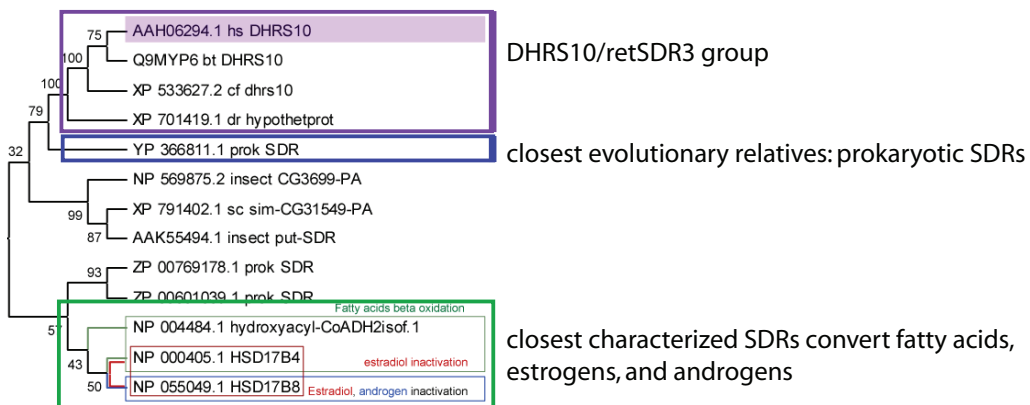


Figure 3.12: Detail from the phylogenetic tree used. The closest relatives found at this point of time are prokaryotic SDRs (only one is exemplarily depicted) and fatty acid and estrogen converting 17β HSD types 4 and 8.

The crystal structure of retSDR3 and its substrate specificity. Phylogeny may provide a hint at retSDR3 substrate specificity. The work on retSDR3 was in large parts conducted in cooperation with the laboratory of Dr. Udo Oppermann, where retSDR3 was crystallized. retSDR3 displays the classical SDR fold. In examination of the substrate binding cleft's dimensions, it became apparent that fatty acids may be substrate to retSDR3. This could however not be shown experimentally. In addition to the activity of retSDR3 shown

3. Discussion

in this work, Petra Lukacik could also detect a minimum activity towards testosterone and 5-androstene- $3\beta,17\beta$ -diol. In the conversion assay in the work at hand, no activity towards testosterone was seen; 5-androstene- $3\beta,17\beta$ -diol was not tested due to lack of availability. These findings are in line with the phylogenetic analyses showing evolutionary relationship with the fatty acids and estrogen converting type 4 17β -HSD and type 8 17β -HSD which in addition can also convert androgens. However, steroids may not be the main substrate of retSDR3.

In time-course experiments, a sudden increase in turn-over of substrate was detected after 36h. This could have several reasons: first, expression of retSDR3 is slow in 293T cells. Second, the increase 36h after addition of the substrate is due to the fact that considerably more cells express retSDR3. 36 h equals approximately two doubling times of these cells. The reasons for this increase were not further investigated. In order to examine this issue, further experiments would be needed as tagged expression and verification (and quantification) with western blot and cell number analysis over time. These experiments were not aim to this study.

In the work of Lukacik and coauthors [67], V_{max} was determined in relation to the cofactor of the reaction, NADH and can therefore not be compared with the values presented here. Furthermore, turnover number K_{cat} was determined in this work. This constant could not be evaluated in the work at hand due to lacking possibilities of protein quantification within the living cells. K_m towards estradiol was determined to be $5.6 \pm 1.7 \mu M$. The value determined in living cells (see table 2.7, fig. 2.52, p. 63f) is only about one third of this value, indicating a much higher affinity towards estradiol *in vivo*. The maximal velocity determined for this reaction is $2.3 \times 10^{-7} \mu mol/min$.

Divergence was shown in values evaluated for K_m and V_{max} under physiological conditions and from purified protein. I could show that the measurements in this thesis relate to retSDR3. They point to a considerably higher affinity towards estradiol than concluded from the experiments with purified protein. Physiological levels of estradiol range from 0.075 to 1.3 nM in blood [82] In target cells, the local concentration may increase to the micro-molar range though. A Michaelis-Menten constant of $1.8 \mu M$ could therefore be rational. To strengthen this concept further, the conduction of Michaelis-Menten kinetics with purified protein should be reconsidered.

Expression analyses. When conducting expression analysis for retSDR3, I could see no especially high expression in the eye with ISBN. High expression of more than one transcript species was detected in brain, liver, and placenta. Furthermore, the transcripts observed were longer than the one described before [38]. The high expression in placenta corroborates the shown involvement in steroid metabolism. It is important to remember that lower levels of steroid hormones can also be present in peripheral tissues. The fact

that expression of retSDR3 is not restricted to placenta does therefore not interfere with this hypothesis.

Subcellular localization of retSDR3. The experiments for the subcellular localization of retSDR3 were conducted both in HeLa cells and in SaOS-2 cells, a human osteosarcomic cell line. From both cell lines, the same result, a cytoplasmic localization, was obtained. I could therefore show the localization of retSDR3 is cell-type-independent (see fig. 3.9, p. 107).

Conclusions. Wrapping everything up, retSDR3 may well play an important role in the inactivation of estradiol. In placenta, it might cooperate with type 2 17 β -HSD2, especially being active at high levels of the steroid hormone. In the liver, it could inactivate falsely delivered estradiol and in the brain take part in the neurosteroidogenic pathways. Based on these results, we proposed retSDR3 to be a new member of 17 β -HSD-group, type 14 [67].

3.8.3. Rat SDRs under investigation: dhrs7b and dhrs8

On the topic of rat dhrs7b, there is no publication available. In fact, only when conducting final database research before summarizing all results, I could find out that this protein, LOC287380 is the homologue of human DHRS7B and is accordingly called like its human homologue. Its previous name is however still depicted in fig. 2.2 in the results chapter (p. 23). The overall situation for rat dhrs8 is similar to rat dhrs7b: no further information is available, no substrate specificity could be found within the set of substrates tested. In regard to their subcellular localization, I could show that both enzymes are located in the endoplasmic reticulum. The most striking results for both enzymes were the expression patterns (see fig. 2.15, p. 39 and fig. 2.17, p. 40).

dhrs7b For dhrs7b, expression is almost opposite in the two genders. No expression was detected in the classical sex-hormones dependent tissues, ovaries and testis. Especially from the large deviations in expression both between the two genders and also between experimental and *in silico* data, prediction of possible substrate specificities is challenging. Taking the experimental expression analysis into account, one might think of energy metabolism, that is, conversion of sugars or fatty acids. Based on the results obtained from the characterization of rat dhrs7b, few conclusions can be drawn. Despite the lack of expression of rat dhrs7b in ovaries and testis the divergence of expression in female and male rats could point to a function that is sex-specific or within sex-specific pathways. On the human homologue, no information was found.

3. Discussion

dhrs8 Dhrs8 also displays a gender specific difference in expression but not as striking as drhs7b. Dhrs8 is expressed in testis (and prostate) but not in the ovaries. This might point to a predominantly male specific function. The fact, that females only seem to express the gene in colon and cerebellum but that males show a broader expression pattern is in agreement with this hypothesis. The subcellular localization is in line with this speculation: also the androgen-metabolizing type 3 17β -HSD localizes to the ER [76]. Human DHRS8 is known to convert androgens and estrogens [14]. Further studies point to additional involvement in lipid metabolism [16,80]. In the study by Brereton and coauthors [14], androstanediol was the steroid hormone preferentially converted by DHRS8. This substrate could however not be tested due to availability.

Further knowledge on these proteins has to be gained in order to define the physiological roles of both rat dhrs7b and dhrs8.

3.8.4. Retinol dehydrogenases under investigation: murine type 12, human types 12 and 13

Haeseleer and coauthors provided characterization of retinol dehydrogenases type 11 to 14 in 2002 [37]. Their characterization was based on retinol conversion and phylogenetic properties showing that the four different retinol dehydrogenases are closely related. Especially for the human RDH12, many new perceptions have been published during the last two years. It has been shown, that the protein has a crucial function in the visual cycle. If dysfunctional, retinal degeneration and Leber Congenital Amaurosis (LCA) can be the consequences [46, 92, 115]. Furthermore, Belyaeva *et al.* described the biochemical properties of retinoid conversion by RDH12.

Phylogenetics and substrate specificities. All three retinol dehydrogenases under investigation for their ability of steroid hormone conversion clustered in one branch of retinol dehydrogenases (see fig. 3.13).

While murine Rdh12 and human RDH13 did not convert any substrate applied, I could show that human type 12 retinol dehydrogenase converts dihydrotestosterone to androstanediol. In addition to activity towards retinoids, human RDH12 therefore displays 17β -HSD activity. Biochemical data is available for RDH12 conversion of retinoids. In the above-mentioned publication [7] RDH12 showed K_m values between 0.04 and 0.14 μM towards all-trans-, 11-cis- and 9cis-retinal, between 0.16 and 0.4 μM towards all-trans-, 11-cis- and 9cis-retinol, and of 3.1 μM for the conversion of nonanal. Furthermore, RDH12 revealed a preference for the phosphorylated cofactors NADP $^+$ and NADPH/H $^+$ with a several hundred-fold lower Michaelis-Menten constant. As most SDRs prefer the phosphorylated cofactor for reduction and NAD $^+$ for oxidation [93], this might indicate that RDH12 mainly acts reductive under physiological conditions. This would be in line with

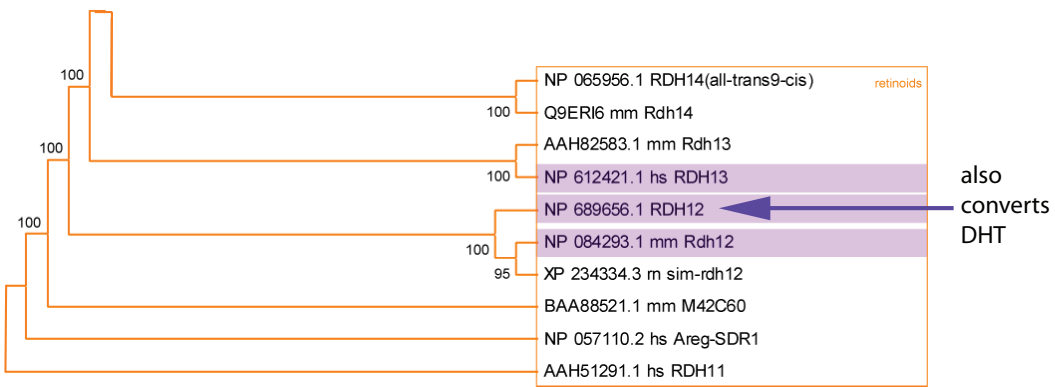


Figure 3.13: Detail of phylogenetic tree (see bottom of fig. 2.37 on p. 50) showing the cluster of retinol dehydrogenases. In this work, RDH12 was shown to possess conversational activity towards dihydrotestosterone in addition to its retinol specificities that were previously shown (see text).

the finding that RDH12 reduced dihydrotestosterone to androstanediol. The determined K_m of $1.6 \mu\text{M}$ lies in the same range as the values shown for retinoid conversion. This conversion could therefore very well be of physiological relevance. However, nonanal is a retinoid from plants and thus not a main substrate of human RDH12. In conclusion, DHT is probably more of a side track for RDH12 besides the main physiological task, conversion of retinoids. There has been no description for the involvement of steroid hormones to Leber's congenital amaurosis. However, ophthalmologists being busy preventing blindness might not lay the focus on searching for additional, not obvious errors of metabolism. Taking into consideration that Michaelis-Menten constant of retSDR3 was only about 40% in living cells compared to conduction with purified protein, it is even more likely that RDH12 will not convert much dihydrotestosterone *in vivo*.

Expression patterns and substrate conversion. For the murine Rdh12, northern blot analysis suggested low, almost ubiquitous expression with proportionally highest levels in heart, brain, liver, and spleen (see fig. 2.19 on p. 40). The bands detected on this membrane can not be remains from murine Dhrs4 as Rdh12 had been hybridized to the membrane prior to mDhtrs4. ISNB however, clearly suggests retinoids as likely substrate with most prominent expression levels in skin, brain and neuronal tissue and the eye. The latter is in accordance with the annotation of the gene as a retinol dehydrogenase. Also in case of the human RDH12, ESTs were predominantly eye-derived. This would be in line with the finding that almost no RDH12 expression was seen in northern blot analysis (cf. to fig.s 2.21 and 2.21 on p. 41). For RDH13, a ubiquitous expression pattern was

3. Discussion

observed both in wet lab and *in silico* analysis (refer to fig.s 2.23 and 2.23 on p. 42).

The subcellular localization. Both homologues of retinol dehydrogenase type 12 co-localized with ER staining. RDH13 displayed mitochondrial distribution. In case of murine Rdh12 and human RDH13, no references could be found on localization data. Human RDH12 data was published by Thompson and coauthors in 2005 [115]. These experiments showed the intracellular localization of the wildtype and several mutated proteins. The authors did however not determine the exact subcellular localization of the protein.

Conclusions on the investigation of retinol dehydrogenases type 12 and 13. For all three retinol dehydrogenases I obtained mostly faint signals on northern blot - RNA from eye was not included. However, the RDHs seem to be ubiquitously expressed at least at low levels. Both homologues of RDH12 (human and murine) localize to the endoplasmic reticulum, while human RDH13 is imported to mitochondria. Interestingly, for the best-characterized of these enzymes, human RDH12 I could show an additional substrate specificity towards dihydrotestosterone.

3.8.5. Murine Dhrs4

Data are completely lacking on murine Dhrs4. The determination of subcellular localization in my experiments displayed surprising results: while the five servers applied predicted a mitochondrial localization, the human homologue DHRS4 is annotated as peroxisomal SDR. The selection of prediction servers was partly arbitrary though. By use of different prediction servers localizations other than mitochondrial were predicted (not shown). In the experimental analysis murine Dhrs4 turned out to be cytosolic. However, proteins lacking the right signal sequences are also directed to the cytosol. Need of both a free N- and C-terminus for the correct localization is an alternative that could disprove the experimental data. This issue could be addressed by either addition of an internal epitope detectable for these studies or by use of an antibody against the mDhrs4 protein itself. No Dhrs4-specific antibody is however available so far.

In northern blot, there was a rather broad expression detected though with distinct bands neither in testis nor in ovaries, being in accordance with the ISNB results. In addition to the tissues analyzed, ISNB displayed expression in breast, bone and cartilage, and tumor tissue (see p. 43). From the expression pattern, mDhrs4 suggested no sex specific steroid substrate specificity but rather help to the decision on the branch of steroid synthesis (sex steroids or corticoids). In the analysis of substrate specificity however, murine Dhrs4 displayed the broadest acceptance of offered substrates of all enzymes investigated:

3.8. Conclusions about the enzymes under investigation

it converts estrone, to a lesser extent androstenedione and dihydrotestosterone. This observation is supported by the respective values from Michaelis-Menten kinetics. For estrone, a Michaelis-Menten constant of $4.3 \mu\text{M}$ was determined. When compared to the respective constant of human 17β -HSD1 ($0.02 \mu\text{M}$, [43]) it is obvious that the enzyme has a much lower affinity than the main estradiol-forming enzyme described. However, mDhrs4 shows high levels of expression in peripheral tissues where 17β -HSD1 is not expressed.

Murine Dhrs4 could therefore play a role in the activation of estrone and androstenedione in peripheral tissues. The high expression in breast and tumor tissue corroborates this conclusion. Murine Dhrs4 may be yet another enzyme complementing 17β -HSD type 1 (and eventually type 7) thus further underlining the importance of steroid hormone metabolism. In conclusion, murine Dhrs4 is a new 17β -HSD.

3.8.6. Human DHRSX

Human X-linked SDR (DHRSX) was cloned in 2001 by Gianfrancesco and coauthors [36]. They described the chromosomal annotation in the pseudo-autosomal regions of X- and Y-chromosome and consequently named the gene DHRSXY. In most database entries, it is only called DHRSX and is referred to by this name within the work at hand. Furthermore, a rather broad expression spectrum was described with two transcripts of about 5 kb and 2 kb, respectively. Highest levels of expression were detected in heart, muscle, pancreas and also thymus. As the control (β -actin) also showed elevated levels in these tissues, it seemed that the gene DHRSXY is ubiquitously expressed at low levels.

In the work at hand, expression was detected at higher levels than shown before and detected the existence two transcripts: a 2.5 kb transcript was seen and additionally, a smaller transcript of approximately 1.8 kb. The transcripts detected were thus much smaller than the ones described before [36]. Furthermore, I could show high levels of mRNA in spleen, prostate, testis, and ovaries but also considerable amounts in the rest of tissues analyzed, confirming with the ubiquitous expression described before [36].

In localization studies I found DHRSX localized to the ER. When subject to the steroid hormone conversion assay, turn-over of dihydrotestosterone to androstanediol was detected at a K_m of $1.8 \mu\text{M}$ and with a V_{max} of $3.7 \times 10^{-7} \mu\text{mol}/\text{min}$. The results suggest role of DHRSX in androgen metabolism both in the classic target and in peripheral tissues. As the Michaelis-Menten constant is however rather high, it may well be that the DHT conversion is not the main task of this enzyme. Especially when judging from the high expression levels in steroidogenic tissues there may well be further steroidogenic compounds to be found that are converted by DHRSX.

3. Discussion

3.8.7. Human and murine WW-box containing oxidoreductases

Much is known about the WW domain containing oxidoreductases in both human and mouse. They are localized in the mitochondria but upon activation, are translocated to the nucleus where they display pro-apoptotic properties (for a review, see [17]). Human WWOX had been described to be a tumor-suppressor gene interacting with several intracellular signaling proteins [6, 18]. However, the substrates converted by both homologues remained unknown.

Expression of mWwox in the mouse embryo. During the work on this thesis, investigations on the expression of murine Wwox during embryonal development were started. Wwox was described to possess pro-apoptotic abilities [17]. Whole mount *in situ* hybridizations were conducted on embryos at dpc 13.5, 14.5 and 15.5 (not shown). Preliminary results show similar patterns of expression as described for the apoptosis and expression of cholesterol biosynthesis genes. Unfortunately, this aspect expanded beyond the frame of this thesis. Further experiments will be needed for definite conclusions.

Implications of northern blot and ISNB results. In expression analysis, several transcripts were found for both human and murine WWOX. In the NCBI database, at least eight splice variants are described (fig. 3.14). This has been subject to several publications (e.g. [27]). Splice variants are also known for the murine gene but are not depicted.

The comparison of the variants with the protein scheme (fig. 3.14 3) shows that the five variants 3-7 can not produce a functional SDR type protein as they lack the active center, and in case of variant seven also the cofactor binding region. Theoretically, variants 1, 2, and 8 could result in functional SDR-type proteins with variant 8 lacking the second WW box.

When comparing these splice variants to the result of the northern blot, it is obvious that the band sizes (between 1 and 5 kb) and lengths of the splice variants do not converge. Due to resolution of the marker applied to the northern blot membrane, signals and WWOX isoforms (cf. to fig. 3.14 in chapter Discussion) can not be correlated to their tissue-specific expression. However, most bands are larger than would be expected with the longest isoform being 2.2 kb in size. Two explanations are possible for this fact: first, the mRNAs deposited to the database lack parts of the 5' or 3'UTRs. In addition, the signal at 5 kb could depict a new isoform of WWOX.

The northern blot for both genes showed rather broad spectra of expression with highest levels of the human gene in spleen and of the murine gene in ovaries, but also in brain, kidney, and testis. *In silico* analyses revealed high expression in neuronal and tumor tissues for both homologues. At the first glance, this may be surprising. It is however conceivable that in those tissues pro-apoptotic genes are up-regulated as means of the organism to

3.8. Conclusions about the enzymes under investigation



Figure 3.14: Splice variants of human WWOX as deposited in the NCBI database. 1: CDS of the SDR putatively functional as enzyme (length is depicted as nt) 2: exons annotated 3: Protein deduced from 1, SDR motifs and the WW boxes are indicated, protein length is given in aa. 4 a-h: Exons included to the the respective splice variants, lengths are depicted in nt.

defeat the tumor.

The substrate specificity. Regarding the knowledge about human WWOX, this work does not add much to what is already known. From the expression patterns, a steroidogenic substrate seemed more likely for murine than for human WWOX. Accordingly, in substrate conversion assays, human WWOX did not show any activity towards the substrates offered - the murine homologue converted androstenedione and androsterone with values for the Michealis-Menten constant of 0.7 and 2.2 μ M, respectively. On the other hand, the homologues are highly conserved and, even though did not convert the same substances. This is however also known for other proteins: rodent 17 β -HSD1 converts androgens besides estrogens, while the human enzyme shows activity only towards estrogens [78]. As conversion rates displayed by mWwox are not very high, androgens may not be the main substrate to this enzyme. It is not unlikely that the WW-box containing oxidoreductases may convert a steroidogenic substrate which still needs to be identified.

3. Discussion

Perhaps, this could be oxysteroids, a recently identified group of physiologically important sterols [47]. These substances seem to display hormonal properties [47] and are intermediates from cholesterol metabolism. In earlier phylogenetic analyses, WWOX proteins were seen in close vicinity to 17β -HSD 7 which was shown to be part of cholesterol biosynthesis converting zymosterone to zymosterol [71]. Alternatively, the main physiological function of these proteins may not be an enzymatic conversion but the proapoptotic role that was described several times.

3.8.8. MGC4172 and MGC18716

For both homologues, MGC4172 and MGC18716, no literature or other data are available so far.

When identified, the protein sequences were annotated too short lacking the cofactor binding site. In the meantime, a human full-length protein was submitted to the database and is accessible with the code AAQ89074. In preparation for phylogenetic analyses, a BLINK search was conducted with this accession code and revealed few related sequences. Most were originating from prokaryotes or from insects. Furthermore, one closely related sequence each from different vertebrates was identified - these sequences presumably depict the respective homologues from these species.

While conducting the database analyses, I observed that most SDRs display only the adh_short domain in the conserved domain search. For MGC4172 and its murine homologue, more possibilities are given with low probability of false-positive hits. All domain-alternatives (adh_short, shikimate/quinate 5-dehydrogenase, and several SDR subfamily domains) are typical for different SDR-subfamilies with regard to substrate specificity. It is, however, striking, that most of these point to an involvement in amino acid metabolism (not shown). Phylogenetic analyses (see fig. 2.37, p. 50) did also not display close relationship with steroid or retinol dehydrogenases included.

Expression analyses yielded differences between MGC4172 and MGC18716. The human gene, MGC4172, was seen ubiquitously expressed at low levels the higher levels in spleen, prostate, testis, and ovaries. The murine MGC18716 on the other hand was only seen in spleen, thymus, kidney, and lung. Overall, it is difficult to conclude much from the expression patterns displayed by both human MGC4172 and MGC18716. The safest conclusion may be that it is unlikely that both proteins convert the same substrates *in vivo*. Though displaying overall 92% identical amino acids, the vicinity of the active center is not as conserved (see fig. 3.15, blue ellipse).

Both proteins showed no conversion of the substrates offered under the conditions chosen. Especially for human MGC4172, it is unclear whether it was expressed from the transfected pcDNA3-plasmid. Subcellular localization could be shown only for MGC18716 in the endoplasmic reticulum. From the high conservation of the two proteins, the same

3.8. Conclusions about the enzymes under investigation

mouse: 1	MTRAGMERWRDRLALV	TGASGG	G	AAVARALVQQGLKVVGCARTVGNIEELAAECKSAGY	60
	M R GMEWRDRLALV	TGASGG	G	AAVARALVQQGLKVVGCARTVGNIEELAAECKSAGY	
human: 1	MARPGRMERWRDRLALV	TGASGG	G	AAVARALVQQGLKVVGCARTVGNIEELAAECKSAGY	60
mouse: 61	PGTLIPYRCDSLNEEDILSMFSAVRSQHSGVDICI	NNAG	MARPDTLLSGSTSGWKDMFNV	120	
	PGTLIPYRCDSLNEEDILSMFSA+RSQHSGVDICI	NNAG	+ARPDTLLSGSTSGWKDMFNV		
human: 61	PGTLIPYRCDSLNEEDILSMFSAIRSQHSGVDICI	NNAG	LARPDTLLSGSTSGWKDMFNV	120	
mouse: 121	N VLA NVLALSIC	TREAYQSMKERNIDDGHIININ	S	MCGHRVPPQSIVHF	180
	NVLALSIC	TREAYQSMKERN+DDGHIININ	S	M GHRV P SV HFYSATKYAVTALTEGL	
human: 121	N VLA NVLALSIC	TREAYQSMKERNVDDGHIININ	S	MSGHRVLPLSVTHF	180
mouse: 181	RQELLEAQTHRATCIS	PG LVET	QFAFKLHDKDPEAAATYEHIKCLRPEDVAEAVIYVL	240	
	RQEL EAQTHRATCIS	PG+VETQFAFKLHDKDPEAAATYE +KCL+PEDVAEAVIYVL			
human: 181	RQELREAQTHRATCIS	PG VVET	QFAFKLHDKDPEKAAATYEQMKCLKPEDVAEAVIYVL	240	
mouse: 241	STPPHVQVGDI	QMRPTEQVT	260		
	STP H+Q+GDIQMRPTEQVT				
human: 241	STPAHIQIGDI	QMRPTEQVT	260		

Figure 3.15: Alignment of MGC18716 (mouse) and MGC4172 (human). SDR motifs detected by the SDR Finder are shaded in gray, SDR motifs described in [86] are depicted in red. Green ellipses highlight differences at C- and N-terminus of the proteins, blue ellipse in the vicinity of the active center.

subcellular localization is likely. Furthermore, the predictions on that topic are very similar for both proteins (refer to table 2.22, p. 85). This points at least to conservation of the terminal sequences which are often important for subcellular localization. As on amino acid level, both share a high identity of 92%, I would predict MGC4172 to have the same subcellular localization as its murine homologue in the ER. Furthermore, the differences in the N- and C-terminus of the proteins are quite low (see fig. 3.15, green ellipses).

There is little but hypotheses to conclude from the results obtained in the investigation of MGC4172 and MGC18716. Especially the expression pattern displayed by murine MGC18716 leaves room for speculations on its substrate specificity. It could correlate with a conversion of corticosteroids: in the kidney, they are needed for regulation of water and electrolyte balance. As glucocorticoids are known as immunosuppressors, an enzyme converting these steroids could be expressed in spleen and thymus, two tissues important for T-cell maturation. Furthermore, immunological responses are needed in the gastrointestinal system and the skin in order to protect the organisms from incoming threats, the ESTs found in these tissues may point to this direction. This theory may also provide further explanation for the low expression level observed both in the northern blot and in *in silico* analysis: if the enzyme really was active in an immunological context, it could be expressed only under very defined conditions and therefore be tightly regulated. This hypothesis does not hold true for the human homologue, MGC4172. Fig. 2.33 clearly shows high expression levels for steroidogenic tissues, namely prostate, testis, and ovary

3. Discussion

next to the most prominent signal from spleen. Therefore, MGC4172 could additionally be important in the conversion of sex steroids. Despite the high degree of conservation, the same could hold true as for 17β -HSD6: while the rodent enzyme converts steroids, the human homologue is involved in retinoid metabolism but can also convert steroids [10, 42]. The conserved domains rather point to involvement in amino acid metabolism.

3.9. What else could be done?

Additional possibilities for addressing protein function in wet lab analysis

There are of course many more aspects in the complete functional characterization of a new protein than were addressed in this thesis. Further experiments could be conducted for example on the following topics. Yeast-two-hybrid screens, promoter studies and the generation and characterization of knock-out mice is rather deep-drilling analysis and so far not achievable for a medium-throughput scale of analysis as conducted in the work at hand.

Determination of substrate specificity. For further evaluation of the substrate specificities of the enzymes under investigation, screens against chemical libraries with putative SDR substrates (fatty acids, sugars, amino acids, further steroids, ...) could be performed. With purified protein or cell pellets (after transient overexpression) this could be done by measuring cofactor conversion with application of UV/VIS spectroscopy.

Search for protein interaction partners. Proteins usually do not fight single combats but are part of complex networks working by direct short-term or complex-forming interactions [13]. Therefore, interaction analysis would be helpful to understand the full dimensions of a protein's task. First hints for the implication of WWOX with apoptosis were achieved by two-hybrid screens and based on the observation, that it interacts with cell-cycle controlling proteins indispensable for signal transduction [18]. To address this question, yeast-two-hybrid screens or co-immuno-precipitation could be used.

Addressing the regulation of the enzymes under investigation: promoter studies. Expression patterns and their regulation can also be addressed from the other side by looking at the transcription and endogenous factors that drive (or inhibit) the transcription of a certain gene. Promoter studies have become an important tool of getting further hints on protein function and also on the underlying concepts of how organisms manage to have the proteins they need. Analyses of the promoters of human and murine 17β -HSD7 further supported the finding, that this protein is part of cholesterol biosynthesis [85].

Generation of knock-out mice. Last but not least, knock out mice deficient of a certain gene can be generated. If viable, these mice can show the defects caused by lack of the given gene product. This, however, can only work if the gene product's function is not redundant.

3.10. Outlook

In this thesis, several *in silico* based or *laptop biology* [45] methods were applied to infer the metabolic function of the enzymes under investigation. In detail, the methods were phylogenetic and *in silico* expression analyses, and prediction of subcellular localization. Exploration of expression patterns and of subcellular localization were also conducted experimentally. In conclusion, the use of bioinformatics is still rather restricted [33]. Prior to the development of even more *in silico* methods we should therefore develop a more detailed understanding of the metabolic pathways and intersections. So far, all applications in this field require extensive database or experimental review.

For more detailed conclusions about the physiological role of the SDRs investigated here, further experiments are needed. Having gone so far in the identification and characterization of new murine, rat, and human SDRs it would be most interesting to pinpoint their individual position in the metabolic network of cell and organism. The comparison of the same protein from different species can help to highlight not only the metabolic role of these enzymes but also species-dependent differences as shown for RDH12 and WWOX. Presenting five enzymes with newly described steroidogenic substrate specificity I could show, that there are still more enzymes converting steroid hormones to be discovered.

These enzymes display functions mostly redundant to enzymes already known which does not necessarily mean that they are physiologically of lesser importance. The presence of proteins with redundant functions underlines the importance of the steroid metabolism. Besides other functions, steroid hormones have a pivotal role regulating reproduction (sex steroids), but also take part in the regulation of blood pressure (mineralocorticoids), glucose metabolism and inflammation (glucocorticosteroids).

On the level of enzymatic catalysis, many central metabolic pathways depend on SDR-type proteins. Inborn errors of metabolism for example Congenital Hemidysplasia with Ichtyoform Erythroderma and Limb Defects (CHILD) with a single dysfunctional enzyme (NSDHL) illustrate the importance of one enzyme governing a single step in a long chain of reactions. In CHILD, malformations go along with the biochemical disruption of the cholesterol biosynthesis leading to early mortality [96]. The inherited diseases have a low incidence but model character for disease mechanisms. On the other hand, wide spread multifactorial diseases as obesity or malignant tumors are influenced in their development by environmental factors as well as by disturbances of metabolism. Obesity affects the

3. Discussion

whole organism, including the endocrine system with side effects as decreased gonadal androgens, dysmenorrhea, and polycystic ovarian syndrome [63]. Carcinoma of the breast and prostate cancer are two examples where a defined role of SDRs (17 β -HSD type 1 in breast, type 3 in prostate cancer [77]) could be discovered.

Learning more about the basal metabolic regulations by exploring the function of the pertinent enzymes, for example SDRs, should help in the future to develop more intelligent therapeutic agents to combat disease. In conclusion, there is still much knowledge to be gained on steroid hormones, the enzymes metabolizing them and the regulation of their metabolic pathways.

4. Methods

4.1. Work with *E. coli*

4.1.1. Culture media

All used culture media were autoclaved at 121°C for 20 min. For solid media, agar-agar was added at a concentration of 1.5% (w/v) before sterilization. Temperature-sensitive ingredients were sterile filtrated and added after autoclaving.

- **LB medium [9]**

10 g casein hydrolysate
5 g yeast extract
4 g NaCl
 H_2O_{bidest} ad 1 L, pH 7.4

- **SOC medium [102]**

2 g tryptone
0.5 g yeast extract
0.2 g $MgCl_2 \times 6 H_2O$
0.25 g $MgSO_4 \times 7 H_2O$
0.36 g glucose
 H_2O_{bidest} ad 0.1 L

4.1.2. Inhibitory and selective media supplements

Used supplements were sterile filtrated and added directly before inoculation for liquid or after cooling below ~45°C for solid culture media. As selection antibiotics, ampicillin at a working concentration of 50-100 $\mu\text{g}/\text{mL}$ or kanamycin at 30 $\mu\text{g}/\text{mL}$ (both dissolved in H_2O_{bidest}) were used.

4.1.3. Growing of bacteria

Inoculation of *E. coli* on solid or in liquid media was conducted with an inoculating loop sterilized by heating or a sterile pipet tip from single colonies on agar plates or from

4. Methods

glycerol stocks. Liquid cultures of more than 30 mL volume were inoculated 1:100 from overnight grown liquid cultures (5 mL). *E. coli*-cultures were grown at 37°C, in case of liquid culture under vigorous shaking (\geq 200 rpm).

4.1.4. Short- and long-term-storage of bacterial culture

E.coli-cultures can be kept on agar plates for several months at 4°C when wrapped into Parafilm (American National Can, Chicago, USA) after overnight incubation at 37°C. For long-term storage, glycerol stocks were prepared by mixing the overnight grown liquid culture and sterile 80% glycerol 1:1 in Nunc Cryo Tube™ vials and kept at -80°C.

4.1.5. Production of competent *E. coli* and transformation of plasmid DNA

Production of electrocompetent *E. coli*

5 mL overnight grown culture of the respective bacterial strain were added to 500 mL prewarmed LB medium. Without selective antibiotics, the culture was grown to an optical density (OD) of 0.6-0.8 at 600 nm. For the following steps, all instruments and solutions were cooled to 4°C. After centrifugation (4000x g, 4°C, 15 min) the bacterial pellet was gently resuspended in 1 volume ice-cold 10% glycerol and again collected by centrifugation. Washing was repeated with 0.5 volumes and 0.02 volumes ice-cold 10% glycerol. The resulting bacterial pellet was then resuspended in 1/500 volume of 20% glycerol and split into aliquots of 50 μ L each. After shock-freezing in liquid nitrogen, the electrocompetent *E.coli* were stored at -80°C.

Electroporation: Transformation of electrocompetent *E. coli*

Commercially available or self-made electrocompetent bacteria were thawed on ice and gently mixed with 1-5 ng plasmid DNA or a maximum of 2 μ L DNA from ligation. After 10 min of incubation on ice, DNA-cell-suspension was put into an ice-cold, sterile electroporation cuvette and electroporated in a Gene Pulser (BioRad, Munich, Germany) at 200 Ω , 2.5 kV and 25 mF. After immediate addition of 400 μ L of SOC medium, bacteria were transferred into a 1.5 mL ERC and incubated under vigorous shaking at 37°C for 45 min. Subsequently, 150 μ L of this transformation were plated onto LB agar plates containing the respective selective antibiotics and incubated overnight at 37°C.

Production of chemocompetent *E. coli* (RbCl Method, The NEB Transcript, 1994)

- TFB1
 - 30 mM KAc
 - 100 mM RbCl

10 mM CaCl₂
50 mM MnCl₂
15% glycerol
pH 5.8

• **TFB2**

10 mM MOPS
75 mM CaCl₂
10 mM RbCl
15% glycerol
pH 6.5

2.5 mL overnight culture were added to 250 mL LB medium with 20 mM MgSO₄ without antibiotics and grown under vigorous shaking at 37°C up to OD₆₀₀ 0.6-0.8. After centrifugation (4000x g, 4°C, 15 min) the pellet was resuspended in 100 mL ice-cold TFB1, incubated on ice for 5 min and centrifugation repeated. After resuspension in 10 mL ice-cold TFB2, bacterial suspension was incubated on ice for 30 min. Cells were split into 100 μL aliquots, shock-frozen in liquid nitrogen and stored at -80°C.

Transformation of chemocompetent E. coli by heat shock

Commercially available or self-made chemocompetent bacteria were thawed on ice and gently mixed with 1-5 ng plasmid DNA or a maximum of 2 μL DNA from ligation reaction. After 20 min of incubation on ice, cells were heat-shocked at 42°C in a waterbath for 30-60 sec (depending on the bacterial strain) and immediately placed on ice for at least 1 min. After addition of 400 μL SOC medium, cells were incubated under vigorous shaking at 37°C for 45-60 min. Subsequently, 150 μL of this reaction were plated onto LB agar plates containing the respective selection antibiotics and incubated overnight at 37°C.

4.2. Methods with eukaryotic cell lines

4.2.1. Cultivation of cells

293T cells are a subline of human embryonic kidney (HEK) 293 cells which additionally to being transformed with adenovirus contain the SV-40 T large antigen. 293T cells were cultured in High Glucose Dulbecco's Modified Eagle Medium (DMEM) supplemented with 10% Fetal Bovine Serum (FBS), 2 mM L-glutamine, 100 U/mL penicillin and 100 μg/mL streptomycin. The cells were grown at 37°C and 5% CO₂ in humidified atmosphere.

4. Methods

HepG2 and HEPA1-6 are hepatocarcinomic cell lines of human and murine origin, respectively. Both cell lines were grown on High Glucose Dulbecco's Modified Eagle Medium (DMEM) supplemented with 10% Fetal Bovine Serum (FBS), 2 mM L-glutamine, 100 U/mL penicillin and 100 µg/mL streptomycin. Cells were kept at 37°C and 5% CO₂ in humidified atmosphere.

HeLa is a well-established human cervix carcinoma cell line. Good adhesive and transfection properties and relatively large cell volume make HeLa cells suitable for subcellular localization studies. They were cultured in Modified Eagle Medium (MEM) supplemented with 10% FBS, 2 mM L-glutamine, 100 U/mL penicillin and 100 µg/mL streptomycin. Cells were grown at 37°C and 5% CO₂ in humidified atmosphere.

SaOS-2 is a cell line of human osteosarcoma origin. These cells were used for purposes alternatively to HeLa cells. Culture conditions were 37°C in humidified atmosphere containing 5% CO₂. McCoy's 5A Medium containing 15% FBS, 2 mM L-glutamine, 100 U/mL penicillin and 100 µg/mL streptomycin was used as a culture medium.

4.2.2. Maintenance of cell culture: Splitting, thawing, freezing, and long-term storage of eukaryotic cells

Splitting

All cells used in this work grow adhesively in epithelial-like monolayers. While HeLa cells have a doubling time of 40-48 h, 293T cells rather double in 24 h. Before cells reach confluence, transfer to a new culture flask is necessary. Therefore, the culture medium is removed, cells are washed with pre-warmed phosphate buffered saline (PBS, ~ 30°C) and subsequently covered with trypsin/EDTA (3 mL for T80, 0.8 mL for T25 culture flasks). After incubation for 3-5 min at 37°C, cells were dissolved from the flask and could be resuspended in pre-warmed culture-media. HeLa and SaOS-2 cells were usually splitted in 1:4 - 1:8, 293T cells in 1:4 - 1:16 ratio because of growing more rapidly. This procedure was repeated every 2-3 days.

• PBS

- 10 mM sodium-phosphate buffer, pH 7.4
- 150 mM NaCl

Thawing

For thawing eukaryotic cells, one vial was taken from liquid nitrogen and quickly thawed in a 37°C waterbath. The cell suspension was then diluted in 9 mL of culture medium and

centrifuged for 3 min at 1000x g. After resuspension, cells were added to a T80 culture flask. As the freeze medium contains the toxic substance DMSO (dimethylsulfoxid) for viable cells, thawing should be conducted rapidly.

Freezing and long-term storage

Cells at about 80-90% confluence were trypsinized from a T80 flask, resuspended in culture media and then collected by centrifugation. For freezing, freezing medium is prepared from culture medium with usual amounts of antibiotics, 20% FBS and 10% DMSO. The cell pellet was resuspended in 2 mL of this freeze medium and distributed into two cryotubes (NUNC). As eukaryotic cells are not to be shock-frosted but should cool down 1°C/min, they were frozen in specialized boxes (also NUNC) overnight at -80°C. The slow decrease in temperature and the addition of DMSO to the freeze medium prevent cell contents from crystallization. Cells were then transferred to liquid nitrogen for long-term-storage. Up to six months, cells can alternatively be stored at -80°C.

4.2.3. Transfection of eukaryotic cells

In this study, cells were transfected with FuGene6 (Roche). FuGene6 works on the basis of lipofection by including the transfected plasmid into lipid droplets. Delivery of the transfectant to the host cell is achieved by fusion of these lipid droplets with the cells' plasma membrane.

Based on the manufacturer's protocol, transfection was optimized. For all cell lines used in this work a 3:1 ratio of μ L FuGene per μ g DNA was found to yield the expected results. As described in the protocol, FuGene6 was first mixed with DMEM or MEM medium without FBS and incubated at room temperature for 5 min. Then, DNA was added and gently mixed by inversion. Drops were collected by brief centrifugation. Before transfection, the mixture was incubated for another 20-25 min at room temperature for formation of the FuGene-DNA complexes.

If more than one identical transfections was carried out, the reactions were set up in one and aliquoted in the process of transfection.

4.2.4. Seeding of cells and transfection in different formats

For all purposes described here, cells were seeded into 12 or 6 well plates. For even distribution, plates were shaked horizontally in eight-like manner. Before transfection, cells were grown over night.

Growing of 293T cells for substrate conversion assays. For substrate conversion assays (cf. chapter 4.6.1), 293T cells were seeded into 12 well plates containing 900 μ L cell culture

4. Methods

medium. Cells were grown to confluence in a T80 flask, trypsinized and resuspended in a 15 mL cell culture medium (resulting in a total volume of 18 mL). One drop from a 10 mL pipet contained approximately 5×10^4 cells. 3 drops from a 10 mL pipet were seeded into each well for 24 h incubation, for 96 h long incubations 1 drop was seeded. For transfection, 0.5-1 μg DNA was applied per well. For initial testing of endogenous conversion, all cell lines were seeded in alike manner.

Growing of HeLa and SaOS-2 cells for subcellular localization studies. For subcellular localization studies (cf. chapter 4.2.5), 5×10^4 to 10^5 cells were seeded into each well of a 6 well plate which contained a glass cover slip. Transfection was performed with 1 μg of DNA per well.

4.2.5. Immuncytochemical methods for subcellular localization studies

For determination of the subcellular localization, HeLa or SaOS-2 cells were grown and transfected as described above (4.2.4). Both cell lines contain rather large cellular volumes facilitating visualization of subcellular localization. The staining procedure is summarized in fig. 4.1.

Staining of mitochondria and ER using compartment-specific trackers. For staining of mitochondria and ER, fluorescence-coupled trackers were used. These trackers are transported actively to the respective subcellular compartments within the living cells. Therefore, the trackers were diluted in culture medium (mitochondrial tracker: 300 nM, ER tracker: 600 nM; both Invitrogen) and added to the cells. After incubation at 37°C for 30-35 min, culture medium was removed and cells were washed 2x with PBS.

Fixation. Fixation of the cells was conducted applying 1 mL of 3.7% formaldehyde in PBS and incubation at 37°C for 10-15 min. Following fixation, cells were washed 2x with PBS.

Permeabilization. If necessary for antibody or phalloidin staining, permeabilization of the cells was carried out by adding 1 mL 0.5% Triton-X in PBS to each well and incubated at room temperature for 5-10 min. Prior to other steps cells were washed 3x in PBS.

Antibody staining. For antibody staining of distinct cellular compartments or myc-tagged proteins under investigation, permeabilized cells were first blocked using 10% FBS in PBS at room temperature for 30 min up to 1 h. Primary and secondary antibody solutions were prepared in 1:2000 dilutions (or as indicated) in blocking solution and incubated at room temperature for 1 h each. Before and after application of the antibody

solutions, cells were washed 3x with PBS. All antibodies used for cell staining are depicted in table 4.1.

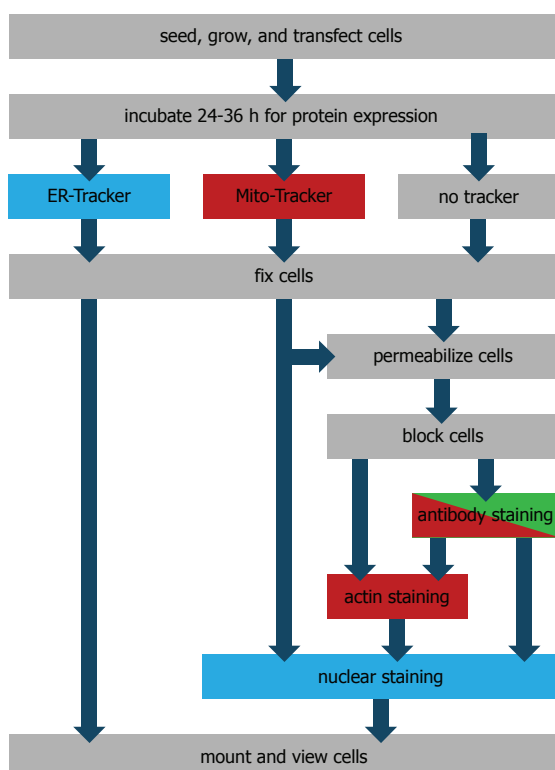


Figure 4.1: Summary of cell staining procedures. Gray staining steps without addition of color for detection, colored boxes: color detected in microscopy. If proteins under investigation were expressed recombinantly with GFP, no green staining was conducted. In combination with ER tracker no further staining was conducted as ER staining was otherwise washed out.

Immunofluorescent detection of FLAG-tagged recombinant proteins. Alternatively to staining ER using ER-Tracker (see above), ER was dyed by transfecting N-FLAG-tagged rabbit sarcolipin (supplied by A. Odermatt, University Berne, Switzerland) or human 17 β hydroxysteroid dehydrogenase type 7 (supplied by Christina Guggenberger). FLAG-tag was detected by using polyclonal FLAG tag antibody from rabbit (Sigma) in 1:1000 dilution. As secondary antibody, goat-anti-rabbit AlexaFluor488 IgG (Invitrogen) was used in 1:2000 dilution.

Myc-tagged recombinant proteins. Myc-tagged proteins were detected by use of mouse monoclonal antibody 9B11 (NEB). Secondary antibody was goat-anti mouse IgG labeled with AlexaFluor488 (green) or AlexaFluor568 (red), respectively.

Staining of the cytoskeleton. Cytoskeletal staining was conducted by staining f-actin with the fungid toxin phalloidin. Phalloidin was labeled with AlexaFluor350 (blue) or AlexaFluor568 (red; both Invitrogen), respectively. Staining procedure was conducted according to the manufacturer's recommendations. After staining, cells were again washed 2-3x with PBS.

Nuclear staining. Nuclear staining was performed with either DAPI (4',6-diamidino-2-phenylindole,dihydrochloride) or Hoechst33342 (both Invitrogen). DAPI was applied in

4. Methods

Table 4.1: Antibodies used for immunocytochemical staining

Primary antibody	Dilution
monoclonal mouse IgG anti myc 9B11	1:2000
polyclonal rabbit IgG anti FLAG	1:2000
monoclonal mouse IgG anti FLAG	1:2000
Secondary antibody	Dilution
goat-anti-mouse IgG AlexaFluor488 coupled	1:2000
goat-anti-mouse IgG AlexaFluor568 coupled	1:2000
goat-anti-rabbit IgG AlexaFluor488 coupled	1:2000

300 nM concentration in water and exposed to the cells for 1-2 min. Hoechst33342 staining was performed in 1:5000 to 1:10000 dilution in PBS and exposed for 1-5 min.

Mounting of the stained cells. After the staining procedure, cells were washed 3x with PBS prior to mounting on Super-Frost Plus coverslides (Menzel Glaeser) using Vectashield (Vectalabs).

Detection of fluorescence and documentation. Fluorescence was detected using a Zeiss Axiophot fluorescence microscope with respective filters. Camera was controlled for taking photographs by ISIS software. For initial processing of the photographs (defining lower and upper thresholds), ISIS software was used. For separation of R-, G-, and B-channel, Adobe Photoshop CS was used.

4.3. DNA-based molecular biological methods

4.3.1. Isolation and purification procedures

Isolation of plasmid DNA from bacteria

Isolation of plasmid DNA from *E. coli* was carried out in two different scales: mini-preparation using 1-5 mL of an overnight culture and the NucleoSpin Plasmid Kit (Macherey& Nagel), and midi-preparation using 50 mL of an overnight culture and the NucleoBond PC100 Kit (Macherey&Nagel). Bacteria were harvested by centrifugation at 4°C and the pellet resuspended in the appropriate buffer of the kit. DNA was isolated according to the manufacturer's protocol. In the mini-preparation procedure, DNA was eluted from the column with 50 µL AE buffer (provided with kit) or H₂O_{bidest}. DNA from midi-preparations was resuspended in 100-200 µL H₂O_{bidest}.

Purification of linear dsDNA from aqueous solutions and agarose gels

DNA purification from solutions containing enzymes, dNTPs, salts from buffers etc. was carried out by use of the Wizard SV Gel and PCR Clean-Up System (Promega) according to manufacturer's protocol. For elution, 35 µL H₂O_{dest} were applied. For DNA purification from agarose gels, TAE buffer based 1% agarose gels (w/v) were used.

- **50x TAE**

2 M Tris
1 M acetic acid
0.1 M EDTA
ad 1 L H₂O_{dest}

Radioactively labeled DNA was purified by use of μSpinTM S-200 HR columns (Pharmacia Biotech) according to manufacturer's protocol. Products for DNA sequencing (4.3.4) were cleaned up using the Qiagen Dye Ex Kit according to the manufacturer's protocol. Restriction reactions for RNA *in vitro* transcription (4.4.1) were purified using QIAquick PCR purification Kit (Qiagen).

Precipitation of DNA

Very diluted or impure DNA can be precipitated for increase of concentration or purity. Therefore, 0.1 volume 3 M sodium acetate (pH 5.2) and 2.5 volumes of ethanol p.a. were added to the DNA solution, mixed, and incubated for at least 2 h at -20°C. After centrifugation (17000x g, 4°C, 15 min), the supernatant was removed, and the pellet washed (centrifugation at 17000x g, 4°C, 10 min) in -20°C cold 70% ethanol. After removal of the supernatant, the pellet could be dried and resuspended in an appropriate amount of H₂O_{dest}.

4.3.2. Measurement and quality assessment of DNA solutions

Separation and monitoring by agarose gel electrophoresis

For qualitative measurement of DNA or subsequent isolation, DNA solutions were subject to agarose gel electrophoresis. Different w/v-percentages of agarose in 1x TBE were used for optimal analysis according to the expected size of the DNA fragments: 0.5% for dsDNA ≥5 kb, 1% for dsDNA ~2-5 kb, 2% for dsDNA ~0.5-2 kb and 3% for dsDNA ≤0.5 kb. For analysis, Loading Dye was added to the DNA solution, mixed, and loaded on a gel containing ethidium bromide (0.5 µg/mL). The DNA was separated in a constant electric field of 80-160 V depending on gel size and percentage of agarose. DNA bands were monitored and photographed with UV transillumination ($\lambda=254$ nm) on a BioVision gel

4. Methods

documentation system (PeqLab).

By adding 6x Loading Dye to the sample, the gel run could be optically monitored during electrophoresis and accordantly stopped. The included dyes, bromophenol blue and xylene cyanol FF behave on a 0.8% agarose gel like dsDNA fragments of 0.3 and 4 kb size, respectively.

- **10x TBE**

108 g Tris
55 g boric acid
9.3 g EDTA
ad 1 L H₂O_{dest}

- **6x Loading Dye**

15% Ficoll 400 (Pharmacia)
0.25% bromophenol blue
0.25% xylene cyanol FF
or purchased as ready-to-use solution from Fermentas.

On determination of DNA fragment size. Within an agarose gel matrix, running velocity of linear dsDNA fragments is inversely proportional with the decadic logarithm of their molecular weight. It is therefore possible to estimate the length of a fragment of unknown size by comparison with the R_f values of lengths of standardized fragments. Usually, this is achieved by inclusion of DNA standards to gel electrophoresis. In this thesis, λ-Markers 3 and 8 (both Fermentas) were used.

Measurement by optical density (OD)

To monitor the quantity and quality of nucleic acid preparations, DNA (or RNA) containing solutions were diluted with H₂O_{dest} and the optical density (OD) of this dilution measured at $\lambda=260$ nm for quantification and additionally at $\lambda=280$ nm for qualification. The concentration of the nucleic acid solution was calculated according to the following formula (adapted from [21]):

$$\text{OD}_{260} \times \text{dilution factor} \times 50 \text{ ng}/\mu\text{L} = c \text{ [ng}/\mu\text{L}]$$

The quality was assessed by the ratio value R (OD₂₆₀ nm/OD₂₈₀ nm) where R = 1.8 for dsDNA in an optimum case.

All OD measurements were conducted using the Beckman DU 530 Life Sciences UV/Vis Spectrophotometer (Beckman, Unterschleissheim, Germany).

4.3.3. Cloning strategies

TOPO-TA cloning

For direct cloning of DNA fragments from PCR reactions with no prior cleanup, the TOPO-TA cloning Kit (Invitrogen) was used. For this method, A-overhangs produced in the elongation step of the PCR by the Taq-polymerase are ligated to T-overhangs in the respective vector (TA-cloning). The yield of ligation products is enhanced by topoisomerase, attached to the vector's cloning sites (TOPO-cloning). After amplification of the DNA by PCR 4 μ L of the reaction mixture were subjected to the ligation procedure into vector pCRII or pCR2.1 and transformed into chemocompetent TOP 10 cells as recommended by the manufacturer.

Cloning via restriction sites

For most applications, DNA fragments were inserted into vectors via restriction sites. Digestion of DNA fragment and vector with restriction enzymes yields complementary (so-called sticky) DNA ends which can then be used for ligation. In contrast to TA-cloning, utilization of two different restriction sites additionally allows for a site-directed insertion.

Cleavage of DNA by restriction endonucleases

For cloning purposes or analysis of plasmids, DNA fragments and vectors were digested with the particular restriction enzymes. 1-10 μ g DNA were digested in 20-50 μ L reaction volume containing appropriate concentrations of buffer, BSA (if enzymes from NEB were used) and 5-20 U enzyme for 2-16 h at 37°C. The adequate amount of enzyme was calculated according to the assumption that 1 U of enzyme digests 1 μ g DNA in 1 h under optimum conditions. The reaction was stopped by heat inactivation or removal of the enzyme using the Wizard SV Gel and PCR Clean-Up System (Promega; see also chapter 4.3.1).

Dephosphorylation of linear DNA fragments by alkaline phosphatase

Alkaline phosphatase can be used to cleave terminal 5'-phosphate groups. This is especially suitable to inhibit religation of restriction digested, linearized vectors. Dephosphorylation can be conducted in common restriction enzyme buffers or in a separate buffer provided with the enzyme. Usually, calf intestine alkaline phosphatase (CIAP, Fermentas) was added directly to vector digestions for the last 30 min of incubation and heat-inactivated or cleaned-up with the restriction reaction.

4. Methods

Ligation of DNA fragments

For ligation of inserts and respective vectors, DNA fragments were mixed in a 4:1 molar ratio (insert:vector) and incubated with 1x ligase buffer and T4-DNA-Ligase (NEB or Promega). Incubation was conducted at room temperature for 2-4 h or at 14°C overnight. DNA amounts were adjusted according to the manufacturer's recommendations. For transformation protocol, see chapter 4.1.5.

4.3.4. PCR-based methods

PCR (polymerase chain reaction)

For site-specific amplification, PCR was used. PCRs were conducted on DNA templates in 20 or 50 μ L formats containing 200 nM dNTP-mix, 0.5 μ M forward and reverse primer each, and 1-2 U polymerase in 1x PCR Buffer. Usually, inhouse made Taq-polymerase was used. For cloning purposes, Taq was substituted by proof-reading polymerases as Pfu Turbo DNA-polymerase (Stratagene) or Pfx Polymerase (Invitrogen) for better performance and accuracy. DNA templates included genomic DNA, plasmid DNA, linear dsDNA, cDNA, primary PCR (without prior cleanup) or bacterial culture. The standard program on a Robo-Cycler PCR machine (Stratagene) implied an initial denaturing for 5 min at 95°C followed by 35 cycles with 30 sec at 95°C, 35 sec at annealing temperature (T_a), 1 min per 1 kb at 72°C, where T_a is the melting temperature $T_m - 5^\circ\text{C}$ specific for the applied primer pair. This cyclic reaction was usually followed by a 10 min final elongation step at 72°C. For bacterial culture as PCR template, initial denaturing was prolonged to 10 min.

- **10x PCR Buffer**

100 mM Tris-HCl, pH 9.0

500 mM KCl

15 mM MgCl₂

On PCR optimization. In case of unspecific or too little yielded PCR product, three strategies were followed. Mainly, this was the case for PCR reactions where primers contained large overhangs due to restriction sites included. First, DMSO was added to the PCR reaction in minimum amounts recommended in the Stratagene Pfu Turbo protocol. Second, cycling during PCR program was split into two parts: 10 cycles at 50°C T_a followed by 25 cycles of the optimum temperature calculated. If possible, a primary PCR was conducted with primers containing no overhangs yielding a product of slightly bigger size than initially needed. The secondary, nested PCR-reaction was then performed on 1 μ L of the initial PCR reaction with the cloning primers now binding closer to the core of the primary PCR product (nested PCR).

DNA Sequencing

To identify or verify sequences and to check for mutations, DNA fragments or plasmids were either sent to SequiServe company (Vaterstetten, Germany) or sequenced on the ABI3730 (Applied Biosystems) by the method of controlled termination of replication (Sanger dideoxy method) according to the manufacturer's protocol.

Site-directed mutagenesis: QuikChange

Insert-sequences of plasmids can be manipulated by site-directed mutagenesis changing, deleting, or adding a certain amount of nucleotides. For this procedure, a pair of complementary specific primers were designed containing the mutation in their core region and flanking it to both sides by ~15-20 bp. In this work, site-directed mutagenesis was employed to exchange single nucleotides to yield a full length wild-type cDNA for expression. Therefore, the QuikChange method (Stratagene) was applied and conducted according to the protocol enclosed with the kit. The maximum amount of recommended template DNA was used.

4.4. RNA-based methods

4.4.1. Synthesis of RNA by in vitro transcription and digoxigenin labelling

Constructs containing the template for RNA probes were linearized by use of an appropriate restriction endonuclease and purified as described above (4.3.1). Elution was carried out in RNase free H₂O. Probes were synthesized by viral T7, T3 or SP6 RNA polymerases (all Fermentas) with DIG RNA Labelling Mix (containing digoxigenin labeled UTP; Roche) and RNase inhibitor for 2 h at 37°C. Previously linearized DNA template was degraded by 10 U RNase free DNaseI (Promega; 15 min, 37°C). RNA synthesis was monitored by agarose gelectrophoresis.

4.4.2. Isolation and purification methods

Isolation of total RNA from tissues

RNA was prepared from murine or rat tissues for expression analysis by RT-PCR. For tissue preparation, mice were killed by cervical dislocation; rats were suffocated in CO₂. For isolation, ~150 mg tissue were homogenized using a Braun Mikro-Dismembrator U after the capsules containing tissue and grinding ball freezing in liquid nitrogen. The thus homogenized tissue was then resuspended in TRIzol (Invitrogen) and subject to RNA isolation following a modified protocol for the RNeasy Midi Kit (Qiagen). After resuspension, RNA was extracted by addition of 2/10 volume of chloroform, vortexing

4. Methods

for 15 sec, incubation for 3 min at room temperature and centrifugation for 15 min at 4°C at maximum speed in a table-top Eppendorf centrifuge. 0.53 volumes of ethanol were added to the supernatant while slowly vortexing. The solution was applied to a pre-equilibrated column of the RNeasy Midi Kit (Qiagen) and further processed according to the manufacturer's protocol. Amount and quality of the total RNA were assessed by spectrophotometry or gel electrophoresis, respectively (cf 4.4.3).

Isolation of total RNA from cells

For RNA preparation from cells, the SV Total RNA Isolation Kit (Promega) was used according to the protocol included therein. Usually, 3×10^6 cells or one confluent grown well from a 6well plate were used. Instead of trypsinizing and collecting the cells before lysis, cells were washed 2x with cool PBS (4°C). Subsequently, 200 μL of β -mercapto ethanol supplemented lysis buffer from the kit were directly applied to the cell layer. During lysis, cells were kept on ice. After collection of the lysate by use of a cell scraper and transfer to a sterile 1.5 mL Eppendorf cap, the manufacturer's protocol was followed. Alternatively, the lysate was kept at -80°C until RNA extraction. Elution was carried out in 35 μL H₂O_{bidest}. After isolation, amount and quality of the obtained RNA were assessed as described below (cf 4.4.3).

Precipitation of RNA

Very diluted or impure RNA can be precipitated for increase of concentration or purity with the same protocol as described for DNA (see 4.3.1).

Purification of RNA from aqueous solutions

RNA probes for whole mount mRNA *in situ* hybridizations were purified using the RNeasy Mini Kit (Qiagen) following the RNA Cleanup Protocol included therein. Probes could be stored at -80°C up to 8 weeks.

4.4.3. Handling and measurement

Following preparation of RNA, 20-40 U of Ribonuclease Inhibitor (Fermentas) were added (to prevent breakdown of labile RNA) and the RNA stored at -80C.

Determination of RNA concentration by measurement of OD

RNA concentrations were determined in the same way as described for DNA (see 4.3.2) but calculated with the following formula:

$$\text{OD}_{260} \times \text{dilution factor} \times 40 \text{ ng}/\mu\text{L} = c \text{ [ng}/\mu\text{L}]$$

The quality was assessed by the ratio value R (OD_{260 nm}/OD_{280 nm}) where R = 2.0 for RNA in an optimum case.

Determination of RNA integrity by gel electrophoresis

To survey the integrity of isolated RNA it was separated on a 1% agarose gel in TBE (as described for DNA in chapter 4.3.2). Though for RNA separation usually denaturing formaldehyde gels using MOPS buffer are recommended, separation on agarose gels in TBE buffer is sufficient for quality assessment.

4.5. Analysis of Gene Expression

4.5.1. Reverse transcription of mRNA into cDNA

Transcription into cDNA was performed by use of RevertAidTM First Strand cDNA Synthesis Kit (Fermentas) according to manufacturers protocol. cDNA used in expression analysis was generated from 1 μ g total RNA with poly dT-primers in a total volume of 20 μ L, from which 0.5-1 μ L was then subjected to PCR. For better quantification in case of high expression level of the gene under investigation, additionally 0.5 μ L of a 1:10 and 1:100 dilution were also subjected to PCR testing.

4.5.2. Hybridization of cDNA probes to membrane bound RNA: Northern Blot

For gene expression analysis, RNA can be immobilized on nylon membranes and then hybridized with DNA or RNA probes. The process of transferring and immobilizing RNA on such a membrane is called Northern blotting following the naming of the respective DNA technique which after its developer, Edward Southern, is conferred to as Southern Blot.

In this work, ready-to-use Northern Blot membranes, FirstChoice Northern Blot Human Blot II and FirstChoice Northern Blot Mouse, both purchased from Ambion, were used with recommended wash solutions and Ultrahyb hybridization solution according to manufacturer's instructions.

PCR products containing parts of the respective cDNA under investigation, were used as probe for hybridization. They were labeled with Strip-EZ DNA Kit (AFermentation, Huntington, UK) with radioactively labeled 32 P- α -ATP nucleotides (Amersham Biosciences) also according to the manufacturer's instructions. Before adding the labeled probe to prehybridization incubation it was purified as described earlier (4.3.1).

Prehybridization and hybridization of the Northern blot membrane were carried out in a rotating oven at 42°C with Ultrahyb solution pre-warmed to 68°C. The next day,

4. Methods

hybridized membranes were washed 2x with each Ambion's NorthernMax Low Stringency Wash and Ambion's NorthernMax High Stringency Wash both conducted at 42°C.

After washing, membranes were sealed in plastic wrap and transferred to film cassettes containing an intensifier screen (Kodak).

Signal detection and documentation. For rapid detection, Fuji phosphorimager screens were exposed to the membrane for 2 h and the signal read out on the Fuji phosphoimager. Images were scanned by use of AIDA software.

If signals were too weak for detection by phosphorimaging, detection was done by autoradiography using BioMax XAR films (Kodak). X-ray films were exposed to the radioactive membranes overnight or for up to several days at -80°C.

Stripping. Before re-hybridization, stripping of Northern Blot membranes was done as indicated in the Strip-EZ DNA Kit. This procedure is especially gentle and therefore suitable for RNA blots. After stripping, measurement of radioactive signal with an ionization chamber was conducted for success control.

4.5.3. Analysis of gene expression in mouse embryos

Preparation of mouse embryos from gravid mice

Gravid C3HT1/2 mice were killed by cervical dislocation, ovariectomized and the embryos transferred to ice-cold PBS. By dislocation of the uterine lining and the extraembryonal tissues (chorion, yolk sac, and amnion) the embryos were uncovered, transferred to ice-cold 4%PFA/PBS immediately and fixed overnight at 4°C. After fixation, the embryos were dehydrated by an increasingly graded methanol/DEPC-PBS series (25, 50, 75, 100% methanol) and stored in 100% methanol at -20°C. Storage up to 6 months does not influence hybridization results.

Whole mount mRNA in situ hybridization of mouse embryos

Whole mount mRNA in situ hybridization of mouse embryos was based on the protocols of [100] and [110] and done in 6 well plates (Falcon or Nunc) with 100 μ -cell strainers (Becton Dickinson Labware) under moderate shaking.

Rehydration and equilibration of the embryos. All prehybridisation steps are conducted at 4°C. The embryos fixed and stored in methanol were rehydrated by an increasingly graded methanol/DEPC-PBS series (75, 50, 25, 0% methanol/DEPC-PBS) for 10 min each. To inhibit substrate precipitates brain ventricles were opened by needle stitch. After bleaching (6% H₂O₂/PBT, 4°C, 1h) embryos were washed in PBT 3x for 15 min

each. For embryos older than 10.0 dpc, a proteinase K digestion followed (depending on the age, 1-15 min at 5 µg proteinase K/mL proteinase K buffer). Digestion was stopped by washing 2x (5 min each) in freshly prepared PBT/glycine, followed by two washing steps in PBT (again 5 min each). For permeabilization, embryos were treated with RIPA buffer (3x 5 min each) and again, washed in PBT (also 3x, 5 min each). For recovery of fixation, embryos were treated with 4% PFA/0.2% glutaraldehyde in PBT.

Hybridisation and washing. Embryos were then equilibrated in 1:1 hybe buffer/PBT and then hybe buffer for 10 min each. Before addition of the denatured digoxigenin-marked probe (denaturation at 80°C, 3 min; for production and purification, cf. chapters 4.4.1 and 4.4.2) embryos were pre-hybridized in hybe buffer for 3 h at 65°C in a humid chamber. At the same temperature, hybridization followed overnight in hybe buffer supplemented with 100 µg/mL tRNA and 0.25-1 µg/mL probe. For removal of unbound probe, 2-3 washing steps at 65-68°C were conducted in hybe buffer followed by 2 washing steps for 5 min each, first in 1:1 hybe buffer/RNase buffer and then in RNase buffer. For RNA digestion, 3 incubation steps at 37°C of 30 min each with 100 µg/mL RNase in RNase buffer followed. Under shaking in a waterbath at 65-68°C, 5 h of washing in SSC/FA/Tween-20 buffer were conducted (buffer was changed ~10x).

Antibody incubation. The embryos were cooled to room temperature and equilibrated by a series of washing steps of 10 min each: 1x in a 1:1 mixture of SSC/FA/Tween-20 and TBST, 2x in TBST, 2x in MABT. Embryos were then incubated in 10% blocking solution/MABT. The dig-antibody (Roche, alkaline phosphatase coupled) was simultaneously incubated 1:5000 in 1% blocking solution/MABT on ice. Antibody incubation took place overnight at 4°C. For removal of the unbound antibody, embryos were washed in 3x 5 min in MABT, then washing was continued in 1xTBST over 24 h with changing the buffer several times. During 2-3 days, washing was further continued in TBST with 1 change of buffer per day.

Staining reaction. The dig-antibody used in this thesis is coupled with alkaline phosphatase (Roche) which catalyzes the precipitation of a dyed substrate and thus enables visualization of dig-labeled RNA probes. For staining, the embryos were first washed 3x for 20 min each in alkaline phosphatase buffer. Staining reaction was set up from BM Purple AB substrate solution (Roche) with 0.5% Tween-20 and 2mM Levamisol. Levamisol is added for inhibition of endogenous alkaline phosphatases ergo for reduction of background staining. Before usage, this staining solution was cleared by centrifugation (7 min, 2400 rpm). Staining was conducted in the dark without shaking at 4°C for 2-4 days. When staining was sufficiently intense, embryos were washed 2x in alkaline phosphatase buffer

4. Methods

(also in the dark) and reaction stopped with 4% PFA/PBS overnight at 4°C. Staining is stably retained over years in this solution.

Documentation. Stained embryos were put in petri dishes containing 1% agarosegel in TBE (cf. to chapter 4.3.2) and covered with PBS. Embryos were photographed using a Zeiss microscope and respective camera and software. Images were processed with Adobe Photoshop CS (correction of color balance, saturation and levels).

4.6. Measurement of substrate specificity

4.6.1. Measurement of substrate conversion in living cells

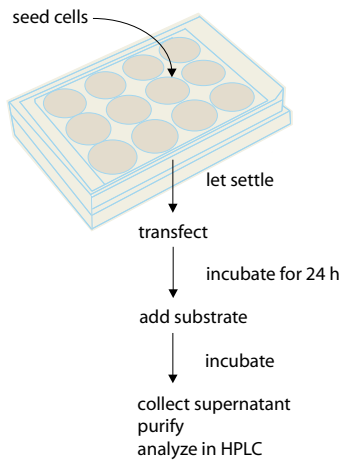


Figure 4.2: Summary of intracellular conversion assays.

incubation time was 24 h for initial tests. For time-course experiments, several samples were prepared over 96 h (every 12 h, one incubation was stopped by removing the supernatant). For this procedure, 3 wells were set up for every time point to be measured (see section 4.2.4). Following incubation, cell culture supernatant was collected and purified prior to HPLC analysis (for purification and HPLC procedure, see below). Each test was performed in triplicates.

The aim of this work was the identification and characterization of novel SDR family members for steroidogenic substrate specificity. Therefore, several steroidogenic substances (Perkin-Elmer, ARC) were tested as putative substrates for mammalian expressed SDR enzymes. Tested substrates and their respective concentrations are indicated in table 4.2.

For *in vivo* measurement of substrate conversion, an assay with tritiated substrates was adapted from [15]. As established during the work on this thesis, the exact procedure is described in the results chapter (see 2.6.2). A summary is given in fig. 4.2. In short, after seeding and transfection on 12 well plates, cells were incubated for 24 h. Tritiated substrates were added to the cell culture supernatant (usually 1 μ L substrate solution was given).

4.6.2. Determination of Michaelis-Menten kinetics

On Michaelis-Menten kinetics. Michaelis-Menten kinetics are a mean of enzymatic characterization which is often employed to describe the affinity of a given enzyme towards a substrate. The Michaelis constant, K_M describes the substrate concentration at which

Table 4.2: Tritiated steroids used in substrate conversion assays

Steroid	^3H labeled positions	Stock concentration
Androst-4-ene-3,17-dione	1, 2, 6, 7- ^3H (N)	11 μM
Androsterone	9,11- ^3H	30.3 μM
Corticosterone	1,2- ^3H	20.8 μM
Cortisol	1,2,6,7- ^3H	12.6 μM
Dihydrotestosterone	1,2,4,5,6,7- ^3H	8.4 μM
Estrone	2,4,6,7- ^3H (N)	23.9 μM
Estradiol	6,7- ^3H (N)	20-24 μM^*
20 α -Hydroxyprogesterone	1,2- ^3H	10 μM
Progesterone	1,2,6,7- ^3H	11.1 μM
Testosterone	3,7- ^3H (N)	14.3 μM

* = concentration lot dependent

the enzyme converts the substrate under investigation at 50% of its maximum velocity (v_{\max}). It is important to notice, that Michaelis-Menten kinetics do not apply to conversion within multi-enzyme complexes. Overall, the determination of K_M is based on the assumption that from enzyme (E) and substrate (S) during the first step, a complex [ES] is being formed, which then dissociates to unbound enzyme and the product P of the reaction. It has been shown that for many enzymes, K_M is close to the physiological concentration of the substrate of interest ([8], p. 224). Though not all enzymes follow this kind of steady state kinetics it was performed in order to be able to evaluate the physiological relevance of the found substrates. Therefore, kinetic measurements were performed by use of the same assay which has been employed for test of substrate conversion (4.6.1). Preferably, substrate concentrations were chosen within the linear area of the conversion (cf. to fig. 4.3, A) before saturation of the curve occurs.

Panel B in this figure depicts the Lineweaver Burk diagram for the evaluation of K_M and v_{\max} . In this diagram, reciprocal values of conversion velocity and substrate concentration are depicted on the y- and x-axes, respectively. The two intersection points of the graph represent the reciprocal values of v_{\max} (on the y-axis) and the negative reciprocal value of K_M (on the x-axis).

As from the substrate concentrations applied, values for K_M and V_{\max} cannot be determined, usually Lineweaver Burk diagrams (4.3, B) are chosen for evaluation of results. From this graph, where reciprocal values of conversion velocity and substrate concentration are depicted on the y- and x-axis, respectively, values for K_M and V_{\max} can be inferred by interpolating the resulting line through its intersection points of the two axes.

4. Methods

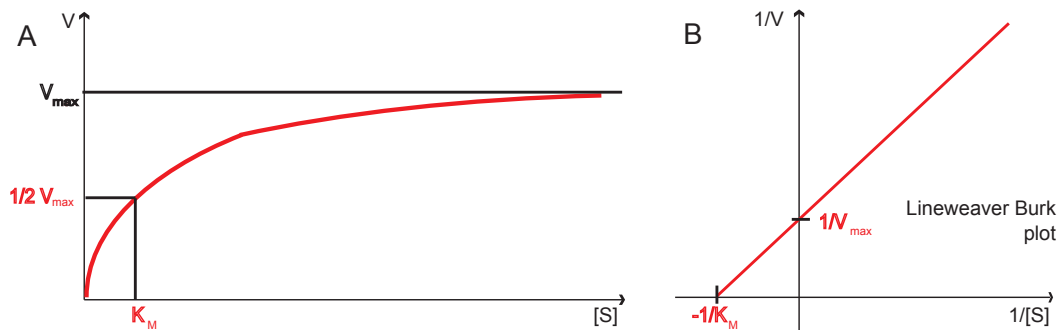


Figure 4.3: Graphical depiction of Michaelis-Menten kinetics. Panel A shows an example curve for an enzyme following Michaelis-Menten kinetics with saturation of the velocity. The half maximal velocity corresponds to the substrate concentration of the Michaelis constant on the x-axis. Panel B depicts the Lineweaver Burk diagram where the reciprocal values in comparison to panel A are depicted on x- and y-axes resulting in a straight line. Lineweaver Burk representation was chosen for evaluation of maximal velocity and the Michaelis constant.

Determination of the Michaelis-Menten constant and maximum velocity of substrate conversion.

Cells were seeded and transfected as for conversion assays (see section 4.2.4). Michaelis-Menten kinetics were conducted by choosing five different substrate concentrations in such a way that the reciprocal values would be approximately equally distributed. The amount of substrate corresponding to the lowest concentration was added from tritiated substrates (see table 4.2) to all samples. For increase of concentration, the respective non-radioactively labeled substances were added to the needed final concentrations. For exact approaches, see fig. 4.4. Concentrations for the assay were kept low in order to avoid hormonal effects of the substrates added to the cells. Cell culture supernatant was harvested after 24 h of incubation, purified by solid phase extraction and analyzed on HPLC (for exact procedures, see below). Samples were prepared in triplicates. Data for Michaelis-Menten kinetics was evaluated using the enzyme kinetics module of Sigma Plot (version 2002, Windows8.02) software.

4.6.3. Purification of HPLC samples by solid phase extraction

For and samples afterwards preliminary purified on Strata C18-E (Phenomenex) or Varian BondElut C18 (Varian, EA Middelburg, The Netherlands) columns (solid phase extraction). After equilibration of the column (application of 2x1 mL methanol followed by 2x1 mL water), samples were applied and rinsed with 0.5 mL water. Elution was carried out 2x with 200 μ L methanol each.

4.6. Measurement of substrate specificity

Estrone		final concentration [nM = pmol/ μ L]				
		18,15	22,69	30,25	45,38	90,75
μ L 3H-substrate	1,00	1,00	1,00	1,00	1,00	
pmol to final concentration	0,00	4,54	12,10	27,23	72,60	pmol
add		1,00	2,67	6,00	16,00	μ L from 4,5375 μ M solution

Estradiol		final concentration [nM = pmol/ μ L]				
		20,12	25,15	33,53	50,30	100,60
μ L 3H-substrate	1,00	1,00	1,00	1,00	1,00	
pmol to final concentration	0,00	5,03	13,41	30,18	80,48	pmol
add		1,00	2,67	6,00	16,00	μ L from 5,03 μ M solution

Androstendione		final concentration [nM = pmol/ μ L]				
		10,99	13,74	18,32	27,48	54,95
μ L 3H-substrate	1,00	1,00	1,00	1,00	1,00	
pmol to final concentration	0,00	2,75	7,33	16,49	43,96	pmol
add		1,00	2,67	6,00	16,00	μ L from 2,75 μ M solution

Androsterone		final concentration [nM = pmol/ μ L]				
		30,30	37,88	50,50	75,75	151,50
μ L 3H-substrate	1,00	1,00	1,00	1,00	1,00	
pmol to final concentration	0,00	7,58	20,20	45,45	121,20	pmol
add		1,00	2,67	6,00	16,00	μ L from 7,58 μ M solution

Dihydrotestosterone		final concentration [nM = pmol/ μ L]				
		9,09	11,36	15,15	22,73	45,45
μ L 3H-substrate	1,00	1,00	1,00	1,00	1,00	
pmol to final concentration	0,00	2,27	6,06	13,64	36,36	pmol
add		1,00	2,67	6,00	16,00	μ L from 2,27 μ M solution

Figure 4.4: Set-up for Michaelis-Menten kinetics. Substrates and their final concentrations are highlighted. The minimal concentration applied equals the concentration used for initial testing of substrate specificity.

4.6.4. HPLC measurement

The separation of the steroids in a 20 μ L sample was performed through HPLC running isocratic H_2O /acetonitrile on a reverse phase LUNA 5 μ m C18 (2) column (Phenomenex) with a flowrate of 1 mL/min [3]. Due to the apolar column, substances of greater polarity are kept longer on the column. Greater similarity with the immobile phase, the column, leads to a shorter retention time. The water/acetonitril percentages used as well as the retention times of the different tritiated steroids are depicted in table 2.6. The HPLC consisted of a Beckman Coulter system assembly composed of two HPLC pumps, a UV detector and was controlled with the 32Karat software (Beckman). The detection of the tritiated steroids proceeded with an online liquid scintillator (Berthold) after mixing with scintillation solution (Ready Flow III, Beckman). The amount of the respective steroids was calculated through integration of the peaks in the HPLC chromatograms using the above mentioned software. Each measurement was performed in triplicates; errors were calculated as standard deviation of the means (SDM) or standard error of the means (SEM), respectively.

4. Methods

4.7. Bioinformatic methods

4.7.1. Identification of SDR candidate genes

Identification of novel SDRs was done by use of SDR Finder, a proprietary software of BioNetWorks company (Munich, Germany). Protein sequences were downloaded from the NCBI server (<ftp://ftp.ncbi.nih.gov/blast/db/FASTA>). A threshold of 11 at minimum conserved amino acids in the motifs detected by the program was set. SDR Finder was used as described in the results chapter.

4.7.2. In silico Northern Blot

For analysis of RNA expression pattern complementing RT-PCR experiments and data from literature, *in silico* Northern blots were performed. For this, an automated version of the by-hand procedure was implemented. A given mRNA sequence was compared against the EST database of the organism of the sequence's origin at NCBI using blastn. Results were screened for specific transcripts assuming that more than 85% sequence identity indicated congruence with the gene of interest. These ESTs were investigated for information about their origin concerning tissue, and counted according to these data. The resulting profile was indicative for the general level of expression as well as occurrence and amount of transcripts in certain tissues in relation to others.

The Algorithm of ISBN was written by Korbinian Grote according to my needs. ISBN can conveniently be accessed through a web interface (<http://anthea.gsf.de/isbn2.html>) and is still easy to setup and maintain. The system relies on the blastn service at the NCBI (<http://www.ncbi.nlm.nih.gov/blast>) for mapping the mRNA sequences of interest onto the EST databases. Due to vast public availability of BLAST servers through the world wide web there did not appear the need of setting up a new server for this task. The NCBI blastn service provides several different output formats including XML (eXtensible Markup Language) which can be parsed for information using openly available software like the HTML::Parse package for the perl programming language. Using these tools, accession numbers and alignment quality for all ESTs matching against the given mRNA sequence are collected as well as the annotation of the identified EST sequences and informations on originating organisms, strains, tissues, and organs. This is accomplished by a perl program. Additionally, download of the human, mouse, rodent, mammal, and other vertebrate EST data files from the EMBL institute (<http://www.embl.org>) is performed and scanned the contained sequence annotation for tissue and organ information. This download is useful as it leads to a faster performance of ISBN. These data together with accession numbers and sequence lengths are then stored into a MySQL database for direct accessibility. In order to keep the MySQL database up to date, we added a mechanism to automatically

include information on any newly released EST sequences. Using the XML information from the blast file and the EST data, our tool produces HTML-output giving an overview on all tissues and organs attributed to the given mRNA via the aligned EST-sequences. Information on found ESTs is stored on the web server and can be retrieved at any later time. Storage of the XML data of the blast output enables re-analysis of the same data with different filter settings.

4.7.3. Alignments and phylogeny

Two protein or DNA sequences were compared to each other using bl2seq at NCBI. For multiple sequence alignments, protein sequences were aligned by clustalW [116]. In these programs penalty gaps, word size, and substitution matrix were kept at default values. For phylogenetic analyses, multiple alignments were also created in MEGA v3.1 ([56] and references therein).

For phylogenetic analysis, data sets were created by retrieving related sequences from the BLINK-link of the respective protein entries in the NCBI database and proteins therein. For comparison of the found proteins, SDRs of known substrate specificities were included to the phylogenetic analyses. Sequences were processed in the same way as for direct comparisons and phylogenetic analyses subsequently conducted with MEGA v3.1 using the Neighbor Joining (NJ) algorithm.

4.7.4. Bioinformatic assessment of subcellular localization

For preliminary bioinformatical analysis several servers are publically available. For this analysis, I compared the results given by five servers. The servers used are depicted in table 5.1 (p. 152).

4. Methods

5. Programs, organisms, material

5.1. Programs

SigmaPlot (version 2002, Windows8.02), enzyme kinetics module:
for evaluation of results from Michaelis-Menten kinetics.

Vector NTI (Informax):

Program for administration and analysis of amino and nucleic acid sequences

BLAST-programs:

BLAST = basic linear alignment search tool

Internet accessible tool for comparison of protein and nucleic acid sequences against databases or against each other (in case of bl2seq)

Employed BLAST-programs:

bl2seq: compares two sequences against each other using any of the given blast programs

blastn: nucleotides vs. nucleotides

blastp: proteins vs. proteins

blastx: translated nucleotides vs. translated nucleotides

psi-blast: iterative search of protein motifs vs. proteins

tblastn: translated nucleotide vs. proteins

<http://www.ncbi.nlm.nih.gov>

BioEdit:

Free-download program (via internet) for the analysis of protein and nucleic acid sequences with stress on alignment and phylogenetics

<http://www.mbio.ncsu.edu/BioEdit/bioedit.html>

5. Programs, organisms, material

clustalW:

Internet accessible tool for multiple sequence alignment of proteins or nucleic acids
<http://www2.ebi.ac.uk/clustalw>

LALIGN:

Internet accessible tool to align two amino or nucleic acid sequences
<http://www2.igh.cnrs.fr/bin/align-guess.cgi>

MEGA (version 3.1):

Phylogenetic analysis of protein and nucleic acid sequences (free download from internet),
<http://www.megasoftware.net>

Servers used for the bioinformatic assessment of subcellular localization are listed in table 5.1.

Table 5.1: Servers used for bioinformatic assessment of subcellular localization

Server	URL
pSORTII	http://psort.nibb.ac.jp/form2.html
pTarget	http://bioinformatics.albany.edu/~pttarget/
SubLoc 1.1	http://www.bioinfo.tsinghua.edu.cn/SubLoc/cgi-bin/eu_subloc.cgi
TargetP 1.1	http://www.cbs.dtu.dk/services/TargetP/
LOCtree	http://cubic.bioc.coluFermentasa.edu/services/loctree
WOLF Sort	http://wolfpsort.seq.cbrc.jp/

5.2. Organisms

5.2.1. *E. coli* strains used

Top 10 (Invitrogen)

JM107

DH5 α (Life Technologies)

E. coli strains provided by RZPD as hosts of ordered ESTs:

GeneHogs DH10B

XL1blue

5.2.2. Cell lines used

HEK293T and SaOS-2 cells were purchased from ATCC /LGC Promochem. HeLa, HEPA1-6, and HepG2 cell lines were distributed by DSMZ.

5.3. Material

Vectors

pAcGFP1-N1	BD Clontech
pcDNA3	Invitrogen
pcDNA4 myc-his Version B	Invitrogen
pCMV-SPORT6	RZPD
pCR2.1	Invitrogen
pCRII	Invitrogen
pEGFP-C2	BD Clontech
pGEX 2T PL2	initially Amersham
pT7T3D-PAC	RZPD

Primary Antibodies

anti-GST	Zymed
Monoclonal mouse anti myc 9B11	NEB
Polyclonal rabbit IgG anti FLAG	Sigma

Secondary Antibodies

Goat anti mouse IgG, AlexaFluor488 coupled	Invitrogen
Goat anti mouse IgG, AlexaFluor568 coupled	Invitrogen
Goat anti mouse IgG, peroxidase coupled IgG	Dianova
Goat anti rabbit IgG, AlexaFluor488 coupled	Invitrogen
Goat anti rat IgG, Cy3 coupled	Dianova
Goat anti rat IgG, peroxidase coupled IgG	Dianova

5. Programs, organisms, material

Radionuclides

Phosphor-labeled Substances

α -³²P-dATP GE Healthcare

³H-labeled substances

Androst-4-ene-3,17-dione (1, 2, 6, 7- ³ H (N))	NEN
Estrone (2, 4, 6, 7- ³ H (N))	NEN
Estradiol (6, 7- ³ H (N))	NEN
Testosterone (1, 2- ³ H (N))	NEN
Corticosterone (1,2- ³ H)	NEN
Cortisol (1,2,6,7- ³ H)	NEN
Androsterone (9,11- ³ H)	NEN
Dihydrotestosterone (1,2,4,5,6,7- ³ H)	NEN
Progesterone (1,2,6,7- ³ H)	NEN
20 α hydroxy progesterone (1,2- ³ H)	NEN

Chemicals, supplements, sera, and media

Acrylamide/Bisacrylamide (30%/0.8%)	Roth
Agarose	Biozym
Ammoniumperoxodisulphate (APS)	Biozym
Ampicillin	Sigma
Bacto-Pepton	Difco
Bacto-Agar	Difco
β -Mercaptoethanol	Merck
BM Purple AB substrate solution	Roche
BSA	NEB
Coomassie blue G250	Biomol
Diaminobenzidine (DAB)	Biomol
DIG RNA Labelling Mix	Roche
Dimethylsulfoxide (DMSO)	Sigma
DMEM	Invitrogen
dNTPs	Fermentas
Ethanol	Merck
Ethidiumbromide	Sigma
Ethylenediamintetraacetate (EDTA)	Biomol
FBS	Biochrom
FluoroTrans W Membrane (PVDF)	Pall
Formaldehyde, 37%	Roth
FuGene6	Roche

Chemicals, supplements, sera, and media (continued)

Glucose	Merck
L-Glutamine	Invitrogen
Imidazol	Sigma
Isopropylthiogalaktosid (IPTG)	Fermentas
Kanamycin	Sigma
λ -Markers 3 and 8	Fermentas
6x Loading Dye	Fermentas
Mangan chloride (tetrahydrate)	Sigma
Magnesium hexahydrate	Merck
McCoy's 5A	Invitrogen
MEM	Invitrogen
NN-Dimethylformamid	Merck
NorthernMax High Stringency Wash	Ambion
NorthernMax Low Stringency Wash	Ambion
Parafilm	American National Can
Penicillin/Streptamycin	Invitrogen
Potassium chloride	Merck
Potassium hydrogen phosphate	Merck
Potassium acetate	Merck
2-Propanol	Merck
Ready Flow III	Beckman
reverse phase LUNA 5u C18 (2) column	Phenomenex
RIPA buffer	Sigma
Rubidiumchlorid	Sigma
Sodiumacetat	Merck
Sodium chloride	Merck
Sodiumdodecylsulfat (SDS)	Serva
Sodiumhydrogenphosphate monohydrate	Merck
Sodiumhydroxid tablets	Merck
TEMED	Sigma
Trisbase	Merck
Triton-X100	Merck
TRIzol	Invitrogen
Trypsin/EDTA	Invitrogen
Tween-20	Merck
Ultrahyb Solution	Ambion
XAR-5 (X-ray films)	Kodak
Yeast extract	Difco

5. Programs, organisms, material

Enzymes

Alkaline Phosphatase	Roche
Benzonase	Sigma
Calf Intestine Alkaline Phosphatase (CIAP)	Fermentas
Herculase	Stratagene
Lysozyme	Merck
PfuTurbo	Stratagene
Pfx Polymerase	Invitrogen
Restriktion endonucleases	NEB
Ribonuclease Inhibitor	Fermentas
RQ1 RNase-free DNase I	Promega
Taq-DNA-Polymerase	Fermentas or made inhouse
T3, T7 and SP6 RNA polymerases	Fermentas
T4-DNA-Ligase	NEB, Promega

Kits

BondElut 18	Varian
Cycle Sequencing Kit	Applied Biosystems
DyeEx or DyeEX96	QIAGEN
MicroSpin™ S-200 HR columns	GE Healthcare
Nucleobond PC 100 Kit	MACHERY & NAGEL
NucleoSpin Plasmid Kit	MACHERY & NAGEL
QuikChange	Stratagene
QIAquick Gel Extraction Kit	QIAGEN
QIAquick PCR Purification Kit	QIAGEN
TA Cloning Kit	Invitrogen
RNeasy Midi Kit	QIAGEN
RNeasy Mini Kit	QIAGEN
RevertAid™ First Strand cDNA Synthesis Kit	Fermentas
Strata C18-E columns	Phenomenex
StripEZ DNA Kit	Ambion
SV Total RNA Isolation Kit	Promega
Wizard SV Gel and PCR Vlean-Up System	Promega

Solutions for cell staining

DAPI	Invitrogen
ER-Tracker Blue-White DPX	Invitrogen
Hoechst33342	Invitrogen
MitoTrackerOrange	Invitrogen
Phalloidin, AlexaFluor350 or 568	Invitrogen

Solutions for cell staining	(continued)
Vectashield	Vectalabs
rabbit N-FLAG sarcolipin plasmid	Dr. A. Odermatt, Berne

Laboratory Equipment

Sub Cell GT	BIO-RAD
Centrifuges	Beckman Avanti J-20 Hettich Universal 32R Eppendorf 5415C
Concentrator	Eppendorf Concentrator 5301
DNA sequencer	Applied Biosystems ABI3730
Elektroporation	Biorad Gene Pulser II
Gel dokumentation	PeqLab BioVision
HPLC radioactivity monitor LB 506D	Berthold
HPLC system assembly 32Karat Gold	Beckman
Incubation shaker innova 4230	New Brunswick Scientific
Incubators	Haereus Instruments
Mikropipettes	Gilson
Mini-PROTEAN II	BIO-RAD
PCR machines	Stratagene Robocycler 96
pH-Meter	pH Meter 766 calimetric Knick
Power supply	Biorad, Power PA300
Precision balance	Sartorius 1205 MD
Spektralphotometer	Beckman DU 530
Thermomixer comfort	Eppendorf
Trans-Blot SD - Semidry Transfer Cell	BIO-RAD
Vortexer	Scientific Industries Vortex Genie

Tubes and Containers

6 well, 12 well, and 96 well plates	Becton & Dickinson or NUNC
100 μ -cell strainer	Becton & Dickinson
Cell culture flasks, T25 and T80	NUNC
Cover slips, SuperFrost plus Cover Slides	Menzel Glaeser
Cryo tubes, 1.8 mL	NUNC or Greiner
Eppendorf Caps, 1.5 mL and 2 mL	Eppendorf
Falcon tubes, 15 mL and 50 mL	Becton & Dickinson
PCR tubes, stripes and plates	Applied Biosystems
Petri dishes	Becton & Dickinson

5. Programs, organisms, material

Bibliography

- [1] J. S. Adams. Bound to work: the free hormone hypothesis revisited. *Cell*, 122(September 9):647–649, 2005.
- [2] J. Adamski. *Lokale Aktivierung und Inaktivierung der Steroidhormone, insbesondere der Sexualhormone*. In: Ganten, D., Ruckpaul, K., Köhrle, J. - Molekularmedizinische Grundlagen von para- und autokrinen Regulationsstörungen. Springer, Berlin, Heidelberg, New York, 2006.
- [3] J. Adamski, W. D. Sierralta, and P. W. Jungblut. Assignment of estradiol-17 beta dehydrogenase and of estrone reductase to cytoplasmic structures of porcine endometrium cells. *Acta Endocrinol (Copenh)*, 121(2):161–7, 1989.
- [4] S. F. Altschul, T. L. Madden, A. A. Schaffer, J. Zhang, Z. Zhang, W. Miller, and D. J. Lipman. Gapped blast and psi-blast: a new generation of protein database search programs. *Nucleic Acids Res*, 25(17):3389–3402, 1997.
- [5] S. Andersson and N. Moghrabi. Physiology and molecular genetics of 17 beta-hydroxysteroid dehydrogenases. *Steroids*, 62(1):143–147, 1997.
- [6] A. K. Bednarek, C. L. Keck-Waggner, R. L. Daniel, K. J. Laflin, P. L. Bergsagel, K. Kiguchi, A. J. Brenner, and C. M. Aldaz. Wwox, the fra16d gene, behaves as a suppressor of tumor growth. *Cancer Res*, 61(22):8068–8073, 2001.
- [7] O.V. Belyaeva, O.V. Korkina, A.V. Stetsenko, T. Kim, P.S. Nelson, and N.Y. Kedishvili. Biochemical properties of purified human retinol dehydrogenase 12 (rdh12): catalytic efficiency towards retinoids and c9 aldehydes ad effects of cellular retinol-binding-protein type 1 (crbp1) and cellular retinaldehyde-binding protein (cralbp) on the oxidation and reduction of retinoids. *Biochemistry*, 44:7035–7047, 2005.
- [8] J. M. Berg, J. L. Tymoczko, and L. Stryer. *Biochemie*. Spektrum Akademischer Verlag, Heidelberg, Berlin, 2003.
- [9] G. Bertani. Studies on lysogenesis. i. the mode of phage liberation by lysogenic escherichia coli. *J Bacteriol*, 62(3):293–300, 1951.

Bibliography

- [10] M. G. Biswas and D. W. Russell. Expression cloning and characterization of oxidative 17beta- and 3alpha- hydroxysteroid dehydrogenases from rat and human prostate. *J Biol Chem*, 272(25):15959–15966, 1997.
- [11] D. Boffelli, J. McAuliffe, D. Ovcharenko, K. D. Lewis, I. Ovcharenko, L. Pachter, and E. M. Rubin. Phylogenetic shadowing of primate sequences to find functional regions of the human genome. *Science*, 299(5611):1391–1394, 2003.
- [12] V. Boggaram, B. Funkenstein, M. R. Waterman, and E. R. Simpson. Lipoproteins and the regulation of adrenal steroidogenesis. *Endocr Res*, 10(3-4):387–409, 1984.
- [13] R. Brent and Jr. Finley, R. L. Understanding gene and allele function with two-hybrid methods. *Annu Rev Genet*, 31:663–704, 1997.
- [14] P. Brereton, T. Suzuki, H. Sasano, K. Li, C. Duarte, V. Obeyesekere, F. Haeseleer, K. Palczewski, I. Smith, P. Komesaroff, and Z. Krozowski. Pan1b (17betaahsd11)-enzymatic activity and distribution in the lung. *Mol Cell Endocrinol*, 171(1-2):111–117, 2001.
- [15] L. A. Castagnetta, G. Carruba, A. Traina, O. M. Granata, M. Markus, M. Pavone-Macaluso, C. H. Blomquist, and J. Adamski. Expression of different 17beta-hydroxysteroid dehydrogenase types and their activities in human prostate cancer cells. *Endocrinology*, 138(11):4876–4882, 1997.
- [16] Z. Chai, P. Brereton, T. Suzuki, H. Sasano, V. Obeyesekere, G. Escher, R. Saffery, P. Fuller, C. Enriquez, and Z. Krozowski. 17 beta-hydroxysteroid dehydrogenase type xi localizes to human steroidogenic cells. *Endocrinology*, 144(5):2084–91, 2003.
- [17] N. S. Chang. A potential role of p53 and wox1 in mitochondrial apoptosis (review). *Int J Mol Med*, 9(1):19–24, 2002.
- [18] N. S. Chang, J. Doherty, and A. Ensign. Jnk1 physically interacts with ww domain-containing oxidoreductase (wox1) and inhibits wox1-mediated apoptosis. *J Biol Chem*, 278(11):9195–9202, 2003.
- [19] W. Chen, M. S. Song, and J. L. Napoli. Sdr-o: an orphan short-chain dehydrogenase/reductase localized at mouse chromosome 10/human chromosome 12. *Gene*, 294(1-2):141–146, 2002.
- [20] K. S.. Crowley and R. M. Payye. Ribosome binding to mitochondria is regulated by gtp and the transit peptide. *J Biol Chem*, 273:17278–17285, 1998.
- [21] D. R. Cryer, R. Eccleshall, and J. Marmur. Isolation of yeast dna. *Methods Cell Biol*, 12:39–44, 1975.

- [22] D. Deluca, A. Krazeisen, R. Breitling, C. Prehn, G. Moeller, and J. Adamski. Inhibition of 17beta-hydroxysteroid dehydrogenases by phytoestrogens. *J. Ster.Biochem.Mol.Biol.*, 93:285–292, 2005.
- [23] D. Deluca, G. Moeller, A. Rosinus, W. Elger, A. Hillisch, and J. Adamski. Inhibitory effects of fluorine-substituted estrogens on the activity of 17beta-hydroxysteroid dehydrogenases. *Mol Cell Endocrinol*, 248(1-2):218–224, 2006.
- [24] B. Desvergne, L. Michalik, and W. Wahli. Transcriptional regulation of metabolism. *Physiol Rev*, 86(2):465–514, 2006.
- [25] J. M. Dothie, J. R. Giglio, C. B. Moore, S. S. Taylor, and B. S. Hartley. Ribitol dehydrogenase of klebsiella aerogenes. sequence and properties of wild-type and mutant strains. *Biochem J*, 230(3):569–578, 1985.
- [26] N. Draper and P.M. Stewart. 11beta-hydroxysteroid dehydrogenase and the pre-receptor regulation of corticosteroid hormone action. *J Endocrinol*, 186:251–271, 2005.
- [27] K. Driouch, H. Prydz, R. Monese, H. Johansen, R. Lidereau, and E. Frengen. Alternative transcripts of the candidate tumor suppressor gene, wwox, are expressed at high levels in human breast tumors. *Oncogene*, 21(12):1832–1840, 2002.
- [28] W.L. Duax and D. Ghosh. Structure and function of steroid dehydrogenases involved in hypertension, fertility, and cancer. *Steroids*, 62:95–100, 1997.
- [29] R. Ebert, N. Schuetze, J. Adamski, and F. Jakob. Vitamin d signaling is modulated on multiple levels in health and disease. *Mol Cell Endocrinol*, 248(1-2):149–159, 2006. 0303-7207 (Print) Journal Article.
- [30] D. P. Edwards, J. O Conner, E. D. Bransome Jr., and W. E. Braselton Jr. Human placental 3beta-hydroxysteroid dehydrogenase:delta5-isomerase. *J Biol Chem*, 251(6):1632–1638, 1976.
- [31] J. A. Eisen and C. M. Fraser. Phylogenomics: intersection of evolution and genomics. *Science*, 300(5626):1706–1707, 2003.
- [32] O. Emanuelsson, H. Nielssen, S. Brunak, and G. von Heijne. Predicting subcellular localization of proteins based on thei n-terminal amino acid sequence. *J Mol Biol*, 300:1005–1016, 2000.

Bibliography

- [33] T. Gabaldon and M. A. Huynen. Prediction of protein function and pathways in the genome era. *CMLS*, 61:930–944, 2004.
- [34] M.T. Geraghty, D Bassett, J.C. Morrell, G.J. Gatto Jr., J. Bai, B.V. Geisbrecht, P. Hieter, and S.J. Gould. Detecting patterns of protein distribution and gene expression in silico. *PNAS*, 96(6):2937–2942, 1999.
- [35] D. Ghosh, M. Sawicki, V. Pletnev, M. Erman, S. Ohno, S. Nakajin, and W.L. Duax. Porcine carbonyl reductase. structural basis for a functional monmer in short chain dehydrogenases/reductases. *J Biol Chem*, 276:18457–18463, 2001.
- [36] F. Gianfrancesco, R. Sanges, T. Esposito, S. Tempesta, E. Rao, G. Rappold, N. Aichidiacono, J.A.M. Graves, A. Forabosco, and D' Urso M. Differential divergence of three human psudoautosomal genes and their mouse homologs: Implications for sex chromosome evolution. *Genome Res*, 2001(11):2095–2100, 2001.
- [37] F. Haeseler, G. F. Jang, Y. Imanishi, C. A. Driessens, M. Matsumura, P. S. Nelson, and K. Palczewski. Dual-substrate specificity short chain retinol dehydrogenases from the vertebrate retina. *J Biol Chem*, 277(47):45537–45546, 2002.
- [38] F. Haeseler and K. Palczewski. Short-chain dehydrogenases/reductases in retina. *Methods Enzymol*, 316:372–383, 2000.
- [39] A. Hammes, T. K. Andreassen, R. Spoelgen, J. Raila, N. Hubner, H. Schulz, J. Metzger, F. J. Schweigert, P. B. Lappa, A. Nykjaer, and T. E. Willnow. Role of endocytosis in cellular uptake of sex steroids. *Cell*, 122(September 9):751–762, 2005.
- [40] J. Hodgkin. What does a worm want with 20,000 genes? *Genome Biol*, 2(11):2008.1–2008.4, 2001.
- [41] S. Hua and Z. Sun. Support vector machine approach for protein subcellular localization prediction. *Bioinformatics*, 17(8):721–728, 2001.
- [42] X. F. Huang and V. Luu-The. Molecular characterization of a first human 3(alpha- β -hydroxysteroid epimerase. *J Biol Chem*, 275(38):29452–7, 2000.
- [43] Y.-W. Huang, I. Pineau, H.-J. Chang, A. Azzi, V. Bellemare, S. Laberge, and S.-X. Lin. Critical residues for the specificity of cofactors and substrates in human estrogenis 17beta-hydroxysteroid dehydrogenase 1: Variants designed from the three-dimensional structure of the enzyme. *Mol Endocrinol*, 15(11):2010–2020, 2001.

- [44] S. V. Hughes, E. Robinson, R. Bland, H. M. Lewis, P. M. Stewart, and M. Hewison. 1,25-dihydroxyvitamin d₃ regulates estrogen metabolism in cultured keratinocytes. *Endocrinology*, 138(9):3711–3718, 1997.
- [45] P. Hunter. Laptop biology. *EMBO reports*, 6(3):208–210, 2005.
- [46] A.R. Janecke, D.A. Thompson, G. Utermann, C. Becker, C.A. Huebner, E. Schmid, C.L. McHenry, A.R. Nair, F. Rueschendorf, J.R. Heckenlively, B. Wissinger, P. Nuernberg, and A. Gal. Mutations in rdh12 encoding a photoreceptor-cell retinol dehydrogenase cause childhood-onset severe retinal dystrophy. *Nature Genetics*, 36(8):850–854, 2004.
- [47] N.B. Javitt. Oxysteroids: a new class of steroids with autocrine and paracrine functions. *Trends in Endocrinology and Metabolism*, 15(8):393–397, 2004.
- [48] H. Joernvall, B. Persson, M. Krook, S. Atrian, R. Gozales-Duarte, J. Jeffery, and D. Ghosh. Short-chain dehydrogenases/reductases (sdr). *Biochemistry*, 34(18):6003–6013, 1995.
- [49] I. Jung-Testas, A. Do Thi, H. Koenig, F. Dsarnaud, K. Shazand, M. Schumacher, and K. Baulieu. Progesterone as a neurosteroid: synthesis and actions in rat glial cells. *J Steroid Biochem Molec Biol*, 69:97–107, 1999.
- [50] Y. Kallberg, U. Oppermann, H. Joernvall, and B. Persson. Short-chain dehydrogenases/reductases (sdrs). *Eur J Biochem*, 269(18):4409–4417, 2002.
- [51] B. Keller, A. Volkmann, T. Wilckens, G. Moeller, and J. Adamski. Bioinformatic identification and characterization of new members of short-chain dehydrogenase/reductase superfamily. *Mol Cell Endocrinol*, 248(1-2):56–60, 2006.
- [52] N. Khan, K. K. Sharma, S. Andersson, and R. J. Auchus. Human 17beta-hydroxysteroid dehydrogenases types 1, 2, and 3 catalyze bi-directional equilibrium reactions, rather than unidirectional metabolism, in hek-293 cells. *Arch Biochem Biophys*, 429(1):50–59, 2004.
- [53] K. Kimura, M. Markowski, C. Bowen, and E.P. Gelmann. Androgen blocks apoptosis of hormone-dependent prostate cancer cells. *Cancer Res*, 61(July 15):5611–5618, 2001.
- [54] G. Kleiger and D. Eisenberg. Gxxg ang gxxxa motifs stabilize fad and nad(p)-bindung rossmann folds through c-h...o hydrogen bonds and van der waals interactions. *J Mol Biol*, 323:36–76, 2002.

Bibliography

- [55] M. Krook, L. Marekov, and H. Jornvall. Purification and structural characterization of placental nad(+) -linked 15-hydroxyprostaglandin dehydrogenase. the primary structure reveals the enzyme to belong to the short-chain alcohol dehydrogenase family. *Biochemistry*, 29(3):738–743, 1990.
- [56] S. Kumar, K. Tamura, and M. Nei. Mega3: Integrated software for molecular evolutionary genetics analysis and sequence alignment. *Brief Bioinform*, 5(2):150–163, 2004.
- [57] F. Labrie. Introcrinology. *Mol Cell Endocrinol*, 78(3):113–118, 1991.
- [58] C. A. Lange. Making sense of cross-talk between steroid hormone receptors and intracellular signaling pathways: who will have the last word? *Mol Endocrinol*, 18(2):269–278, 2004.
- [59] D. Laubner, R. Breitling, and J. Adamski. Surprising expression pattern of cholesterogenic enzymes during embryonic mouse development. *Developmental Biology*, 235(1):195–198, 2001.
- [60] D. Laubner, R. Breitling, and J. Adamski. Embryonic expression of cholesterogenic genes is restricted to distinct domains and colocalizes with apoptotic regions in mice. *Brain Res Mol Brain Res*, 115(1):87–92, 2003.
- [61] F. Leenders, J. G. Tesdorp, M. Markus, T. Engel, U. Seedorf, and J. Adamski. Porcine 80-kda protein reveals intrinsic 17 beta-hydroxysteroid dehydrogenase, fatty acyl-coa-hydrolase/dehydrogenase, and sterol transfer activities. *J Biol Chem*, 271(10):5438–5442, 1996.
- [62] M. P. Leese, H. A. Hejaz, M. F. Mahon, S. P. Newman, A. Purohit, M. J. Reed, and B. V. Potter. A-ring-substituted estrogen-3-o-sulfamates: potent multitargeted anticancer agents. *J Med Chem*, 48(16):5243–5256, 2005.
- [63] R. L. Leibel, C. C Streamson, and M. Rosenbaum. *Obesity*, volume 3 of *Scriver, C. R., Beaudet, A. L., Sly, W. S.: The Metabolic & Molecular Basis of Inherited Disease*. McGraw-Hill, New York, 8 edition, 2001.
- [64] K. X. Li, R. E. Smith, and Z. S. Krozowski. Cloning and expression of a novel tissue specific 17beta-hydroxysteroid dehydrogenase. *Endocr Res*, 24(3-4):663–667, 1998.
- [65] R. Losel and M. Wehling. Nongenomic actions of steroid hormones. *Nat Rev Mol Cell Biol*, 4(1):46–56, 2003.

- [66] R. M. Losel, E. Falkenstein, M. Feuring, A. Schultz, H. C. Tillmann, K. Rossol-Haseroth, and M. Wehling. Nongenomic steroid action: controversies, questions, and answers. *Physiol Rev*, 83(3):965–1016, 2003.
- [67] P. Lukacik, B. Keller, G. Bunkoczi, K. Kavanagh, W.H. Lee, J. Adamski, and U. Oppermann. Structural and biochemical characterization establishes human dhrs10 as a novel 17-hydroxysteroid dehydrogenase. *Manuscript in revision*, 2006.
- [68] V. Luu-The, P. Tremblay, and F. Labrie. Characterization of type 12 17beta-hydroxysteroid dehydrogenase (17beta-hsd12), an isoform of type 3 17beta-hydroxysteroid dehydrogenase responsible for estradiol formation in women. *Mol Endocrinol*, 20(2):437, 2006.
- [69] V. Luu-The, J. Zhang, D. Poirier, and F. Labrie. Characteristics of human types 1, 2 and 3 17beta-hydroxysteroid dehydrogenase activities: Oxidation/reduction and inhibition. *J. Ster. Biochem. Mol. Biol.*, 55(5/6):581–587, 1995.
- [70] P.J. Malloy, W. Pike, and D. Feldman. The vitamin d receptor and the syndrome of hereditary 1,25-dihydroxyvitamin d-resistant rickets. *Endocr Reviews*, 20(20):156–188, 1999.
- [71] Z. Marijanovic, D. Laubner, G. Moller, C. Gege, B. Husen, J. Adamski, and R. Breitling. Closing the gap: identification of human 3-ketosteroid reductase, the last unknown enzyme of mammalian cholesterol biosynthesis. *Mol Endocrinol*, 17(9):1715–1725, 2003.
- [72] M. Mark, N. B. Ghyselinck, O. Wendling, V. Dupe, B. Mascrez, P. Kastner, and P. Chambon. A genetic dissection of the retinoid signalling pathway in the mouse. *Proc Nutr Soc*, 58:609–613, 1999.
- [73] C.M. Mendel. The free hormone hypothesis. distinction from the free hormone transport hypothesis. *J Androl*, 13(2):107–116, 1992.
- [74] G. (Ed.) Michal. *Biochemical Pathways*. Spektrum Akademischer Verlag, Heidelberg, 1 edition, 1999.
- [75] R. Mindnich. *Identification and characterization of zebrafish 17beta HSD type 1 and type 3: A comparative analysis of androgen/estrogen activity regulators*. PhD thesis, GSF - National Research Institute, 2004.
- [76] R. Mindnich, F. Haller, F. Halbach, G. Moeller, M. Hrabe de Angelis, and J. Adamski. Androgen metabolism via 17beta-hydroxysteroid dehydrogenase type 3 in mammalian and non-mammalian vertebrates: comparison of the human and the zebrafish enzyme. *J Mol Endocrinol*, 35(2):305–316, 2005.

Bibliography

- [77] R. Mindnich, G. Moeller, and J. Adamski. The role of 17 beta-hydroxysteroid dehydrogenases. *Mol Cell Endocrinol*, 218(1-2):7–20, 2004.
- [78] G. Moeller and J. Adamski. Multifunctionality of human 17beta-hydroxysteroid dehydrogenases. *Mol Cell Endocrinol*, 248(1-2):47–55, 2006.
- [79] CH Moore, SS Taylor, MJ Smith, and BS Hartley. *Atlas of Protein Sequence*, volume 5. National Biomedical Research Foundation, Washington, D.C., 1978.
- [80] K. Motojima. 17beta-hydroxysteroid dehydrogenase type 11 is a major peroxisome proliferator-activated receptor alpha-regulated gene in mouse intestine. *Eur J Biochem*, 271(20):4141–4146, 2004.
- [81] P. Nokelainen, T. Puranen, H. Peltoketo, M. Orava, P. Vihko, and R. Vihko. Molecular cloning of mouse 17 beta-hydroxysteroid dehydrogenase type 1 and characterization of enzyme activity. *Eur J Biochem*, 236(2):482–490, 1996.
- [82] A.W. Norman and H Litwack. *Hormones*. Academic Press, San Diego, London, 2nd edition, 1997.
- [83] T. Normand, B. Husen, F. Leenders, H. Pelczar, J. L. Baert, A. Begue, A. C. Flourens, J. Adamski, and Y. de Launoit. Molecular characterization of mouse 17 beta-hydroxysteroid dehydrogenase iv. *J. Steroid Biochem. Mol. Biol*, 55(5-6):541–548, 1995.
- [84] A. Odermatt, S. Becker, Khannam V.K., K. Kurzydlowski, E. Leisner, D. Pette, and MacLennan D.H. Sarcolipin regulates the activity of serca1, the fast-twitch skeletal muscle sarcoplasmic reticulum ca2. *J Biol Chem*, 273(20):12360–12369, 1998.
- [85] T. Ohnesorg, B. Keller, M. Hrabe de Angelis, and J. Adamski. Transcriptional regulation of human and murine 17beta hydroxysteroid dehydrogenase type 7 confers its 3 participation in cholesterol biosynthesis. *J Mol Endocrinol*, page In Press, 2006.
- [86] U. Oppermann, C. Filling, M. Hult, N. Shafqat, X. Wu, M. Lindh, J. Shafqat, E. Nordling, Y. Kallberg, B. Persson, and H. Jornvall. Short-chain dehydrogenases/reductases (sdr): the 2002 update. *Chem Biol Interact*, 143-144:247–253, 2003.
- [87] A. H. Payne and D. B. Hales. Overview of steroidogenic enzymes in the pathway from cholesterol to active steroid hormones. *Endocr Rev*, 25(6):947–970, 2004.

- [88] H. Peltoketo, V. Isomaa, O. Mentausta, and R. Vihko. Complete amino acid sequence of human placental 17b-hydroxysteroid dehydrogenase deduced from cdna. *FEBS Letters*, 239(1):73–77, 1988.
- [89] H. Peltoketo, P. Nokelainen, Y. S. Piao, R. Vihko, and P. Vihko. Two 17beta-hydroxysteroid dehydrogenases (17hsds) of estradiol biosynthesis: 17hsd type 1 and type 7. *J Steroid Biochem Molec Biol*, 69(1-6):431–439, 1999.
- [90] H. Peltoketo, P. Vihko, and R. Vihko. Regulation of estrogen action: role of 17 beta-hydroxysteroid dehydrogenases. *Vitam Horm*, 55:353–398, 1999.
- [91] T. M. Penning. Hydroxysteroid dehydrogenases and pre-receptor regulation of steroid hormone action. *Hum Reprod Update*, 9(3):193–205, 2003.
- [92] I. Perrault, S. Hanein, S. Gerber, F. Barbet, D. Ducrocq, H. Dollfus, C. Hamel, J. Dufier, A. Munnich, J. Kaplan, and J.-M. Rozet. Retinal dehydrogenase 12 (rdh12) mutations in leber congenital amaurosis. *Am J Hum Genet*, 75:639–646, 2004.
- [93] B. Persson, Y. Kallberg, U. Oppermann, and H. Joernvall. Coenzyme-based functional assignments of short-chain dehydrogenases/reductases (sdrs). *Chem Biol Interact*, 143-144:271–278, 2003.
- [94] D. Poirier. Inhibitors of 17beta-hydroxysteroid dehydrogenases. *Curr Med Chem*, 10(6):453–477, 2003.
- [95] A. Poletti and L. Martini. Androgen-activating enzymes in the central nervous system. *J Steroid Biochem Molec Biol*, 69:117–122, 1999.
- [96] F. D. Porter. Malformation syndromes due to inborn errors of cholesterol synthesis. *J Clin Invest*, 110(6):715–24, 2002.
- [97] J. P. Preslock. A review of in vitro testicular steroidogenesis in rodents, monkeys and humans. *J Steroid Biochem*, 13(8):965–975, 1980.
- [98] J. Reboul, P. Vaglio, N. Tzellas, N. Thierry-Mieg, T. Moore, C. Jackson, T. Shin-i, Y. Kohara, D. Thierry-Mieg, J. Thierry-Mieg, H. Lee, J. Hitti, L. Doucette-Stamm, J. L. Hartley, G. F. Temple, M. A. Brasch, J. Vandenhaut, P. E. Lamesch, D. E. Hill, and M. Vidal. Open-reading-frame sequence tags (osts) support the existence of at least 17,300 genes in c. elegans. *Nature Genetics*, 27(3):332–336, 2001.
- [99] P. Robel and E. E. Baulieu. Neurosteroids: biosynthesis and function. *Crit Rev Neurobiol*, 9(4):383–394, 1995.

Bibliography

- [100] B. Rosen and R. Beddington. Detection of mrna in whole mounts of mouse embryos using digoxigenin riboprobes. *Methods Mol Biol*, 28:201–208, 1994.
- [101] M.G. Rossmann, D. Moras, and K.W. Olsen. Chemical and biological evolution of a nucleotide-binding protein. *Nature*, 205:194–199, 1974.
- [102] J. Sambrook and D.W. Russell. *Molecular Cloning: A Laboratory Manual*. Cold Spring Harbor Laboratory Press, Woodbury NY, 2001.
- [103] P. Sazani and R. Kole. Therapeutic potential of antisense oligonucleotides as modulators of alternative splicing. *J Clin Invest*, 112(4):481–486, 2003.
- [104] G. Schneider and U. Fechner. Advances in the predictions of protein targeting signals. *Proteomics*, 4:1571–1580, 2004.
- [105] G. D. Schuler. Sequence mapping by electronic pcr. *Genome Res*, 7:541–550, 1997.
- [106] M.F. Schwartz and H. Joernvall. Structural analyses of mutant and wild-type alcohol dehydrogenases from drosophila melanogaster. *Eur J Biochem*, 68:159–168, 1976.
- [107] D. Shen, J. He, and H.R. Chang. In silico identification of breast cancer genes by combined multiple high throughput analyses. *Int J Mol Med*, 15(2):205–212, 2005.
- [108] J. Simard, M.-L. Ricketts, S. Gingras, P. Soucy, A. Feltus, and Melner M.H. Molecular biology of the 3beta-hydroxysteroid dehydrogenase/delta5-delta4-isomerase gene family. *Endocrine Reviews*, 26(4):525–582, 2005.
- [109] A. Slominski, I. Semak, J. Zjawiony, J. Wortsman, W. Li, A. Szczesniewski, and R. C. Tuckey. The cytochrome p450syy system opens an alternate pathway of vitamin d3 metabolism. *FEBS Journal*, 272:4080–4090, 2005.
- [110] R. Spoerle and K. Schughart. System to identify individual somites and their derivatives in the developing mouse embryo. *Dev Dyn*, 210(3):216–226, 1997.
- [111] S. Steckelbroek, B. Oyesamni, Y. Jin, S.-H. Lee, H. J. Kloosterboer, and T. M. Penning. Tibolone metabolism in human liver is catalyzed by 3alpha/3beta hydroxysteroid dehydrogenase activities of the four isoforms of the also-keto reductase (akr) 1c subfamily. *J Pharmacol Exp Therap*, 316(3):1300–1309, 2006.
- [112] B. Tchedam Ngatcha, V. Luu-The, F. Labrie, and D. Poirier. Androsterone 3alpha-ether-3beta-substituted and androsterone 3beta-substituted derivatives as inhibitors of type 3 17beta-hydroxysteroid dehydrogenase: chemical synthesis and structure-activity relationship. *J Med Chem*, 48(16):5257–5268, 2005.

- [113] D.R. Thatcher. The complete amino acid sequence of three alcohol dehydrogenase alleloenzymes (adh_n-11, adhs, and adh_f) from the fruitfly *drosophila melanogaster*. *Biochem J*, 187:875–883, 1980.
- [114] J.L. Thomas, W.L. Duax, A. Addlagatta, S. Brandt, R.R. Fuller, and W. Norris. Structure/function relationships for coenzyme specificity and the isomerase activity of human type 1 3beta-hydroxysteroid dehydrogenase/isomerase. *J Biol Chem*, 278:35483–35490, 2003.
- [115] D.A. Thompson, A.R. Janecke, J. Lange, K.L. Feathers, C.A. Huebner, C.L. McHenry, D.W. Stockton, G. Rammesmayer, J.R. Lupski, G. Antinolo, C. Ayuso, M. Baiget, P. Gouras, J.R. Heckenlively, A. den Hollander, S.G. Jacobson, R.A. Lewis, P.A. Sieving, B. Wissinger, S. Yzer, E. Zrenner, G. Utermann, and A. Gal. Retinal degeneration associated with rdh12 mutations results from decreased 11-cis retinal synthesis due to disruption of the visual cycle. *Human Molec Genet*, 14(24):3865–3875, 2005.
- [116] J. D. Thompson, D. G. Higgins, and T. J. Gibson. Clustal w: improving the sensitivity of progressive multiple sequence alignment through sequence weighting, position-specific gap penalties and weight matrix choice. *Nucleic Acids Res*, 22(22):4673–4680, 1994.
- [117] J. W. Tomlinson, E. A. Walker, I. J. Bujalska, N. Draper, G. G. Lavery, M. S. Cooper, M. Hewison, and P. M. Stewart. 11beta-hydroxysteroid dehydrogenase type 1: a tissue-specific regulator of glucocorticoid response. *Endocr Rev*, 25(5):831–866, 2004.
- [118] T. E. Vaskivuo, U. Ottander, O. Oduwole, V. Isomaa, P. Vihko, J. I. Olofsson, and J. S. Tapanainen. Role of apoptosis, apoptosis-related factors and 17beta-hydroxysteroid dehydrogenases in human corpus luteum regression. *Mol Cell Endocrinol*, 194(1-2):191–200, 2002.
- [119] N. Vicker, X. Su, H. Lawrence, A. Cruttenden, A. Purohit, M. J. Reed, and B. V. Potter. A novel 18beta-glycyrrhetic acid analogue as a potent and selective inhibitor of 11beta-hydroxysteroid dehydrogenase 2. *Bioorg Med Chem Lett*, 14(12):3263–3267, 2004.
- [120] P. Vihko, P. Harkonen, P. Soronen, S. Torn, A. Herrala, R. Kurkela, A. Pulkka, O. Oduwole, and V. Isomaa. 17beta-hydroxysteroid dehydrogenases-their role in pathophysiology. *Mol Cell Endocrinol*, 215(1-2):83–88, 2004.

Bibliography

- [121] P. Vihko, A. Herrala, P. Harkonen, V. Isomaa, H. Kaija, R. Kurkela, Y. Li, L. Patrikainen, A. Pulkka, P. Soronen, and S. Torn. Enzymes as modulators in malignant transformation. *J Steroid Biochem Molec Biol*, 93(2-5):277–283, 2005.
- [122] M. Warner and J. A. Gustafsson. Nongenomic effects of estrogen: why all the uncertainty? *Steroids*, 71(2):91–95, 2006.
- [123] G. E. Weitsman, R. Koren, E. Zuck, C. Rotem, U. A. Liberman, and A. Ravid. Vitamin d sensitizes breast cancer cells to the action of h2o2: Mitochondria as a convergence point in the death pathway. *Free Radical Biology & Medicine*, 39:266–278, 2005.
- [124] O. Wendling, P. Chambon, and M. Mark. Retinoid x receptors are essential for early mouse development and placentogenesis. *PNAS*, 96:547–551, 1999.
- [125] K. Yoon, L. Pellaroni, Ramamoorthy K., K. Gaido, and S. Safe. Ligand structure-dependent differences in activation of estrogen receptor alpha in human hepg2 liver and u2 osteogenic cancer cell lines. *Mol Cell Endocrinol*, 162:211–220, 2000.
- [126] Y. Zhang, I. Dufort, P. Rheault, and V. Luu-The. Characterization of a human 20alpha-hydroxysteroid dehydrogenase. *J Mol Endocrinol*, 25(2):221–228, 2000.
- [127] L. Zhong, J. Ou, U. Barkai, J.F. Mao, J. Frasor, and Gibori G. Molecular cloning and characterization of the rat ovarian 20alpha-hydroxysteroid dehydrogenase gene. *Biochem Biophys Res Commun*, 149:797–803, 1998.
- [128] I. H. Zwain and S. S. Yen. Neurosteroidogenesis in astrocytes, oligodendrocytes, and neurons of cerebral cortex of rat brain. *Endocrinology*, 140(8):3843–2852, 1999.

A. Appendix

A.1. Accession numbers of the dataset for the phylogenetic trees

All phylogenetic trees shown are based on the data set consisting of the following accession numbers from NCBI database.

AAH06294.1, Q9MYP6, XP_533627.2, XP_701419.1, ZP_00997073.1, YP_299653.1, ZP_01137081.1, ZP_00619341.1, AAK73164.1, ZP_00601805.1, NP_961862.1, NP_959636.1, ZP_00769178.1, NP_625887.1, ZP_00816771.1, ZP_00601039.1, ZP_00658990.1, ZP_00601484.1, NP_856527.1, YP_385178.1, YP_366811.1, XP_792550.1, XP_474658.1, BAC53872.1, XP_479614.1, NP_569875.2, XP_320665.2, XP_791402.1, AAK55494.1, NP_056540.1, NP_742034.1, NP_065956.1, NP_066284.2, NP_954674.1, NP_683695.1, NP_620419.2, NP_004744.2, NP_000187.2, NP_002144.1, NP_861420.1, NP_000405.1, NP_057455.1, NP_115679.2, NP_113651.3, XP_945902.1, NP_000853.1, NP_000189.1, NP_004484.1, NP_878249.1, NP_005318.1, NP_057226.1, NP_057006.1, NP_000188.1, NP_055049.1, NP_057329.1, NP_001748.1, NP_660151.1, BAA92883.1, NP_000404.1, NP_001008507.1, NP_001004209.1, Q5M875, CAI35261.1, CAG33405.1, AAD34088.1, XP_943583.1, NP_510793.2, BAE42129.1, AAM51176.1, NP_835236.1, AAI04136.1, XP_910581.1, XP_943009.1, XP_578441.1, BAB71545.1, NP_001032276.1, AAH10972.1, NP_689656.1, BAA88521.1, Q9ERI6, CAI25703.1, AAF82054.1, NP_653284.1, CAI95431.1, AAH82583.1, NP_612421.1, AAH03484.1, Q8VID1, XP_946607.1, AAH07339.2, NP_082066.1, P50169, AAB07997.1, AAH98650.1, NP_536684.1, AAH89612.1, AAC39922.1, NP_694773.1, NP_003699.2, NP_663399.1, AAH62000.1, O88451, NP_003716.2, NP_671755.1, AAH21836.1, AAH91114.1, AAB88252.1, NP_002896.2, Q8VD48, AAB93668.1, Q58NB6, AAF31693.1, AAP94227.1, AAF82053.1, NP_084293.1, XP_234334.3, NP_057110.2, AAH19696.2, AAQ89074.1, Q3U0B3, CAI24984.1, NP_001028498.1, AAH51291.1

A. Appendix

A.2. Primers used

Forward (for) primer bind at the 5'-, reverse (rev) primers at the 3'-side of the respective PCR products.

A.2.1. Primers used for test of overexpression of the constructs and generation of northern blot probes

gene		primer sequence	product length (bp)
h β ACTIN	for	GGATTCCCTATGTGGCGACGAGG	868
	rev	CACGGAGTACTTGCCTCAGGAGG	
m β Actin	for	GGGTCAGAAGGACTCCTATGTGGG	884
	rev	CGATCCACACAGAGTACTTGC	
mSdr-o	for	GCCCTCACAGACTTGCTTTATGTACC	527
	rev	AACTTGGAGACACAGTAACCACCG	
hretSDR3	for	GCTACGGAACCGCGCTATGC	627
	rev	CATGCCCTCTCGGATTGTGG	
rdhrs7b	for	GTCACCCAGACGACCATCCTACC	728
	rev	CTTGTCTAGAGCTCCATATCTGGAGCC	
rdhrs8	for	GCTGGAGAGATCGTTCTGATCACC	587
	rev	GCTCGGGTTCTTGATGAAGCC	
mRdh12	for	ATACCAAGAACTCCCAGGTGCTAGTGC	643
	rev	GCTGTTTCTTGTCCGGGC	
hRDH12	for	GATGCTGGTCACCTGGGACTG	664
	rev	GGTGCCTTGGAGCCTTGG	
hRDH13	for	CGTGCTGCTCAAGGACTATGTCAC	560
	rev	GCTTGCTCTGGCAGTAGGCC	
mDhrs4	for	CCAGACAGCAGCTGGATCAGC	734
	rev	CCTCGTGCTGCTACTCCTCTAC	
hDHRSX	for	GGTGATCCTGGCGCAGCTG	904
	rev	CAAGGACCCCAGTCATCTCACAACTC	
hMGC4172	for	CAGCAGGGACTGAAGGTGGTGG	649
	rev	CCAATCTGGATGTGTGCGGG	
mMGC18716	for	GGACTGAAGGTTGTGGTTGTGC	559
	rev	TAGGTGGCAGCTGCTTCCCC	
hWWOX	for	GGACGACACGGACAGTGAGGACGAG	667
	rev	CACTTGAAAGGTGGCTCCAGG	
mWwox	for	GGACGACACGGACAGTGAGGATGAG	547
	rev	CTGCACGCTACGGAGCACGG	
mHsd17b11	for	ATGAAGTATCTTCTTGACTTGATCC	600
	rev	AGCCGGTGTATGAAGTTG	

A.2.2. Primers and restriction sites used for cloning

Gene		Primer sequence	Vector	RE
mSdr-o	for	TATAGGATCCATGGCGGCCCTCACAGACTTGCT	1, 2	BamHI
	rev	TTAAGAATTCTCAAACACTGTCTGCTGGTCTTGG	1	EcoRI
	rev	TTAACCGCGGAACACTGTCTGCTGGTCTTGGCAA	2	SacII
	for	TATAGAATTCATGGCGGCCCTCACAGACTTGCT	3, 4	EcoRI
	rev	TTAAGGATCCTCAAACACTGTCTGCTGGTCTTGG	3	BamHI
	rev	TTAAGAATTCAACACTGTCTGCTGGTCTTGGCAA	4	BamHI
h retSDR3	for	TATAGGATCCATGGCTACGGGAACGCGCTATGCC	1, 2	BamHI
	rev	TTAAGAATTCTCAGGAAGGGATATCGGGGGCGTC	1	EcoRI
	rev	TTAACCGCGGGGAAGGGATATCGGGGGCGTCCAC	2	SacII
	for	TATAGAATTCATGGCTACGGGAACGCGCTATGCC	3	EcoRI
	rev	TTAAGGATCCTCAGGAAGGGATATCGGGGGCGTC	3	BamHI
r dhrs7b	for	TATAGGATCCATGCTCAAGGAGAGGGCCATGGAC	1, 2	BamHI
	rev	TTAAGAATTCTCAGGAGTTCTGGATTTCGCTC	1	EcoRI
	rev	TTAACCGCGGGGAGTTCTGGATTTCGCTCTT	2	SacII
	for	TATAGAATTCATGCTCAAGGAGAGGGCCATGGAC	3	EcoRI
	rev	TTAAGGATCCTCAGGAGTTCTGGATTTCGCTC	3	BamHI
r dhrs8	for	TATAGGATCCATGAAGTACCTTCTGACCTGATC	1	BamHI
	rev	TTAAGAATTCTCATTATCTTGTAGCCAACAAAC	1	EcoRI
	for	TATAGAATTCATGAAGTACCTTCTGACCTGATC	3, 4	EcoRI
	rev	TTAAGGATCCTCATTATCTTGTAGCCAACAAAC	3	BamHI
	rev	TTAAGAATTCTTATCTTGTAGCCAACAAACAGC	4	BamHI
m Rdh12	for	TATAGGATCCATGCTTTATCTTGGTACTGCTT	1, 2	BamHI
	rev	TTAAGAATT CCTATTCCC ACTGGATT CCTAGAAG	1	EcoRI
	rev	TTAACCGCGGTTCCC ACTGGATT CCTAGAAG CTC	2	SacII
	for	TATAGAATT CATGCTTTATCTTGGTACTGCTT	3	EcoRI
	rev	TTAAGGATCCCTATTCCC ACTGGATT CCTAGAAG	3	BamHI
h RDH12	for	TATAGGATCCATGCTGGCACCTGGGACTGCTC	1, 2	EcoRI
	rev	TTAAGAATT CCTACTCCC ACCGGATT CCTAGAAG	1	BamHI
	rev	TTAACCGCGGCTCCC ACCGGATT CCTAGAAG CTC	2	SacII
	for	TATAGAATT CATGCTGGCACCTGGGACTGCTC	3	EcoRI
	rev	TTAAGGATCCCTACTCCC ACCGGATT CCTAGAAG	3	BamHI
h RDH13	for	TATAGGATCCATGAGCCGCTACCTGCTGCCGCTG	1	BamHI
	rev	TTAAGAATTCTTATCTGGGAGGGGCTGCTCCCT	1	EcoRI
	for	TATAGAATT CATGAGCCGCTACCTGCTGCCGCTG	3, 4	EcoRI
	rev	TTAAGGATCCTATCTGGGAGGGGCTGCTCCCT	3	BamHI
	rev	TTAAGAATTCTCTGGGAGGGGCTGCTCCCTCAC	4	BamHI
m Dhrs4	for	TATAGGATCCATGGCCAGTTCCGGTTGACTCGT	1, 2	BamHI
	rev	TTAAGAATTCTCAGAGGC GAGAAGGGGTT CCTCC	1	EcoRI
	rev	TTAACCGCGGGAGGGC GAGAAGGGGTT CCTCCCC	2	SacII
	for	TATAGAATT CATGCCAGTTCCGGGTTGACTCGT	3, 4	EcoRI

A. Appendix

	rev	TTAAGGATCCTCAGAGCGAGAAGGGTTCCTCC	3	BamHI
	rev	TTAAGAATTGAGGCAGAGAAGGGTTCCTCCCC	4	BamHI
h DHRSX	for	TATAGGATCCATGTCGCCATTGTCTGCGCGCGG	1, 2	BamHI
	rev	TTAAGAATTCTCACAGGTCACATCAAGGACCCC	1	EcoRI
	rev	TTAAGAATTGAGGCAGGGTCACATCAAGGACCCCAGT	2	EcoRI
MGC4172	for	TATAGGATCCATGGCCAGGCCGGCATGGAGCGG	1	BamHI
	rev	TTAAGAATTCTAGGTACACTGCTCCGTGGCCT	1	EcoRI
MGC18716	for	TATAGGATCCATGACTAGAGCTGGCATGGAGCGG	1, 2	BamHI
	rev	TTAAGAATTCTAGGTACACTGCTCTGTGGCCT	1	EcoRI
	rev	TTAACCGCGGGTCACCTGCTCTGTGGCCTCAT	2	SacII
	for	TATAGAATTGACTAGAGCTGGCATGGAGCGG	3	EcoRI
	rev	TTAAGGATCCCTAGGTACACTGCTCTGTGGCCT	3	BamHI

Vectors are indicated by the following numbers: pcDNA3 = 1, pcDNA4 myc-his Version B = 2, pEGFP-C2 = 3, pAcGFP1-N1 = 4. Column 'RE' depicts the restriction site included to the primers and subsequently used for cloning.

Both **murine and human WWOX** were cloned blunt end via the EcoRV restriction site of pcDNA3. For Amplification of the CDS, the following primers were used:

hWWOX

for: ATGGCAGCGCTGCGCTACGCGG

rev: GCCGGACTGGCTGCCAAGCCG

mWwox

for: ATGGCAGCTCTGCGCTATGCGGGC

rev: GCTGGATGGACTACCCAGTCGGTCCTGG The murine PCR fragment was additionally cloned into pCRII for whole mount *in situ* hybridization probes.

A.3. IMAGE clones ordered (RZPD)

The following IMAGE clones were used for the amplification of the CDS of the respective products:

mSdr-o: IMAGp998C119435Q3 (pCMV-SPORT6, ampicillin resistance)

hretSDR3: IMAGp958BC006283Q3 (pOTB7, chloramphenicol resistance)

rdhrs7b: IMAGp998M1012446Q3 (pCMV-SPORT6, ampicillin resistance)

rdhrs8: IMAGp958L083175Q2 (pDNR-LIB, chloramphenicol resistance)

mRdh12: IMAGp998J1210437Q3 (pCMV-SPORT6, ampicillin resistance)

hRDH12: IMAGp998M1111498Q3 (pCMV-SPORT6, ampicillin resistance)

hRDH13: IMAGp998M1111411Q3 (pCMV-SPORT6, ampicillin resistance)

mDhrs4: IMAGp998N136958Q (pCMV-SPORT6, ampicillin resistance)

hDHRSX: IMAGp998A035188Q (pT7T3D-PacI, ampicillin resistance)

Coding sequences of hWWOX, mWwox, MGC4172, and MGC18716 were amplified from cDNA gained from cultured cells.

A.4. List of publications

Publications included in this thesis

Keller, B., Grote, K. and Adamski, J. **2006**. In silico Northern blot, an automated method to determine expression patterns from EST databases, reveals tissue specificity of murine 17 β -hydroxysteroid dehydrogenase type 11. *Mol Cell Endocrinol* 248 (1-2): 242-5.

Keller, B., Volkmann, A., Wilckens, T., Möller, G. and Adamski, J. **2006**. Bioinformatic identification and characterization of new members of short-chain dehydrogenase/reductase superfamily. *Mol Cell Endocrinol* 248 (1-2): 56-60.

Lukacik, P., **Keller, B.**, Bunkoczi, G., Kavanagh, K., Lee, W. H., Adamski, J., and Oppermann, U. **2006**. Structural and biochemical characterization establishes human DHRS10 as a novel 17 β -hydroxysteroid dehydrogenase. Manuscript in revision.

Keller, B., Meier, M., and Adamski, J. **2006**. In search of hydroxysteroid dehydrogenase function: systematic ways to analyze subcellular localization. Manuscript in preparation.

Keller, B., and Adamski, J. **2006** Analysis of steroidogenic activities of retinol dehydrogenases. RDH12, responsible for Leber's congenital amaurosis, takes part in steroid metabolism. Manuscript in preparation.

Publications not included in this thesis

Keller, B., Ohnesorg, T., Mindnich, R., Glöckner, C. J., Breitling, R., Scharfe, M., Möller, G., Blöcker, H. and Adamski, J. **2006**. Interspecies comparison of gene structure and computational analysis of gene regulation of 17 β -hydroxysteroid dehydrogenase type 1. *Mol Cell Endocrinol* 248(1-2): 168-71.

Ohnesorg, T., **Keller, B.**, Hrabé de Angelis, M. and Adamski, J. **2006**. Transcriptional regulation of human and murine 17 β -hydroxysteroid dehydrogenase type 7 confers its participation in cholesterol biosynthesis. *Journal of Molecular Endocrinology*, in press.

Scientific presentations

Keller, B., and Adamski, J. Analysis of steroidogenic activities of retinol dehydrogenases. RDH12, responsible for Leber's congenital amaurosis, takes part in steroid metabolism.

A. Appendix

Poster presentation at the 17th International Symposium of the Journal of Steroid Biochemistry & Molecular Biology, Seefeld, Austria.

Keller, B., Meier, M., and Adamski, J. In search of hydroxysteroid dehydrogenase function: systematic ways to analyze subcellular localization. Poster presentation at the 17th International Symposium of the Journal of Steroid Biochemistry & Molecular Biology. May 31 - June 3, 2006, Seefeld, Austria.

Keller, B., Grote, K. and Adamski, J. In silico Northern blot, an automated method to determine expression patterns from EST databases, reveals tissue specificity of murine 17 β -hydroxysteroid dehydrogenase type 11. Poster presentation at The International Workshop on 11 β - and 17 β -Hydroxysteroid Dehydrogenases, May 8-11, 2005, Elmau, Germany.

Keller, B., Ohnesorg, T., Mindnich, R., Glöckner, C. J., Breitling, R., Scharfe, M., Möller, G., Blöcker, H. and Adamski, J. Interspecies comparison of gene structure and computational analysis of gene regulation of 17 β -hydroxysteroid dehydrogenase type 1. Poster presentation at The International Workshop on 11 β - and 17 β -Hydroxysteroid Dehydrogenases, May 8-11, 2005, Elmau, Germany.

Keller, B., Volkmann, A., Wilckens, T., Möller, G. and Adamski, J. Bioinformatic identification and characterization of new members of short-chain dehydrogenase/reductase superfamily. Poster presentation at The International Workshop on 11 β - and 17 β -Hydroxysteroid Dehydrogenases, May 8-11, 2005, Elmau, Germany.

Breitling, R., Deluca, D., Enseleit, A., Gerber, J.-K., Graedler, F., Glöckner, J. C., Laubner, D., Ohnesorg, T., **Keller, B.**, Marijanovic, Z., Mindnich, R., Möller, G., Perovic, D., Schertel, C., Schieweg, M., Schüren, S., Völkl, A., Ziegelmeyer, G., and Adamski, J. 17beta-Hydroxysteroid dehydrogenases - Tackling them from all directions. Poster presentation at the 15th International Symposium of the Journal of Steroid Biochemistry & Molecular Biology. May 17-20, 2002. Munich, Germany.

Filling, C., Kalaitzakis, E., **Keller, B.**, Bennett, M., and Oppermann, U. Short-Chain hydroxyacyl CoA (SCHAD) deficiency: biochemical and genetic analysis of target gene candidates. Poster presentation at the 11th International Congress Genes, Gene Families and Isozymes. June 30 - July 4, 2001. Stockholm, Sweden.

Danksagung

An dieser Stelle möchte ich all denen danken, die zum Gelingen dieser Doktorarbeit direkt oder indirekt beigetragen haben:

Zuerst meinem Doktorvater, Herrn Prof. Dr. Jerzy Adamski nicht nur für die Überlassung des Themas. Besonders zu erwähnen ist die liberale Art seiner Betreuung und Führung. Ohne sein stets für Ideen und Probleme offenes Ohr und den Freiraum zur Verwirklichung dieser Ideen, aber auch ohne seinen kreativen Input und seine moralische Unterstützung wäre diese Arbeit nicht möglich gewesen. Seine Art und Weise, Wissenschaft zu betreiben hat mich sehr geprägt.

Frau Dr. Gabi Möller möchte ich ebenso für ihre stete Hilfsbereitschaft danken wie für die große Mühe, die sie sich immer beim Korrekturlesen meiner Texte, und nicht zuletzt meiner Doktorarbeit, gegeben hat. Frau Dr. Rebekka Mindnich gilt ebenso großer Dank für das kritische Lesen (aber auch für vieles andere - du weißt, was ich meine). Eure Korrekturen haben diese Arbeit entscheidend verbessert!

Herrn Dr. A. Odermatt, Universität Bern, Schweiz möchte ich herzlich für die Überlassung des N-FLAG Sarcolipin Plasmids danken.

Ein herzliches Dankeschön gilt der gesamten JAG für das erfrischende Arbeitsklima und die allgemeinwährtige Hilfsbereitschaft. Ganz besonderen Dank möchte ich Frau Gabriele Zieglmeier (unserer Labormama, die uns immer mit Rat und Tat zur Seite steht, auch wenn wir noch so nerven), Frau Kerstin Schwerdtner und Frau Marion Schieweg aussprechen. Ebenso danken möchte ich Frau Christina Guggenberger (nicht zuletzt für deine meist sehr ähnliche Sicht der Dinge - nein, ich bin nicht alleine auf dem Holzweg 😊 - und dafür, dass deine Zunge ebenso spitz sein kann wie die meine) und Herrn Marc Meier - der mit seiner unerschütterlich positiven Einstellung immer wieder für ☀️-strahlen in den dunklen Momenten sorgte. Den Praktikanten und Praktikantinnen, die ich im Verlauf meiner Doktorarbeit betreuen durfte - dabei habe ich viel gelernt. Labortechnisch last, but for sure not least möchte ich Herrn Dr. Thomas Ohnesorg für guten Rat nicht nur in Laborbelangen danken. Auch deine Korrekturen waren mir wichtig - danke besonders dafür, daß du dich durch den Methoden-Teil gequält hast... 😊

Von Herzen danken möchte ich auch meinen Freunden - die mir hoffentlich verzeihen, dass ich sie so schändlich vernachlässigt habe, und die mir trotzdem immer den Rücken freigehalten, mich unterstützt und an mich geglaubt haben (auch wenn ich es selber nicht mehr getan habe). Dieser Dank gilt auch meiner Familie und ganz besonders meinen Eltern - für eure Unterstützung kann es keine adequaten Worte geben, ebensowenig wie für meine Dankbarkeit.